Three Dimensional Modelling and Optimisation of Multistage Collectors

Tushar Kanti Ghosh

BEng (Electronics and Tele-Communication), Calcutta University (CU), 1990

MEng (Electronics and Tele-Communication), Jadavpur University (JU), 1993

A Thesis Submitted for the degree of Doctor of Philosophy

June 2002

Engineering Department
Lancaster University
United Kingdom

DECLARATION

I hereby declare that the thesis is my own work, and has not been submitted in substantially the same form for the award of a higher degree elsewhere. Any sections of the thesis which have been published are clearly identified.

ACKNOWLEDGEMENTS

- This work was carried out under the *Commonwealth Scholarship/Fellowship Plan*, administered by the Association of Commonwealth Universities, UK. The British Council in UK financially supported it. Thanks to my sponsors.
- The final part of the work was financially supported by the IEEE Electron Devices Society, USA in the form of *2001 Graduate Student Fellowship*. Thanks to the IEEE EDS technical committee.
- I am grateful to my supervisor Prof. Richard Carter for his valuable guidance throughout the project without which it could not have been seen the light of success. He was always helpful in solving technical as well as personal problems. Thank you very much Prof. Carter.
- Thanks to Mrs Awena Carter for her help; I always felt homely with their company.
- Prof. BN Basu supported and encouraged me through occasional e-mails. Thanks to Prof. Basu.
- Thanks to Prof. RN Biswas, Director UACT (Ex-Director CEERI), for his constant encouragement to carry out this project.
- Thanks to the Director, CEERI, Mr SN Joshi, the late Mr HN Bandyopadhyay, Dr Vishnu Srivastava, Dr RS Raju, Dr AK Sinha, Dr HK Dwivedi, Mr LM Joshi, Mr RK Gupta and other members of the CEERI for their encouragement.
- Thanks to Richard Jenkins for supplying me with a set of spent beam data, which I have used for the sensitivity analysis in Chapter 5.
- The English of my thesis was mostly checked by Mrs Penelope Andrews. Thank you very much Penelope for your help. Thanks to Dr. Paul Beker, for proof reading two chapters of my thesis.
- Thanks to Dr. D Bhattacharya, Corning Research Centre, for his encouragement and support.
- Thanks to my parents for their encouragement to pursue higher studies. Thanks to my other members of the family for their support. My special thanks are for my son Sushobhan (Sayan) for sharing his “valuable” playtime with me occasionally. Last but not the least thanks to my wife for her love, understanding and support throughout this project. She is an inspiration to me.

To my family

Three Dimensional Modelling and Optimisation of Multistage Collectors

Tushar Kanti Ghosh

BEng (Electronics and Tele-Communication), Calcutta University (CU), 1990
MEng (Electronics and Tele-Communication), Jadavpur University (JU), 1993

A Thesis Submitted for the degree of Doctor of Philosophy

ABSTRACT

Multistage collectors are commonly used in travelling wave tubes (TWTs), klystrons, gyrotrons and inductive output tubes (IOTs). A dc beam transfers some of its energy to the input RF wave during its travel through the interaction circuit. The purpose of a collector is to recover most of the remaining dc power from the spent beam and thereby increase both the collector and the overall efficiency. Secondary electrons play a detrimental role in collector performance. Use of the asymmetric collector geometries and application of a magnetic field in the collector region have proved to be effective in recapturing the secondaries. A fully three-dimensional simulator LKOBRA (MF) – the mainframe version of Lancaster KOBRA, has been developed at Lancaster University; this is capable of simulating multistage collectors including the effects of secondary electron emission and magnetic field. It is based on KOBRA3-INP[1] but has been modified and improved together with the pre- and post-processors of the package.

Efficiency is an important parameter in space applications of microwave tubes so it is always desirable to optimise the collector performance to maximise the overall tube

[1] KOBRA3-INP is distributed by INP-DME, Junkernstrasse 99, Wiesbaden, 65205 Germany

efficiency. As a first step the potentials at the collector electrodes are optimised to achieve the maximum possible theoretical efficiency. A computer code based on the well-known enumerative technique has been developed for this purpose. In the next step the geometry of the collector electrodes is optimised using an automated design package that is based on a genetic algorithm. The genetic algorithm creates a new geometry through a search procedure that works from a population of possible geometries. A new set of geometries is generated using three basic operators namely reproduction, crossover and mutation. The collector efficiency is used as the fitness parameter in the genetic algorithm that produces a new population of geometries. This package has been used to optimise the efficiency of a 4-stage symmetric collector and a 2-stage asymmetric collector.

June 2002
Engineering Department
Lancaster University
United Kingdom

CONTENTS

FIGURES

TABLES

Chapter 1

Introduction

The collector is a major component of a linear beam microwave tube. The travelling wave tube (TWT), klystron, gyrotron [1] and inductive output tube (IOT) [2] are different members of this tube family. Figure 1-1 shows the block diagram of a linear beam tube. It has three main components, the electron gun, the RF structure and the collector. The electron gun produces a dc electron beam. The input RF wave interacts with the dc beam in the RF structure and the wave is amplified taking energy from the beam. The rest of the energy remains in the beam after the RF energy is taken out. The beam is then called the spent beam. The purpose of a collector is to collect the spent beam efficiently.

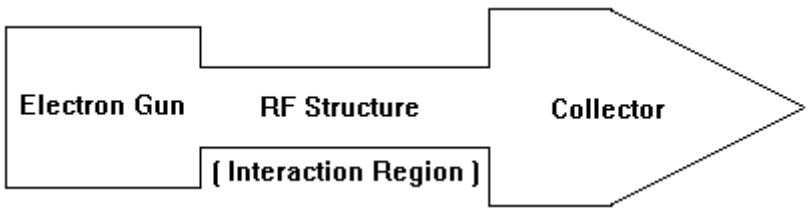

Figure 1-1: Block diagram of a linear beam tube

In this chapter, the purpose of collectors is discussed in brief in section 1.1. The principles of operation of single stage and multistage collectors are explained in sections 1.2 and 1.3 respectively. Different aspects of designing the collector and the aim of the project are discussed in sections 1.4 and 1.5. Finally a brief summary and the novelty of the thesis are described in sections 1.6 and 1.7 respectively.

1.1 THE FUNCTION OF THE COLLECTOR

- *Advantages of spent beam energy recovery*

There are basically two ways to improve the overall efficiency of a linear beam tube, either by increasing the dc to RF conversion efficiency (defined as electronic efficiency) or by recovering the power from the spent beam. It is possible to optimise the interaction between the beam and the RF wave to improve the electronic efficiency but the amount of dc power transferred from the beam to the wave is limited. An efficient collector recovers most of the power from the spent beam and thereby improves the overall tube efficiency. The latter method is valuable because the improvement in efficiency is quite large; it is also reliable and predictable.

When the collector potential is same as that of the body of the tube, the electrons strike the electrode surface at high velocities and the kinetic energy in the spent beam is converted into heat. This energy is also high enough to produce secondary electrons in the collector. In high power tubes x-rays may be produced because of the high energy of the spent beam. To summarise, the advantages of the spent beam recovery are as follows:

- Higher overall tube efficiency
- Lower cooling requirements
- Lower x-ray emission

- *How the spent beam energy is recovered*

As the modulated electron beam enters the collector the axial magnetic field, which controls it in the interaction region is removed and the spent beam is allowed to expand under the influence of the space charge forces. If the collector potential is depressed relative to that of the ground potential then the electrons face a retarding force and land on the electrode surfaces with a lower kinetic energy and power is recovered from the spent beam. These collectors are called depressed collectors. It was first proposed by A. V. Haeff [3] in 1940 that potential depression of the collector might help to recover some of the spent beam power. In practical applications the body of the tube is kept at ground potential. Depression means that the potential of the collector is made negative with respect to the body potential.

Therefore greater depression means a more negative potential with respect to the body and lower depression means a less negative potential with respect to the body. The concept of recovering energy from the beam through collector potential depression can be easily understood by an analogy: when the energy is given as input, then the electrons are accelerated; conversely if the electrons are decelerated, then energy is recovered from them.

1.2 SINGLE STAGE DEPRESSED COLLECTOR

A collector with only one electrode having a depressed potential is known as a single stage depressed collector. The geometry of a single stage depressed collector is shown in Figure 1-2. With no RF modulation in the beam all the electrons travel at the same speed with which they were generated by the electron gun. It is seen in Figure 1-3 that the energy of these electrons are same (dotted line). They can be collected efficiently by a single stage depressed collector at the same potential as the cathode. It is theoretically possible to recover all the dc beam power in this way. If the beam is modulated its average velocity changes because of the transfer of dc beam power to the RF wave. The velocities of the electrons also vary over a wide range as shown in the typical spent beam distribution curves in Figure 1-3. The nature of these curves varies for different tubes because of the different interaction mechanisms. From these curves it is evident that the interaction between the RF and the beam is more intense in klystron than in a TWT. Therefore some of the electrons in klystron lose nearly all of their energy whereas the energy of some is nearly doubled. In this case a small depression may cause reflection of the slower electrons. In a TWT the interaction is not so strong. But some of the electrons are decelerated losing nearly 30% of their energy and some are accelerated gaining nearly the same amount. Because of the wide variation of energy in the spent beam a single stage depressed collector cannot collect the spent beam efficiently. The high velocity electrons can be collected at a lower potential but slower electrons will be reflected and stream back towards the interaction region (RF structure). These electrons introduce noise in the output RF signal either through interception or by providing an unwanted feedback path. The noise gets amplified and can introduce instability and oscillation through feedback. At a less

negative potential it is possible to reduce the back streaming but a greater part of the spent beam power will be dissipated as heat in the collector making it less efficient. A more detailed discussion of the energy recovery process in a single stage collector is given in Chapter 2.

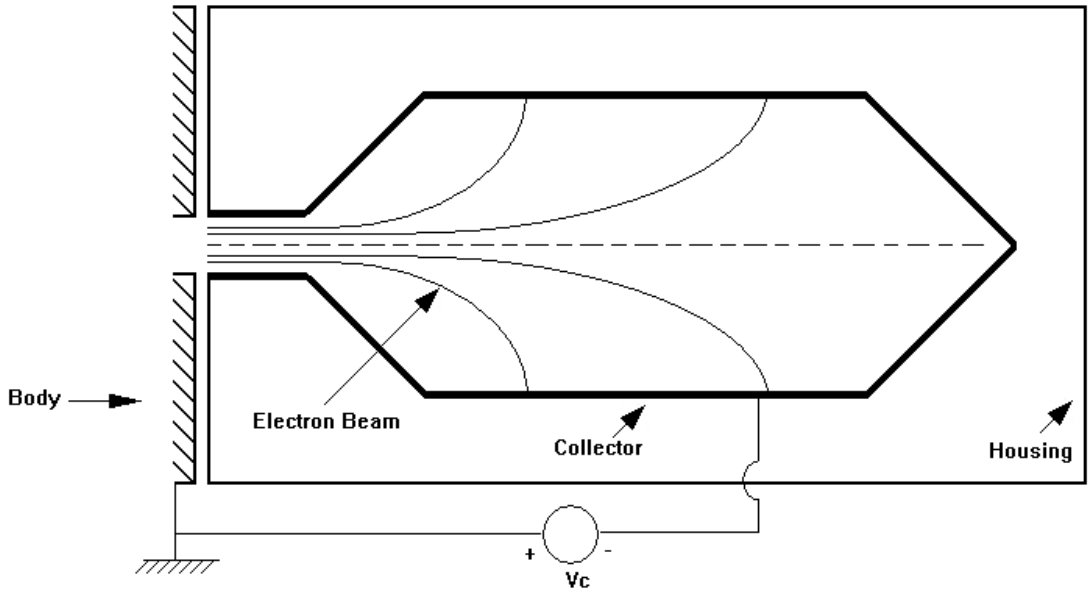

Figure 1-2: Geometry of a single stage depressed collector

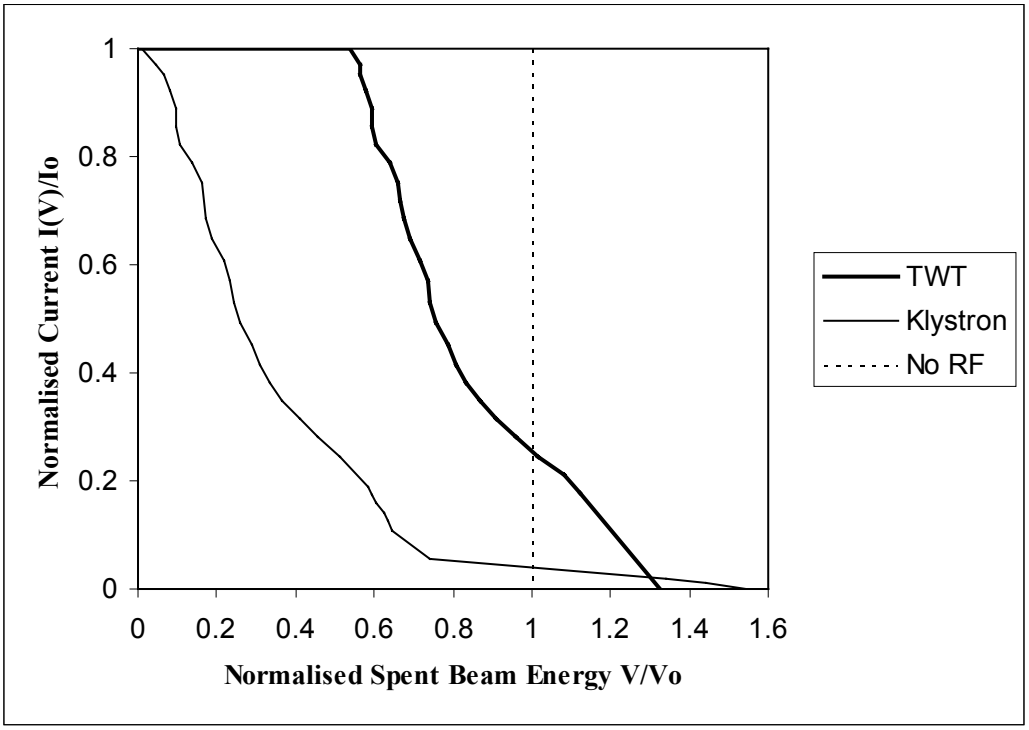

Figure 1-3: Spent beam energy distributions for different linear beam tubes

1.3 MULTISTAGE DEPRESSED COLLECTOR

To overcome the limitations of the single stage collector a multistage depressed collector is used that recovers the spent beam energy in a more efficient way. A collector with a number of electrodes at different potentials is called a multistage collector. The number of stages is defined as the number of potentials on the collector electrodes other than the body potential. The geometry of a typical 4-stage collector is shown in Figure 1-4 where the electrodes (shaded in black) are electrically isolated by high voltage ceramic insulators (shown in grey). An interfacing ring between the RF structure and the collector is kept at ground potential. The potentials of the electrodes are progressively more negative with increasing distance from the body.

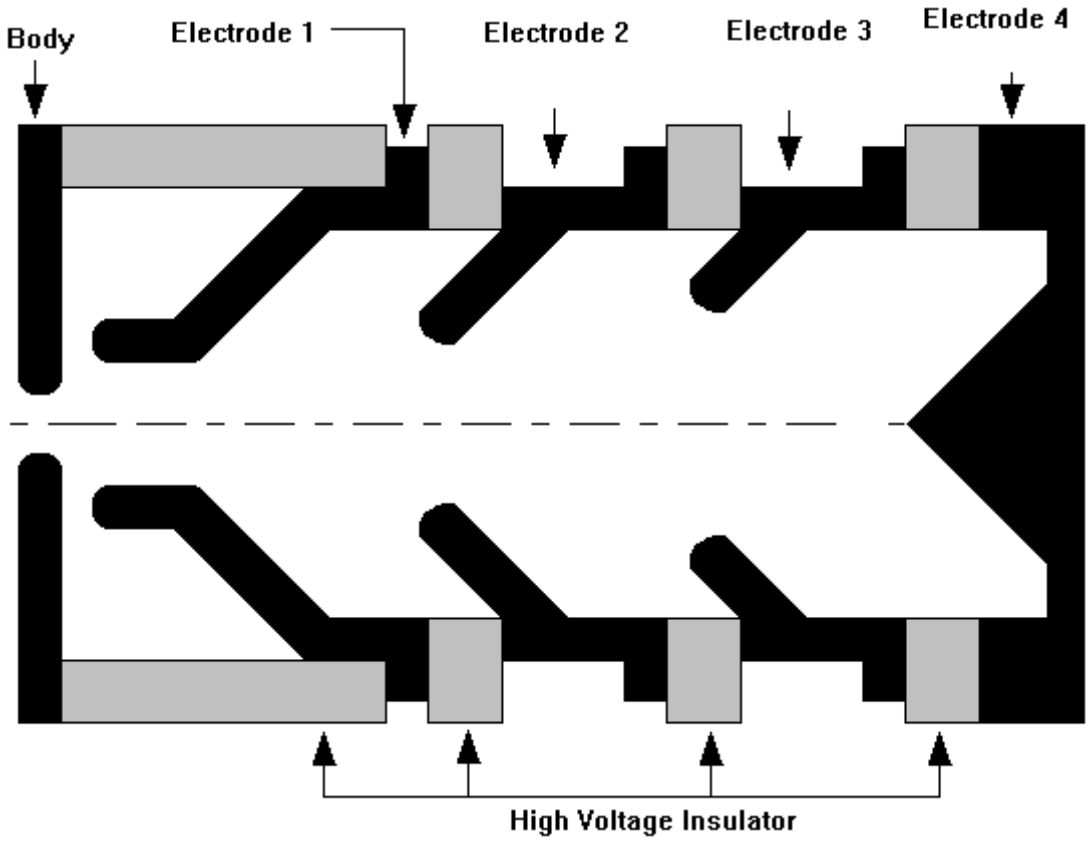

Figure 1-4: A typical 4-stage collector

The main purpose of a multistage collector is to sort the electrons according to their energies and collect them at the lowest possible potential. Electrons with least energy are collected at the highest potential whereas the electrons with higher energies are collected at the electrodes with lower potentials. The potential of the last electrode (furthest from the RF structure, electrode 4 in Figure 1-4) is usually kept at or close to the cathode potential because it is not possible to recover the power from the accelerated electrons using a conventional power supply.

1.3.1 Axi-symmetric Collector

The concept of the multistage depressed collector was originally proposed in the 1950s [4]. But due to the lack of proper understanding of the principle of operation, the early collectors increased the reflection of primary electrons when the number of stages was greater than two. As a result of this, most of the collectors were 2-stage [5]. The shape of the modern multistage collector was first proposed by H. G. Kosmahl [6] in the 1970s. Since then a lot of research has been done to improve its performance [7], [8], [9]. A recent survey of the literature has shown that different companies are using multistage collectors in space TWTs [10], klystrons [11], [12] and IOTs [2]. A detailed review of multistage depressed collectors is presented in Chapter 2.

- *Problems in axi-symmetric collector*

In theory it is possible to recover 100% of the power from the spent beam but with the increase in the number of stages the complexity of fabrication and of the power supply increases. Most modern day collectors are axi-symmetric and they use either 4 or 5 depressed stages [12], [2]. An excerpt form a recent report on space TWTs manufactured by the Thales Electron Devices (TED) is given below [19]:

> "Today, the 4-stage collector provides the optimum trade off between the additional complexity of the TWT amplifier (including the power supply) and energy savings. ….at saturation, about 70% of dissipated heat is generated in the collector; and at small signal, this figure increases to about 90%".

The number of sorted energy classes of the spent beam electrons is same as the number of depressed stages in the collector. When only a few stages are used it is not possible to collect all electrons of the same energy class with very low kinetic energy because the energy of the electrons may vary over a wide range in each class. These electrons thus hit the collector electrodes with sufficient energy to knock secondary electrons out.

1.3.2 Secondary Electron Emission

One of the factors degrading the collector performance is secondary electron emission. Secondary electrons generated on the back of the electrode (facing away from the RF structure) face a decelerating electric field due to the lower potential of the adjacent electrode which forces them back towards the electrode where they were generated. But the secondary electrons generated on the front of the electrode (facing towards the RF structure) face an accelerating electric field from the higher potential of the adjacent electrode. These secondary electrons may either be collected at a higher potential or stream back towards the interaction region. An example is shown in Figure 1-5 where the primary and secondary trajectories are shown in solid and dashed lines respectively. Two primary electrons primary 1 and primary 2 land on the back of electrode 2 and the front of electrode 3 respectively. Secondary electrons generated from primary 1 are decelerated (because the potential of electrode 3 is negative with respect to electrode 2) and recaptured on the same electrode. But the secondary electrons generated by primary 2 are accelerated by electrode 2; one of them is collected at electrode 2 and the other is continuously accelerated (first, by electrode 2, then by electrode 1) towards the RF structure.

Secondary electrons generated from primary 1 have no effect on collector performance. However both secondary electrons generated from primary 2 reduce the collector efficiency and degrade the tube performance. Therefore the secondary electron emission should be as small as possible in the collector or there should be some mechanism to recapture these electrons on the same electrode where they were generated.

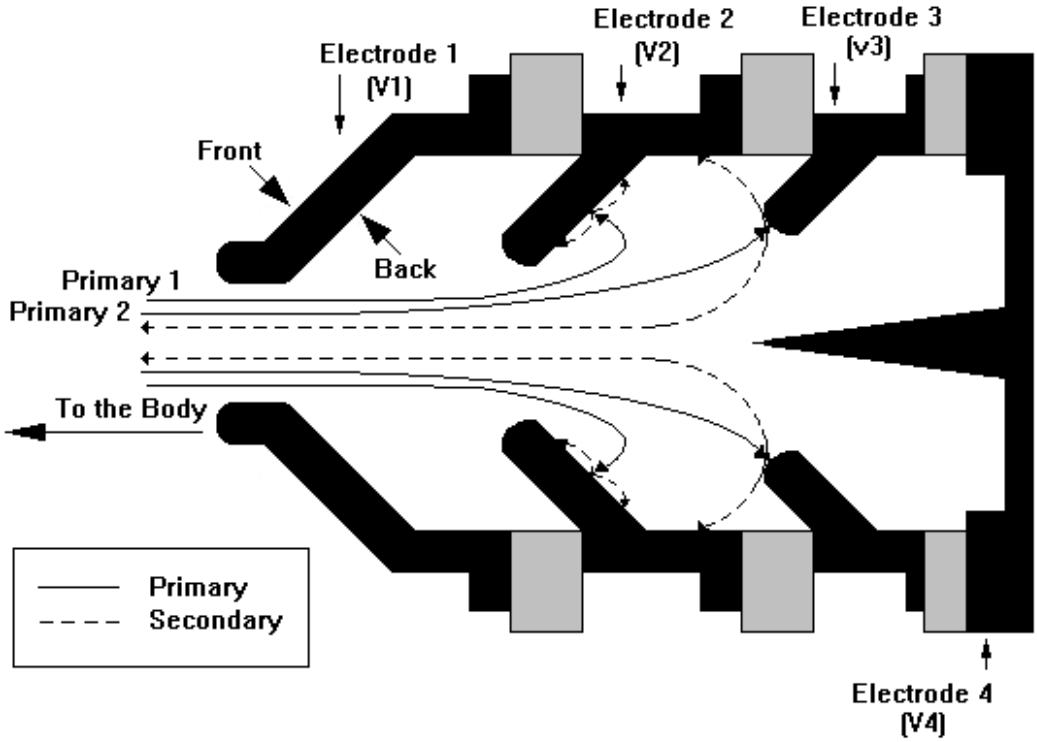

Figure 1-5: Secondary electron trajectories in an axi-symmetric collector

1.3.3 Asymmetric Collector

Asymmetric multistage collectors can be used to recapture the secondary electrons efficiently. A diagram of such an asymmetric collector, called a tilted electric field (TEF) collector, is shown in Figure 1-6. The design and the theory of this collector were first proposed by T. Okoshi et al [13]. A tilted retarding electric field together with an axial magnetic field is applied in the collector. The electron motion in such a collector consists of a uniform deceleration in the axial direction and a uniform transverse drift motion. As a result of this the secondary electrons generated on a collector electrode will continuously move away from the axis of the collector. The primary and secondary trajectories in a TEF collector are shown in Figure 1-7 where the dotted lines are the secondary trajectories.

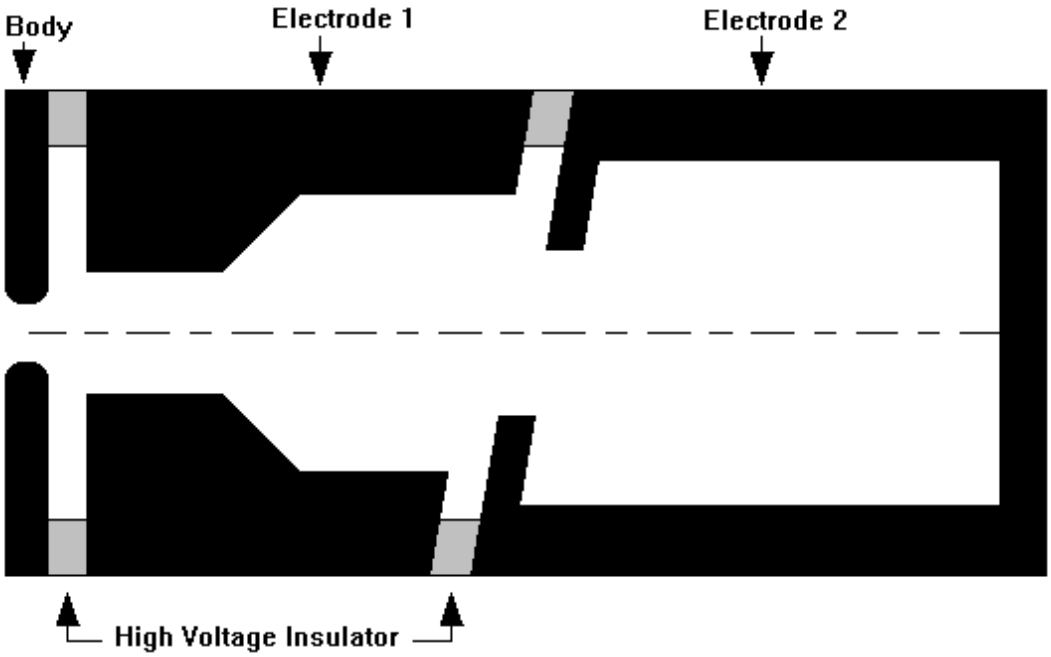

Figure 1-6: A typical 2-stage asymmetric tilted electric field (TEF) collector

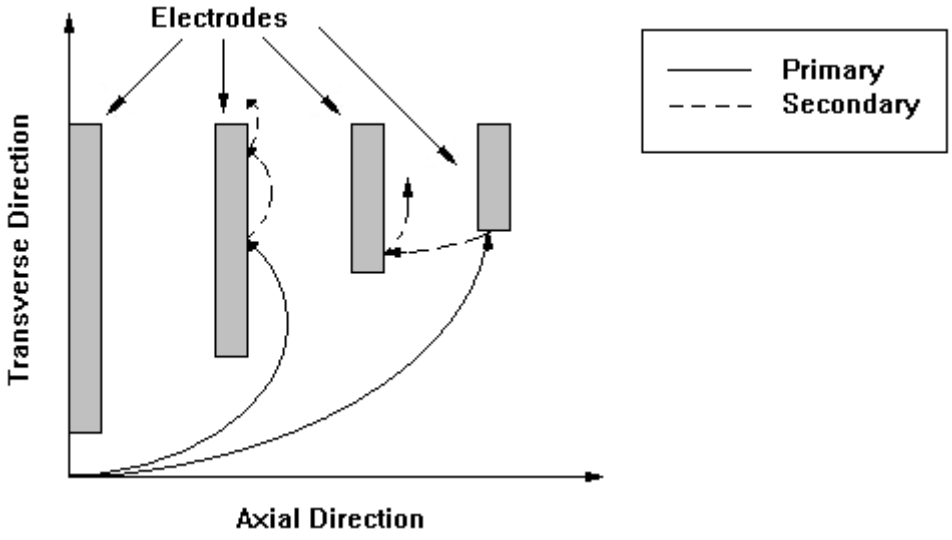

Figure 1-7: Primary and secondary electron trajectories in TEF collector

Another asymmetric collector was proposed by J. R. Hechtel [14] in 1977. A hyperbolic electric field with focusing properties is applied in the collector region as shown in Figure 1-8. The advantage of this collector is that most of the trajectories land on the back of the electrodes and hence the probability of secondary electrons streaming back is much reduced.

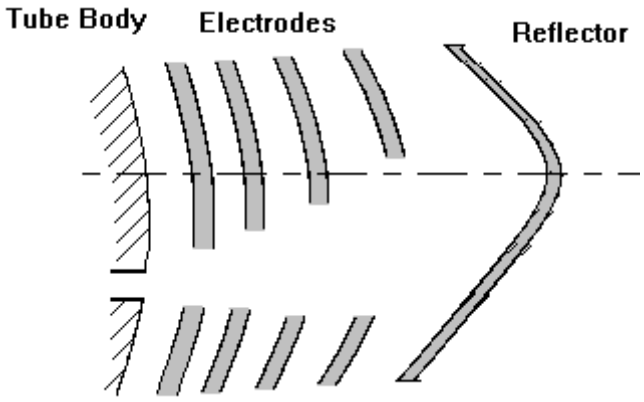

Figure 1-8: Hyperbolic electric field collector

The three dimensional modelling and simulation of asymmetric collectors was first reported by L. Kumar et al [15] in 1991. Simulated results for a TEF collector and a hyperbolic electric field collector were presented in this paper. Later the simulated results for the same TEF collector using a different package were reported by S. Coco et al [16] in 2001. The simulation of this collector using an improved three-dimensional package has been reported by this author [17], [18]. More details of the asymmetric collectors are given in Chapter 2.

1.3.4 Application

Multistage collectors are used to improve the overall efficiency of the tube. Higher overall efficiency is advantageous in different ways:

- For the same output power a higher efficiency tube needs less input power than the lower efficiency tube.
- For higher efficiency tube the power dissipation at the collector is lower than a lower efficiency tube. This reduces the cooling requirements of the tube.
- Less kinetic energy in the spent beam reduces the probability of x-ray emission from the high power tubes.

Reduced input power and lower cooling requirements make the multistage collector an obvious choice for tubes used in space application. The reported overall efficiencies for space TWTs using multistage depressed collectors are 65 to 68% in C-band (20 to 40 W, 250 MHz bandwidth) and 70% in Ku-band (30 to 50 W, 500 MHz bandwidth) [20]. In another publication the efficiency of a C-Band (50 W, 400 MHz bandwidth) TWT fitted with a 4-stage depressed collector was reported to be 66% [21]. For ground-based applications the multistage collector can be used with tubes used in TV transmissions, which can save a lot of power. A recent publication has shown that the use of multistage collectors in klystron tubes used in TV transmission has saved almost 500 Mega Watts of power and more than $50 million in the USA during the last 11 years [12].

1.3.5 Conclusion

From the above discussions it is clear that a lot of effort has been made to improve the performance of axi-symmetric collectors during last three decades. These collectors are mostly electrostatic. Because of their simplicity in fabrication and no requirement for a magnetic field these collectors have been adopted by the industry. Most of the multistage collectors used at present are axi-symmetric. Until recently multistage collectors were used in space TWTs and high power klystrons. But new fields have emerged for the use of multistage collectors in IOT [2]. Research is still under way for the use of multistage collectors in Free Electron Masers (FEM) [22] and gyrotrons [24].

Asymmetric collectors have shown good performance in terms of efficiency and reduced back streaming. But, due to the lack of proper three dimensional computer packages, and better understanding of the theory of operation the possibility of using asymmetric collectors have not been explored much.

Therefore it was concluded that the modelling of both symmetric and asymmetric multistage collectors should be carried out in improved ways using a fully three-dimensional computer package.

1.4 PROBLEMS IN DESIGNING THE COLLECTOR

An ideal collector should be able to sort the electrons according to energy class, collect them at the lowest potential that they have enough energy to reach. It should suppress secondaries by recollecting on the electrode where they were generated. But the effect of space charge forces in the beam, the velocity variations due to RF modulation, secondary electron emission and the limitations in the fabrication of the number of electrodes make it difficult to achieve this goal. However it is possible to overcome these problems to some extent and to optimise the collector performance. The collector should have the following properties for that purpose:

- *Sorting of electrons*

To sort the electrons by energy the electric field in the collector should be designed in such way that it has the focussing properties. If there is a potential difference between two parallel plates then the equipotential lines between them are parallel but in a collector structure they are different as shown in Figure 1-9(a). The equipotential lines on the left side of each set act as a converging lens but they bend near the aperture and form a diverging lens at the right side. If the aperture is small the distortion of equipotential lines is less and limited only in the aperture region as is evident from the figure. An electron beam passing through a set of equipotential lines gets converged first due to the converging lens effect, which helps to counter the space charge force in the beam. Near the aperture the beam diverges (due to the diverging lens effect and the space charge force within the beam) in a direction perpendicular to the equipotential lines. This type of structure is widely known as a "Dispersive-Lens" collector (DLC). Sometimes another type of electrostatic lens is used for collector design, which is called the "Individual-Lens" collector (ILC) [23]. One such geometry and its equipotential lines are shown in Figure 1-9 (b) where the electrostatic lens is formed at the aperture. The shapes of the equipotential lines depend on the size of the aperture unlike DLC. An electrostatic lens of this kind is sometimes disadvantageous as it repulses the low energy electrons and increase back streaming. The advantage of ILC is that the size is always smaller than a comparable DLC and the designer has the flexibility to choose the location and number of electrodes. But the smaller size in the ILC reduces the collector efficiency [23].

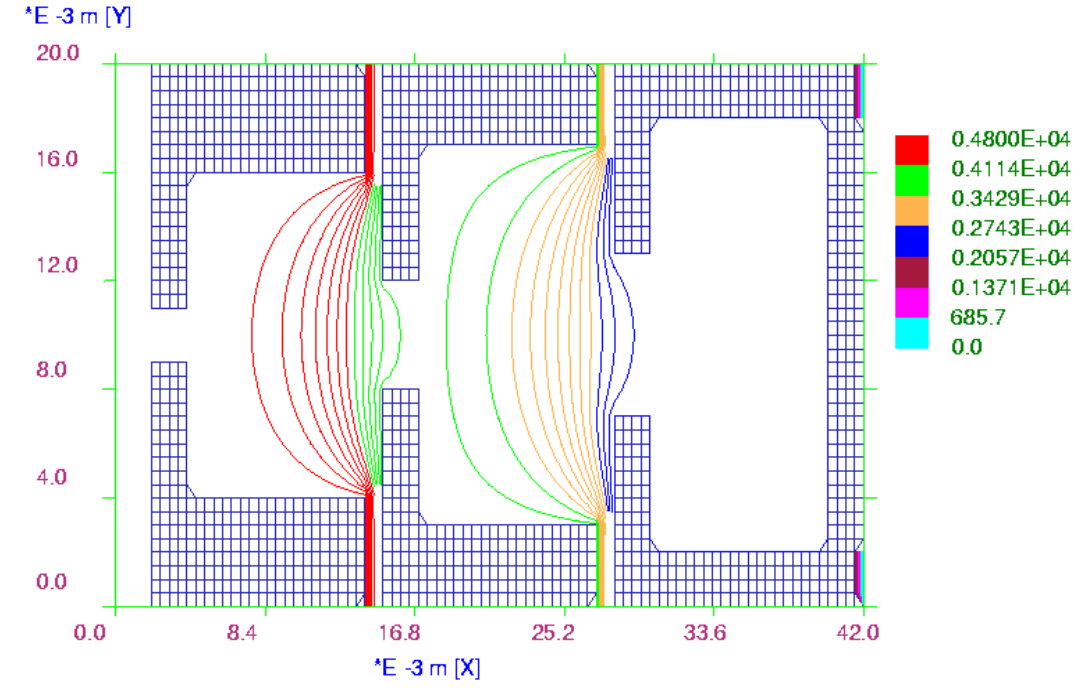

(a)

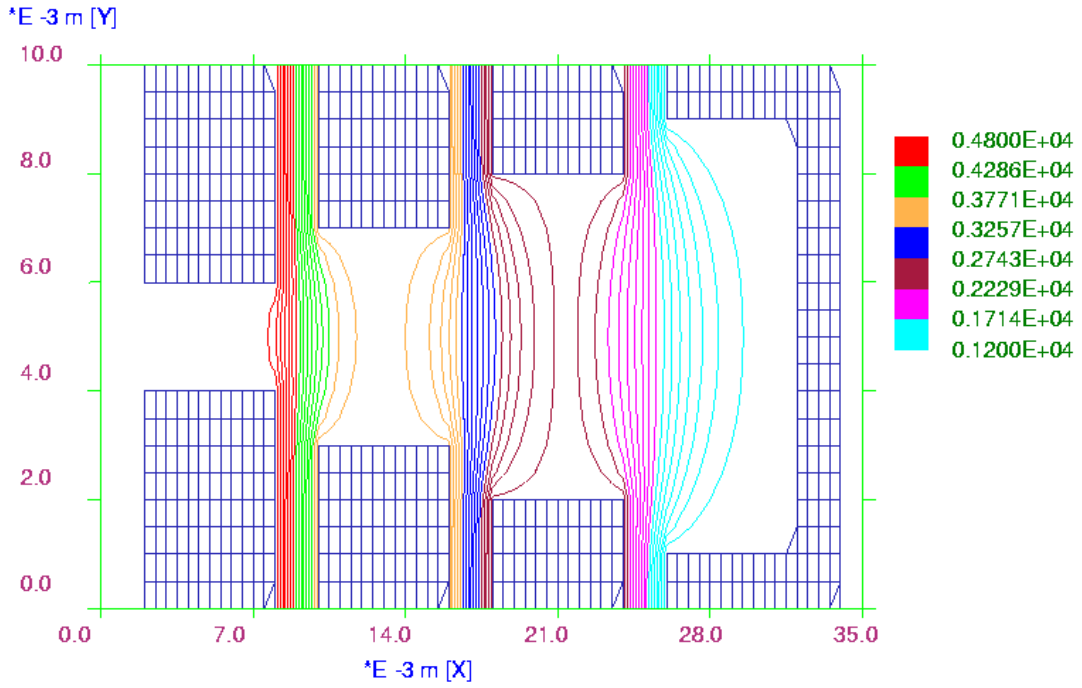

(b)

Figure 1-9: Equipotential lines (a) dispersive lens collector (b) individual lens collector.

The number of lenses formed determines the number of energy classes within the collector.

- *External magnetic field*

The reflected primary and secondary electrons generated at the front of the electrodes are either collected at the electrodes with higher potentials or tend to move towards the interaction region because of the accelerating electric field produced by the adjacent electrode (towards the RF structure). A transverse component of the magnetic field pushes the electrons towards the sidewalls where they are collected. An external magnetic field in the collector should be applied at an angle to the direction of the electric field.

An example is shown in Figure 1-10 where an electron is moving along the direction of v, and B is the transverse magnetic field. The force on the electron is F = qvB and its direction is perpendicular to the motion. Because of this, the electron has a transverse velocity component that moves the electron away from the axis.

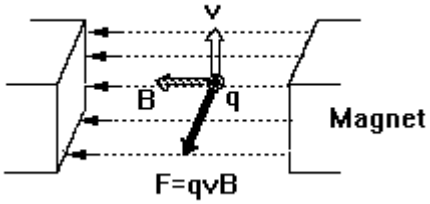

Figure 1-10: Influence of transverse magnetic field on an electron

- *Transverse energy*

The electric field lines are perpendicular to any metal boundary surface. The design of the collector should be such that the electrons do not travel at a large angle to the electric field lines. In this case the electrons will have a large transverse energy component when they strike the electrode. This energy cannot be recovered from the electrons. The electric field lines and the primary trajectory are shown in Figure 1-11. The transverse energy (E_x) increases as the angle θ between the electric field and the primary trajectory increases. Another disadvantage of the increase of θ is that the

secondary electron emission co-efficient increases which increases the secondary electron emission current.

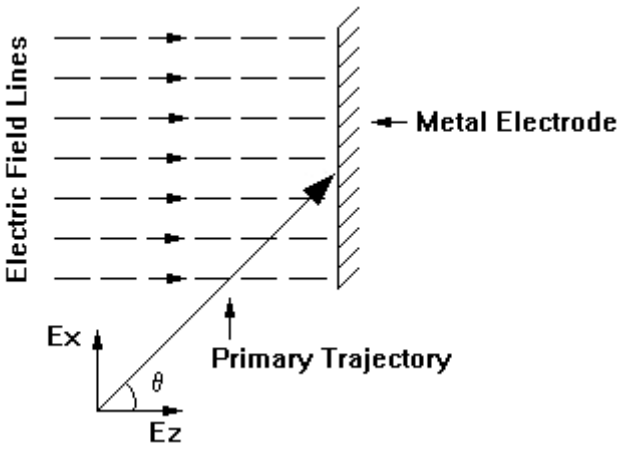

Figure 1-11: Primary trajectory and the electric field lines

- *Electric field*

The electric field in the collector should be such that the reflected primary electrons and the secondary electrons always see a retarding field. This is possible by collecting the primaries on the back of the electrodes (facing away from the RF structure) where the secondaries generated can be recaptured. But in the case of the last electrode this condition can never be achieved because it is always kept at the most negative potential with respect to the body and the adjacent electrode (towards the RF structure) is at higher potential. However a spike in the electrode can direct the electrons towards the sidewalls where they can be collected. Presumably we could try to collect the electrons on the back of electrode N-1 by making the spike potential so low that no electrons could reach it. But with the conventional power supply it is not possible to make the spike potential lower than the cathode potential.

- *Constant efficiency*

The input RF drive level changes the output power and hence the characteristics of the spent beam. If the collector is designed for only one spent beam condition (in a static condition) then it may not be able to maintain maximum efficiency in other operating conditions. In a multi-carrier operation the input drive signal is made low to operate the tube well below saturation to reduce the intermodulation products. The lower input drive reduces the output power and the overall efficiency of the tube. But it is

necessary for some operations to maintain a certain level of overall efficiency with varying drive levels. The collector performance can be optimised for that purpose in two steps:

- A number of different spent beam energy distribution curves are used to optimise the electrode potentials to give nearly constant efficiency over a wide variation of the input drive levels.
- In the next step the collector geometry can be optimised by changing the electrode shapes.

- *Dynamic operation*

The velocity distribution of the electrons changes with the change in phase of the RF cycles. The typical transit time of electrons within the collector is a few RF cycles. After several RF periods a steady state condition is achieved within the collector [25]. A time domain approach is required to incorporate the velocity variation in the simulation of collector performance. Instead of that a steady state solver can be used if it is assumed that the time scale of the variation is less than the transit time of electrons in the collector.

- *Optimisation*

Generally, the optimisation in the performance is carried out manually through several iterations. It may not be possible always to achieve an optimised design, which is very close to the ideal design. In that case an automated design procedure will be a great help. A new geometry can be generated by iteration and its performance can be predicted through simulation. An algorithm to generate a new geometry that uses the performance of the old geometry to produce a better design may be the best choice [26], [27].

1.5 AIM OF THE PROJECT

It is necessary to predict the performance of a multistage collector before it is fabricated. Computer packages can be used for design and simulation purposes to

avoid the repetition of fabrication that is otherwise necessary to optimise the collector performance through experimentation. But the problems in designing the collector and the remedial procedures have been discussed in the previous section. The main aims of the project have been decided on the basis of this discussion. Broadly they are:

1. To find improved ways of modelling and simulation of symmetric and asymmetric collectors
2. To find a suitable methodology for optimising the collector performance

For this purpose it is necessary to have a fully three-dimensional particle-in-cell (PIC) code that includes a secondary electron emission model. The package should incorporate an automated process for the collector design, which generally needs a large number of iterations for the optimisation of collector performance. Emphasis has been given to the validation of simulated results by comparison with experimental data.

1.6 THESIS STRUCTURE

Chapter 2 of the thesis is a background study and up-to-date literature review of the modelling and simulation of MDCs. A review of the different three-dimensional computer codes is included in this chapter.

The development of a three-dimensional package along with its pre- and post processors is discussed in Chapter 3. The package has been validated through some basic tests. The simulated results of an asymmetric collector have been compared with the experimental data to validate the package.

A secondary electron emission model has been developed and included in the package. The development of this model is discussed in Chapter 4. Some tests are carried out on this model and the simulated results are compared with the experimental data.

Chapters 5 and 6 of the thesis deal with the optimisation of the design procedure of multistage collectors. The first part of the optimisation procedure is dealt with in Chapter 5. An algorithm to optimise the electrode potentials is described in detail. The sensitivity of the collector performance at different input drive levels is discussed with an example. The optimisation procedure for the collector geometry using a genetic algorithm is described in Chapter 6.

The last chapter summarises the thesis and suggests areas of further research in the field of MDC.

1.7 NOVELTY OF THE THESIS

The thesis demonstrates the modelling and simulation of high efficiency axi-symmetric and asymmetric multistage collectors. All these simulations consider the effect of secondary electrons inside the collector. A three-dimensional simulator including pre- and the post-processors has been developed for this purpose. This is based on an existing ion source simulator KOBRA3-INP[1], which has been modified and improved. The pre-processor has been modified and some new options are added. The post-processor that includes a secondary electron emission model and an analysis program has been developed afresh.

A technique has been developed for the optimisation of multistage collector performance. In the first part of this work an algorithm based on the enumerative technique has been developed to optimise the electrode potentials for maximum power recovery. It is also capable of doing sensitivity analysis of the collector performance for different input drive levels. Finally two algorithms have been developed based on random walk and genetic algorithms for the optimisation of collector geometry. The genetic algorithm is based on natural selection and natural genetics; it uses a random method as a tool for optimisation. *For the first time the genetic algorithm has been used for optimisation of any microwave tube component*. In that sense this method is unique. Two separate automated packages have been developed using these

[1] KOBRA3-INP is distributed by INP-DME, Junkernstrasse 99, Wiesbaden, 65205 Germany

algorithms. Both of them include the three-dimensional simulator. The performance of the genetic algorithm has been compared with the random walk algorithm by optimising two different collectors.

REFERENCES

[1] M. E. Read, W. G. Lawson, A. J. Dudas, A. Singh, "Depressed Collectors for High-Power Gyrotrons," *IEEE Trans. on Electron Devices*, vol. 37, no. 6, pp. 1579-1589, June 1990.

[2] R. S. Symons. (1999, June). The Constant Efficiency Amplifier. Presented at Accelerator Driven Transmutation Technologies and Applications, Czech Republic [Online]. Available: http://www.fjfi.cvut.cz/con_adtt99

[3] A. V. Haeff and L. S. Nergaard, "A Wide Band Inductive Output Amplifier," *Proc. of IRE*, vol. 28, pp. 126-130, March 1940.

[4] F. Sterzer, "Improvement of Travelling-Wave Tube Efficiency Through Collector Potential Depression," *IRE Trans. on Electron Devices*, pp. 300-305, October 1958.

[5] W. Neugebauer and T. Mihran, "A ten stage depressed collector for Improving Klystron Efficiency," *IEEE Trans. on Electron Devices*, vol. ED-19, No. 1, pp. 111-121, Jan. 1972.

[6] H. G. Kosmahl, A Novel Axi-symmetric Electrostatic Collector For Linear Beam Microwave Tubes, NASA Tech. Note TN D-6093, 1971.

[7] J. A. Dayton, JR., H. G. Kosmahl, P. Ramins and N. Stankiewicz, "Analytical Prediction and Experimental Verification of TWT and Depressed Collector Performance Using Multidimensional Computer Programs," *IEEE Trans. on Electron Devices*, vol. ED-26, No. 10, pp. 1589-1597, 1979.

[8] P. Ramins, H. G. Kosmahl, D. A. Force, R. W. Palmer and J. A. Dayton, JR., "Verification of an Improved Computational Design Procedure for TWT-Dynamic Refocuser-MDC Systems with Secondary Electron Emission Losses," *IEEE Trans. on Electron Devices*, vol. ED-33, No. 1, pp. 85-90, January 1986.

[9] K. R. Vaden, V. O. Heinen and J. A. Dayton, Jr., "Three-Dimensional Modelling of Multistage Depressed Collectors," *IEEE Trans. on Electron Devices*, vol. 46, No. 8, pp. 1810-1811, August 1999

[10] P. Ehret, E. Bosch and H. Seidel, "L- and S-Band Travelling Wave Tubes for Satellite Application," in *Proc. of IVEC 2001,* April 2001, pp. 35-38.

[11] A. Shabazian, E. L. Wright, R. Batra, E. McCune, R. Begum and L. Zitelli, "Development and Production of a High-power S-band MSDC Klystron for Satellite Digital Radio," in *Proc. of IVEC 2002,* April 2002, pp. 326-327.

[12] R. Batra, E. L. Wright, E. McCune, "Reliability of TV Klystron with Multi Stage Depressed Collector," in *Proc. of IVEC 2002,* April 2002, pp. 328-329.

[13] T. Okoshi, E. Chiu and S. Matsuki, "The Tilted Electric Field Soft-Landing Collector and Its Application to a Travelling-Wave Tube," *IEEE Trans. on Electron Devices*, vol. ED-19, No. 1, pp. 104-110, 1972.

[14] J. R. Hechtel, "A Novel Electrostatic-Focusing Depressed Collector for Linear Beam Tubes," *IEEE Trans. on Electron Devices*, vol. ED-24, No. 1, pp. 45-52, January 1977.

[15] L. Kumar, R. G. Carter and D. Perring, "Three-Dimensional Modeling of Asymmetric Depressed Collectors," in *Proc. ESA Workshop on Space TWTA's 1991*, ESTEC, Noordwijk, 15-16 May, 1991, ESA WPP-22, pp. 6.3.1-18.

[16] S. Coco, F. Emma, A. Laudani, S. Pulvirenti and M. Sergi, "COCA: A Novel 3-D FE Simulator for the Design of TWTs Multistage Collectors," *IEEE Trans. on Electron Devices*, vol. 48, no. 1, pp. 24-31, January 2001.

[17] T. K. Ghosh and R. G. Carter, "3-D Simulation of Asymmetric Multistage Depressed Collectors with Secondary Electron Emission Effects for High Efficiency Space TWTs," in *Proc. ITG Conference on Displays and Vacuum Electronics*, May 2-3, 2001, pp. 67-71.

[18] T. K. Ghosh and R. G. Carter, "Improved Three Dimensional Simulation of Multistage Depressed Collectors for High Efficiency Travelling Wave Tubes," in *Proc. of 2nd IEEE International Vacuum Electronics Conference 2001*, April 2-4, 2001, pp. 215-220.

[19] Thales Electron Devices (Website).
Available: http://www.thales-electrondevices.com/

[20] E. Bosch, H. P. Rothacker, A. Jager, "High Efficiency, Low Power C- and Ku-Band Travelling Wave Tubes for Satellite Application," in *Proc. of IVEC 2002,* April 2002, pp. 186-187.

[21] R. T. Benton, U. R. Hallsten, J. A. Hill, K. P. Mallon, W. L. Meninger, X. Zhai, "High Efficiency S-band and C-band Travelling Wave Tubes for Satellite Communications," in *Proc. of IVEC 2002,* April 2002, pp. 184-185.

[22] C. G. Whyte, A. W. Cross, D. A. Jaroszynski, W. He, K. Ronald and A. D. R. Phelps, "Free Electron Maser Amplifier Energy Recovery Experiments," in *Proc. of IVEC 2002,* April 2002, pp. 91-92.

[23] H. G. Kosmahl, "Modern Multistage Depressed Collectors – A Review," *IEEE Trans. on Electron Devices*, vol. ED-70, No. 11, pp. 1325-1334, Nov. 1982.

[24] A. Singh, S. Rajapatirana, Y. Men, V. L. Granatstein, R. L. Ives, and A. J. Antolak, "Design of a Multistage Depressed Collector System for 1-MW CW Gyrotrons-Part I: Trajectories Control of Primary and Secondary Electrons in a Two-Stage Depressed Collector," *IEEE Trans. on Plasma Science*, vol. 27, No. 2, pp. 490-502, 1999.

[25] Y. Goren, R. Wilson, P. Lally, "2.5-Dimensional Time Domain Particle-In-Cell Simulation Code for Collector Design," in *IEDM (Technical Digest)*, pp. 877-880, IEEE 1990.

[26] T. K. Ghosh and R. G. Carter, "Design Optimisation of Multistage Depressed Collectors for High Efficiency Travelling Wave Tubes Using Genetic Algorithm," in *Proc. of 3rd IEEE International Vacuum Electronics Conference 2002*, April 23-25, 2002, pp. 158-159.

[27] K. R. Vaden, J. D. Wilson, and B. A. Bulson, "A Simulated Annealing Algorithm for the Optimization of Multistage Depressed Collector Efficiency," in *Proc. of 3rd IEEE International Vacuum Electronics Conference 2002*, April 23-25, 2002, pp. 164-165.

Chapter 2

Background Study

2.1 INTRODUCTION

The basic theory of the depressed collector is quite old and the technology is well established. But the computer packages used for simulation of multistage collectors were not very reliable and complete until the 1970s. These packages were used earlier for a better understanding of the physical aspects of the collector. Sometimes these packages were modified to match the experimental results. Until recently, the different components of a microwave tube used to be designed through scaling an existing component due to the lack of powerful and reliable simulation tools. After several cycles of design, fabrication and experiments, the new design could be established. Clearly this was a time-consuming and expensive process. So, different simulation packages have been developed during the last two decades for the design of collectors. Once the basic design is complete, the simulator can be used as a tool to tune the performance of the device.

The advantage of the multistage collector over the single stage one and the impact of collector efficiency on the overall tube efficiency are discussed in 2.2 and 2.3 respectively. In section 2.4 the review of codes is discussed on the basis of the criteria chosen for an ideal code. Finally, the literature review of the modelling is presented in section 2.5, which covers both symmetric and asymmetric collectors. Sections 2.4 and 2.5 are both concluded by summarising the findings.

2.2 SINGLE STAGE VERSUS MULTISTAGE COLLECTOR

The origins of the "scientific" depressed collectors [8] to increase the overall efficiency of a tube started in the 1960s however the depressed collectors were suggested as long ago as 1940s [38]. It was shown experimentally by F. Sterzer [39] in 1958 that the potential depression at the collector improves the efficiency of collection. Before the 1970s there was a misconception that collectors with more than two stages would increase the back streaming of electrons by an enormous amount. With the better understanding of the theory of collectors it is now feasible to fabricate and use multistage collectors to increase the overall tube efficiency without significant back streaming.

2.2.1 Spent Beam Curve

The amount of power that can be recovered by a collector depends on the nature of the spent beam, if the number of stages in the collector is kept fixed. A typical spent beam distribution curve for a TWT is shown in Figure 2-1 where the horizontal axis represents the collector voltage and the vertical axis represents the collector current. In practical TWTs the body current (electron current intercepted either by the RF interaction circuit or the anode in the electron gun) is quite small; therefore it can be neglected. The cathode voltage and current are denoted by V_o and I_o respectively and the dc beam power is calculated from the area of the rectangle (V_o * I_o). The grey shaded area (less area under the V_{max} - V_o tail) represents the dc beam power converted to RF power and different losses in the tube (circuit interception loss, reflection loss, sever loss etc.). The hatched area under the curve represents the power remaining in the spent beam that can be recovered by the collector. The square hatched area (alternate black and white) under the V_{max} - V_o tail represents the energy of those electrons, which are accelerated during the interaction between the RF wave and the beam.

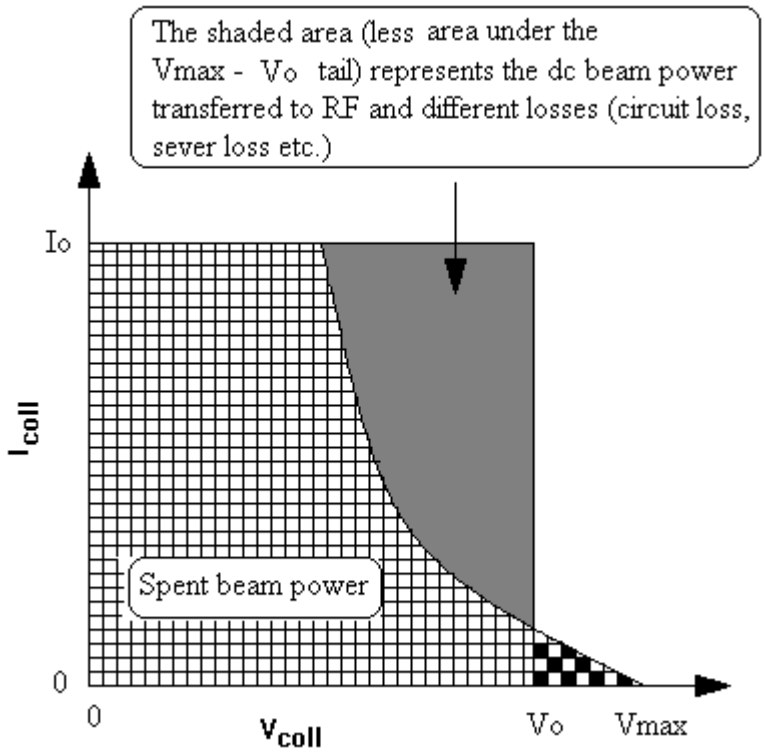

Figure 2-1: Spent beam power distribution

2.2.2 Single Stage Collector

A typical spent beam power distribution curve is shown in Figure 2-2 where the shaded area represents the maximum power that can be recovered by any single stage collector. The depressed potential at which the collector is to be operated to recover this power is called the knee voltage. In the present case the knee voltage is 0.58 times the cathode potential V_o. Electrons with lower energy are reflected towards the interaction region if the collector voltage is lowered than the knee voltage. The spent beam curve for a collector varies due to different operating conditions and input drive levels. So the knee voltage cannot be sharply defined for a specific collector. Generally, the collector is operated at a less negative voltage (with respect to ground) than the knee voltage to avoid the reflections of electrons from the collector in any operating condition. Moreover, the complexity in the power supply increases due to the tight voltage regulation that might be required to operate the collector sharply at the knee. From Figure 2-2 it is clear that a large amount of power is still left in the

spent beam, which is not recovered by the single stage collector. In the present case the collector can recover a maximum of 71.4% of the spent beam power.

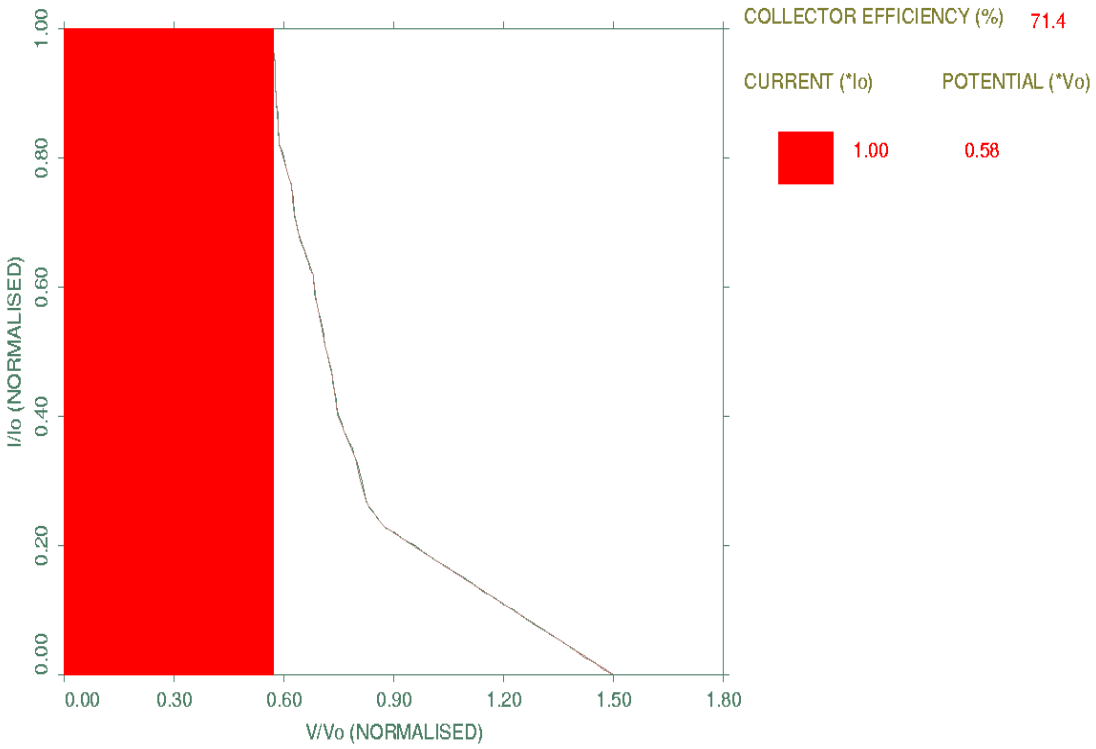

Figure 2-2: Spent beam power recovered by a single stage depressed collector

2.2.3 Multistage Collector

To recover more power from the spent beam the number of stages in the collector should be increased. The same spent beam distribution curve (shown earlier) with four different potentials of a 4-stage depressed collector is shown in Figure 2-3. The shaded area represents the maximum power that can be recovered by the collector. Different shadings represent the power recovered by different electrodes. Normalised potentials (normalised with respect to cathode potential) and currents at different stages are tabulated at the top right corner of the plot. This indicates that the power within the V_{max} - V_o tail is lost (Figure 2-1*)*. In theory it is possible to lower the last electrode potential below the cathode potential to recover the power from the

accelerating electrons. But due to the limitations in the power supply the last electrode potential is generally kept at positive potential with respect to the cathode.

In the present case the multistage collector recovers 89.4% of the spent beam power, nearly 1.25 times higher than that of a single stage, which illustrates that a multistage collector is more efficient for recovering the power from the spent beam than a single stage. Power recovered by the 4-stage collector, P_{rec}, is

$$P_{rec} = V_1 I_1 + V_2 I_2 + V_3 I_3 + V_4 I_4 \tag{2-1}$$

where V_1, V_2, V_3, V_4 are the potentials at electrodes 1, 2, 3 and 4 respectively and I_1, I_2, I_3, I_4 are the current collected by them.

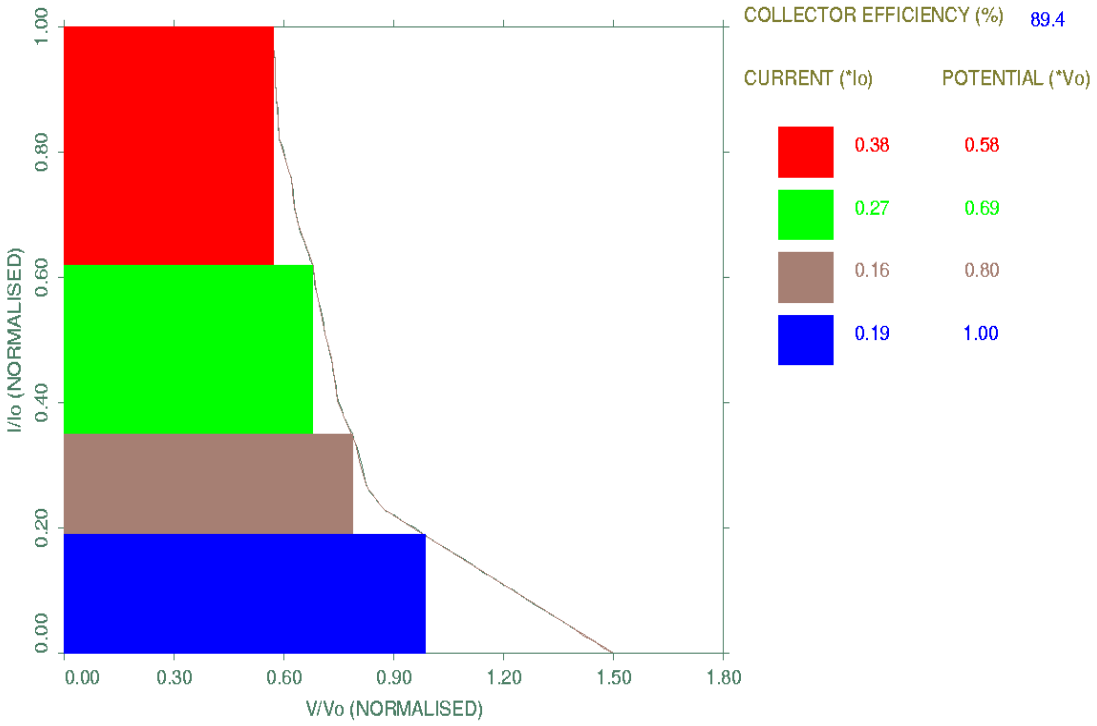

Figure 2-3: Power recovered by a 4-stage collector

2.3 EFFECT OF COLLECTOR ON TUBE EFFICIENCY

The basic tube efficiency, commonly known as the electronic efficiency, is defined as the efficiency with which the dc beam power is converted to RF power during the interaction process. In mathematical terms, the basic tube efficiency, η_e, can be expressed as

$$\eta_e = \frac{P_{out}}{P_{dc}} \tag{2-2}$$

where P_{out} *is the RF output power*

P_{dc} *is the input dc power*

The performance of a collector is evaluated by determining its efficiency to recover the power from the spent beam. By definition, efficiency is the ratio of the power recovered from the spent beam to the power entering the collector. The collector efficiency, η_{coll}, is expressed as

$$\eta_{coll} = \frac{P_{rec}}{P_{spent}} \tag{2-3}$$

where P_{rec} *is the power recovered from spent beam*

P_{spent} *is the total spent beam power*

If the losses in the circuit (circuit loss, heater loss, interception loss etc.) are assumed to be negligible, then the overall efficiency can be expressed only in terms of the collector and basic tube efficiency. The overall efficiency, η, is

$$\eta = \frac{\eta_e}{1 - \eta_{coll}(1 - \eta_e)} \tag{2-4}$$

where η_{coll} *and* η_e *are as defined above*

The curves for overall efficiency versus basic tube efficiency for different collector efficiencies are plotted in Figure 2-4 (reproduced from [4]). The x-axis of the curve represents the basic tube efficiency and the y-axis represents the overall tube

efficiency. For any curve the collector efficiency is kept constant. It is seen from the curves that an increase in collector efficiency increases the net tube efficiency remarkably. In the first curve (η_{coll} = 0%) the overall efficiency of the tube is same as the basic tube efficiency for no collector depression. If the collector efficiency is 80% then it is possible to achieve 64% overall efficiency for a basic tube efficiency of 25%. This gives an increase of the overall tube efficiency by more that 2.5 times with collector depression. However in practice it is not so simple because the collector efficiency depends on the basic tube efficiency and the beam perveance. The collector efficiency decreases with both increasing perveance and electronic efficiency [8]. So the designer may have to compromise on the electronic efficiency to achieve a maximum overall efficiency.

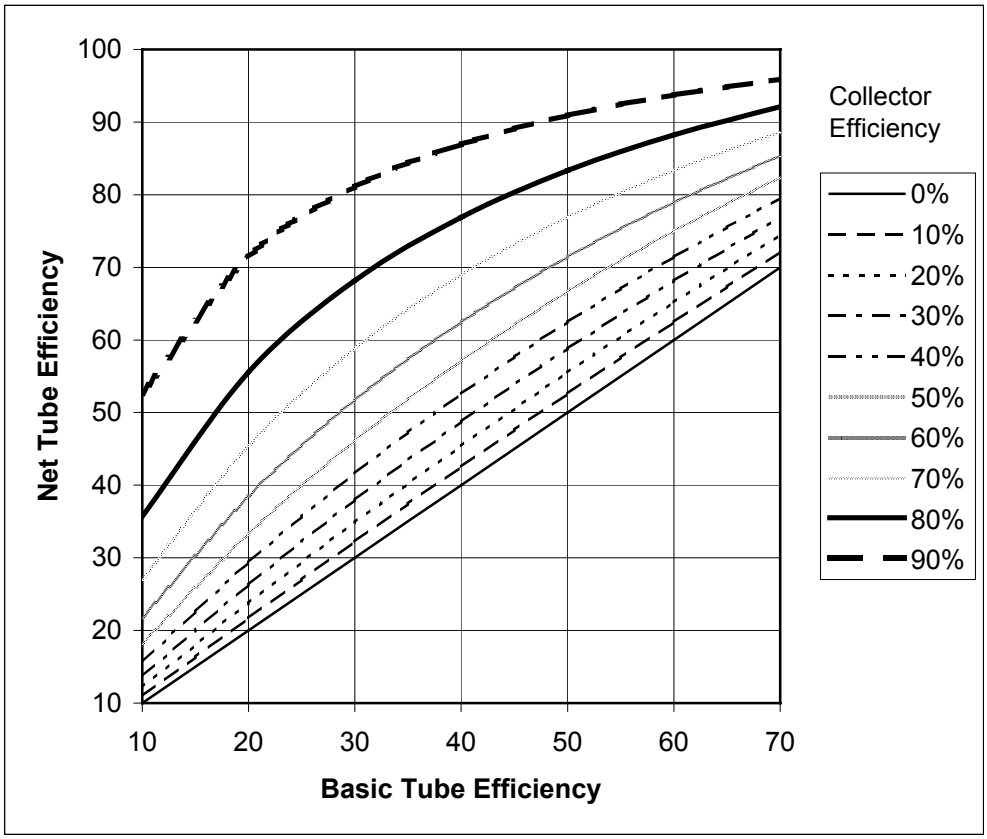

Figure 2-4: Basic tube efficiency versus net tube efficiency for different collector efficiencies

2.4 REVIEW OF CODES FOR SIMULATION

In the 1960s the trend was to develop two-dimensional PIC (particle-in-cell) codes, which are suitable for simulation of axi-symmetric collectors in static condition. But to model any asymmetry either in the geometry or in the external magnetic field a three-dimensional package should be used. The modelling of a complicated multistage collector in three dimensions was done as early as in the 1980s [3]. This collector was a standard azimuthally symmetric device but with vanes attached to the third electrode to shield the collector plates from the space charge of the incoming electrons. Although the development of three-dimensional packages is not very new, the use of a three-dimensional package for the simulation of asymmetric collectors was only reported for the first time in 1991 [2]. The simulated results were compared with the experiments and these were reported to be in good agreement. In this section, the properties of an ideal code are described in detail. The features of different well-known computer packages are compared to test their suitability for the purpose of simulation and further improvements or additions to do the design optimisation.

2.4.1 Criteria for an Ideal Code

Some important features, which the simulator should have for the design and simulation of a multistage collector, have been identified. The simulator should be a three-dimensional PIC code with the following features:

1. *Collector geometry*

   The collector should have the capability to sort electrons according to their energy distribution in the spent beam. Electrons with a different class of energy should be collected at different electrodes depending upon the potential of that electrode. A simulator should have the capability to design at least 4- to 5- electrodes (depending upon the application of the tube) with different potentials assigned to each of them. The number of stages in the collector is restricted due to the compromise between efficiency, weight, and complexity in fabrication and power supply. Most modern multistage collectors have a maximum of four stages (four different electrode potentials other than ground).

The geometry of the collector is designed according to the requirement of the electric and the magnetic field inside the collector. Different types of collectors such as asymmetric, symmetric, tilted electric field and crossed-field are used depending upon the application and efficiency requirements. A detailed classification of various possible orientations of electric and magnetic fields in a collector is given in Mihran and Neugebauer's report [4]. It is a common practice to apply an external magnetic field in the collector region to reduce the back streaming of trajectories towards the RF structure of the tube. The leakage magnetic field from the PPM focussing system into the collector also influences its performance. So the simulator should have the ability to define complex electrode geometry of different shapes and to incorporate static electric and magnetic fields in any direction. It should be capable of solving the space charge forces for these geometries using numerical methods like finite difference, finite element etc.

2. *Boundaries*

In multistage collectors the electrodes are separated by the high voltage ceramic insulators. So the simulator should have the capability to define at least two different types of boundaries, e.g. Dirichlet and Neumann. The electric-wall (E_t=0, B_n= 0) or the Dirichlet boundary condition is applied when there is no electric field component parallel to the boundary, which corresponds to a metallic boundary at the edge. The magnetic-wall boundary (E_n=0, B_t= 0) or the Neumann boundary condition is applied when there is no perpendicular component of electric field to the boundary. The subscripts n and t correspond to the normal and tangential components.

3. *Spent beam data*

The simulator should take the arbitrary set of data (such as spent beam data) as input for positional co-ordinates and velocity components as an initial condition for each trajectory. Facilities should be included to modify the starting conditions before the trajectory computations. The number of electrons (particles) should be large enough to represent the electron beam accurately.

4. *Secondary electrons*

The effect of secondary electron emission is to be incorporated in the simulation as it plays a detrimental role in the operation of a collector and its efficiency. A model should be included to compute the secondary electron yield as a function of energy and incident angle of the primary electrons. To include the secondary electron emission in the simulator, it is necessary to find the exact point of impact of the primary with the surface of the collector electrode. The simulator should be able to deal with different currents for the electrons, as each secondary trajectory carries different currents due to different yield. It will be helpful if the simulator includes a library of data for the secondary electron emission properties of different materials, which are commonly used in the fabrication of the multistage collectors.

5. *Dynamic model*

The velocity of an electron is changed due to the change in phase of the RF cycle and the presence of multiple carriers in the input signal. The change in velocity of the electrons in the spent beam should be considered in the design so that the collector performance can be optimised for all conditions. The time scales of these variations should be less than the transit time of electrons in the collectors. The simulator should also be able to compute the effects of stimulated RF fields in the collector.

6. *Different materials are to be modelled*

The simulator should be able to model different materials with their physical characteristics like resistors with conductivity, dielectrics with permittivity, conductors with voltages, permeable materials with permeability. There should not be any limitations in the number of materials.

7. *Unlimited mesh points with mesh refinement capability*

The package should not limit the total number of mesh points required to model the collector; it should be dependent upon the memory only. There should be some options to refine the meshes so that fine details can be modelled in the gap region between the electrodes, and close to the axis. This improves the accuracy of the simulated results.

8. Parameters to be calculated

The main parameters to be calculated are beam current, beam perveance, collector efficiency, time variation of the electrode currents and voltages, back streaming current, back streaming power, recovered and dissipated power at the electrodes and energy.

9. Input interface

(a) Different types of input options are necessary depending upon the available data so that the user has the flexibility to choose any option. Some or all of the following options may be included in the simulator: (i) batch input via name list file (ii) menu driven input with graphics compatibility (iii) interactive interface (iv) input through data file(s).

(b) There should be some options for segmented input of complex electrode shapes. Some simple geometric structures (like cylinder, funnel, flat plate, circular disc etc) should be predefined in a built-in library so that these shapes can be easily used (by Boolean operations, e.g. and, or, not) to make complex geometries. A facility for rotating the predefined shapes in three dimensions could be included to facilitate their representation in all possible orientations for which co-ordinate transformation subroutines are to be added to the program.

(c) There should be some means of defining potentials on different electrodes.

(d) Particle starting conditions are to be defined by their co-ordinates and velocity components.

(e) The input file should be in ASCII format so that any editor can edit it.

(f) The input data should be plotted so that if there is any mistake in the data file it can be modified easily without executing the full program.

(g) The input interface with other programs should be provided (if possible).

10. External magnetic field

As discussed earlier the simulator should have the capability to incorporate the external magnetic field for computational purposes. But it is not a wise idea to incorporate an option in the simulator to model a magnetic circuit as this can

be done using any of the specialised and easily available packages like ANSYS. The focussing system can be modelled externally and the magnetic field data can be mapped onto each mesh point. If the meshing is different in two cases then an interface program can be used in the simulator to find the field at all mesh points through interpolation.

11. Output interface

The output should be in a dumped file, a text file, two-dimensional and three-dimensional graphics files, and a postscript file. A graphics package should be supplied (if there is any), otherwise it should be specifically explained how to plot the graphical output. There should be options to plot the geometry, the primary and secondary trajectories, the potential and field and the energy. The format of the output data files should be documented in the manual so that they can be used for further computation. These files can also be used for other plotting purposes (if required) for better understanding of the performance of the collector.

12. Operating systems

The simulator should work in most popular working environments like DOS, Windows, VAX/VMS or unix based systems in a PC or in a workstation. It should use efficient algorithms so that the computations are fast enough to simulate the collector within a reasonable time.

13. Validation of the package

The package should be validated by comparing the simulated data with the experimental results. In cases where practical results are not available some basic tests can be done to check the accuracy of the computation. Some analytical formula may be used for this purpose. The repeatability and the reliability of the computed results should be tested properly over a wide range of operating conditions.

14. Documentation

The source code should be well commented (it is good programming practice) and a detailed documentation of the package describing its operation and

capability should be supplied. This is necessary for further work or improvement on the package.

The features of an ideal package have been discussed above. It will be an added advantage if the package can be used to design a collector and/or optimise it using an advanced procedure like a genetic algorithm.

2.4.2 Literature Review on Different PIC Codes

The development of a computer package with all these features is a challenging task. A survey of three-dimensional PIC codes was carried out to see the capability and applications of these codes. Detailed information on these codes is available in the form of the published works, catalogues, and from the websites [5], [6]. Salient features, numerical methods of solving any problem, applications, input and output interface, hardware and software requirements, capabilities and drawbacks of these codes have been studied thoroughly. A summary of salient features of these codes is given in Table 2-1. The suitability of these codes is evaluated on the basis of the criteria selected for an ideal code.

A detailed review of the techniques of modelling and simulation of vacuum electronics devices was published by T. M. Antonsen et al [1] where the features and capabilities of some special purpose codes were reported. Some new aspects of the computer codes were dealt with by R. G. Carter [7]. This publication also updated the information about the computer codes in use. A comparison of all these codes (which are mostly available for purchase) on the basis of the criteria for an ideal code is presented in Table 2-2(a)-(e). It is evident from Table 2-2(a)-(e) that none of these codes have all the facilities to design and simulate asymmetric collectors fully. It was therefore necessary to find the most suitable PIC code as a basis, which serves our purpose maximally. It was planned to modify the source code to satisfy our requirements for the three-dimensional modelling and simulation of both symmetric and asymmetric collectors.

Table 2-1: Salient features of some 3-D PIC codes

CODE	APPLICATION	PLATFORM	SOURCE
ARGUS	- time and frequency domain FDM - electrostatic and electromagnetic - gun design - ion and electron sources - RF cavities - plasmas -MMIC circuits and packaging	-CRAY (Unicos and CTSS) -IBM RS/6000(AIX)	SAIC, Burlington, MA, USA
COCA	- depressed collectors	-PC based -Windows 95/98	Catania Univ., Italy
EMX	-2D and 3D time-domain -Relativistic particle-in-cell -Custom geometry definition -Single or multiprocessor -Animated and 3D visualisation	-Sun and HP - PCs - Intel Paragon - IBM SP2.	Culham Electromagn--etics and Lightning, UK
GUN3D	- frequency domain FDM - electromagnetic - gun design - depressed collectors - cathode ray tubes	-IBM 4341 -VAX-11/780 -HP-9000 -Harris-300	Electrocon International Michigan, USA
HERCULES	- inertial confinement fusion (ICF) - ion driven parametric instabilities - electromagnetic - laser and plasma interaction	-CRAY-T3D	Los Alamos National Lab. (LANL) USA
ISIS	-electromagnetic -modelling 3D electrodynamics -intense beam and plasmas -open boundary -body fitted co-ordinate systems	-Not known	Los Alamos National Lab. USA
KARAT	-time domain FE, electromag. -gun design -ion and electron sources, FEL -plasmas, secondary emission	-DOS PC -UNIX -VAX/VMS	VP Tarakanov Moscow Russia

CODE	APPLICATION	PLATFORM	SOURCE
LKOBRA	-ion sources -depressed collectors	-IBM-3090 -IBM-PC	INP, Germany & UoL, UK
MAFIA	-time domain finite integration -electromagnetic -permanent magnet -transient and resonant RF -eddy currents	-Sun Sparc xx, Solaris -HP9000/7xx, HP-UX -IBM RS6000 xxx, AIX -DEC Alpha, DEC-OSF	CST GmbH Darmstadt Germany
MAGIC (SOS)	-time domain FDM -electromagnetic -electron gun -plasmas -magnetic insulation -diodes and switches	-UNIX -UNICOS -VMS -DOS	Mission Research Corp. (MRC) Virginia USA
MHPCC	-inertial confin. fusion (ICF) -electromagnetic -laser and plasma interaction	-CRAY –T3D	UCLA USA
MICHELLE	-electron gun -multistage collector -ion sources	-Not known	SAIC, Burlington MA, USA
PICNS	-electromagnetic -plasmas -charged particle dynamics	-OS Solaris	MRC Albuquerque USA
QUICK- SILVER	-frequency domain FDM -electromagnetic -ion diodes and electron beam -microwave devices	-CRAY (Unicos and CTSS) -UNIX -VAX/VMS	SNL Albuquerque New Mexico USA
WARP3d	- inertial confin. fusion (ICF) -electromagnetic -simulates bent accel. Lattices -electrost. Quadrupole inject.	-CRAY C90	LANL

Table 2-2(a): Comparison of 3-D PIC codes on the basis of an ideal code

Code Name	**Numerical Method**	**Coordinate System**	**Mesh Points**	**Refine Mesh**
ARGUS	FDM (time domain)	Cartesian, cylindrical	No limit	No
COCA	FEM	*	*	*
GUN3D	FDM	Cartesian, cylindrical	127x63x13 for 180 deg. Symm.	No
KARAT	FEM (time domain)	*	*	*
LKOBRA	FDM (static solver)	Cartesian, cylindrical	*	To limt. extent
MAFIA	FIT(freq., time domain)	Cartesian, cylindrical	No limit	Yes
MAGIC (SOS)	FDM (time domain)	Cartesian, cylindrical, spherical	500, 000	Yes
MICHELLE	FEM	Cartesian, cylindrical	No limit	No
QUICKSILVER	FDM (time domain)	Cartesian, cylindrical, spherical	No limit	Yes

Table 2-2(b): Comparison of 3-D PIC codes on the basis of an ideal code

Code Name	**Arbitrary 3D Electrode**	**How Define Potential**	**3D Spent Beam in Electric and Magnetic Field**	**Max. number of Particles**
ARGUS	Yes	On boundary or grids	Yes	Unlimited
COCA	Yes	On boundary	Yes	*
GUN3D	To limt. extent	On boundary	Yes	*
KARAT	Yes	*	Yes	Unlimited
LKOBRA	Yes	On boundary	Yes	Unlimited
MAFIA	Yes	Solver-s	Yes	*
MAGIC (SOS)	Yes	On boundary	Yes	80, 000
MICHELLE	Yes	On boundary or grids	Yes	Unlimited
QUICKSILVER	Yes	Can not be defined	Yes	Unlimited

* Not known

Table 2-2(c): Comparison of 3-D PIC codes on the basis of an ideal code

Code Name	Boundaries	Electrostatic Potential	Language Used
ARGUS	Neumann, Dirichlet, periodic	Yes	FORTRAN
COCA	Neumann, Dirichlet	Yes	C++
GUN3D	Neumann	Yes	FORTRAN
KARAT	*	*	*
LKOBRA	Neumann, Dirichlet	Yes	FORTRAN
MAFIA	Neumann, Dirichlet, periodic	Yes	FORTRAN
MAGIC (SOS)	Perfect conductors, incident and outgoing e-m waves, mirror and periodic symm.	Yes	FORTRAN
MICHELLE	Neumann, Dirichlet, periodic	Yes	C++
QUICKSILVER	Perfect conductors, incident and outgoing e-m waves, mirror and periodic symm.	*	FORTRAN and C

* Not known

Table 2-2(d): Comparison of 3-D PIC codes on the basis of an ideal code

Code Name	Parameters Calculated	Secondary Electrons
ARGUS	Capacitance, inductance, impedance, Q, sws parameters	No
COCA	Beam current, current density distribution, eq. potentials	Yes
GUN3D	Beam current, current density distribution, eq. potentials	No
KARAT	Useful for gun design, FEL gyrotrons, BWO etc.	Yes
LKOBRA	Beam current, current density distribution, eq. potentials	Yes
MAFIA	Eddy current, resonant mode, impedance, wakefield etc.	No
MAGIC (SOS)	Meas. Parameters, surface heating rates, field vs. time	Yes
MICHELLE	Gun and collector parameters	Yes
QUICKSILVER	Electric and magnetic fields, current and charge density, particle position and momentum etc.	No

Table 2-2(e): Comparison of 3-D PIC codes on the basis of an ideal code

Code Name	Input Interface	Output Interface	Source Code Available	Docum-entation
ARGUS	Input via namelist, ASCII file	Output via graphics, dump files, text files	No	Yes
COCA	User interactive	Graphics and text file	No	*
GUN3D	Input via namelist, ASCII file	Graphics and text file	Yes	Yes
KARAT	*	*	*	Yes
LKOBRA	User interactive	Graphics and text file	Yes (partly)	Yes
MAFIA	Menu driven	Graphics and text	No	Yes
MAGIC (SOS)	Input file using MCL	Graphics, text, dump	No	Yes
MICHELLE	Input via namelist, ASCII file	Output via graphics, dump files, text files	No	Yes
QUICKSILVER	Menu driven	Graphics, text, dump	No	Yes

* Not known

None of the codes mentioned in this section could be verified, as they were not available. This is also beyond the scope of this thesis. The information presented here is based on the literature by the developers of the packages and publications in different journals. Some of the codes might have been modified recently to improve their performances and overcome the shortcomings but this is not known to the author. Most of the industries have their own proprietary codes [1] such as DEMEOS (developed by Litton Systems, Inc.), the THERMGUN code (developed at the Hughes Electron Dynamic Division), the HGUN and TGUN code (developed at Communication and Power Industries, CPI – formerly known as Varian), UGUN code (developed at Raytheon Corporation) and COLLECT3D (developed by Thales Electron Devices). The details of these codes are missing here due to their non-availability.

2.4.3 Conclusion

Some of the codes described above are special purpose codes, which are not available for purchase. The details of these codes are not available as they are either proprietary software or classified for security reasons. From the comparisons made it is observed that the source codes of nearly all the packages are not available. Considering all these points, LKOBRA (Lancaster KOBRA) has been found to be the most suitable code. It has already been tested for the three-dimensional modelling and simulation of asymmetric collectors. It consists of a three-dimensional PIC code KOBRA3-INP (PC version) and its pre- and post-processor. But this package has serious limitations, which could not be removed due to the non-availability of the source code of KOBRA3-INP (PC version). Moreover, it was found difficult to change the interface package every time when the KOBRA3-INP package is upgraded by the developers. It was therefore decided to use the mainframe version of KOBRA3-INP as a basic package (the source code of this package is available) and modify it according to our requirements. A new version of LKOBRA has been developed during this project based on the modified mainframe version of KOBRA3-INP. The details of the development of this package are described in Chapter 3.

None of the computer packages mentioned in this section can be used for the preliminary design of the multistage collectors. They are basically simulators, which can be used to test the performance of the collectors before they are fabricated. Prior knowledge and experience is necessary for the optimisation of the collector performance using the simulator. Otherwise a trial and error method may take time and effort, sometimes without much success. Another reason to choose LKOBRA is to develop a computer code that can be included in the package for the design automation. It can also be used for the optimisation of the designs using genetic algorithm. This will enhance the capability of the package by reducing the monotonous manual labour and improving the collector performance. The details of the development of optimisation and automation algorithms can be seen in Chapters 5 and 6.

2.5 LITERATURE REVIEW ON SIMULATION OF MDC

The modelling and simulation of a multistage collector is a challenging task. It is difficult to compute the effect of the electric and the magnetic fields on the electron beam accurately over a region that is several wavelengths long. The number of particles to be modelled is quite large in order to represent accurately the nature of the beam. This makes it more computationally extensive. In the case of high frequency devices the frequency dependent parameters should be considered for computation purposes so that the simulation is more realistic. Finally, the relativistic velocity of the particles should be considered in the simulation [1].

A review on modern multistage collectors was published by H. G. Kosmahl in 1982 [8], which describes different types of multistage depressed collectors and their design technique. This was updated in a later report by L. Kumar et al in 1990 [9]. An attempt has been made to avoid repeating the previous works. A survey on actual computer simulations of multistage depressed collectors by different researchers has been carried out and the findings are presented in this section. Based on the geometry, the collectors are divided broadly into two types, (a) axi-symmetric and (b) asymmetric. Therefore the simulation has been categorised into two groups.

2.5.1 Axi-symmetric Collector

In the 1970s, the symmetric nature of the MDCs was exploited to make the computation easier and faster and to overcome the limitations of the computers. The first reported simulation on MDC was carried out at NASA Lewis Research Center (LeRC), now NASA Glenn Research Center, in 1971 by H. G. Kosmahl [10]. Here, an axi-symmetric electrostatic collector was used in a linear beam microwave tube. Since then, the multistage collectors have mostly been used in TWTs.

In the same year W. Neugebauer at LeRC carried out simulations for two 5-stage and 10-stage electrostatic collectors for klystrons [11]. A PACE analog computer was used for the simulation. The computation of trajectories was done with and without any space charge. In this paper a cylindrical can collector was studied with a retarding

spike protruding from the back wall, which deflected the electrons radially. These electrons were then reflected by the back and sidewalls toward the input plane of the collector. To evaluate the performance, these two collectors were fabricated and different parameters were measured. The computed electron trajectories for a 5-stage collector are shown in Figure 2-5. The electrodes (heavy lines) were located approximately along the equipotential lines (dashed lines), which result when the last electrode is kept at cathode potential and the housing is kept at the beam potential. The measured results are in good agreement with the simulation. A magnetic coil was used between the output coupler and the collector to improve the efficiency of the collector. The effect of secondary electron emission was not computed in the simulation, but it was assumed for the computation of the collector as well as tube efficiency.

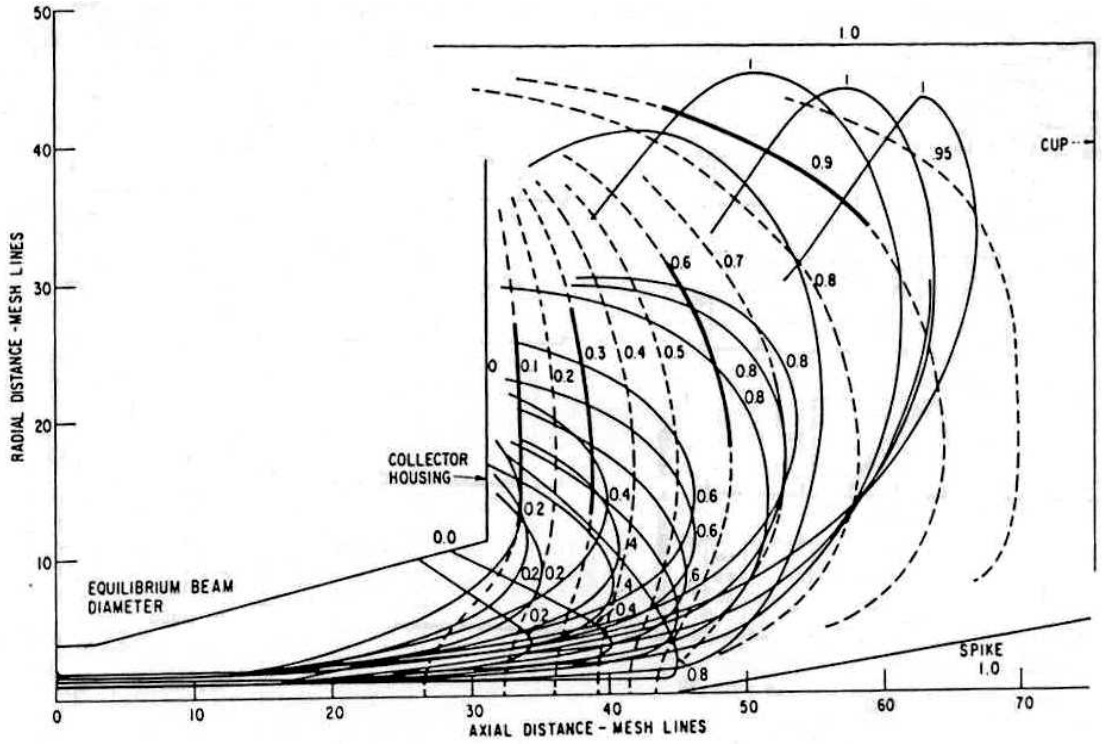

Figure 2-5: Computed trajectories in a 5-stage collector [11]

A collector design technique developed at Teledyne in 1975 was reported by A. C. Schram [12]. Design and simulation of two 2-stage and 3–stage collectors were carried out utilising the simplicity of the magnetically shielded axi-symmetric electrostatic design. Current rays with predetermined velocity distributions and densities were chosen to simulate the beam and were fed into the Stanford Linear

Accelerator Electron Optic Program. The current density was estimated to be three times that of the dc condition to simulate the worst RF bunching conditions. A beam radius of 75% of the inner radius of the helix was estimated and the electron trajectories were computed using fully relativistic equations and accounting for all possible electric and magnetic fields. Since the effects of secondary electrons, beam non-laminarity, RF modulation and beam scalloping could not be modelled through the simulation an experimental program was used to supplement the computer work. Experimental efficiencies were reported to be within 75 to 83% for two different collectors.

Present-day collectors are sometimes equipped with a spent beam refocusing (SBR) section placed between the output coupler and the collector of a linear beam tube to improve the collector efficiency. This section effectively reduces the spent beam turbulence by magnetic refocusing of the beam before injecting it into the collector. It has two purposes, (a) dilution of the space charge and (b) reduction of the radial velocity component of the beam. The beam turbulence is measured by the rms deviation of particle angles where the angles are calculated from the ratio of radial velocity to axial velocity. The detailed analysis of the SBR to achieve the optimum collector efficiency was published by N. Stankiewicz [13]. Efficiency improvement by SBR technique was first proposed by H. G. Kosmahl et al [14]. In this paper the results were published for a coupled-cavity TWT that was fitted with a SBR and a 9-stage collector. The efficiency of the collector and the overall tube were reported to be 81% and 56% respectively. In a separate project, the efficiency improvement of TWTs for use in electronic counter measure (ECM) was carried out by applying MDC and SBR [15]. In this technique three-dimensional trajectories are computed throughout the spent beam refocusing section and finally at the collector. The three-dimensional theory predicts the efficiencies of 2-stage and 4-stage axi-symmetric collectors with SBR section of 81% and 83.5% respectively. Experimental values for these collectors are 81% and 83% respectively which are in close agreement with the values predicted analytically.

An approach to simulate the multistage depressed collector was presented by James A. Dayton, JR. et al [16]. A multidimensional computer program was used to predict and experimentally verify the TWT and depressed collector performance. This was the

first time that the trajectories were computed using a multidimensional program from the RF input to the end of the MDC through the BRS rather than injecting "representative" angles and velocity classes into the MDC. A version of the Stanford Linear Accelerator Center (SLAC) computer program EGUN developed by Herrmannsfeldt [17] was used to compute the electron trajectories both in MDC and BRS. The electron trajectory equations in the program are relativistic and account for the axi-symmetric electric field distribution within the collector including the space charge effects. The secondary electron emission was estimated (secondary electron emission yield δ = ½ for carbon black) with the local electric field determining whether the electrons are suppressed or accelerated. Two collectors, a 3-stage and a 5-stage electrostatic collector, were simulated and the performances were evaluated by the experimental results. The computed efficiency of the 3-stage collector is 81.6%, which is close to the experimental value 81.9%. In case of the 5-stage collector the computed efficiency is 84.9%, which is close to the theoretical value 84.2%.

The computational procedure of the TWT–refocuser-MDC system was experimentally verified and published by James A. Dayton, JR. et al [18]. The simulation was carried out for a dual mode TWT, which is equipped with a SBR and a 5-stage collector. It was operated at high mode in saturation (electronic efficiency of 0.205) and at a lower mode (electronic efficiency 0.023 at $1/10^{th}$ of the pulse repetition rate of the high mode). The refocusing profile was optimised largely for the low mode and produced a well-ordered beam but in the high mode the beam expansion was excessive and almost touched the tunnel. However in the linear region the beam was confined well within the tunnel. The analytical efficiency of the collector at high mode is 81.4%, which is close to the experimental value 84.3%. In the low mode the analytical efficiency is 84.4%, which is also close to the experimental value 85.5%. results match well with the simulated predictions for both modes.

A computational procedure to design a dynamic refocusing system (with simultaneous beam de-bunching and re-conditioning) and a highly efficient 4-stage depressed collector for a 200 W 8-18 GHz TWT was presented by P. Ramins et al [19]. It is an extension of the previous work [16], [18]. But here the electrodes of the collector are made of isotropic graphite material with very low secondary electron emission yield. A change in the TWT program [17] helped in computing the electron beam flow in a

region where the beam diameter changes discontinuously. The secondary electron emission effect was computed semi-quantitatively. A 4-stage collector was fabricated and the voltages were optimised experimentally. The cross section of a 4-stage depressed collector and permanent magnet refocuser is shown in the Figure 2-6. Further studies on the effects of SBR on MDC performance were carried out by P. Ramins et al at NASA [20], [21].

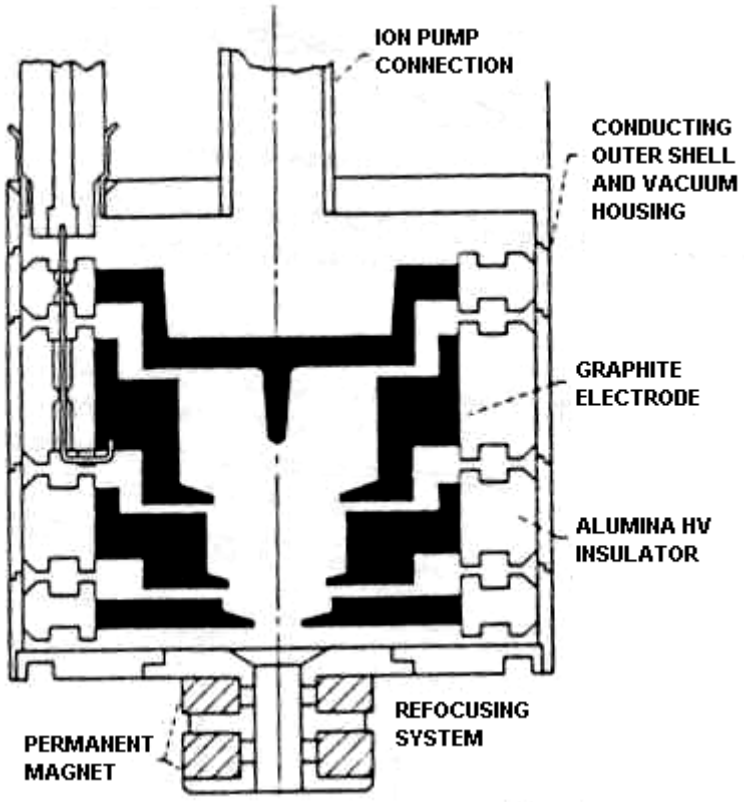

Figure 2-6: Cross section of a 4-stage brazed graphite depressed collector and a permanent magnet refocusing system [19]

Simulation of collectors in dynamic conditions was reported by Y Goren [22]. For this case a 2.5 – dimensional time-domain PIC simulation code was used to design a single stage and a 2-stage axi-symmetric collector. This code was integrated with the Teledyne MEC's gun code, which was developed based on the EGUN code. Several electrostatic features and external magnetic fields were used for the simulation purpose. The analysis was carried out using a finite difference time domain algorithm where an electrostatic field is calculated using the two-dimensional fast Poisson

solver. A self-magnetic field and the external magnetic field were included in the simulation. An attempt was made to design the whole TWT from the gun to the collector by integrating all indigenously developed codes, but the secondary electron emission effect was not considered for the simulation purpose.

M. E. Read et al carried out a feasibility study of the MDCs for gyrotrons at Maryland University and published the simulated results of a 3-stage axi-symmetric collector [23]. The SLAC computer code EGUN was used for the simulation purpose and the design was optimised by adjusting the voltages on the collector electrodes. Simulated results for the cases of 0% and 30% electronic efficiency were reported to be close to the theoretical maximum neglecting the secondary emissions. Particular emphasis was given to collecting most of the electrons at the backside of the electrode (to avoid secondaries streaming back) and to protect the insulators from electron bombardment. Simulated results of a 2-stage collector for gyrotrons were published by A. Singh et al [24]. A computer code PROFILEM was developed for the simulation that includes the back-scattered electrons.

The simulation of multistage collectors for an Inductive Output Tube (IOT) was reported by R. S. Symons [25]. It was assumed that the RF voltage at the output gap equals 90% of the dc voltage and the number of collector stages was reduced to five. The electrodes of the collector were assigned potentials to give constant efficiency. Different beam currents with a consistent energy spread were assumed in a way such that ten different levels could be achieved with a power range from a very low output level to a maximum. These beams were introduced into DEMEOS that solves Poisson's equation and determines the trajectories for a set of electrodes. After a large number of simulations with different sets of electrodes at different output RF power levels the performance of the collector was optimised. Simulated plots of a 5-stage collector were published for both low and high RF output power but no comparison between the theoretical and practical values was given. The simulation does not include the secondary electrons as it is assumed that all secondaries are collected on the same electrode where they are generated.

The three-dimensional time domain version of the MAFIA code was used by K. R. Vaden et al [34] to validate its use as a tool for the simulation of MDC. A 4-stage

collector fitted in a 32 GHz 10 W TWT was simulated. The comparison of electrode currents among the computed results of EGUN and MAFIA and the measured data shows a good agreement. The secondary electron emission was estimated and the current distribution was corrected for its partial effect. The secondary electron current collected at the next lower stage was considered as 40% of the incident current.

A three-dimensional package MICHELLE was used by J. Petillo et al for the simulation of a 4-stage collector for Boeing [37]. The spent beam and the external magnetic fields were generated by two separate programs and used in the simulation. The predicted efficiency is 88% including the effects of secondary electrons, which is close to the theoretical maximum of 91%.

2.5.2 Asymmetric Collectors

An asymmetric multistage collector was first proposed by T. Okoshi [26] as a means of reducing the back streaming of secondary electrons towards the interaction region of the tube by recapturing them. Unlike other conventional collectors it is an electromagnetic collector where the soft landing of electrons was realised. In the proposed scheme, a tilted electric field was applied along with an axial magnetic in the collector region. Therefore it is called a tilted electric field (TEF) collector. The electrodes in this collector are placed at an angle θ with the tube axis as shown in Figure 2-7(a). Design principle, detail theory, preliminary experiment and applications of a TEF collector were published in this paper. The advantage of this collector is that the secondary electrons are always deflected towards the sidewalls and finally recaptured, thus avoiding back streaming. An approximate trajectory is plotted in Figure 2-7(b). The experimental TWT equipped with this collector achieved an efficiency improvement from 19% (basic tube efficiency) to 46%. The performance of a TEF collector was evaluated by L. Kumar et al [42] using computer simulation. Here the electric field is tilted but the magnetic field is transverse to the axial direction, which is slightly different from the proposed Okoshi collector. A fully three-dimensional finite difference simulator LKOBRA (Lancaster KOBRA) was used for simulation. The simulated results of the same collector were published by S. Coco et al [27]. In this case a finite element simulator COCA (COllector CAtania) was used

for the simulation purpose. In both of the above cases only one secondary electron was modelled for each primary. This limitation was removed in recent publications by T. K. Ghosh et al [28]-[31] where six secondaries were modelled per primary to represent the distribution of secondary electron emission more accurately. None of these TEF collector simulations included the actual magnetic field (applied externally) accurately. This is due to the lack of a 3-D magnetic field simulator.

The theory of another asymmetric collector that employs focusing electric field instead of defocusing was proposed by J. R. Hechtel [32]. This is an electrostatic collector and is known as Hechtel's collector. Design methodology, detail theory and advantages of the hyperbolic field collector were published in the paper. A 3-stage collector was fabricated and fitted with a TWT operating in dual mode. The reported experimental efficiencies in low and high power modes are 75.6% and 71.1% respectively. These are close to the theoretical values 79% and 71% respectively. The simulated results of a 3-stage collector were published by L. Kumar et al [42] but this could not be verified due to the lack of experimental results. In a later report the simulated results of the same collector were published by T. K. Ghosh et al [33]. The modified mainframe version of the LKOBRA package was used for simulation instead of the PC version that was used by L. Kumar et al. The simulated trajectories in a 3-stage hyperbolic field collector are shown in Figure 2-8(a). The beam hole is slightly off axis that makes it advantageous over axi-symmetric collectors to suppress the secondaries. Total energy versus path length is plotted in Figure 2-8(b) for all trajectories. The trajectories maintain their total initial energy throughout the path length that checks the correct operation of the program. Details of the simulation can be found in [33].

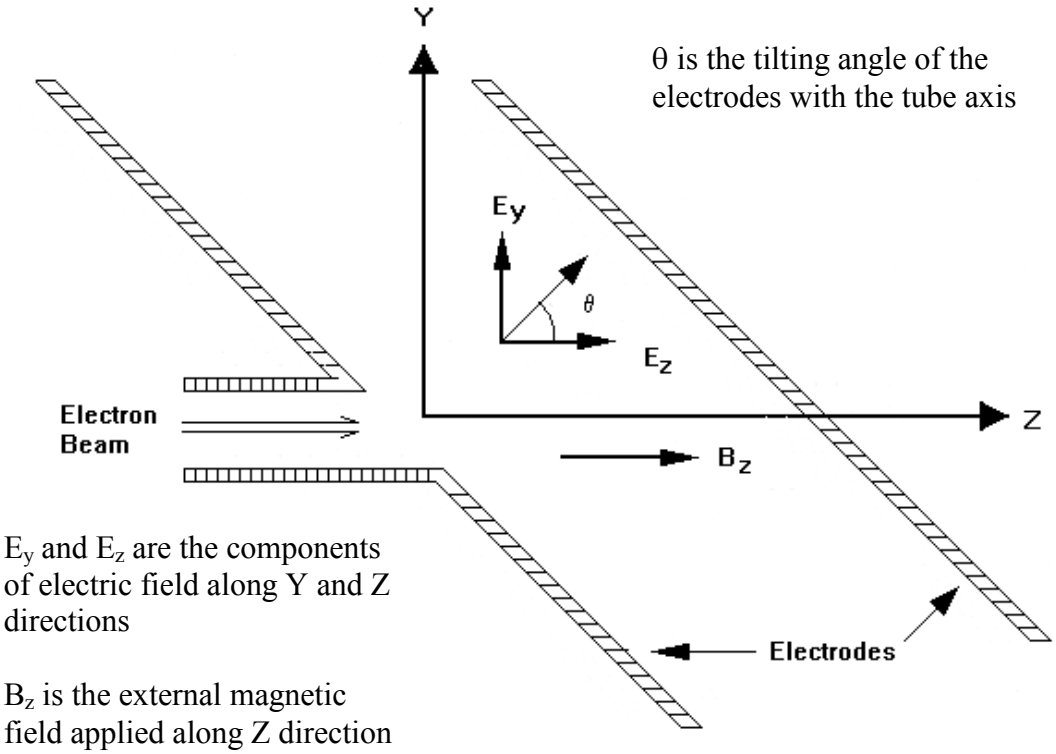

(a)

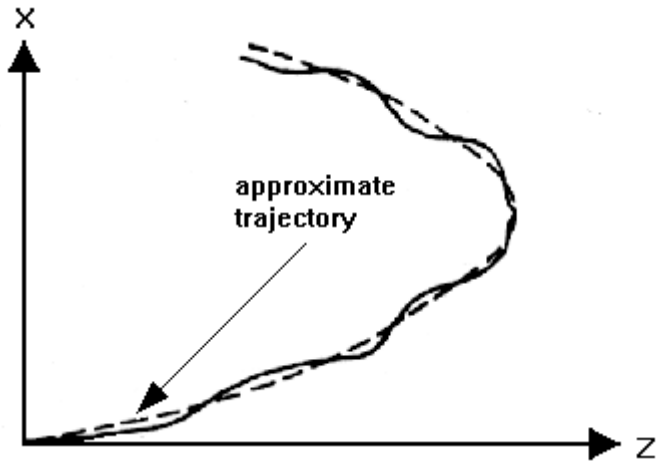

(b)

Figure 2-7: TEF Collector (a) geometry and field (b) electron trajectory [26]

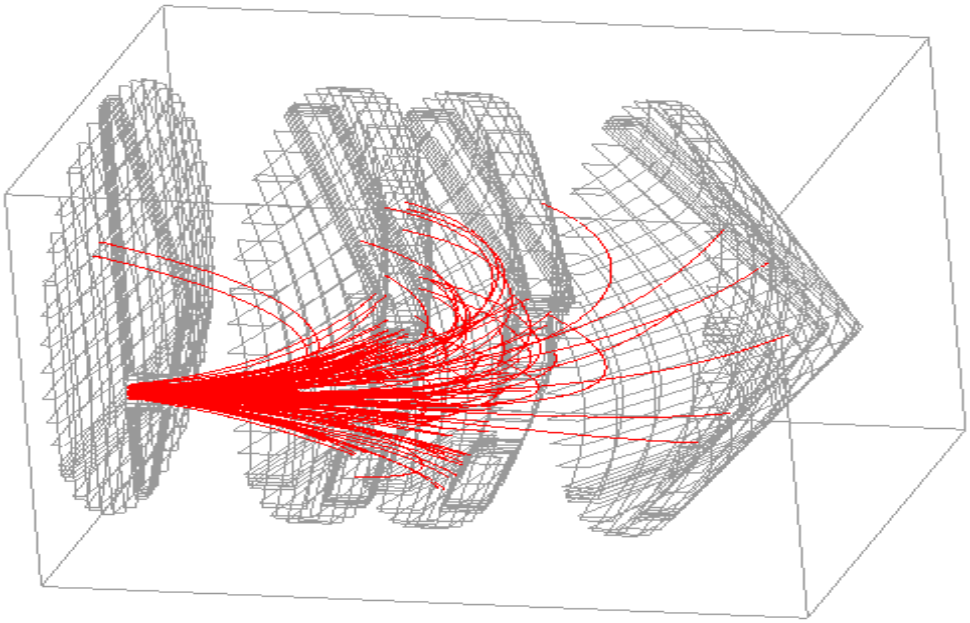

(a)

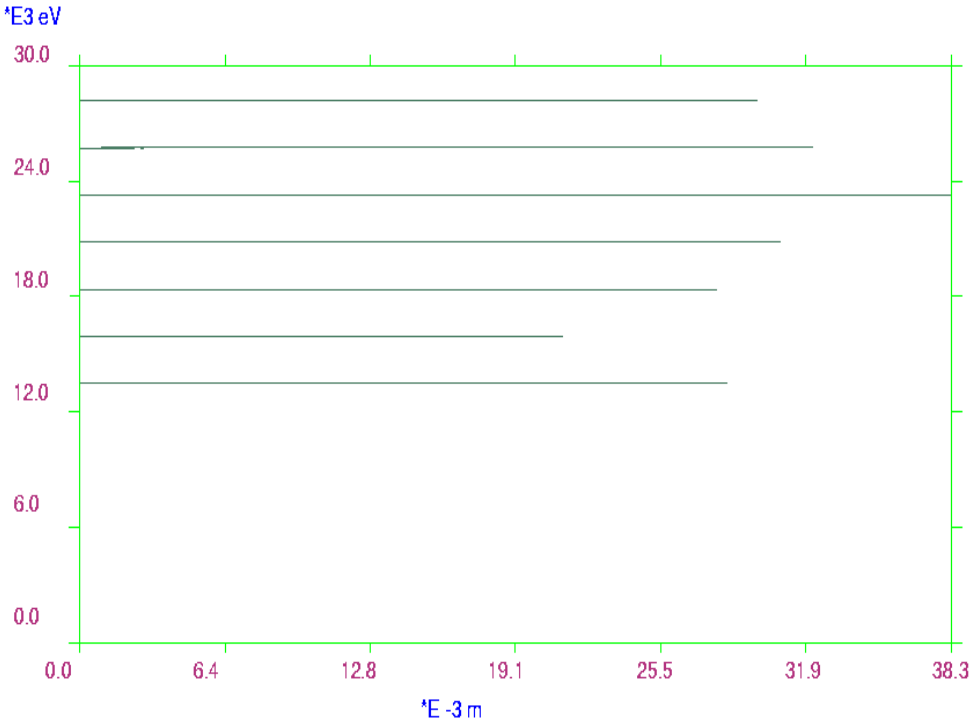

(b)

Figure 2-8: 3-stage hyperbolic electric field collector (a) trajectories (b) total energy versus path length

A summary of the modelling and simulation of collectors by different researchers is shown in Table 2-3 on the basis of the following parameters:

(a) Dimension of analysis (2-D, 2.5-D or 3-D)
(b) Type of analysis (static or dynamic)
(c) Inclusion of secondary electrons

It is not possible to produce a full list of modelling works. Instead, a list of those works is produced when an attempt was made to develop a collector either with some breakthrough achievements or an altogether new package was used for the simulation.

Table 2-3: Review of the literature on simulation of multistage depressed collector

FIRST AUTHOR AND YEAR	TYPE OF ANALYSIS	DIMENSION	SECONDARY ELECTRONS
H G Kosmahl [10], 1971	Static without SBR	2.5-D axi-symmetric	Not included
W Neugebauer [11], 1972	Static without SBR	2.5-D axi-symmetric	Not included
T Okoshi [26], 1972	Static without SBR	Analytic asymmetric	Not included
Y Morishita [35], 1974	Static without SBR	Axi-symmetric	Included
A C Schram [12], 1975	Static without SBR	2.5-D axi-symmetric	Not included
J R Hechtel [32], 1977	Static without SBR	Analytic asymmetric	Not included

SBR = spent beam refocusing

Continued

FIRST AUTHOR AND YEAR	TYPE OF ANALYSIS	DIMENSION	SECONDARY ELECTRONS
H G Kosmahl [15], 1977	Static with SBR	2.5-D axi-symmetric	Not included
J A Dayton JR. [16], 1979	Static with SBR	2.5-D axi-symmetric	Estimated
P Ramins [19], 1986	Static with dynamic SBR	2.5-D axi-symmetric	Semi-quantitative
J. Petillo [3], 1988	Static without SBR	3-D axi-symmetric	Not included
P Ramins [20], 1989	Static with SBR	2.5-D axi-symmetric	Included
Y Goren [22], 1990	Dynamic without SBR	2.5-D axi-symmetric	Not included
L Kumar [2], 1990	Static without SBR	3-D asymmetric	Included
R T Benton [36] 1997	Dynamic	2.5-D axi-symmetric	Included
R S Symons [25], 1999	--------	2.5-D ax-symmetric	Not Included
K R Vaden [34], 1999	Dynamic	3-D axi-symmetric	Estimated
S Coco [27], 2001	Static without SBR	3-D asymmetric	Included
T K Ghosh [31], 2001	Static without SBR	3-D asymmetric	Included

2.5.3 Conclusion

Investigations on different aspects of the symmetric multistage collector have been done either by the scientists in NASA or by scientists in other organisations through collaborative projects with NASA. It was observed that the SLAC computer program EGUN, developed by Herrmannsfeldt [17] was the main computer code used for the simulation of electron guns and multistage collectors. The accuracy in the computed results in individual electrode current and power in some of the cases is seen to be poor [16], [19], although the predicted efficiency matches well with that of the experiment. Some interface packages were developed based on the EGUN code and used for the simulation purpose at Teledyne MEC [22], Maryland University [23] and in other industries as mentioned earlier. Modelling and simulations using fully three-dimensional packages started during the 1980s [3]. Since then several three-dimensional packages e.g., ARGUS, MAGIC, LKOBRA, MICHELLE, COCA and some industry specific proprietary codes, have been developed and used for the simulation of both symmetric and asymmetric collectors. But none of these packages were tested as much as the EGUN code. This may be due to its free availability and reliability. The three-dimensional package MAFIA has been proved to be suitable [34] for the simulation of MDCs, but it does not include the secondary electron emission model. However MAFIA is not much in use for the modelling and simulation of collectors.

It was observed that most of the modelling and design work was done for symmetric collectors. These electrostatic collectors were commonly used without the need for any magnetic field. Due to the simplicity in fabrication and better understanding of the theory, more research has been done on the axi-symmetric collectors. For this reason the theory and the technology of the symmetric collector are well established and adopted in most industries. The concept of asymmetric collectors is relatively new and very little research has been done to improve the collector performance. Moreover, due to the non-availability of proper computer resources it was impossible to simulate collectors in three-dimensions and several assumptions were made to simplify the computation until the 1970s. A review published by W. Neugebauer [11] shows that nearly all the collectors developed before that period were either single stage or 2-

stage. With the invention of high-speed computers it is now possible to simulate the collectors within a reasonable time limit.

Till the 1980s the multistage collector was used only as a major component of either klystron or TWT. Efforts were made during the last decade to use it in gyrotrons once its theory and technology were established [23]. In a recent development the multistage collector was successfully used in an IOT [25]. These are the emerging fields for the possible use of multistage collectors. Material research also played an important role during the last two decades in reducing the secondary electron emission and improving the collector and overall tube efficiency. Several new materials like graphite, carbon etc., were found, and new methods of surface treatment were discovered for this purpose. But the carbon type materials are hard and difficult to machine. It is necessary to do new research to find materials with improved secondary electron suppression properties, which are easy to fabricate. The necessity to develop a new three-dimensional package has been discussed earlier. From a modelling point of view it was observed that different secondary electron emission models were proposed but they lacked the basic experimental data, so they are not very reliable. Accurate models need to be developed that can be used to predict the secondary electron emission effects more accurately. Most of the simulations did not include any external magnetic field. Therefore more research has to be done to find the effects of magnetic field on the electron trajectories inside the collector. Another area of research is the optimisation of collector performance. Very little work has been done in this area [40], [41]. New techniques and algorithms are necessary for this purpose as it is a complex problem.

REFERENCES

[1] T. M. Antonsen et al., "Advances in Modeling and Simulation of Vacuum Electronic Devices," *Proceedings of the IEEE*, vol. 87, no. 5, pp. 804-839, May 1999.

[2] L. Kumar, R. G. Carter and D. Perring, "Three-Dimensional Modeling of Asymmetric Depressed Collectors," in *Proc. ESA Workshop on Space TWTA's 1991*, ESTEC, Noordwijk, 15-16 May, 1991, ESA WPP-22, pp. 6.3.1-18.

[3] J. Petillo, A. Mankofsky, C. L. Chang, A. Drobot and A. Adler, "3-D particle-in-cell simulations for multi-stage depressed collector design," in *Proc. 1988 Microwave Power Tube Conf.*, Monterey, CA, 1988, Paper 2C-5.

[4] T. G. Mihran and W. Neugebauer, Analytical study of depressed collector for linear beam microwave amplifiers, Final Report, NASA Lewis Research Centre, Cleveland, Contract No. NAS3-11530, July 1970.

[5] Computer Codes for Particle Accelerator Design and Analysis: A Compendium, Los Alamos National Laboratory, Second Edition, May 1990.

[6] R. G. Carter and Ian Ashworth, Microwave Tube CAD, Final report, Report MRG/92/7, Lancaster University, September 1992.

[7] R. G. Carter, "Computer Modelling of Microwave Tubes – A Review," in *Proc. IVEC 2001*, April 2-4, 2001, pp. 393-396.

[8] H. G. Kosmahl, "Modern Multistage Depressed Collectors – A Review," *IEEE Trans. on Electron Devices*, vol. ED-70, No. 11, pp. 1325-1334, Nov. 1982.

[9] L. Kumar and R. G. Carter, Microwave Tube Design: 3-D Depressed Collector, ESA Contract Report, Report No. MRG/90/1, Lancaster University, 1990.

[10] H. G. Kosmahl, A Novel Axi-symmetric Electrostatic Collector For Linear Beam Microwave Tubes, NASA Tech. Note TN D-6093, 1971.

[11] W. Neugebauer and T. Mihran, "A ten stage depressed collector for Improving Klystron Efficiency," *IEEE Trans. on Electron Devices*, vol. ED-19, No. 1, pp. 111-121, Jan. 1972.

[12] A. C. Schram, "TWT Efficiency Improvement Using Multi-Stage Collectors," *Microwave Journal*, pp. 31-33, August, 1975.

[13] N. Stankiewicz, "Analysis of Spent Beam Refocusing to Achieve Optimum Collector Efficiency," *IEEE Trans. on Electron Devices*, Vol., ED-24, No. 1, pp. 32-36, January 1977.

[14] H. G. Kosmahl, O. Sauseng, and B. D. McNary, "A 240-W 12-GHz Space Communication TWT with 56 Percent Overall and 81 percent Collector Efficiency," *IEEE Trans. on Electron Devices*, ED-20, page 1169, 1973.

[15] H. G. Kosmahl and P. Ramins, “Small-Size 81- to 83.5-Percent Efficient 2- and 4-Stage Depressed Collectors for Octave-Bandwidth high-performance TWT’s,” *IEEE Trans. on Electron Devices*, vol. ED-24, No. 1, pp. 36-44, January 1977.

[16] J. A. Dayton, JR., H. G. Kosmahl, P. Ramins and N. Stankiewicz, “Analytical Prediction and Experimental Verification of TWT and Depressed Collector Performance Using Multidimensional Computer Programs,” *IEEE Trans. on Electron Devices*, vol. ED-26, No. 10, pp. 1589-1597, 1979.

[17] W. B. Herrmannsfeldt, Electron Trajectory Program, SLAC-166, Stanford Linear Accelerator Center, September 1973.

[18] J. A. Dayton, JR., H. G. Kosmahl, P. Ramins and N. Stankiewicz, “Experimental verification of a computational procedure for the design of TWT-refocuser-MDC systems,” *IEEE Trans. on Electron Devices*, vol. ED-28, No. 10, pp. 1480-1489, 1981.

[19] P. Ramins, H. G. Kosmahl, D. A. Force, R. W. Palmer and J. A. Dayton, JR., “Verification of an Improved Computational Design Procedure for TWT-Dynamic Refocuser-MDC Systems with Secondary Electron Emission Losses,” *IEEE Trans. on Electron Devices*, vol. ED-33, No. 1, pp. 85-90, January 1986.

[20] P. Ramins and B. T. Ebihara, “Isotropic Graphite Multistage Depressed Collectors- A Progress Report,” *IEEE Trans. on Electron Devices*, vol. ED-36, No. 4, pp. 817-824, 1989.

[21] P. Ramins, S. Peet and D. A. Force, “A Re-examination of Spent Beam Refocusing for High Efficiency Helix TWT’s and Small MDC’s,” *IEEE Trans. on Electron Devices*, vol. 35, No. 4, pp. 539-547, 1988.

[22] Y. Goren, R. Wilson, P. Lally, “2.5-Dimensional Time Domain Particle-In-Cell Simulation Code for Collector Design,” in *IEDM (Technical Digest)*, pp. 877-880, IEEE 1990.

[23] M. E. Read, W. G. Lawson, A. J. Dudas, A. Singh, “Depressed Collectors for High-Power Gyrotrons,” *IEEE Trans. on Electron Devices*, vol. 37, no. 6, pp. 1579-1589, June 1990.

[24] A. Singh, S. Rajapatirana, V. L. Granatstein, R. L. Ives, A. J. Antolak, "Design of a Multistage Depressed Collector System for 1-MW CW Gyrotrons-Part I: Trajectory Control of Primary and Secondary Electrons in a Two-stage Depressed Collector," *IEEE Trans. on Plasma Science*, vol. 27, no. 2, pp. 490-502, April 1999.

[25] R. S. Symons. (1999, June) The Constant Efficiency Amplifier. Presented at Accelerator Driven Transmutation Technologies and Applications, Czech Republic [Online]. Available: www.fjfi.cvut.cz/con_adtt99/

[26] T. Okoshi, E. Chiu and S. Matsuki, "The Tilted Electric Field Soft-Landing Collector and Its Application to a Travelling-Wave Tube," *IEEE Trans. on Electron Devices*, vol. ED-19, No. 1, pp. 104-110, 1972.

[27] S. Coco, F. Emma, A. Laudani, S. Pulvirenti and M. Sergi, "COCA: A Novel 3-D FE Simulator for the Design of TWTs Multistage Collectors," *IEEE Trans. on Electron Devices*, vol. 48, no. 1, pp. 24-31, January 2001.

[28] T. K. Ghosh and R. G. Carter. (2001, July). Multistage Depressed Collectors for helix TWTs. Presented at The Northern Vacuum Electronics Conference, UK [Online].
Available: www.comp.lancs.ac.uk/engineering/research/microwave/conference/tushar.pdf

[29] T. K. Ghosh and R. G. Carter. (2000, April). 3-D Simulation of Multistage Depressed Collectors for High Efficiency Space TWT. Presented at The Northern Vacuum Electronics Conference, UK [Online].
Available: epicentre.tay.ac.uk/NVEC2000/tghosh.pdf

[30] T. K. Ghosh and R. G. Carter, "3-D Simulation of Asymmetric Multistage Depressed Collectors with Secondary Electron Emission Effects for High Efficiency Space TWTs," in *Proc. ITG Conference on Displays and Vacuum Electronics*, May 2-3, 2001, pp. 67-71.

[31] T. K. Ghosh and R. G. Carter, "Improved Three Dimensional Simulation of Multistage Depressed Collectors for High Efficiency Travelling Wave Tubes," in *Proc. of 2nd IEEE International Vacuum Electronics Conference 2001*, April 2-4, 2001, pp. 215-220.

[32] J. R. Hechtel, "A Novel Electrostatic-Focusing Depressed Collector for Linear Beam Tubes," *IEEE Trans. on Electron Devices*, vol. ED-24, No. 1, pp. 45-52, January 1977.

[33] T. K. Ghosh and R. G. Carter, 3-D Simulation of Multistage Depressed Collectors for High Efficiency Space TWT" (Progress Report 1), Engineering Department, Lancaster University, MRG/2000/2, March 2000.

[34] K. R. Vaden, V. O. Heinen and J. A. Dayton, Jr., "Three-Dimensional Modelling of Multistage Depressed Collectors," *IEEE Trans. on Electron Devices*, vol. 46, No. 8, pp. 1810-1811, August 1999.

[35] Y. Morishita and S. Murata, "Ion-Trapping Effects in Depressed Collectors," *Electronics and Communications in Japan*, vol. 57-B, No. 2, pp. 99-105, 1974.

[36] R. T. Benton et al., "Efficiency Improvements in KU-Band Space Helix travelling Wave Tubes," Presented in the ESA/NATO Workshop on Microwave Tubes for Space, Military and Commercial Applications, ESTEC, April 7-10, 1997.

[37] J. Petillo et al, "The New 3D Electron Gun And Collector Modelling Tool: MICHELLE," in *Proc. of 2nd IEEE International Vacuum Electronics Conference 2001*, April 2-4, 2001, pp. 199-205.

[38] A. V. Haeff and L. S. Nergaard, "A Wide Band Inductive Output Amplifier," *Proc. of IRE*, vol. 20, pp. 126-130, March 1940.

[39] F. Sterzer, "Improvement of Travelling-Wave Tube Efficiency Through Collector Potential Depression," *IRE Trans. on Electron Devices*, pp. 300-305, October 1958.

[40] T. K. Ghosh and R. G. Carter, "Design Optimisation of Multistage Depressed Collectors for High Efficiency Travelling Wave Tubes Using Genetic Algorithm," in *Proc. of 3rd IEEE International Vacuum Electronics Conference 2002*, April 23-25, 2002, pp. 158-159.

[41] K. R. Vaden, J. D. Wilson, and B. A. Bulson, "A Simulated Annealing Algorithm for the Optimization of Multistage Depressed Collector Efficiency," in *Proc. of 3rd IEEE International Vacuum Electronics Conference 2002*, April 23-25, 2002, pp. 164-165.

[42] L. Kumar, P. Spadtke, R. G. Carter and D. Perring, "Three-Dimensional Simulation of Multistage Depressed Collectors on Micro-computers," *IEEE Trans. on Electron Devices*, vol. 42, No. 9, pp. 1663-1673, September 1995.

Chapter 3

Development of a 3-D Simulator

3.1 INTRODUCTION

To evaluate the performance of any multistage collector and optimise its design it is necessary to have a 3-D software package that can be used to simulate both symmetric and asymmetric collectors. It should be capable of tracing electron trajectories under the influence of electric and magnetic fields. Both secondary and reflected primary electrons have significant roles in the performance of the collector. So the simulator should include the effects of secondaries and reflected primaries. Different parameters of the collector (efficiency, current and power recovered by each electrode and back streaming current) should be calculated using an interface to analyse its performance. It is also intended to optimise the MDC performance through automation. All these tasks can be performed using a fully 3-D simulator along with easy-to-use interfaces.

Keeping these in mind a 3-D simulator, Lancaster KOBRA (mainframe version), has been developed based on the criteria chosen in the previous chapter. From this time onwards we will call it LKOBRA (MF). This package is based on the mainframe version of KOBRA3, which was originally developed for the simulation of ion sources. The LKOBRA (MF) includes the mainframe version of KOBRA3 and its pre- and post-processor.

Another version of LKOBRA, which includes the PC version of KOBRA3-INP and its pre- and post-processor, was developed earlier in 1993 at Lancaster University [1]. This version of the package (v1.13) has some drawbacks. Some of them have been removed in the higher versions but at the same time some have been introduced.

To overcome these limitations it is necessary to modify the PC version of KOBRA3-INP. But due to the non-availability of the source code it was planned to develop the mainframe version of the package. For that purpose the mainframe version of KOBRA3 has been taken as the basis and modified according to our requirements. The major limitations of this package have been removed. The pre-processor of the PC version has been modified and some new features have been included in it. The post-processor has been developed afresh. These pre- and post-processors along with the modified mainframe version of KOBRA3 constitute the LKOBRA (MF). The status of the availability of the source codes of LKOBRA at the beginning of this project is shown in the Table 3-1.

Table 3-1: Status of the availability of the source code of LKOBRA before the start of the project

Code	Components	Source Available
LKOBRA (PC Version)	KOBRA3-INP (PC version)	No
	Pre-processor	Yes
	Post-processor	Yes
LKOBRA (mainframe Version)	KOBRA3-INP (mainframe)	Yes
	Pre-processor	No
	Post-processor	No

3.2 LIMITATIONS OF LKOBRA (PC VERSION)

There are several drawbacks in both the PC version of KOBRA3-INP and the pre- and post-processors of the LKOBRA package. Some of them are listed in [1], [2], [3] and

rest were found during testing of the package. These are discussed in detail in the following sections.

3.2.1 Limitations of KOBRA3-INP (PC Version)

The PC version of KOBRA3-INP was modified by the scientists of INP, Germany, with feedback from Lancaster University, to make it suitable for the 3-D simulation of MDCs. But not all of the limitations of the package were removed during that period. As a result of this the following limitations are still there in the package:

- All trajectories in the input data file are assigned equal current, as the simulator cannot deal with different currents for different trajectories. The geometry generator of the simulator reads the total current and the total number of trajectories from the input file. The total current is then divided equally among the trajectories. This results in an error in the case of computing the primary trajectories. The secondary electron current depends on the primary energy, the incident angle and the surface conditions. In the case of secondary trajectories the current is different for different trajectories even though it is assumed that the primary trajectories carry equal currents. So the calculations of the effects of secondaries are not quite accurate if an equal current is assigned to all trajectories. The space charge of the secondaries cannot be considered.
- Trajectories enter deep inside the electrodes. Due to this, it is often difficult to find out the exact point of impact of the primary on the electrode surface. The point of impact is used as the emerging point of the secondaries.
- Only a constant magnetic field can be applied in all three co-ordinate directions.
- It works only in DOS. The extended-DOS version and the WINDOWS version of the package exist but these were not available.
- The DOS version 1.13 is very slow but the upgraded version 2.16 is fast though mostly all other limitations of the lower version are still there in the higher version of the package.

- Mesh size is limited to 16, 000 only (40 x 20 x 20) and it is not possible to compute the parameters with better accuracy. Complex and large geometries cannot be simulated with reasonable accuracies.
- Only the executable version of the package is available which makes it difficult to make any alterations in the package that are necessary for our purpose.

3.2.2 Limitations of LKOBRA Pre- and Post-processor (PC Version)

The pre- and post-processors of the LKOBRA package were written at Lancaster University for KOBRA3-INP PC version (v1.13). This package is not totally compatible with the higher versions. At the same time it has some limitations, which are removed from the mainframe version. The limitations in the pre-processor are listed below:

- There is no option to modify or recover the input data if any error occurs during the interactive input.
- The trajectory data, generated through the large signal model (LSM), cannot be converted into a format suitable for KOBRA3.
- An option to input through other means (e.g., a data file) is necessary in the pre-processor for design automation and repetitive operations.

The post-processor has been replaced totally due to its limitations, which are listed below:

- The analysis part of the post-processor computes the current and the power recovered at each electrode by assigning the trajectories to different electrodes according to their potential energy. If the potential energy of any trajectory is equal to, or within the tolerance limit, of the potential of the electrode then the trajectory is assigned to that electrode. The disadvantage of this method is that sometimes all trajectories cannot be considered, as some of them do not come under any of the tolerance limits of the electrodes. If the limit is increased to consider all trajectories, then some of them may be considered twice or some of

them may be wrongly assigned to another electrode due to the overlapping potential energy region of the nearest electrodes. This results in error in the analysis of some of the collectors where the potentials of adjacent electrodes are very close.

- The analysis part of the post-processor also does not include the effects of secondary electron emission.
- The secondary electron emission model of the post-processor is based on the experimental results of Jonker [4] and Vaughan's empirical formula [5]. In this model only one secondary electron is considered per primary, which cannot represent the secondary electron emission energy distribution. As the main simulator cannot handle different currents for different trajectories the secondary electron emission model does not calculate separately the current for different secondary trajectories. Instead of that, the current is assumed to be the same for all trajectories, which is not accurate.

3.3 PRE-PROCESSOR AND POST-PROCESSOR OF LKOBRA (MF)

The pre- and post-processor of the 3-D collector simulation package LKOBRA (MF) has been developed and tested to satisfy the requirements of a MDC simulator. Some new features have been added in the pre-processor as necessary. The newly developed post-processor includes a fully 3-D secondary electron emission model that generates the starting conditions of the trajectories and an analysis program that analyses the performance of a collector including the effects of secondary electrons.

3.3.1 Pre-processor of LKOBRA (MF)

The purpose of the pre-processor is to generate the input data file in a format suitable to run the modified mainframe version of KOBRA3. Basic electrode shapes defined in the pre-processor (cone, funnel, cylinder, rectangular plate and circular disc) can be used to

generate the data for electrode geometry. A complex geometry can be formed by combining these basic shapes. The electrodes can be assigned different potentials. The trajectory starting data can be generated through the 3-D beam model when the starting conditions of the trajectories are not available. However the 3-D trajectory data can be used directly if the experimental data is available.

The pre-processor has been modified to make it user-friendly. Some new features have been added to serve our purpose. These are described below:

- *User-Friendly Interactive Interface*

  The interactive interface of the pre-processor is used to create the input data file (geometry and trajectory data) for the main simulator. It is a lengthy process to generate the input data file using the interactive interface, especially for complex geometries where the number of electrodes is large. There is no option to modify the data if there is any mistake during the input. The whole process has to be repeated again from the beginning, which is time-consuming and laborious. To overcome this drawback the pre-processor has been modified to make it user-friendly. A new provision has been added to modify the interactive data (if required) after the input is complete. For that purpose the main program has been split into several subroutines instead of a single program. This interface program has been commented properly. Detail can be seen in [6].

- *Interface through input file*

  A new option to create the input file through a data file has been created. The interactive input interface is useful for one-time operation and not suitable for repetitive operations. It is used only when the design is complete and no further modification is required in the collector geometry to improve its performance. Interface through the input file is useful when a large number of modifications are required for fine-tuning the performance of the collector at the design stage. For a

little modification in the geometry the first method requires the whole process to be run whereas the second method needs only small changes in the data file. This reduces the time needed to create the input file for the modified geometry and avoids the monotonous work involved. Detail can be seen in [7].

Another advantage of the second method is that, as the data file for the collector geometry can be stored instead of the input file, a lot of storage space is saved. The size of the data file is a few hundred bytes whereas the size of the input file is a few hundreds of kilobytes. It takes only few seconds to generate the input file from the data file. The shape and size of the individual electrodes can be easily understood in the data file, which is not possible in the input file.

This new option is especially useful for design optimisation through automation, which requires several alterations in the collector geometry data until an optimised efficiency is achieved. Detail of the geometry optimisation techniques is described in Chapter 6.

- *Interface between the large signal model (LSM) and LKOBRA (MF)*

The 2.5-D trajectory data generated by the large signal model (LSM) cannot be used directly in KOBRA3. An interface program has been developed to convert the data from 2.5-D cylindrical co-ordinates to a 3-D Cartesian co-ordinate format suitable for the main simulator. The LSM data consists of 96 sets (this number varies) of data Z, R, θ, (positional co-ordinates) ZDOT, RDOT and θDOT (velocity components in these three directions) for 96 different trajectories with no θ variation in the position. To convert this data into 3-D it is necessary to introduce sample electrons at different θ angles. If eight sample electrons are created having equal angular spacing (to keep symmetry) at the same radial position of an electron then the total number of trajectories becomes 96 x 8 = 768. It takes a long time to run the trajectory program for such a large number of trajectories and it requires a huge disk space to store this data. The situation becomes worse when secondaries are considered in the simulation

(six trajectories are generated per primary in the secondary electron emission model). To avoid it similar trajectories are grouped together to take an average so that the 96 trajectories can be reduced to 24. For that purpose the electrons are sorted first according to their ZDOT value in ascending order. The ZDOT, RDOT and θDOT values of the first unmarked electron are considered as the base values. These parameters of all remaining unmarked electrons are compared with the base values to form a group. If the ZDOT, RDOT and θDOT values of other electrons fall within specified limits around the base values then these electrons are grouped together and marked as considered. The same process is repeated for the next unmarked electron onwards until all electrons have been marked and grouped. All electrons in a particular group are counted and the parameters mentioned above are averaged separately. Eight sample electrons with different θ values (for each trajectory generated) are generated at an equal angular spacing keeping other parameters the same. Details of this interface can be seen in [7].

The total number of trajectories thus generated is 24 x 8 = 192. A detailed flow diagram of the logic is shown in Figure 3-1. Based on this algorithm two separate programs have been developed for converting the modulated beam data, and the dc beam data.

It is necessary to maintain the nature of the spent beam by keeping its energy nearly the same after the grouping of similar trajectories is done. To check this, a set of two spent beam energy distribution curves is plotted in Figure 3-2. The thin and thick curves represent the spent beam energy distribution before and after the grouping respectively. It is observed from the plot that the nature of the spent beam and total energy remains nearly the same. This implies that the algorithm to reduce the number of particles in the spent beam data can be used efficiently without changing the nature of the spent beam.

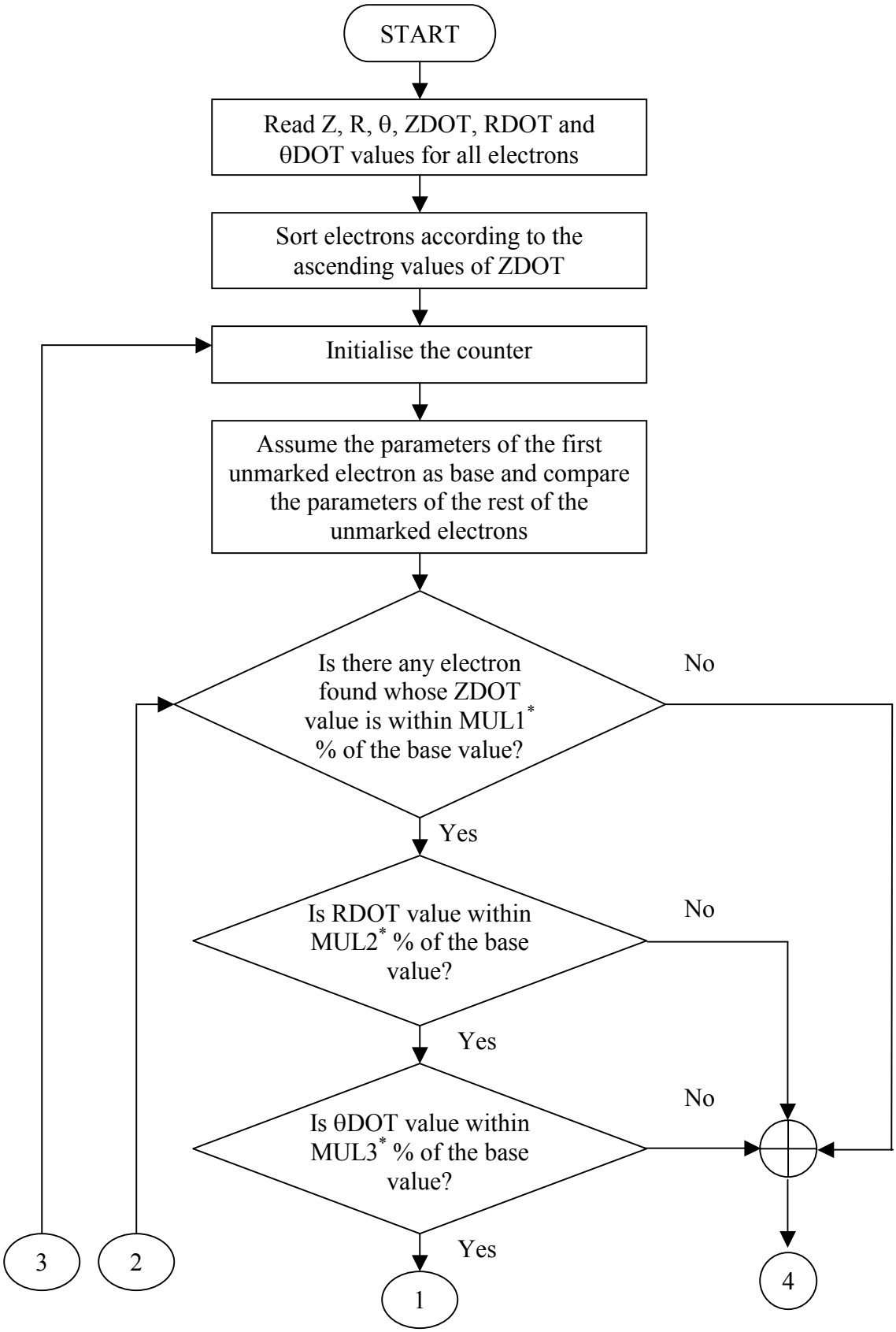
START
Read Z, R, θ, ZDOT, RDOT and θDOT values for all electrons
Sort electrons according to the ascending values of ZDOT
Initialise the counter
Assume the parameters of the first unmarked electron as base and compare the parameters of the rest of the unmarked electrons
Is there any electron found whose ZDOT value is within MUL1* % of the base value?
No
Yes
Is RDOT value within MUL2* % of the base value?
No
Yes
Is θDOT value within MUL3* % of the base value?
No
Yes
3
2
1
4

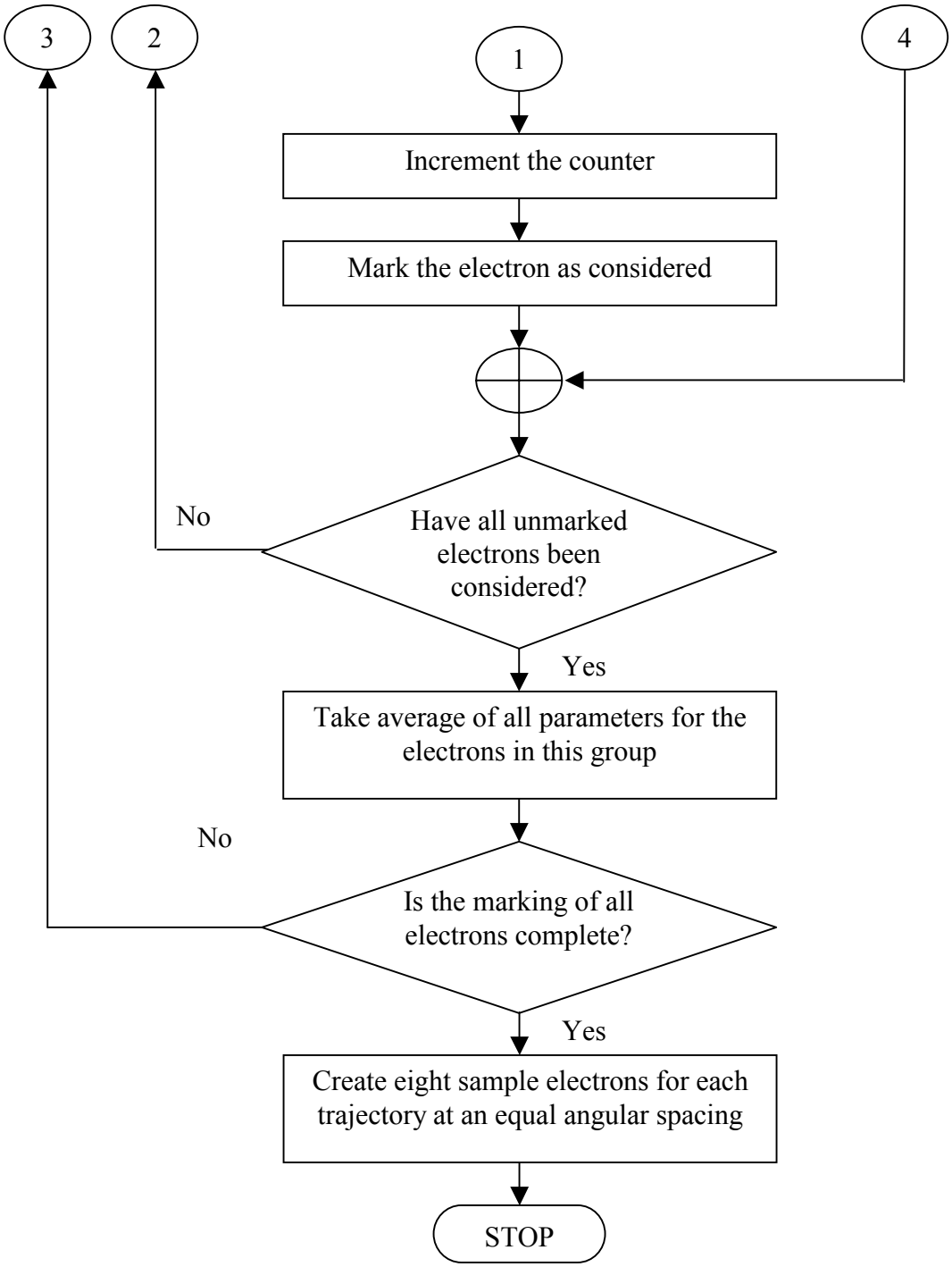

* MUL1, MUL2 and MUL3 are specified by the user

Figure 3-1: Basic flow diagram of the LSM to LKOBRA converter

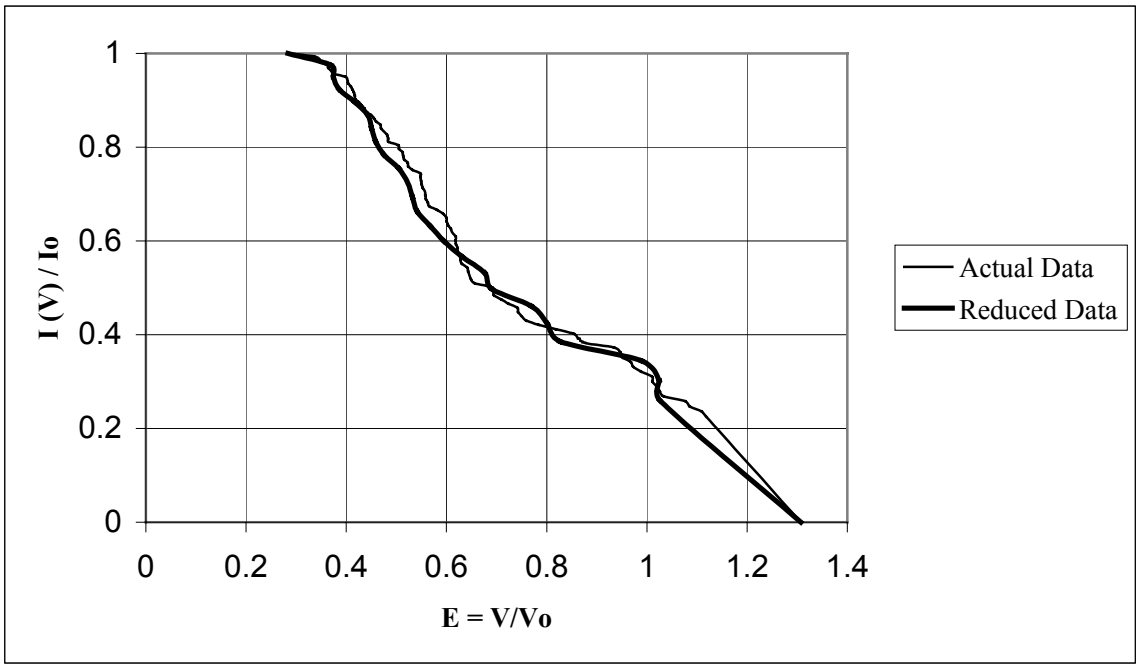

Figure 3-2: Spent beam energy distribution before and after grouping

3.3.2 Post-processor of LKOBRA (MF)

The post-processor performs two operations; it generates the starting conditions of the secondary electrons and analyses the performance of the collector. It has been discussed in the previous section that the PC version of the post-processor suffers from various limitations. A totally new post-processor has been written to replace the old one.

- *Secondary electron effects*

  A model has been developed to incorporate the effects of the secondary electron emission (SEE) based on the experimental results of Jonker [4] and the SEE formula derived by Vaughan [5]. Secondary electrons have been classified broadly into two groups, slow secondaries and fast secondaries. Out of these two categories the slow

secondaries are composed of true secondaries and in-elastically reflected primaries. True secondaries are generated by the bombardment of primary electrons on the collector electrode surface. Fast secondaries are elastically reflected primaries. The starting positions of the secondary electrons are determined by finding the exact point of impact between the primary electrons and the collector surface. Angles of emergence of the secondaries depend upon the angle of incidence of the primary electron. The velocity components of the secondaries in three coordinate directions are determined from the initial energy of the secondary electrons and the angles of their emergence. The secondary electron current is calculated from the SEE yield and the primary current where the value of SEE yield is obtained using the Vaughan's formula. The electrode material and its surface smoothness factor have been considered for the accuracy of the calculation of the SEE yield. In the present model five slow secondaries and one fast secondary are assumed to be emerging for each primary electron. The total slow secondary electron energy is considered to be 50 eV per primary electron. Multiple generations of the secondary electrons can also be considered in this model. The details of the SEE model are described in Chapter 4 of this thesis.

- *Analysis of collector performance*

The analysis part of the post-processor analyses the performance of the collector by computing parameters such as the electrode current at each electrode, the power recovered and dissipated by each electrode, the back streaming current and the collector efficiency. It is capable of computing these parameters with or without the secondary electrons, which is helpful for studying the effects of secondary electron emission.

For any trajectory the position, total energy and the velocity components at all points are stored in a data file by the main simulator. Each trajectory is assigned a specific electrode by finding out the position of its last point (i.e., the point of impact with the electrode). The total input power to the collector is calculated by summing up the

energy at the starting point of the trajectories and the power dissipated at each electrode is calculated from the energy at the end point. The total power entering a collector P_{ent} is defined as

$$P_{ent} = \sum_{k=1}^{N} I_k V_k \tag{3-1}$$

where V_k is the voltage corresponding to the initial kinetic energy

I_k is the current of the k-th trajectory

N is the total number of primary trajectories.

The power recovered by the i-th stage of the collector P_i is defined as

$$P_i = V_i \left(\sum_{l=1}^{S_i} I_l + \sum_{m=1}^{Q_i} I_m - \sum_{n=1}^{R_i} I_n \right) \tag{3-2}$$

where V_i is the potential of the i-th stage with respect to ground

I_l is the current of l-th primary trajectory reaching the i-th electrode

S_i is the number of primary trajectories reaching the i-th stage

I_m is the current of the m-th secondary trajectory reaching the i-th electrode

Q_i is the number of secondary trajectories reaching the i-th electrode

I_n is the current of the n-th secondary trajectory leaving the i-th electrode

R_i is the number of secondary trajectories leaving the i-th electrode

The total power recovered (P_{rec}) is calculated by summing up the power recovered by each stage. Now the collector efficiency η_{coll} can be written as

$$\eta_{coll} = (P_{rec}/P_{ent}) \times 100\ \% \tag{3-3}$$

The back streaming power and the power dissipated at each electrode are calculated to determine the total power loss in the collector. An energy balance is achieved if the sum of the power recovered and the power loss is equal to the total power entering the collector. The details of this post-processor can be seen in [7].

3.4 DEVELOPMENT OF KOBRA3 (MAINFRAME VERSION)

The mainframe version of KOBRA3 simulator consists mainly of the mesh generator, the Poisson solver, the trajectory solver and the 2-D and 3-D graphics programs. Details of the development of the 3-D simulator and its pre- and post-processors have been published in [6], [7] and [8]. The main features and improvements of the mainframe version of KOBRA3 simulator are described below.

3.4.1 The Mesh Generator

The mesh generator reads the data as generated by the pre-processor and discretises the three-dimensional problem box containing the collector geometry. Any geometry can be simulated using arbitrary electrode shapes or through combinations of simple electrode shapes (circular, rectangular etc.). Local mesh refinement is possible in all three directions by defining the mesh interval for better accuracy in the simulation. Boundary conditions for the electric field can be applied at all the six faces of the problem box. In the present version two boundary conditions namely the Neumann or open circuit condition (no field component perpendicular to the boundary) and the Dirichlet condition (no field component parallel to the boundary) are possible. The Neumann condition is possible only on the sides of the problem box. The following improvements have been made in the mesh generator:

- If the geometry has an intersection with a mesh line then the distances of the geometry point from the mesh point in all three directions have to be known. These are stored in an array to calculate the potential using the finite difference method. The mainframe version of the program calculates these distances more accurately.
- In the DOS version the mesh size is limited to 16, 000 whereas in the mainframe version the mesh size has been increased and is limited only by the available memory.

- If any new co-ordinate system is defined then the unit vectors along three directions must be defined to run this input file in the mainframe version. The mainframe version of the program has been modified so that the same geometry data can be used in both DOS and mainframe versions.

3.4.2 The Poisson Solver

Initially fixed potentials are assigned at the electrode mesh points and zero potential is assigned to the vacuum mesh points. The Poisson solver uses a 7-point finite difference formula to calculate the potentials at all vacuum mesh points through successive iterations. The successive over-relaxation method is used for the speedy convergence of the program. It is an iteration algorithm where the finite difference equations are solved for all mesh points.

3.4.3 The Trajectory Solver

The relativistic Lorentz force equations are solved by the trajectory solver. Any type of magnetic field can be used in any or all directions. The number of trajectories is limited only by the disk space available. The trajectory equations are solved using the Runge-Kutta method. The following improvements have been made in the trajectory solver:

- The original mainframe version of KOBRA3 used equal currents for all trajectories. In the improved version either equal or different currents can be assigned to the trajectories.
- The step size of integration for computing the trajectories has been made variable. This helps in finding the point of impact of the electron trajectory on the electrode surface more accurately. Unlike the previous version the trajectories do not enter deep inside the electrodes.

- Either primary or the secondary trajectories can be considered at any time without transferring the trajectory data into separate files. In the original version the trajectories are read from only one data file so the primary trajectory data had to be transferred to a new file in order to compute the secondary trajectories. In the modified version the trajectory data is read from two separate data files (for primary and secondary trajectories) depending on the choice of computation. This is useful for modelling the space charge of the secondary electrons.

3.4.4 Graphics

The package has options to create both 2-D and 3-D graphics. But the graphics in the original version are of poor quality [1]. Major modifications have been made in the graphics programs to improve it. Several new options have also been created which are helpful in analysing the collector performance.

- *2-D Graphics*

  There are two options in the 2-D plot. The first option plots the geometry, potential, electric field and magnetic field in all three planes (xy, yz and zx) and the second option plots the energy components of the trajectories. The following improvements have been made in the 2-D graphics:

  - In the original version, the equipotential and electric field lines enter inside the electrodes and the boundaries of the electrodes are not drawn. There is no axis and scale in the plots. The text headings and descriptions of the plot are missing. All these limitations have been removed in the improved version. Equipotential and electric field lines are plotted in different colours.
  - Different components of energy (total energy, kinetic energy, potential energy, axial component of energy etc.) are computed correctly and plotted against the

distance travelled along the trajectory. Scaling and levelling of the plots have been introduced.

- *3-D Graphics*

  The geometry, the trajectory and the mesh can be plotted in 3-D at different angles. The following new options have been made in the 3-D graphics:

  - The primary trajectories can be plotted with reference to their energies. A group of trajectories, which lie within specified energy limits, can be plotted suppressing the rest.
  - The primary trajectories belonging to different energy groups can be plotted with different colours in the same plot. This helps in analysing the collector performance through visual inspection.
  - All primary and secondary trajectories can be plotted in the same plot with different colours. This is useful for easy distinction between the primary and secondary trajectories.
  - Both primary and secondary trajectories can be plotted with reference to their energy. This is useful to find out the group of primaries, which is responsible for the generation of unwanted secondaries. It is also useful to study the effects of secondary electrons.

3.4.5 Output

A new option has been added to create coloured postscript files for all the graphics. All of the 2-D and 3-D graphics programs mentioned above produce the postscript files by default when they are run. None of the graphics programs plots the graphics on the screen in the unix operating system. However the postscript files can be seen in unix through any postscript viewer. The original source code of a package to generate the postscript files has been received free of cost from the Nova University, USA [9] and has

been modified according to the requirements. The postscript files are easily portable and can be inserted into reports and documents for publication and display.

3.4.6 General Features and Improvements

Apart from specific modifications some general improvements have been made in the package. These have made the package faster and more accurate. The quality and clarity of the graphics have also been improved.

- All programs including pre- and post-processor have been transferred to a unix platform to enhance the speed of the package. As a result the speed is about fifty times faster than under DOS.
- The graphics commands in DOS have been commented out and system commands, like date and time and the random number generator have been substituted with appropriate unix commands and subroutines.
- All programs including the interface package and postscript file generator have been made double precision for better accuracy.
- All newly developed programs have been commented extensively according to good software engineering practice. Modified subroutines of the original package have also been commented.

3.5 VALIDATION OF LKOBRA (MF)

The structure of the mainframe version of LKOBRA is shown in a basic flow diagram in Figure 3-3. After a steady state solution is achieved, the graphics options are used to see different plots. A postscript file is generated as a default output when the plot option is chosen.

The suitability of LKOBRA (MF) for simulating the MDCs in three-dimension has been evaluated through some basic tests. These tests are used to study the effects of:

- Transverse magnetic field
- Asymmetric geometry

The accuracy of the test results is chosen as the main criterion for its suitability.

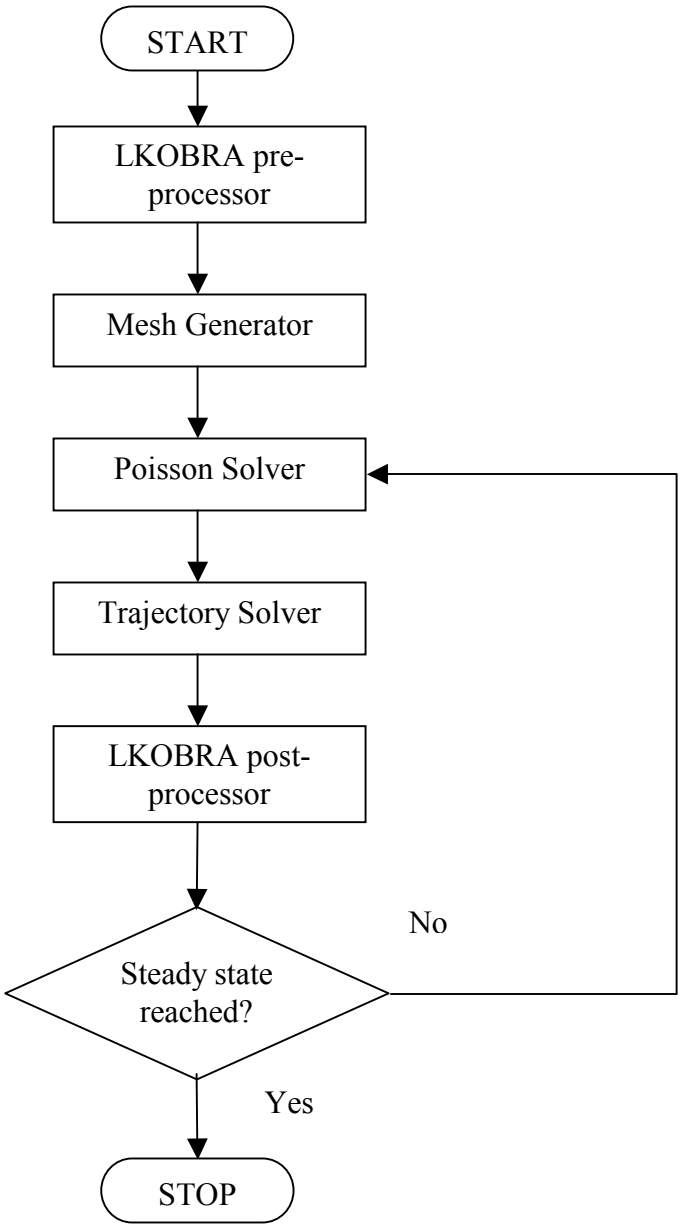

Figure 3-3: Basic flow diagram of the LKOBRA package

3.5.1 Effect of Transverse Magnetic Field on Electron Trajectories

A mass spectrometer test has been carried out to examine the effect of a transverse magnetic field on the electron trajectories. It is well known that if a constant magnetic field is applied to an electron perpendicular to its direction of motion then it will follow the circular path whose radius can be defined as

$$r = 3.37 \times 10^{-6} \ (V^{1/2}/B) \qquad (3\text{-}4)$$

Here the radius r is in meters, the potential V is in Volts and the magnetic field B is in Tesla.

In a test case eight trajectories are started at one end of a box of dimensions 175 mm x 145 mm x 145 mm. Figure 3-4 shows a plot of the electron trajectories. These electrons have a span of energy from 600 to 1300 eV. All trajectories start from the same position at x = 5 mm, y = 71.25 mm and z = 110 mm. A constant transverse magnetic field of strength 9.43 Gauss is applied. The theoretical and experimental data are compared in Table 3-2. The error is less than 0.5%.

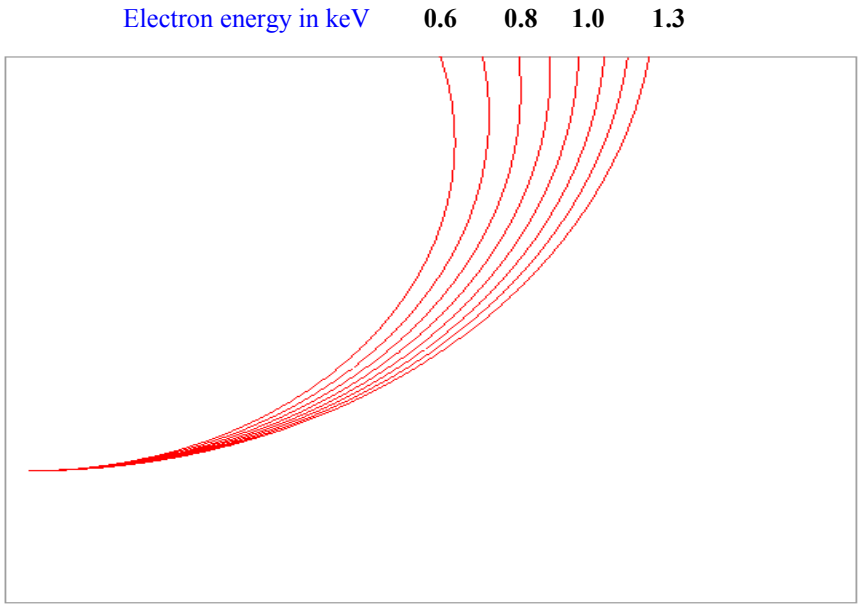

Figure 3-4: Plot of electron trajectories with different initial energy under the influence of transverse magnetic field

In a different test case ten electron trajectories with a span of energy between 500 eV to 950 eV start inside a box of dimensions 400 mm x 300 mm x 300 mm. All electrons start at the same point x = 200 mm, y = 30 mm, z = 70 mm. A transverse magnetic field of 8 Gauss is applied (in the z direction) at all the mesh points of the problem box. Figure 3-5 plots these trajectories under the influence of the magnetic field. The trajectories are seen to follow a circular path, as should be the case. The theoretical and experimental values of the radius of the circular path are compared in Table 3-3. The error is less that 0.5%. The accuracy in both experimental results has proved the capability of the package to simulate the electron trajectories under the influence of an external magnetic field.

Table 3-2: Comparison of experimental and theoretical values of x-co-ordinate of end point of trajectories

Electron energy (eV)	**X-co-ordinate of the end-point of trajectories (mm)**		
	Theoretical	**Computed**	**Error**
600.0	89.52	89.69	0.17
700.0	98.22	98.36	0.14
800.0	105.65	105.77	0.12
900.0	112.15	112.26	0.11
1000.0	117.96	118.05	0.09
1100.0	123.22	123.30	0.08
1200.0	128.04	128.11	0.07
1300.0	132.49	132.55	0.06

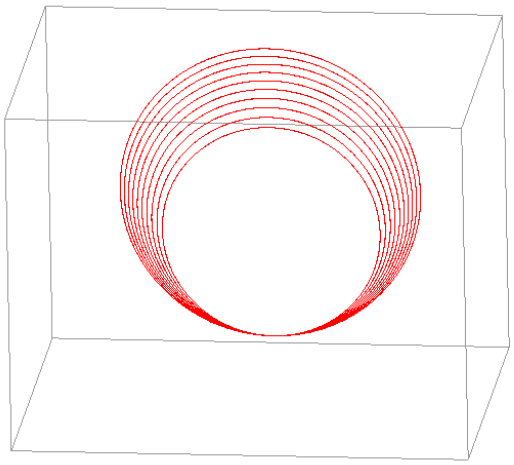

Figure 3-5: Plot of circular electron trajectories with different initial energy under the influence of transverse magnetic field of 8 Gauss (along z direction)

Table 3-3: Comparison of experimental and theoretical values of radius of the circular path traversed by the trajectories

Electron energy (eV)	**Radius of the circular path of the trajectories (mm)**		
	Theoretical	**Computed**	**Error**
500	94.26	94.16	0.10
550	98.87	98.76	0.11
600	103.26	103.15	0.11
650	107.48	107.37	0.11
700	111.54	111.42	0.12
750	115.45	115.34	0.11
800	119.24	119.12	0.12
850	122.91	122.79	0.12
900	126.47	126.35	0.12
950	129.94	129.82	0.12

3.5.2 Effect of Asymmetric Geometry

A two-stage asymmetric tilted electric field (TEF) collector, widely known as Okhosi's collector [10] has been simulated using the LKOBRA (MF) package. This includes the effects of secondary electron emission. The computed results have been compared with experimental values.

The TEF collector was fitted in a TWT with beam radius 0.63 mm, cathode voltage 4.8 kV (V_0) and beam current 54 mA (I_0). The details of the electrical specifications can be found in [6]. In the present simulation we have used an axial electric field similar to Okhosi's original collector.

- *Geometry*

Figure 3-6 shows the diagram of the two-stage TEF collector for which the simulation has been carried out. It consists of three electrodes, which are assigned potentials 4.8 kV, 2.4 kV and 1.2 kV respectively. Since the first electrode is kept at body potential it is regarded as a two-stage collector. An input file for the simulator has been generated by the pre-processor of the package using the geometrical data shown in the Figure 3-6. Some basic pre-defined electrode shapes have been used to create the geometry of the electrodes. The first electrode is a cylinder, the second electrode is a combination of a funnel and a cylinder and the third electrode is a combination of two cylinders and a circular disc.

The mesh size was taken to be 0.5 mm in all three directions. A smaller mesh size of 0.2 mm is used in the gaps between the electrodes and close to the axis of the collector geometry. Though the total number of mesh units is limited only by the disk space it is still necessary to use a smaller number of mesh units if the speed of computation is not to be unacceptably long. There is, thus, a compromise between the disk space, computation time and the accuracy of the results. For this reason a relatively smaller mesh size was used at the gaps and a bigger mesh size at other parts of the collector. The space charge

force is highest on the axis and it becomes lower towards the wall of the collector. For better accuracy in the results the mesh size is smaller than the beam radius near the axis of the beam and it is made larger as the distance from the axis increases.

The experimental spent beam distribution of this tube is shown in Table 3-4. Based on this data the trajectory starting conditions were generated using the 3-D beam model. A total of 183 trajectories were generated and each of them was assigned an angular deviation randomly from -2^0 to $+2^0$. This range was deliberately chosen small as the beam perveance was low (~0.16 μPerv).

Boundary conditions were defined on all the six faces of the box containing the collector geometry. The lower left corner of the problem box was kept as the origin of the 3-D co-ordinate system with the axial direction set as x, the transverse direction as y and the vertical direction as z. The first and the last yz plane were assigned potentials 4.8 kV and 1.2 kV respectively. The four remaining faces were assigned open circuit (Neumann) boundary conditions.

Table 3-4: Spent beam energy distribution for TEF collector

V/V_0	0.55	0.65	0.75	0.85	0.95	1.05	1.15
$I(V/V_0)/I_0$	.056	0.430	0.276	0.067	0.078	0.056	0.037
Number of Trajectories	12	78	51	12	15	9	6

- *Simulation*

The mesh generator of the main simulator generates the mesh in the 3-D problem box containing the collector geometry, assigns the potential to the electrodes and defines the boundary conditions on the faces of the box. After successful mesh generation the Poisson solver and the trajectory solver are run alternately. It took 8 iterations to get a

self-consistent solution in this case. The details of the simulation and the results have been described in [6] and [11].

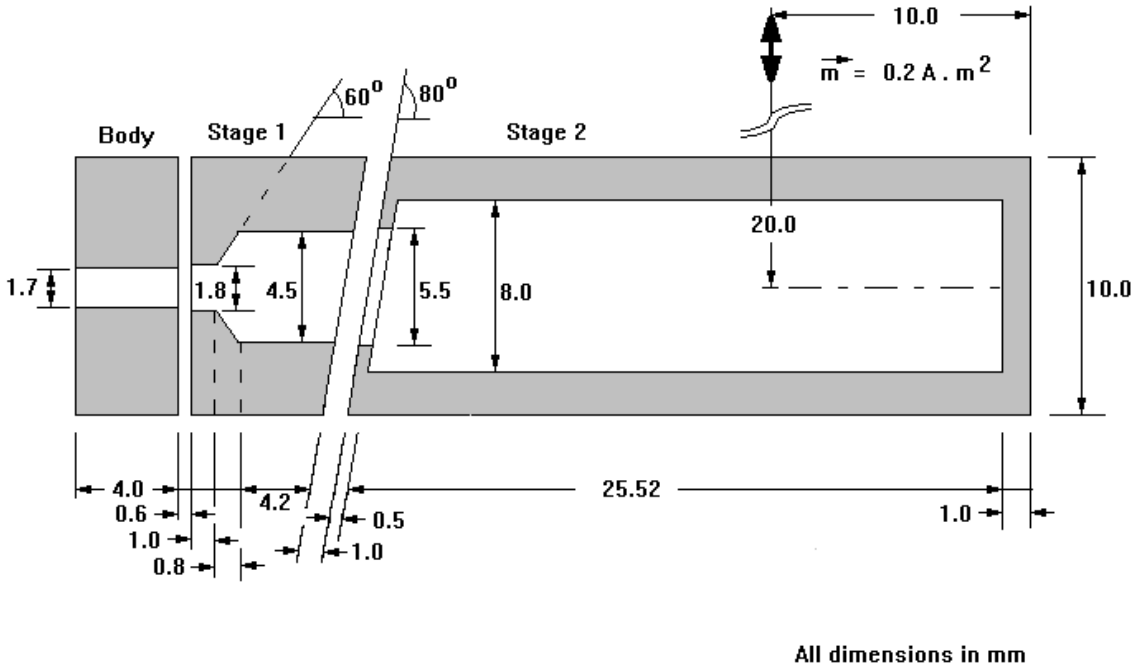

Figure 3-6: Geometry of a 2-stage tilted electric field collector (the magnetic field is applied using a dipole magnet of 0.2 A. m^2 magnetic moment)

Figure 3-7 (a) and (b) shows the geometry of the collector in 3-D at different Euler's angles. The 2-D plot of the collector geometry is shown in Figure 3-8. In this plot the refined mesh is seen to be smaller (compared to mesh size at other places) in the gaps between the electrodes. Both geometry and equipotential lines are plotted in 2-D at different planes in Figure 3-9. The equipotential lines are plotted in the yz plane at the end of the second electrode in Figure 3-9(a). The variation in the strength of potential from the electrode surface towards the axis of the collector is clearly shown in the plot. In Figure 3-9(b) the equipotential lines are plotted in the xy plane at the middle of z.

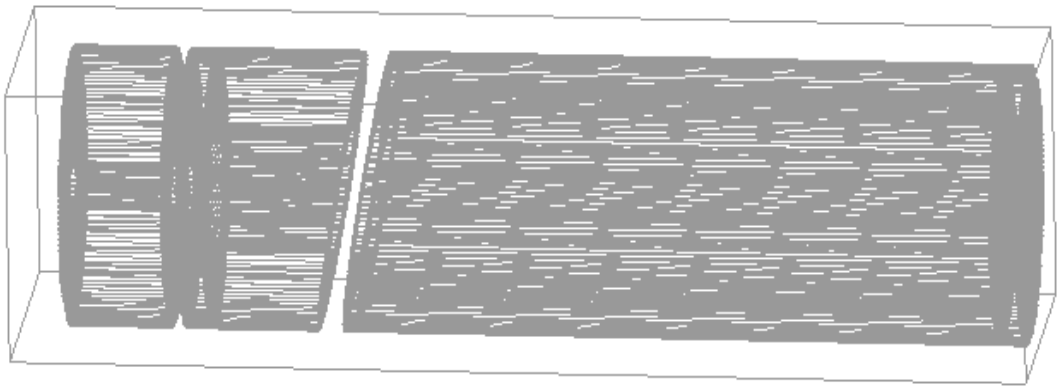

(a)

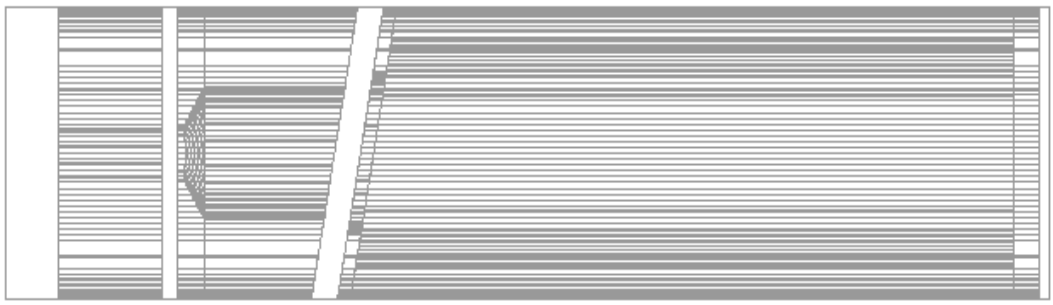

(b)

Figure 3-7: 3-D geometry of the TEF collector at Euler's angle (a) 20,-20,20 (b) 0,0,0

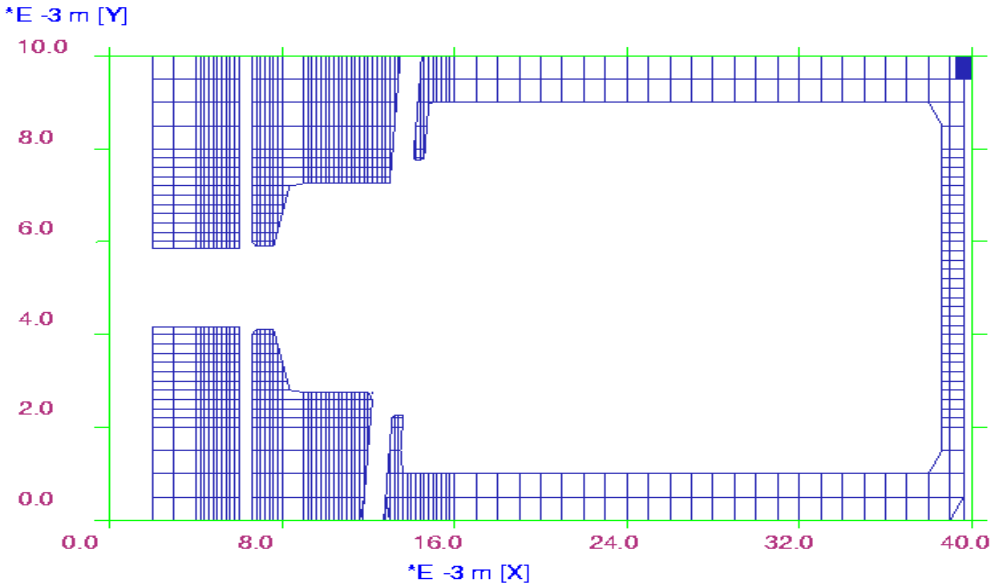

Figure 3-8: 2-D geometry of the TEF collector in the xy plane at the middle of z (z= 20)

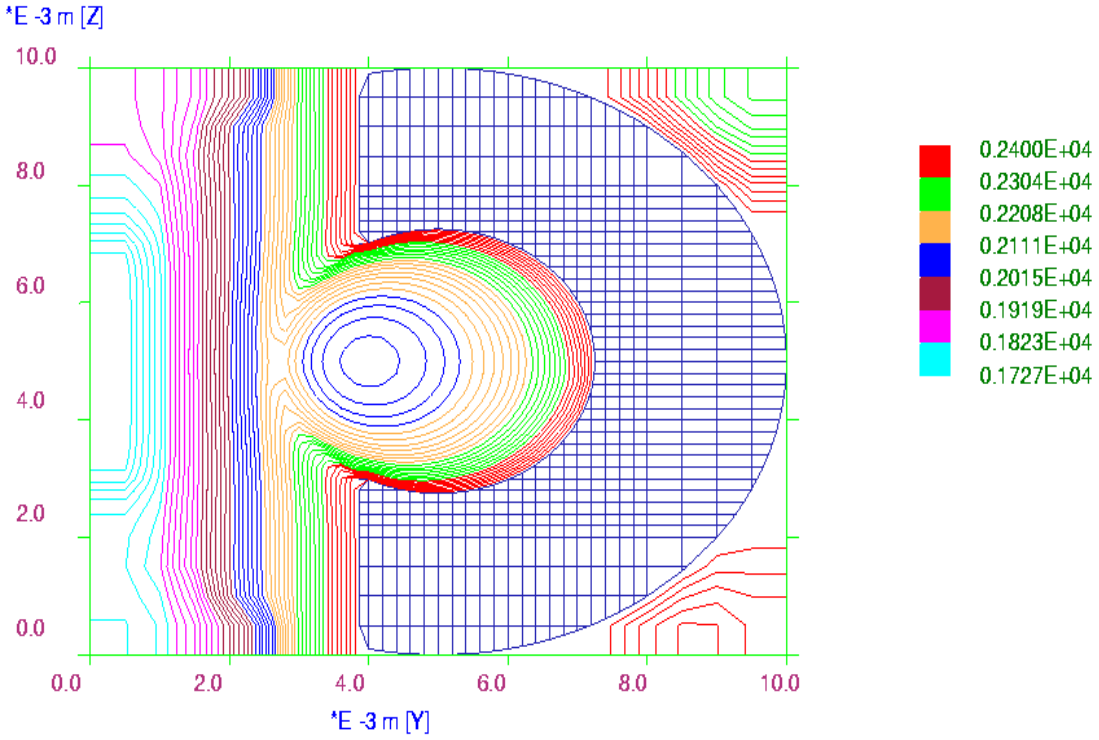

(a)

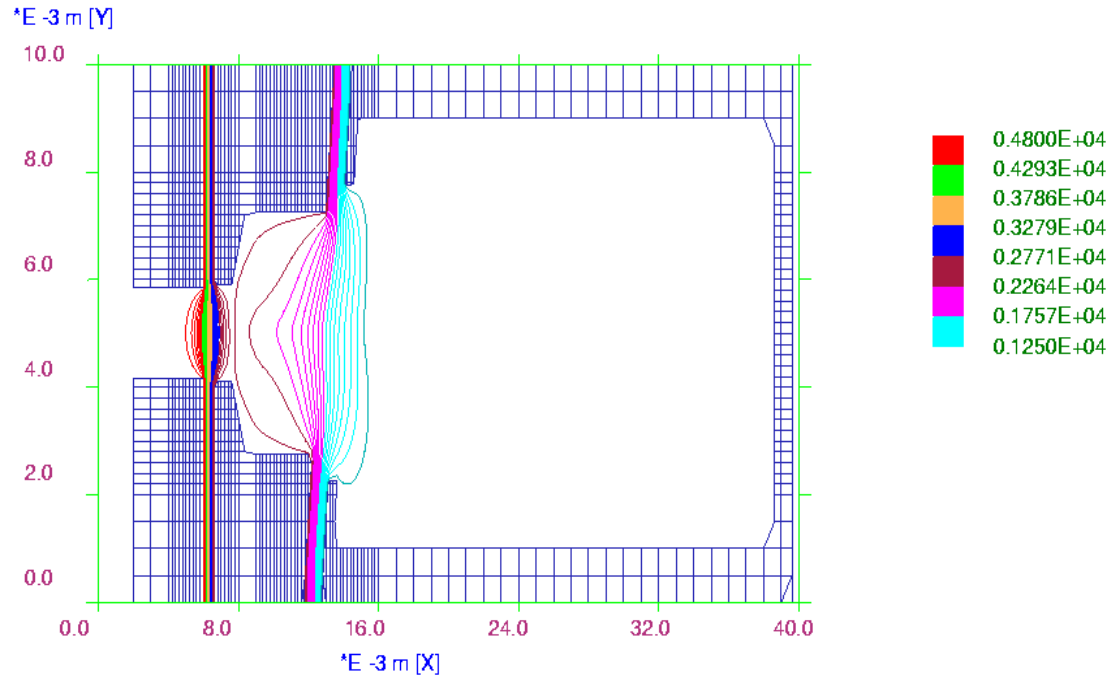

(b)

Figure 3-9: Equipotential lines in the TEF collector (a) yz plane at the end of second electrode (x =43) (b) xy plane at the middle of z (z = 20)

The equipotential lines are symmetric in the gap between the first and the second electrode but they are asymmetric in the other gap between the second and the third electrode due to the asymmetric geometry in this region. Lens effects are prominent in the gaps between the electrodes. A retarding force is exerted on the electrons by the lens in each electrode gap. The strength of force generated by the first lens (between the first and the second electrodes) is less than that generated by the second lens (between the second and third electrodes). The slower electrons are affected more in the first region because the lens is week. On the other hand the second lens influences the higher velocity electrons.

The total energy (sum of kinetic and potential energy) and the total kinetic energy are plotted versus the distance traversed by the primary trajectories in Figures 3-10 (a) and (b) respectively. In Figure 3-10 (a) the trajectories for seven different energy classes maintain their total energy throughout the path length, as it ought to be. In the second plot, in Figure 3-10 (b), the kinetic energy diminishes as the electrons move and it attains a minimum level. All electrons should be collected at this energy level, in an ideal collector to reduce the heat dissipated. But here it is seen that some electrons gain further energy when they turn backward (repulsed by the electrode potential) and hit an electrode with lower depression. The energy with which the electron hits the electrode surface can be determined from the height of the end point of the trajectory.

The electron trajectories can be plotted in different ways to reveal their nature. The primary trajectories are plotted according to their energy in the set of plots in Figure 3-11 (a) – (c). Electron trajectories having energy between 0 and 2640 eV (0.55 V_0) are plotted in Figure 3-11 (a). These electrons are collected at the second electrode, as the potential at the second electrode is 2400 V. The second group of electron trajectories having energies between 2640 eV and 3120 eV (0.65 V_0) are plotted in Figure 3-11 (b). Here nearly all the trajectories cross the second electrode but are repelled by the third and are collected at the second electrode. The third electrode potential, 3600 V (0.75 V_0), is much higher than the electron energies in the group, which causes them to be repelled towards the second

electrode. Electron trajectories with energies higher than 3600 eV are all collected by the third electrode as shown in Figure 3-11 (c). Some of the primary trajectories stream back towards the interaction region, which is highly undesirable. These plots are useful for adjusting the electrode dimensions so that the collector performance is optimised.

Once the primary trajectories have been generated the post-processor uses the data to generate the starting conditions of the secondaries. Secondary trajectories are generated after running the simulator again and taking account of their space charge effects. In Figure 3-12(a) all primary trajectories are plotted with different colour representing a different energy class. The colour-coded value of the trajectory energy is shown at the bottom of the plot. All secondaries are plotted in the Figure 3-12(b). A superimposed view of the secondaries on the primaries is shown in Figure 3-12(c). The details of the modelling of secondary electrons and their effects on this TEF collector are explained in the next chapter.

- *Results and Analysis*

The performance of the collector has been analysed using the post-processor and compared with experimental results in Table 3-5. In Table 3-5(a) the results are compared when no magnetic field is applied in the collector. There is a difference between the theoretical and practical results in the current and power recovered at different stages. This is due to the approximations in the secondary electron emission model. Only one generation of secondaries has been considered in the present case. The theoretical results may be closer to those of experiment if a more accurate secondary electron emission model is developed and the multiple generations of secondaries are considered. The energy balance has been computed by comparing the power entering the collector with the total power (total power recovered + total power loss). The difference between these two values is within a limit of 0.1 W.

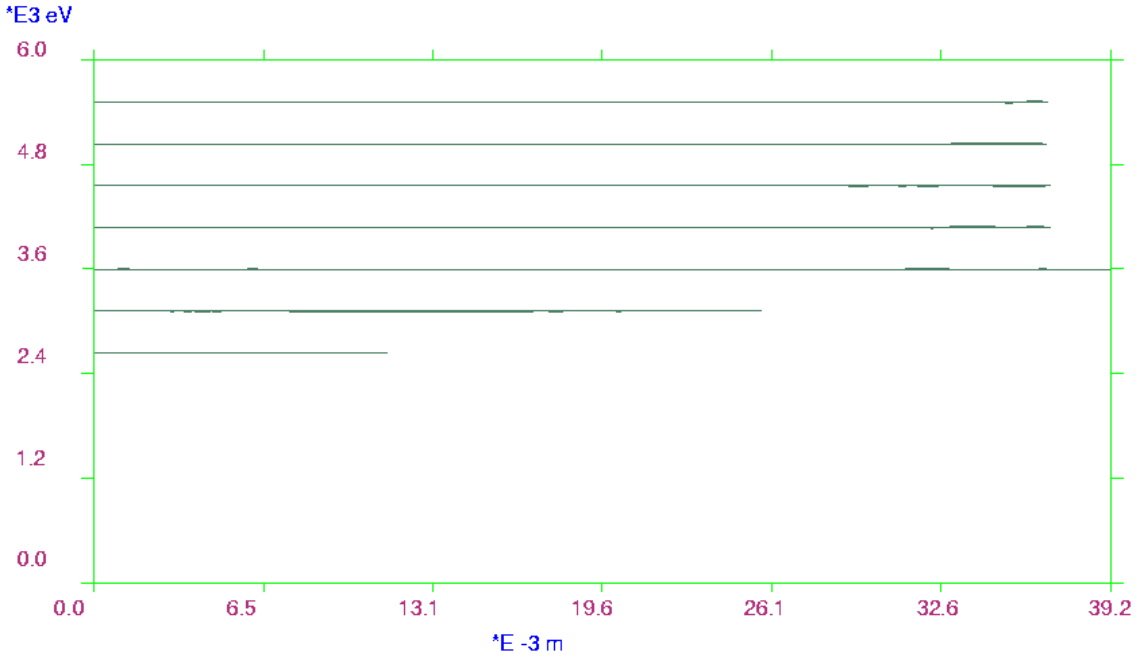

(a)

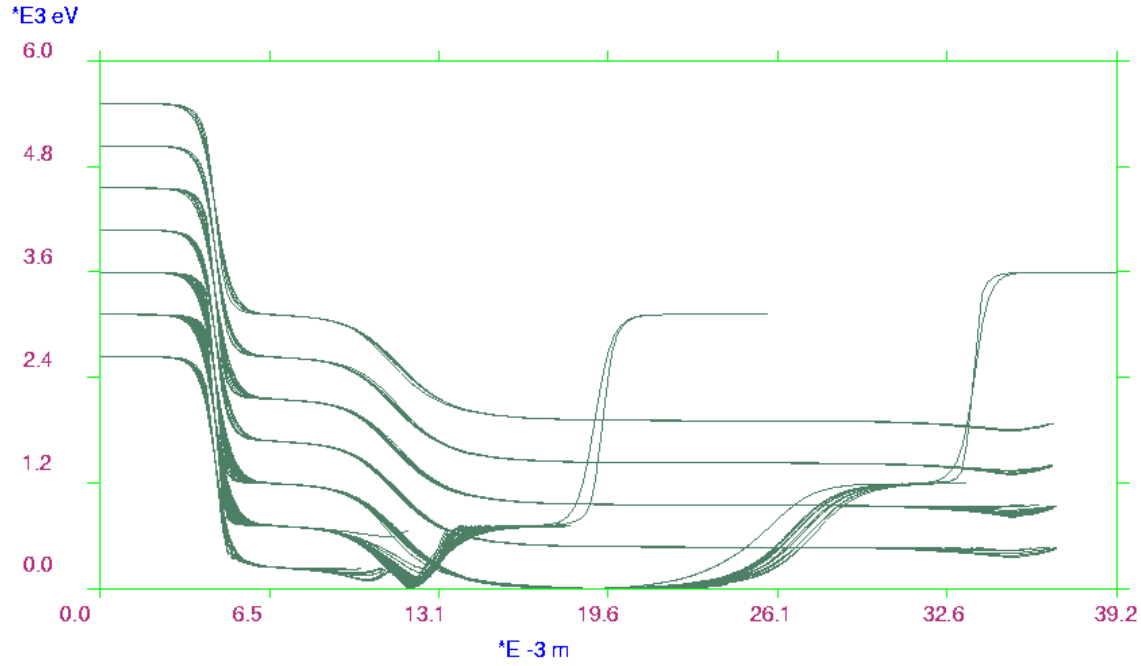

(b)

Figure 3-10: Plot of energy vs distance traversed for all trajectories (a) total energy (b) total kinetic energy

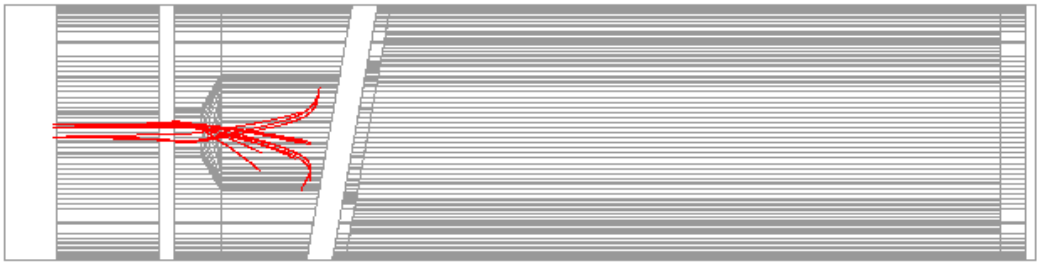

(a)

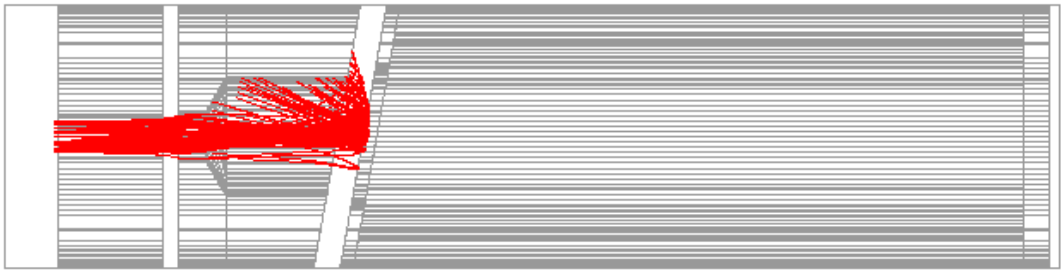

(b)

(c)

Figure 3-11: Primary trajectories according to their energy (a) between 0 and 2640 eV (b) between 2640 and 3120 eV (c) between 3120 and 6000 eV

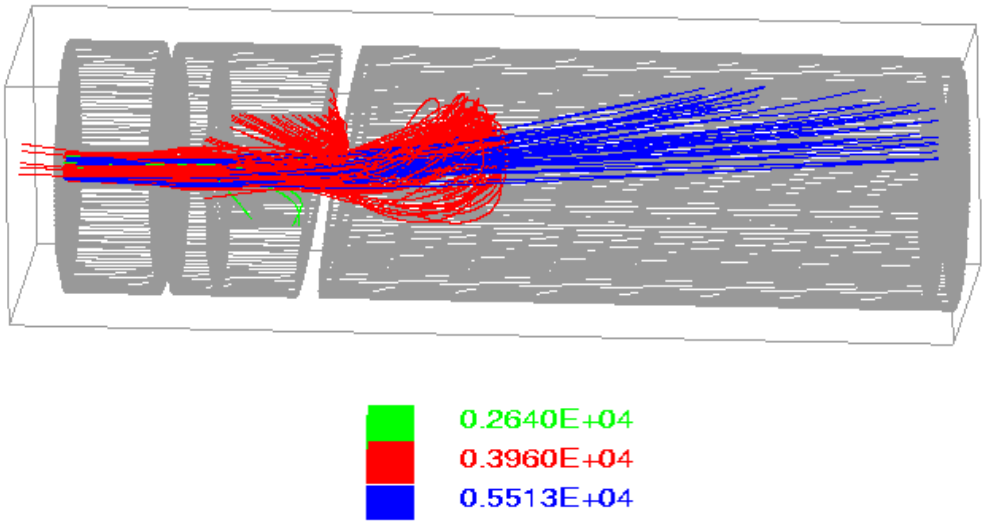

(a)

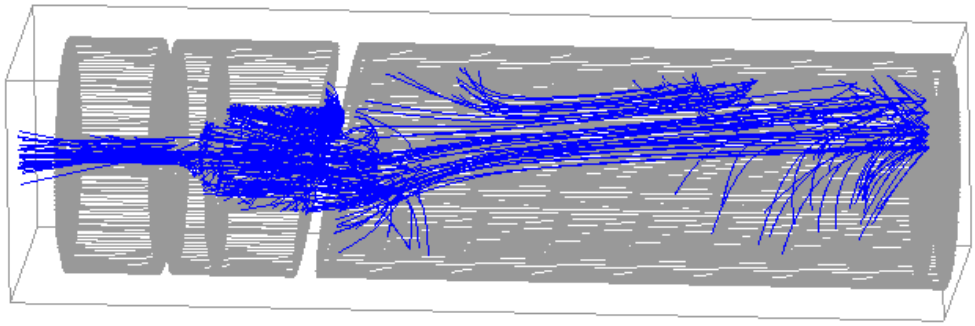

(b)

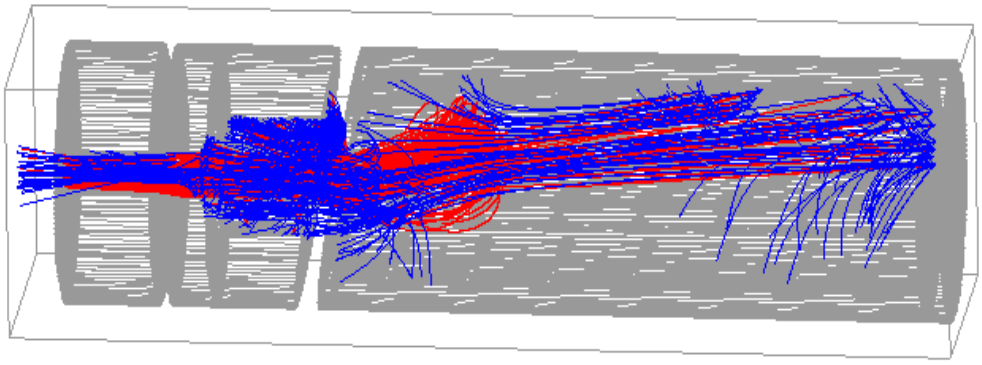

(c)

Figure 3-12: Trajectories for the TEF collector with magnetic field (a) all primaries colour-coded (b) all secondaries (c) both primaries and secondaries

A comparison between the theoretical and practical results under the influence of the magnetic field is shown in Table 3-5(b). In the practical collector a magnetic field with a dipole magnet of 0.2 $A.m^2$ magnetic moment oriented in the y direction and located at a distance of 10 mm inward from the end of the last stage and 20 mm away from the axis was applied (Figure 3-6). The simulator does not include any magnetic field generator of this type. In the present simulation a constant magnetic field of 8 Gauss in the y direction was applied at all mesh points. This may be the reason why the simulated efficiency is a little lower than the experimental value.

3.6 SUMMARY

A fully 3-D package LKOBRA (MF) has been developed and proved to be suitable for simulation of multistage collectors that includes the secondary electron emission effects. The package is equipped with a pre- and a post-processor. The whole package runs both in DOS and unix operating systems. All plots in this package are coloured graphics output that can be transferred into postscript format. This package is capable of simulating secondaries generated through multiple reflections. However the post-processor does not consider multiple reflections for computational purpose of the collector parameters. The effect of magnetic field on the electron trajectories was computed with reasonable accuracies. The simulated results of the asymmetric collector prove the capability of the package to simulate any complex collector geometry in 3-D.

Table 3-5(a): Computed and the Experimental Results of the TEF Collector without magnetic field

QUANTITY	EXPERIMENTAL VALUE	COMPUTED VALUE
Total Power Entering the Collector	191.6 W	190.04 W
Back Streaming Current	#	3.9 mA
Current at Body	#	1.8 mA
Current at Stage 1	45.0 mA	32.8 mA
Current at Stage 2	7.0 mA	14.8 mA
Power Recovered at Stage 1	108.0 W	78.68 W
Power Recovered at Stage 2	25.2 W	53.11 W
Power Dissipated at Body	#	2.02 W
Power Dissipated at Stage 1	#	27.76 W
Power Dissipated at Stage 2	#	22.24 W
Back Streaming Power	#	6.20 W
Total Power Recovered	133.2 W	131.80 W
Total Power Loss	58.4 W	52.03 W
Collector Efficiency	**69.5 %**	**69.4 %**

Table 3-5(b): Computed and the Experimental Results of the TEF Collector with magnetic field

QUANTITY	EXPERIMENTAL VALUE	COMPUTED VALUE
Total Power Entering the Collector	191.6 W	190.04 W
Back Streaming Current	#	3.5 mA
Current at Body	#	1.7 mA
Current at Stage 1	42.2 mA	30.5 mA
Current at Stage 2	11.0 mA	17.5 mA
Power Recovered at Stage 1	101.2 W	73.16 W
Power Recovered at Stage 2	39.6 W	63.13 W
Power Dissipated at Body	#	1.01 W
Power Dissipated at Stage 1	#	31.55 W
Power Dissipated at Stage 2	#	15.77 W
Back Streaming Power	#	5.39 W
Total Power Recovered	140.9 W	136.29 W
Total Power Loss	50.7 W	48.35 W
Collector Efficiency	**73.5 %**	**71.7%**

Experimental values are not known

REFERENCES

[1] L. Kumar, P. Spadtke, R. G. Carter and D. Perring, "Three-Dimensional Simulation of Multistage Depressed Collectors on Micro-computers," *IEEE Trans. on Electron Devices*, vol. 42, No. 9, pp. 1663-1673, September 1995.

[2] L. Kumar and R. G. Carter, "3-D Depressed Collectors (Report on Phase I)," Engineering Department, Lancaster University, MRG/90/1, July 1990.

[3] L. Kumar and R. G. Carter, "3-D Depressed Collectors (Final Report)," Engineering Department, Lancaster University, MRG/91/2, October 1991.

[4] J. L. H. Jonker, "The Angular Distribution of the Secondary Electrons of Nickel," Philips Research Report, No. 6, pp. 372-387, 1951.

[5] J. R. M. Vaughan, "Secondary Emission Formulas," *IEEE Trans. on Electron Devices*, Vol. 40, No. 4, p. 830, April, 1993.

[6] T. K. Ghosh and R. G. Carter, "3-D Simulation of Multistage Depressed Collectors for High Efficiency Space TWT (Progress Report 1)," Engineering Department, Lancaster University, MRG/2000/2, March 2000.

[7] T. K. Ghosh and R. G. Carter, "3-D Simulation of Multistage Depressed Collectors for High Efficiency Space TWT (Progress Report 2)," Engineering Department, Lancaster University, MRG/2001/1, January 2001.

[8] T. K. Ghosh and R. G. Carter, "3-D Simulation of Asymmetric Multistage Depressed Collectors with Secondary Electron Emission Effects for High Efficiency Space TWTs," in *Proc. ITG Conference on Displays and Vacuum Electronics*, May 2-3, 2001, pp. 67-71.

[9] K. E. Kohler, PSPLOT - PostScript for Technical Drawings (A free Fortran-callable PostScript Plotting Library), Nova Southern University Oceanographic Center. Available at: http://www.nova.edu/cwis/oceanography/psplot.html.

[10] T. Okoshi, E. Chiu and S. Matsuki, "The Tilted Electric Field Soft-Landing Collector and Its Application to a Travelling-Wave Tube," *IEEE Trans. on Electron Devices*, vol. ED-19, No. 1, pp. 104-110, 1972.

[11] T. K. Ghosh and R. G. Carter, "Improved Three Dimensional Simulation of Multistage Depressed Collectors for High Efficiency Travelling Wave Tubes," in *Proc. of 2nd IEEE International Vacuum Electronics Conference 2001*, April 2-4, 2001, pp. 215-220.

Chapter 4

Modelling of Secondary Electron Emission

4.1 INTRODUCTION

In any linear beam microwave tube secondary electrons are generated at the collector due to the remaining spent beam energy in the primary electrons. The spent beam electrons carry sufficient energy to knock out secondary electrons from the collector electrodes. Sometimes the primaries are reflected either elastically or in-elastically from the walls of the collector electrodes. The secondaries and reflected primaries play an important role in determining the efficiency of the collector as well as the overall efficiency of the microwave device. Secondary electrons sometimes stream back towards the interaction region, which is highly undesirable for communication and radar tubes as it introduces unwanted noise to the amplified signal either through interception or through unwanted feedback path. The noise gets amplified and can introduce instability and oscillation in the tube. It also causes the signal distortions and heating of the RF circuit.

In this chapter the types of secondary electrons and the distribution of secondaries are presented in section 4.2. A brief review on different secondary electron emission models is discussed in section 4.3. The development of a secondary electron emission model and

the effect of secondaries on the multistage collector performance are described in sections 4.4 and 4.5 respectively. The chapter is concluded with a summary.

4.2 CLASSIFICATION OF SECONDARY ELECTRONS

When the primary electrons hit the surface of an electrode, some of them penetrate into the surface and rest are reflected elastically. The energy of the penetrated electrons excites the electrons inside the metal to a higher energy level. Sometimes these electrons come out of the electrode surface if the energy level is higher than the threshold energy (work function) of the material. It is also possible that some of the primaries loose their energy partially into the solid, but escape from it afterwards. All the electrons, emitted from the metal surface, are called secondary electrons. The secondary electrons are broadly classified into two categories: (a) slow secondary electrons and (b) fast secondary electrons.

Figure 4-1 shows a typical energy distribution of the secondary electrons emitted from any metal when the primary electrons strike the surface at an angle normal to it [1]. The lower part of the curve has a wide peak (region "A"), which indicates that a majority of the secondary electrons have low energy. For most of the solids this value is only few eV. These secondaries are actually true secondaries. There is no clear division between the slow and fast secondary electrons. But it is assumed that the energy below 50 eV is composed of slow secondary electrons whereas the upper energy level, i.e., region "B" consists of fast secondary electrons. The region between "A" and "B" is nearly flat and it consists of the inelastically reflected primaries and some true secondaries. Some researchers suggest that the secondary energy should be half of the primary energy when the primary energy exceeds 100 eV, but the general convention is to assume this energy as 50 eV [1]-[3], [8]. In our modelling we have followed this convention.

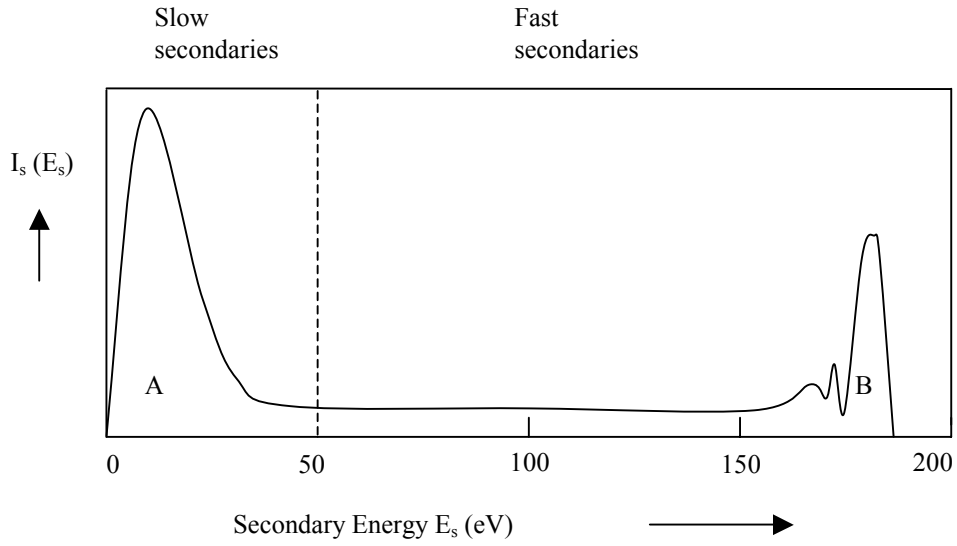

Figure 4-1: Typical energy distribution of secondary electrons emitted from a metal surface

4.2.1 Slow Secondary Electrons

The slow secondary electrons are classified into two subgroups:

(a) True secondaries

(b) Inelastically reflected primaries.

True secondaries are those electrons, which are knocked out from the electrode surface by the high-energy primary electrons. For primary energies below the threshold value (approximately 10 eV) no secondaries are generated. The second group is originated due to the inelastic collision of the primary electrons with the electrode surface. In this case the primary electrons transfer an amount of energy to the electrode. After one or more collisions these electrons are reflected to the surface. Between these two groups only the true secondaries are responsible for any yield greater than 1 as it comprises no primary electron and their energy distribution is also independent of the primary energies [1].

The angular distribution of the true secondary electrons and the reflected primary electrons has been measured and plotted by Jonker [4]. All these experiments have been carried out on polycrystalline nickel. The collector electrode is generally made of copper or other carbon based material like graphite. These materials are crystalline in nature. Therefore it has been assumed that the distribution of secondaries and the reflected primaries will remain unchanged. Due to the lack of experimental data for copper, these results have been used for the present secondary electron emission model.

The angular distribution of the slow secondary electrons as measured by Jonker [4] has been plotted in Figure 4-2 for different angle of incident of primary energy. From Figure 4-2 (a) it is seen that the distribution is approximately cosinusoidal for lower primary energies though it is not perfectly so. But in Figure 4-2 (b) it can be observed that the distribution is more distorted from the true cosinusoidal distribution and the distortion is in the direction anti-parallel to the direction of incidence. This may be due to the higher primary energy than the previous one.

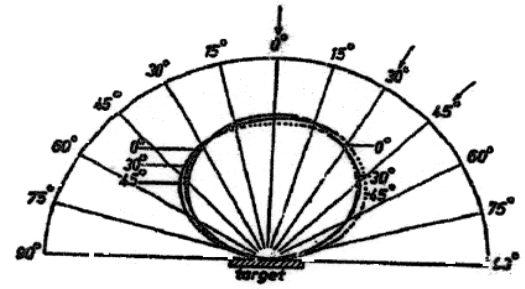

(a)

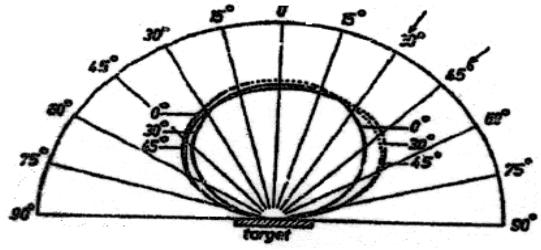

(b)

Figure 4-2: Angular distribution for slow secondaries emitted from polycrystalline nickel as measured by Jonker

(a) Primary energy Ep = 100 eV, distributions for several angle of incidence
(b) Primary energy Ep = 450 eV, distributions for several angle of incidence

The angular distribution of the secondary electrons for different primary energies keeping the angle of incidence fixed is plotted in Figure 4-3. In Figure 4-3 (a), the angular distribution is very close to the cosinusoidal distribution for all levels of primary energy. But in Figure 4-3 (b) and Figure 4-3 (c) it is observed that the distribution is distorted from the true cosinusoidal distribution at higher primary energies and higher angles of incidence. These results are similar to those of Figure 4-2. As all of these experiments were carried out for only three angles and for a maximum energy of 450 eV, no conclusion can be drawn from these results (in practical cases the primary energy may vary up to kVs and angle up to 90 degrees). But it can be assumed that the angular distribution of slow secondaries is close to the cosinusoidal distribution. In our model we have assumed a cosinusoidal distribution for slow secondaries.

Based on the above experimental data the slow secondary electron emission has been modelled in [5] where the distribution was assumed to be cosinusoidal. Some other models were developed based on the Jonker's experimental data [6], [7], [17], [19]. Mostly all these models assumed a cosinusoidal distribution of slow secondaries. However it is not known whether the model developed by A. Singh et al. at Maryland University [7] assumes a cosinusoidal distribution. This package is mainly used for modelling of multistage depressed collectors for high power gyrotrons.

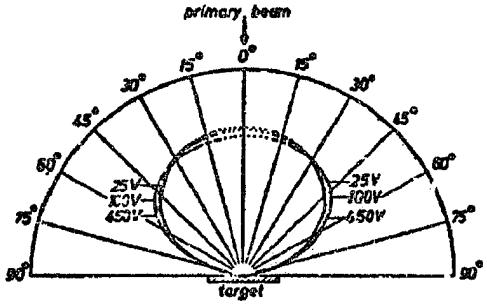

(a)

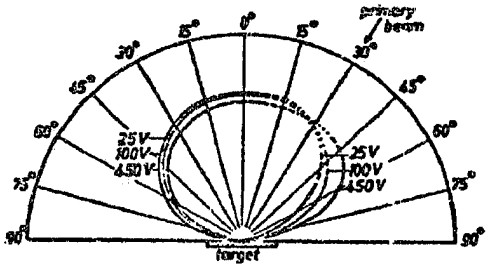

(b)

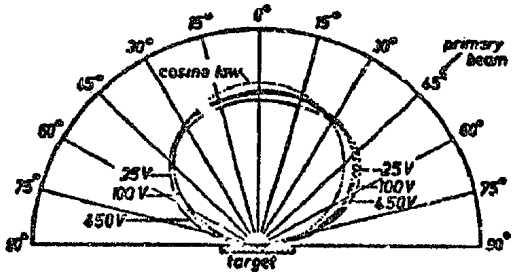

(c)

Figure 4-3: Angular distribution for slow secondaries emitted from polycrystalline nickel as measured by Jonker

(a) $\theta = 0^0$, distribution for several values of primary energy
(b) $\theta = 30^0$ distribution for several values of primary energy
(c) $\theta = 45^0$ distribution for several values of primary energy

4.2.2 Fast Secondary Electrons

Fast secondary electrons are elastically reflected primaries. In almost all the cases these electrons undergo one or more elastic collisions with the metal surface and finally they are liberated from the surface through electron substitution or any other similar process [1]. In our model we have considered the fast secondary electrons collectively irrespective of their origin. The angular distribution for fast secondaries as measured by Jonker is shown in Figure 4-4. Here the angular distribution is plotted with respect to angle of incidence of the primary electrons keeping the primary energy constant. From Figure 4-4 (a) and Figure 4-4 (b) it is observed that there are similarities between the distributions of secondaries; they are bi-directional in nature and in both cases two lobes in the angular distributions are prominent. One is in the backward direction and the other is in forward direction. But at higher primary energies the lobes in the forward direction become smaller.

The angular distribution of fast secondary electrons for different angles of incidence of primary electrons keeping the energy fixed is plotted in Figure 4-5. The distribution was measured and plotted by Jonker. In all of these plots it is seen that the minor lobe is very small for higher energies at all angles of incidence. As the energy of the spent beam electrons in any microwave tube is generally very high and the electrons hit the surface with sufficient energy we may consider that the volume of the minor lobe will be very small. From Figure 4-4 and Figure 4-5 we have so far observed that the direction of the major lobe is backward but not exactly at the same angle of incidence. It is slightly tilted towards the surface normal. As only limited data is available to predict the exact angle of emergence of the fast secondaries we have assumed that angle as approximately 2/3 of the incident angle of the primary electrons. All of the above experiments were carried out by Jonker for polycrystalline nickel, but we will use this data for our modelling purpose, as there is no other data available to the author at present. The same data was used for modelling secondary electrons in [5], [6].

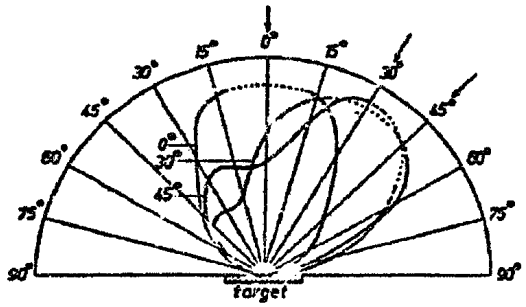

(a)

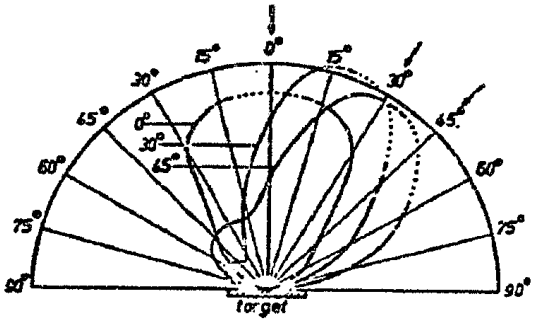

(b)

Figure 4-4: Angular distribution for fast secondaries emitted from polycrystalline nickel as measured by Jonker

(a) Primary energy Ep = 100 eV, distributions for several angle of incidence

(b) Primary energy Ep = 450 eV, distributions for several angle of incidence

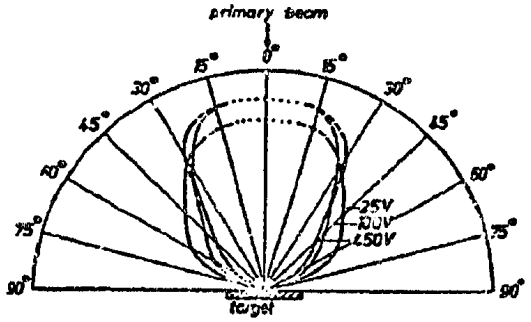

(a)

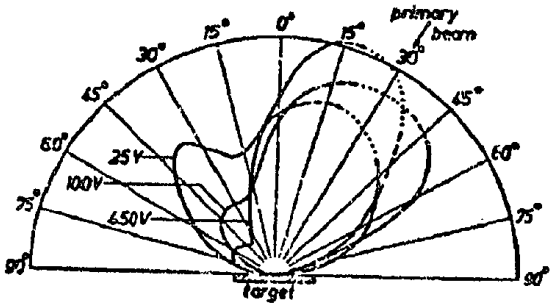

(b)

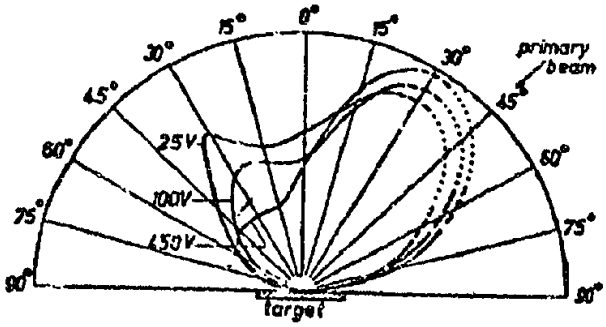

(c)

Figure 4-5: Angular distribution for fast secondaries emitted from polycrystalline nickel as measured by Jonker

(a) $\theta = 0^0$ distribution for several values of primary energy
(b) $\theta = 30^0$ distribution for several values of primary energy
(c) $\theta = 45^0$ distribution for several values of primary energy

4.2.3 Secondary Electron Emission Yield

Secondary electron emission yield is defined as the ratio of secondary electron current to the primary electron current. It is a factor, which determines the number of secondary electrons emitted per primary electron. The process of secondary electron generation is a complex phenomenon, which is difficult to express analytically. An empirical formula to find out the secondary electron emission yield has been derived by Vaughan [8] and it has been modified afterwards by Vaughan himself [9] based on some experimental results carried out by Shih and Hor [10]. The experiments carried out by Shih and Hor proves that the empirical formula derived by Vaughan is correct to well within 10% of the experimental results. But for any theoretical prediction of secondary electron emission yield it is necessary to have a prior knowledge of $V_{\max}$ and $\delta_{\max}$ where $\delta_{\max}$ is the maximum secondary electron emission yield at an impact voltage $V_{\max}$ when the impact is normal to the surface. If the impact is at an angle θ with the normal then these values are modified according to the equations (4-1) and (4-2).

$$V_{\max}(\theta) = V_{\max}(0) * (1 + k_{sv}/2\pi) \tag{4-1}$$

$$\delta_{\max}(\theta) = \delta_{\max}(0) * (1 + k_{s\delta}\theta^2/2\pi) \tag{4-2}$$

Where k_{sv} and $k_{s\delta}$ *are* the separate smoothness factors for V and δ. These factors could have higher values for smoother and lower for dull surfaces. A value 2.0 is assigned for exceptionally smooth surface and a lower than 1.0 value for deliberately roughened surface. Generally both are assigned a default value 1.0 for a typical rough surface, which is common inside the microwave tube.

Now these modified values are used to find out the value of delta, which depends upon the primary energy and the angle of incidence. The empirical formulas derived by Vaughan are shown below [9]:

$$v = \frac{V_i - V_0}{V_{\max}(\theta) - V_i} \tag{4-3}$$

with

$$\delta_\theta = \delta_{\max}(\theta) * (ve^{1-v})^k \tag{4-4}$$

$$k = k_1 = 0.56 \qquad \text{for } v < 1 \tag{4-5}$$

$$k = k_2 = 0.25 \qquad \text{for } 1 < v \leq 3.6 \tag{4-6}$$

$$\delta_\theta = \delta_{\max}(\theta) * 1.125 / v^{0.35} \qquad \text{for } v > 3.6 \tag{4-7}$$

where, V_0 is the impact voltage at which any secondary electron will be generated and it is assumed as 12.5 V; V_i is the impact voltage and θ is the direction of impact relative to the surface normal (in radians). Figure 4-6 shows the variation of secondary electron emission yield with the variation of impact voltage keeping the impact direction θ constant. It is seen from the plot that as the impact angle increases for a particular incident energy the secondary electron emission yield also increases. In this case we have assumed V_{max} = 600 V for δ_{max} = 1.5. Experimental values for V_{max} and δ_{max} are not available for different materials. New research is necessary to find out these values for the materials, which can be used for fabrication of MDCs.

The above equations consider only the slow secondary electrons and they have been used to find out the value of yield for slow secondary electrons in the present model. Finally this value has been used to calculate the secondary electron current.

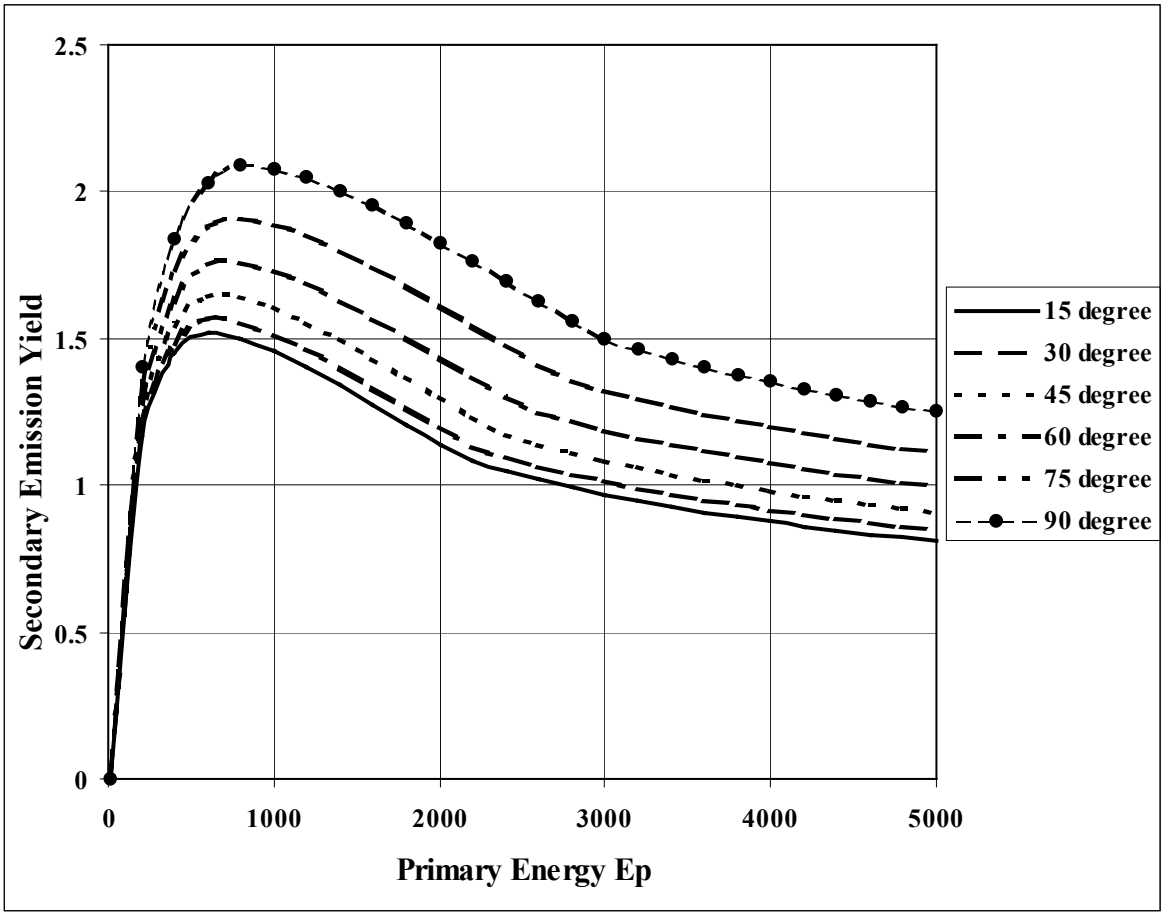

Figure 4-6: Plot of secondary electron emission yield (δ) vs primary energy (E_p) for different impact angles.

The curves were computed from the equations as derived by Vaughan using Vmax = 600 V and $\delta max = 1.5$.

4.3 SECONDARY ELECTRON EMISSION - A REVIEW

The effect of secondary electron emission on MDC performance has been studied by several researchers since 1970s. In early days scientists used 2-D models to represent the secondary electrons due to the following reasons:

(a) The lack of computer resources
(b) Only axi-symmetric collectors were investigated

In some of the cases the effect of secondaries in the MDCs was estimated due to the lack of a proper simulator and the non-availability of the experimental data on the properties (e.g., secondary electron emission yield, surface smoothness etc.) of different materials. Mostly all collectors, used in present days, are symmetric and a 2-D package can simulate them if the external magnetic field is axi-symmetric or no magnetic field is applied in the collector region. Still scientists prefer to use a 3-D computer code for better understanding of the characteristics of both primary and secondary trajectories. Sometimes an asymmetric magnetic field in the collector region may be helpful in reducing the back streaming of secondary electrons, which in turn improves the collector efficiency by collecting the secondaries on the electrode where they were generated. In that case a 2-D code is not suitable to evaluate the effects of magnetic field in the collector. Instead a 3-D computer code can be a good choice to simulate the collectors in all conditions. Different approaches taken by several researchers to model the secondary electron emission effects in MDCs have been discussed in the following section. It was a common practice in 1970s to roughen the surface of the electrodes or coat them with some low secondary electron emission co-efficient materials even though the effects of secondary electron emissions were not accurately quantified. More research has revealed that if the collector is made of the materials with low secondary electron emission co-efficient then the improvement in collector efficiency is higher than in the previous case. A study on the characteristics of different materials and their usefulness as collector electrode material is presented later in this chapter.

4.3.1 Different Models of Secondary Electron Emission

The performance of 2- and 4-stage axi-symmetric collectors with the effect of secondary electron emission was analysed using computer programs and experimentally verified by H. G. Kosmahl et al [11]. The secondary electron yield was assumed to be one half (with

no reflected primaries), for the purpose of this computation, for impinging on the "lower" sides and cone, and zero for impacts on the "upper" sides. “Upper” side of the collector is defined as the side looking away from the tube output where as the “lower” side is the side toward the tube. According to the authors this approximation is optimistic in view of the experimental results and theoretical evaluation.

The axi-symmetric collector and TWT performances were evaluated by multidimensional computer programs and were experimentally verified at NASA Lewis Research Center by J. A. Dayton, Jr., et al [12]. Here the effects of secondary electrons were estimated and it was assumed that all electron impacts on the MDC electrodes generated low-energy secondaries (yield, $\delta=1/2$ for carbon black). The local field was used as the determining factor for the acceleration or suppression of the secondaries. The experimental and theoretical evaluations were carried out for three different 5-stage collectors.

P. Ramins et al verified the performance of a 200 W, 8 - 18 GHz TWT using a multidimensional computer program including the effects of secondary electron emission losses [13]. The secondary electron emission losses in the MDC were treated semi-quantatively by injecting a representative beam at the point of impact of each primary with the electrode surface. Here the slow secondary electrons were injected back along the angle of incidence (the most probable angle in some cases) in the amount I_i $(0.4 + 0.2\ \theta^2)$, where θ is the angle of incidence in radians and I_i is the incident current. The elastically reflected primaries were injected at the equal angle of incidence and the loss due to these electrons was not quantified due to the lack of appropriate data.

MAFIA, which solves the MAxwell’s equations by Finite Integration Algorithm, was used as a tool by R. T. Benton et al to simulate the multistage collector in 3-D for a KU-band helix TWT at Hughes Electron Dynamic Division (HEDD) and NASA Lewis Research Laboratory. In this case the secondary electrons were simulated by in-house developed 2-D program (three dimensional velocity vectors) [14]. According to the authors, MAFIA can be used to simulate the secondaries but it takes much of CPU time.

Results of 2-D simulations of secondary electron emissions were presented in the paper. The details about the secondary electron emission model have not been discussed.

The UGUN program was used to simulate an axi-symmetric 5-stage collector at Raytheon Corporation and the results of the experimental collector were presented by T. M. Antonsen, Jr. et al [6]. The UGUN program was modified based on the Vaughan algorithm [9] and the angular distributions of secondary electrons developed by Jonker [4] to incorporate the secondary electron emission effects. Simulated results have shown that the overall tube efficiency is reduced by 26% points due to the effect of secondary electron emission, which is in good agreement with the experimental results. The theory of the back-scattered algorithm is still less established due to the lack of proper data [6].

A detailed study of the behaviour of secondary electrons in TWTs was carried out by D. J. Ferretti at the University of Utah [5]. A 2-D model of secondary electron emission was developed based on the Jonker's experimental results [4].

In all the above cases the simulation or computation was carried out on multistage axi-symmetric collectors and secondary electron emission was modelled in 2-D. The first 3-D simulation of secondary electron emission in an asymmetric collector was presented by L. Kumar et al [17]. Only one slow secondary electron was considered to be emitted per primary in the direction of the normal to the surface at the point of collision of the primary electron and the electrode surface. No fast secondary electron was included in the secondary electron emission model. Space charge of the secondaries was also not considered for the simulation purpose.

The characteristics of the elastically scattered secondary electrons were studied experimentally by K. R. Vaden et al., at NASA Lewis research Lab, for different materials and this data was used for the simulation of an MDC [15], [16]. None of these publications present anything quantitatively about the backscattered primaries.

A 3-D finite element simulator developed at the University of Catania by S. Coco et al [19] was used to simulate the same asymmetric collector as the one in [17]. The secondary electron emission model has considered only one secondary electron per primary to be emitted in the direction of the surface normal. Users can select the secondary electron energy among the three different values depending upon their requirements. The current carried by each secondary electron is determined from the incident angle of the primary trajectory.

Secondary electron emission has been modelled in MICHELLE (3-D electron beam design tool) by J. Petillo et al at Scientific Application International Corporation (SAIC) to simulate the MDC [18]. The simulated results have been presented for a 4-stage symmetric collector including the effects of symmetric collectors. The simulated results are within the acceptable limit of the experimental results. Both true and backscattered secondaries have been modelled in the package. The slow secondary electron emission yield is derived from the incident energy and angle of inclination. The emission energy and the angular distribution are calculated from the modified Maxwellian distribution. Backscattered secondary electron emission is based on the reconstruction of 3-D angular distribution from the two transverse 2-D probability distribution. This package has been developed with the support of the Office of Naval Research and is not available for all.

Mostly all of the secondary electron emission models use 2-D models. Very few of these packages use 3-D models for the simulation of secondaries in asymmetric collectors. Only two packages have been used to simulate the secondary electrons in asymmetric collectors but in both cases the secondary electron emission model is quite approximate. They do not consider any distribution of secondary electrons and the secondaries are emitted only in the direction normal to the surface. Some of the packages described above are also not available for general use. To overcome all these limitations a fully 3-D secondary electron emission model has been developed by this author based on KOBRA (MF) [20]. Both axi-symmetric and asymmetric collectors have been simulated using this package. Simulated results of asymmetric collectors have been compared with the experimental values and they are in good agreement. The effect of secondary electron

emission on the performance of MDCs has been investigated and published in [21]. The detail about the secondary electron emission model is described later in the next section.

4.3.2 Secondary Electron Emission Suppression Techniques

The most commonly used material for collector electrodes is OFHC (Oxygen Free High Conductivity) copper for its high thermal and electrical conductivity and ease of fabrication. But the disadvantage of this material is that it has a very high secondary electron emission co-efficient. Different methods are adopted by researchers to suppress the secondary electron emissions in MDCs. Application of a thin coating of titanium carbide by sputtering technique on the copper surface has shown to reduce the secondary emission moderately [22]. If the copper surface is subjected to ion bombardment under proper conditions then a highly textured copper surface is formed which is capable of reducing the secondary emission more efficiently than the above method [23]. Though the secondary electron emission is reduced significantly by the above two methods, even lower emission of secondary electrons is desired for high efficiency MDCs. Experimental results have shown that graphite and carbon, which have low secondary electron emission properties, can be used as electrode materials to suppress the secondary electron emission successfully to a significant level. Thus carbon and carbon-coated materials are highly attractive as the electrode materials for high efficiency TWTs [24]. Pyrolytic graphite and high purity isotropic graphite can be used as electrode materials due to its low secondary electron emission properties. The already low secondary electron emission properties can be lowered further by ion-texturing the electrode surface [16]. Properties of ion-textured graphite and textured, carbon coated copper have been experimentally evaluated and shown as the potential material for electrodes in MDCs.

Investigations were carried out by P. Ramins and B. T. Ebihara on different type of graphite materials for their possible use as electrodes. Isotropic graphite (POCO graphite), pyrolytic graphite and ion-textured isotropic graphite were used as the electrode materials and the collector performance was experimentally evaluated. The experimental

results show dramatic improvement in MDC and TWT overall efficiency. The average tube and collector performance across the operating band at saturation for the various collector electrode surfaces is summarised in Table 4-1 [25]. Experimental results have shown that with proper MDC design and the use of low secondary electron yield carbon material the degradation of the collector performance can be reduced to a few percent.

Table 4-1: Summary of average TWT and MDC performance across 2.5 to 5.5 GHz operating band at saturation (optimised at saturation at 4.75 GHz) [25]

MDC electrode characteristics	***Four stage collector***		***Three stage collector***	
	η_{col} *(percent)*	η_{ov} *(percent)*	η_{col} *(percent)*	η_{ov} *(percent)*
Carbon black	76.7	46.2	74.4	44.7
Textured isotropic graphite	76.4	46.0	74.5	44.7
Bead-blasted isotropic graphite	74.9	45.0	73.0	43.7
Pyrolytic graphite	74.8	44.9	72.7	43.5
Machined isotropic graphite	74.3	44.5	72.4	43.2
Copper	66.5	39.9	64.9	39.1

A few measures can be taken other than choosing the electrode materials to suppress the secondary electrons and hence reduce the loss in collector and overall tube efficiency. An application of a retarding electric field at the regions where the slow secondary electrons are generated helps to suppress the secondaries. The primaries should land on the lowest depressed potential at a very low incident angle, which will reduce the secondary electron emission yield and hence the secondary electron emission current. The primaries hitting on the "lower" surface of the electrode or on the inner apertures produce more

secondaries and backscattered primaries. A spent beam refocusing section in between the output coupler and the collector can be used to dilute the space charge forces and reduce the transverse velocity components of the beam. This magnetic refocusing section helps in achieving optimum collector efficiency [26]. If proper measures are taken as mentioned above then it is possible to achieve high collector efficiency with low secondary electron emission.

4.4 MODEL OF SECONDARY ELECTRON EMISSION EFFECTS

The effect of secondary electron emission has been included in the post-processor of the package LKOBRA (MF). The secondary electron emission current generated from different primary electrons is different and has to be considered for the simulation purpose. But the original version of the package deals with equal current for each trajectory. Thus it was necessary to modify the trajectory solver and the input data file format to incorporate different current for different trajectories. Details about the modifications carried out on the input data file format are described in [20].

To simulate the MDCs, the trajectory solver is run initially with primary trajectories. The starting conditions of the secondary trajectories are generated from different parameters of the primary trajectories. The logic to generate the starting conditions of the secondaries is described below.

The positions, velocities and energies of the last two points of each trajectory are read from the primary trajectory data file. The mesh information is read from the mesh data file. The translated geometry information and the potential number of mesh points of the electrodes are read from another data file.

- *Surface normal*

With this information the co-ordinates of eight corners of a cube are found which contains the end point of the trajectory. One such cube is shown in Figure 4-7 (a) where the part of

the cube shaded in light grey represents metal. Rest of the cube is in vacuum. The trajectory vector MN strikes on the metal surface PQRS (deep grey) inside the mesh cube. Some of the corner points of the cube are eliminated which are in the vacuum. The corner points, (here A, B, C and D) which lie inside the electrode with respect to the direction of the trajectory, are also eliminated. It is decided on the basis of the geometry information and the potential values of the corner points. Rest of the corner points are stored to find out the equation of a surface where the primary trajectory hits. In this case, the points E, F, G and H are in the vacuum but they carry the information about the points P, Q, R and S respectively. Therefore these corner points are stored to find out the equation of the surface PQRS where the trajectory hits. Another example is shown in Figure 4-7(b) where the corner points A1, A2, A3, A4 are on the metal surface and they coincide with the edge of the cube. As the trajectory X1X2 hits the metal surface A1A2A3A4, a surface equation can be written from these points and the other four corners of the cube should be eliminated.

A surface normal vector is computed for each surface equation. Another vector is formed with the last two points of the trajectory, which is called the trajectory vector. The angle between the trajectory vector and the surface normal is called the incident angle. From this incident angle the direction of the normal is modified such that the surface normal is always outward to the surface. If the incident angle between these two vectors is less than 90^0 then the direction of normal is towards the surface of the electrode and it is reversed by 180^0 to make it outward to the surface.

- *Angle of emergence*

It is assumed that five slow secondary electrons and one fast secondary electron are emitted at the point of intersection between the trajectory vector and the surface of the electrode. Among the five slow secondary electrons one is emitted in the direction of surface normal. The rest are at an angle of 45^0 with the surface normal and with an angular spacing of 90^0 between them. The fast secondary electron is emitted at an angle equal to the 2/3 of the incident angle. Directions of the secondaries and the reflected

primary are assumed from Jonker's experimental results [4]. The angles of emergence of slow and fast secondary electrons are shown in Figure 4-8.

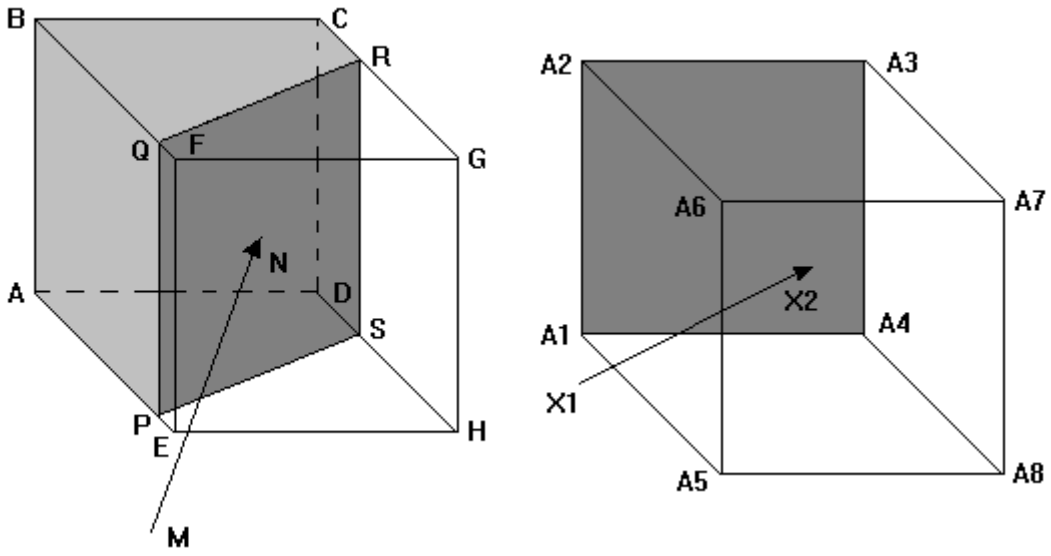

(a) (b)

Figure 4-7: End point of the trajectory in a cube (a) striking surface inside the cube (b) striking surface at the edge of the cube

- *Secondary electron current*

Secondary electron emission yield is defined as the ratio of secondary electron current to the primary current. It is necessary to know the value of secondary emission yield and the primary current to calculate the secondary electron current. This is done in following three steps. In the first step the maximum secondary electron emission yield and the corresponding maximum potential at which this occurs are modified according to the incident angle of each primary trajectory. Equations 4-1 and 4-2 are used to modify these values. The secondary electron emission yield is calculated in the second step from the above values and the impact energy of the primary trajectory. Equations 4-3 to 4-7 are

used to compute the secondary electron emission yield for different primary energies and different incident angles. Finally, the secondary electron current for each trajectory is calculated from the yield and primary current.

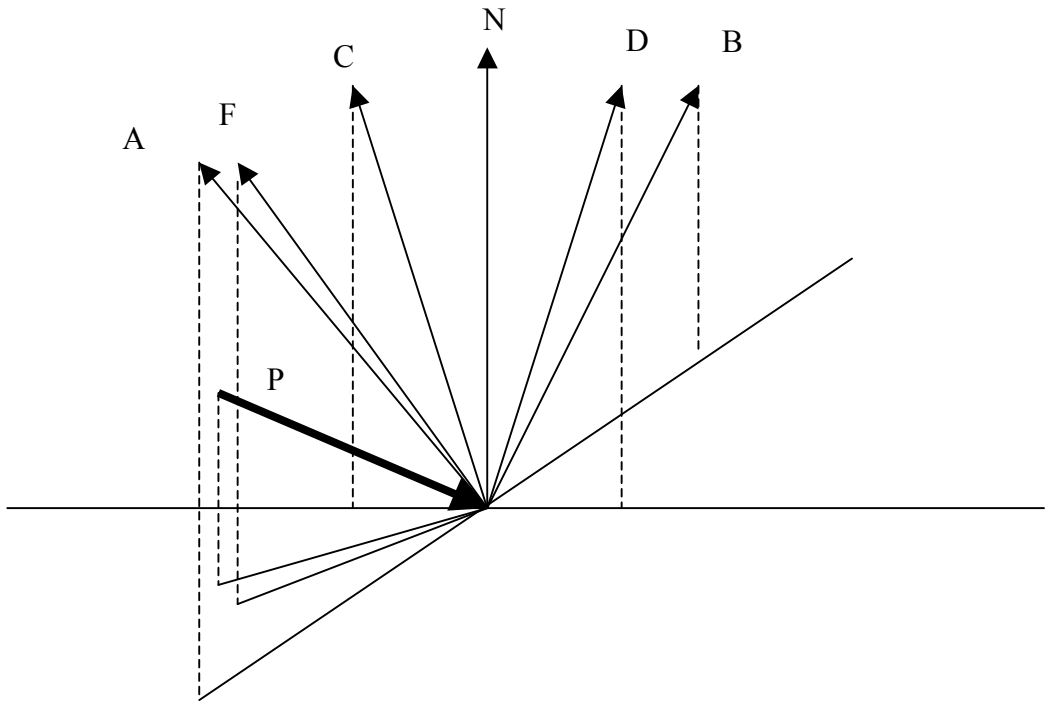

Figure 4-8: Secondary electrons emitted from a single primary electron

P: the primary electron

N: surface normal (direction of one slow secondary)

A, B, C, D: slow secondary electrons (angle between N and A, N and B, N and C, N and D all are 45^0 but the angle between A, B, C and D is 90^0)

F: fast secondary (angle between F and N is 2/3 of the angle between P and N)

- *Secondary electron energy and velocity*

One of the starting conditions of the secondary trajectories is the velocity and it is calculated from the energy. Total slow secondary electron energy is assumed to be 50 eV and it is distributed among five electrons each having energy equal to 10 eV. The velocity of each slow secondary electron generated from a particular primary electron is assumed to be same and it is calculated form the above energy. The kinetic energy at the last point of the primary trajectory is computed to find the energy of the fast secondary electron. Theoretically the energy should be same as the kinetic energy of the primary electron as per the definition of fast secondaries. The probability of any primary being reflected elastically reduces with the increase in primary energy. We have assumed this value as 0.1. An equivalence of this is taken as 1/10 th of the primary current for all primary trajectories which means all primaries will produce a fast secondary with 10% of the primary current. The velocity of the fast secondary electron is calculated from the energy of the primary trajectory. Now the components of these velocities are taken in the direction of emergence of the secondary electrons.

- *Starting position*

The starting position of the secondary electrons is the point of intersection of the trajectory vector with the surface normal. The starting conditions of each secondary i.e., positional co-ordinates, velocity components in all three directions and the current are computed using the model described above. Finally these data are stored in the secondary starting data file in a format suitable for the simulator.

- *Assumptions in the model and its validation*

The following assumptions have been made in this model:

- Energy of the slow secondary electrons is irrelevant
- Current of the fast secondary electrons is irrelevant

These two assumptions have been checked by two separate experiments. These experiments have been carried out for the TEF collector as shown in Chapter 3. In the

first case the energy of each of the slow secondaries is varied from 10 eV to 75 eV and the collector performance is evaluated. The efficiency of the collector varies within 2% points except in a very few places as shown in the Figure 4-9. It is observed from the plot that the collector efficiency is minimum at 10 eV. In our model we have used this value as a conservative choice.

In the second case the current of the fast secondary is varied from 5% to 50% of the primary current to evaluate the collector performance. In Figure 4-10 the collector efficiency versus the fast secondary current is plotted. The fast secondary current is assumed as a fraction of the primary current and it is constant for a specific run. A considerable fraction of the primaries is reflected at energies below 10 eV, but as the primary energy increases the number of reflected electrons is reduced. For primary energies at about 100 eV only 10% of the electrons are reflected [1]. This value is further reduced with the increase of the primary energy. In the present example it was seen that if the fast secondary electron current is increased from 10% of the primary current to 20% of the primary current then change in collector efficiency is within 3% points. Therefore we have assumed the fast secondary current to be 10% of the primary current.

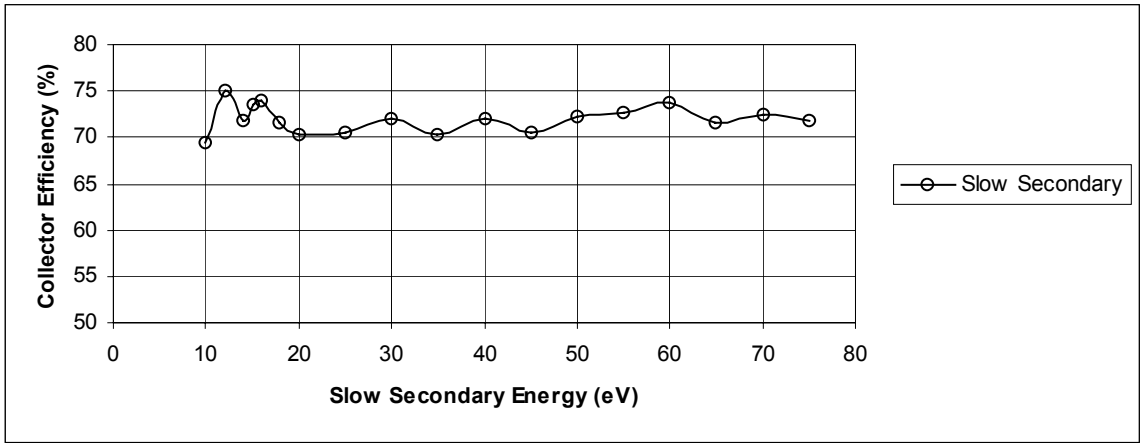

Figure 4-9: Variation of collector efficiency with slow secondary energy

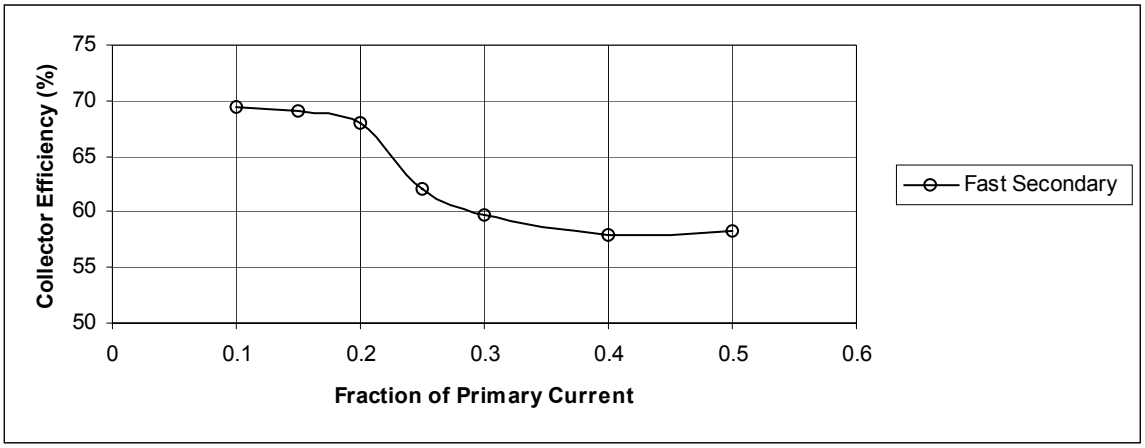

Figure 4-10: Variation of collector efficiency with fast secondary current

4.5 EFFECTS OF SECONDARY ELECTRONS ON MDC

A fully 3-D model has been developed to simulate the secondary electron emission and to find its effects on the collector performance [21]. This package has been used to simulate the secondaries in the asymmetric TEF collector. The geometry and simulated results have been discussed in the previous chapter. Here the effect of secondaries on collector performance has been described in detail.

4.5.1 Secondary Electrons According to Energy

A series of plots of secondaries according to the energy is shown in Figures 4-11(a) – (c) to show their effects on the MDC performance. Primaries with different energy class have been plotted in Figure 3-11(a) – (c) in Chapter 3. Here the same group of primaries and their corresponding secondaries are superimposed on the same plots in Figures 4-11(a)-(c). In all these cases the space charge of both primary and secondary electrons is considered. A transverse magnetic field as mentioned in Chapter 3 is applied.

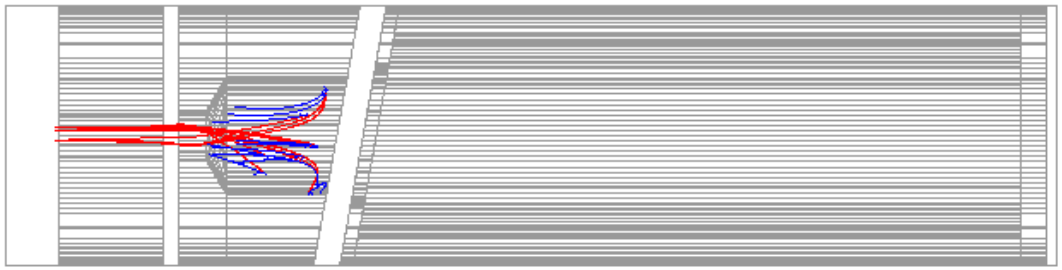

(a)

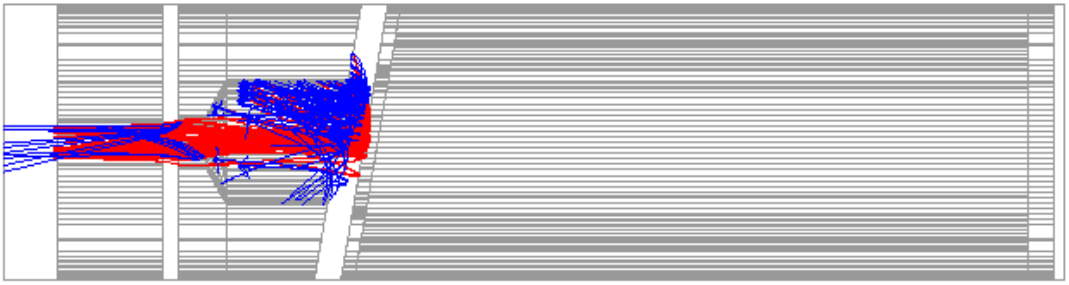

(b)

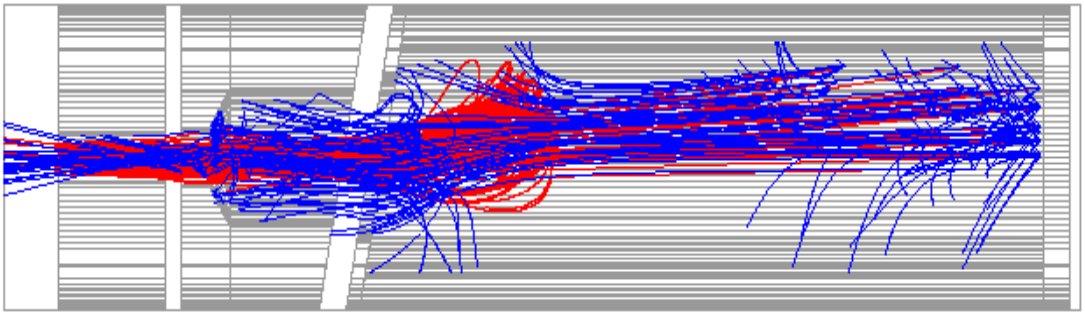

(c)

Figure 4-11: Primary and secondary trajectories according to their energy (a) between 0 and 2640 eV (b) between 2640 and 3120 eV (c) between 3120 and 6000 eV

It is observed from this set of plots that secondary trajectories generated from the primaries with energies between 2640 eV and 3120 eV stream back towards the interaction region, which should be avoided to reduce noise level in the signal. Another group of secondaries generated from the primaries with energies between 3120 eV and 6000 eV are collected at a higher potential compared to the potential where they are generated causing degradation of the collector efficiency. Some secondaries are collected at the same electrode (in all three cases) where they are generated. These electrons do not contribute for any reduction in collector efficiency. The plots are useful to identify a specific group of primaries and corresponding secondary trajectories, which affect the collector performance most. Based on the observations the collector geometry and the potentials can be altered for fine-tuning of its performances.

4.5.2 Comparison of Theoretical Results Without and With Secondaries

To quantify the effect of secondary electron emission, the MDC performance has been evaluated for two different cases. In the first case the collector has been modelled without any secondary electrons. In the second case the space charge of both primary and secondary electrons have been considered. The computed results are shown in Table 4-2. It is not possible to suppress the secondaries totally in the practical case. So the comparison between the theoretical and practical results of the TEF collector without the secondaries is not possible. However the computed results are in good agreement with the practical results when the secondaries are included as shown in Chapter 3. It is observed from the table that the back streaming current and power have been increased from 0.6 mA to 3.9 mA and from 2.09 W to 6.20 W respectively. A comparison between the computed results with and without secondaries shows that the collector efficiency is reduced by 9.5% points if the effects of secondaries are considered. No magnetic field has been applied in the present simulation.

Table 4-2: Computed Results of the TEF Collector without magnetic field

QUANTITY	PRIMARIES ONLY	WITH SECONDARIES
Total Power Entering the Collector	190.04 W	190.04 W
Back Streaming Current	0.6 mA	3.9 mA
Current at Body	0.3 mA	1.8 mA
Current at Stage 1	32.0 mA	32.8 mA
Current at Stage 2	20.3 mA	14.8 mA
Power Recovered at Stage 1	76.74 W	78.68 W
Power Recovered at Stage 2	73.25 W	53.11 W
Power Dissipated at Body	0.9 W	2.02 W
Power Dissipated at Stage 1	24.43 W	27.76 W
Power Dissipated at Stage 2	12.60 W	22.24 W
Back Streaming Power	2.09 W	6.20 W
Total Power Recovered	150.0 W	131.80 W
Total Power Loss	40.03 W	52.03 W
Collector Efficiency	**78.9 %**	**69.4 %**

4.5.3 Space Charge Effect of Secondaries on MDC Performance

The effect of space charge on the MDC performance has been investigated and the computed results are shown in Table 4-3. In the first case the simulator is run through several iterations for the primaries only. When the steady state is achieved, the secondary electrons are generated and run only once to avoid the effects of secondary electrons. So no space charge effect due to the secondaries has been considered. In the second case the space charge effect of the secondaries has been considered for the steady state solution. In both cases the secondary electrons are considered while computing the collector parameters. It is observed from the table that the currents at different electrodes and the power recovered at each stage have been changed significantly though the efficiency of the collector remains nearly the same. Primaries without and with the space charge effects of secondaries are plotted in Figures 4-12(a) and (b) respectively. In the second plot, the number of back streaming primaries has been increased as the space charge effects of the secondaries has been considered in the system.

Table 4-3: Computed Results of the TEF Collector without magnetic field

QUANTITY	WITHOUT SECONDARY SPACE CHARGE	WITH SECONDARY SPACE CHARGE
Total Power Entering the Collector	190.04 W	190.04 W
Back Streaming Current	4.2 mA	3.9 mA
Current at Body	3.9 mA	1.8 mA
Current at Stage 1	24.7 mA	32.8 mA
Current at Stage 2	20.3 mA	14.8 mA
Power Recovered at Stage 1	59.4 W	78.68 W
Power Recovered at Stage 2	73.25 W	53.11 W
Power Dissipated at Body	0.9 W	2.02 W
Power Dissipated at Stage 1	41.66 W	27.76 W
Power Dissipated at Stage 2	12.60 W	22.24 W
Back Streaming Power	2.17 W	6.20 W
Total Power Recovered	132.65 W	131.80 W
Total Power Loss	55.21 W	52.03 W
Collector Efficiency	**69.8 %**	**69.4 %**

4.5.4 Effect of Magnetic Field on Secondaries

The computed results with and without the magnetic field are compared in Table 4-4(a) and (b). A transverse magnetic field of 8 Gauss is applied to see its effects on MDC performance. In Table 4-4(a) the computed results are shown considering only the primary trajectories. This is an ideal case when there is no secondary electron in the collector. It is observed from the table that the collector efficiency is reduced by nearly 0.5% points due to the application of the transverse magnetic field. This shows that the primaries remain nearly unchanged even if a transverse magnetic field is applied in the collector region. In Table 4-4(b) the computed results are shown considering both primaries and secondaries. An improvement in collector efficiency of 2.3% points is achieved when the magnetic field is applied. The back streaming current and the power is also reduced because of the transverse magnetic field. This result is quite significant for the tubes used in communication and radar systems.

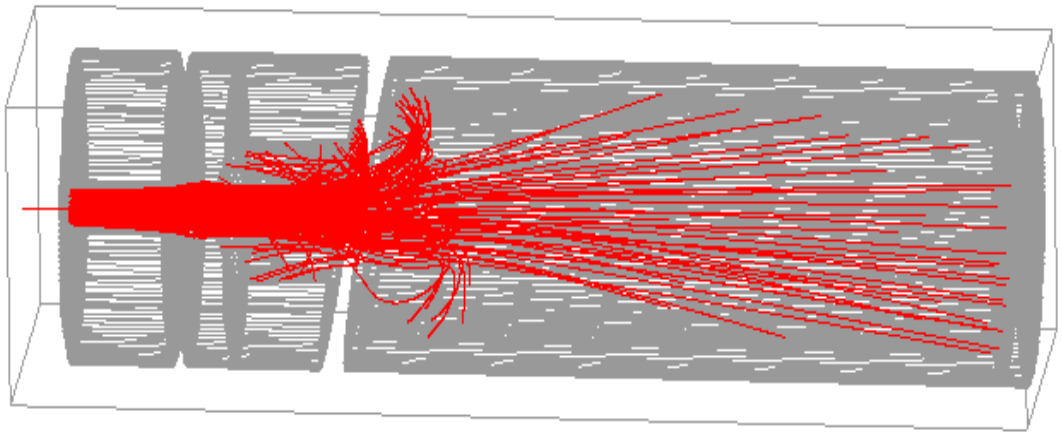

(a)

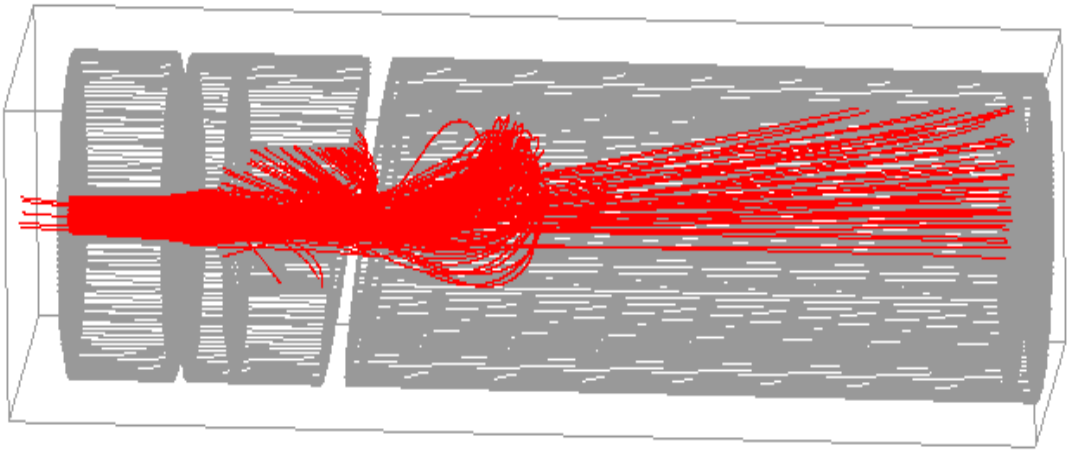

(b)

Figure 4-12: Primary trajectories in a TEF Collector without magnetic field (a) without secondary electron space charge (b) with secondary electron space charge

Table 4-4(a): Effect of magnetic field on the TEF Collector (only primaries considered)

QUANTITY	COMPUTED VALUE (without magnetic field)	COMPUTED VALUE (with magnetic field)
Total Power Entering the Collector	190.04 W	190.04 W
Back Streaming Current	0.6 mA	0.3 mA
Current at Body	0.3 mA	0.3 mA
Current at Stage 1	32.0 mA	33.7 mA
Current at Stage 2	20.3 mA	18.9 mA
Power Recovered at Stage 1	76.74 W	80.93 W
Power Recovered at Stage 2	73.25 W	68.02 W
Power Dissipated at Body	0.9 W	0.90 W
Power Dissipated at Stage 1	24.43 W	26.80 W
Power Dissipated at Stage 2	12.60 W	12.32 W
Back Streaming Power	2.09 W	1.05 W
Total Power Recovered	150.0 W	148.96 W
Total Power Loss	40.03 W	40.03 W
Collector Efficiency	**78.94 %**	**78.38 %**

Table 4-4(b): Effect of magnetic field on the TEF Collector performance (both primaries and secondaries are considered)

QUANTITY	COMPUTED VALUE (without magnetic field)	COMPUTED VALUE (with magnetic field)
Total Power Entering the Collector	190.04 W	190.04 W
Back Streaming Current	3.9 mA	3.5 mA
Current at Body	1.8 mA	1.7 mA
Current at Stage 1	32.8 mA	30.5 mA
Current at Stage 2	14.8 mA	17.5 mA
Power Recovered at Stage 1	78.68 W	73.16 W
Power Recovered at Stage 2	53.11 W	63.13 W
Power Dissipated at Body	2.02 W	1.01 W
Power Dissipated at Stage 1	27.76 W	31.55 W
Power Dissipated at Stage 2	22.24 W	15.77 W
Back Streaming Power	6.20 W	5.39 W
Total Power Recovered	131.80 W	136.29 W
Total Power Loss	52.03 W	48.35 W
Collector Efficiency	**69.4 %**	**71.7%**

The primaries under the influence of a transverse magnetic field are plotted in Figure 4-13. It is observed from this figure that some trajectories, which were collected at the second stage when there was no magnetic field (Figure 4-12(a)), bend under the influence of the magnetic field and repulsed to the first stage where they are collected. This reduces the current and power at the second stage and increases the same at the first stage. The results in Table 4(a) correspond to the plots in Figures 4-12 (a) and 4-13 respectively.

The secondaries under the influence of magnetic field have been plotted in Figure 3-12(b) in the previous chapter. That plot has been reproduced here in Figure 4-14. To study the effect of the magnetic field a similar plot of the secondaries is shown in Figure 4-15 where no magnetic field has been applied in the modelling. A careful observation shows that the secondaries have bent towards the collector walls (away from the axis) under the influence of the magnetic field and a significant number of them have been collected on the same electrode. This has reduced the number of secondaries being collected at a higher potential compared to the potential where they have been generated. At the same time the number of secondaries streaming back has also been reduced.

4.6 SUMMARY

Some basic terms have been defined at the beginning of the chapter. A literature review on different secondary electron emission models has been carried out and the findings are presented. A fully three-dimensional secondary electron emission model has been developed as an integral part of the package LKOBRA (MF). It is based on the experimental results of Jonker and the empirical formula developed by Vaughan. This model considers the effects of both slow and fast secondary electrons. The model has been discussed in detail. Using this model the effect of secondary electrons in an asymmetric 2-stage TEF collector has been investigated. The reduction in collector efficiency is nearly 10% points due to the secondary electron emission. The effect of the secondary electron space charge and the transverse magnetic field on the multistage collector performance has also been investigated.

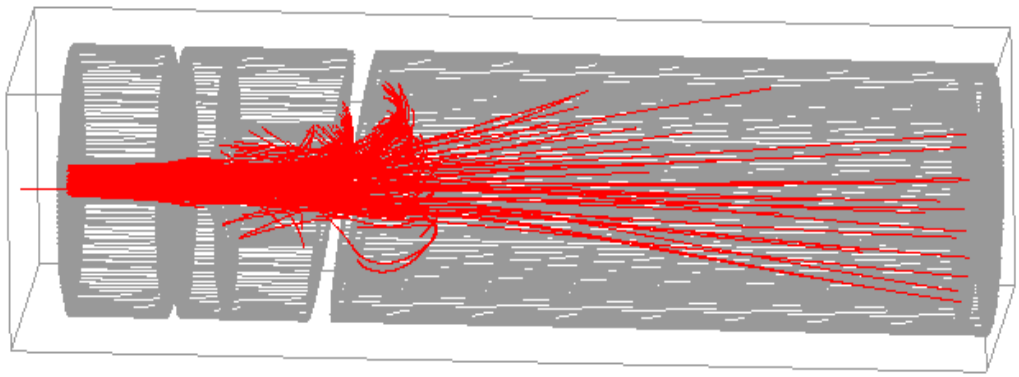

Figure 4-13: Primary trajectories in a TEF Collector with magnetic field

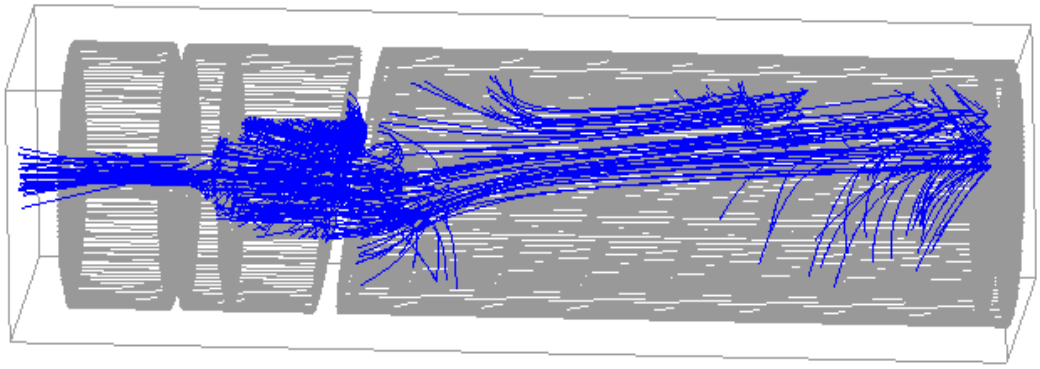

Figure 4-14: Secondary trajectories in a TEF Collector with magnetic field

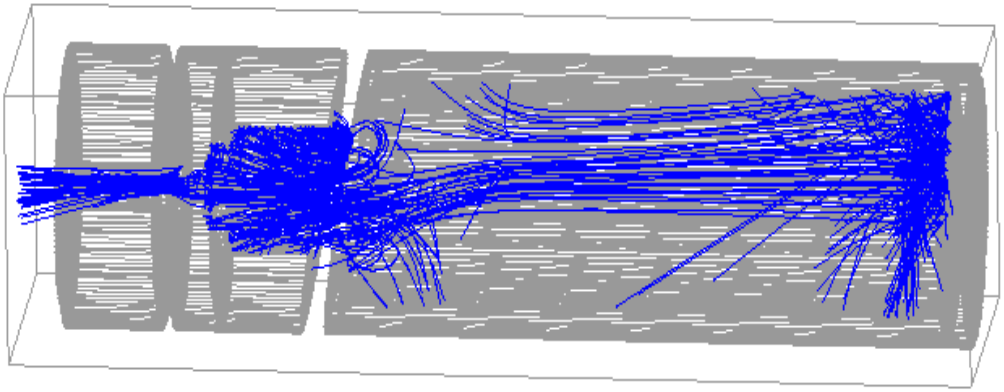

Figure 4-15: Secondary trajectories in a TEF Collector without magnetic field

REFERENCES

[1] A. J. Dekker, *Solid State Physics*, Mac Millan, 1963.

[2] T. Koshikawa and R. Shimizu, "Secondary Electron and Backscattering Measurements for Polycrystalline Copper with a Spherical Retarding Field Analyzer," *Journal Physics D: Applied Physics*, vol. 6, 1973, pp. 1369-1380.

[3] R. E. Kirby and F. K. King, "Secondary Electron Emission Yields From PEP-II Accelerator Materials," SLAC-PUB-8212, October 2000, pp. 1-10.

[4] J. L. H. Jonker, "The Angular distribution of the Secondary Electrons of Nickel," *Philips Research Report*, no. 6, 1951, pp. 372-387.

[5] D. J. Ferretti, "Development of a Dynamic Secondary Electron Emission Model for Use in MDC Simulation," Final Report, No. UTEC MD 86-064, University of Utah, April 1987.

[6] T. M. Antonsen et al., "Advances in Modeling and Simulation of Vacuum Electronic Devices," *Proceedings of the IEEE*, vol. 87, no. 5, May 1999, pp. 804-839.

[7] A. Singh et al, "Design of a Multistage Depressed Collector System for 1-MW CW Gyrotrons-Part I: Trajectory Control of Primary and Secondary Electrons in a Two-stage Depressed Collector", *IEEE Trans. on Plasma Science*, vol. 27, no. 2, April 1999, pp. 490-502.

[8] J. R. M. Vaughan, "A New Formula for Secondary Emission Yield," *IEEE Transactions on Electron Devices*, vol. 36, no. 9, September 1989, pp. 1963-1967.

[9] J. R. M. Vaughan, "Secondary Emission Formulas," *IEEE Transactions on Electron Devices*, Vol. 40, No. 4, April 1993, p. 830.

[10] A. Shih and C. Hor, "Secondary Emission Properties as a Function of the Electron Incidence Angle," *IEEE Trans. on Electron Devices*, vol. 40, no. 4, pp. 824-829, April 1993.

[11] H. G. Kosmahl and P. Ramins, "Small-Size 81- to 83.5-Percent Efficient 2- and 4-Stage Depressed Collectors for Octave-Bandwidth high-performance TWT's," *IEEE Trans. on Electron Devices*, vol. ED-24, no. 1, January 1977, pp. 36-44.

[12] J. A. Dayton, Jr., H. G. Kosmahl, P. Ramins and N. Stankiewicz "Analytical Prediction and Experimental Verification of TWT Depressed Collector Performance Using Multidimensional Computer Programs," *IEEE Transactions on Electron Devices*, vol. ED-26, no. 10, October 1979, pp.1589-1598.

[13] P. Ramins, H. G. Kosmahl, D. A. Force, R. W. Palmer and J. A. Dayton, JR., “Verification of an Improved Computational Design Procedure for TWT-Dynamic Refocuser-MDC Systems with Secondary Electron Emission Losses,” *IEEE Trans. on Electron Devices*, vol. ED-33, no. 1, January 1986, pp. 85-90.

[14] R. T. Benton et al., "Efficiency Improvements in KU-Band Space Helix travelling Wave Tubes," Presented in the ESA/NATO Workshop on Microwave Tubes for Space, Military and Commercial Applications, ESTEC, April 7-10, 1997.

[15] K. R. Vaden and I. K. Krainsky, "The characteristics and Modelling of Secondary Electrons Elastically Scattered From Collector Surfaces," in *Proceedings of IVEC 2000*, May 2-4, 2000, p2.9.

[16] K. R. Vaden, "New Models For Secondary Electrons Elastically Scattered From Copper And Isotropic Graphite Surfaces," in *Proceedings of IVEC 2001*, April 2001, pp. 271-272.

[17] L. Kumar, P. Spadtke, RG Carter and D. Perring, “Three-Dimensional Simulation of Multistage Depressed Collectors on Micro-computers,” *IEEE Trans. on Electron Devices*, vol. 42, no. 9, September 1995, pp. 1663-1673.

[18] J. Petillo et al., "The New 3D Electron Gun And Collector Modeling Tool: MICHELLE," in *Proceedings of IVEC 2001*, April 2001, pp. 199-204.

[19] S. Coco, Francesco Emma, Antonio Laudani, Sabrina Pulvirenti and Mirko Sergi, “COCA: A Novel 3-D FE Simulator for the Design of TWTs Multistage Collectors,” *IEEE Trans. on Electron Devices*, vol. 48, no. 1, January 2001, pp. 24-31.

[20] T. K. Ghosh and R. G. Carter, "3-D Simulation of Multistage Depressed Collectors for High Efficiency Space TWT - Progress Report 2," Report No. MRG/2001/1, January 2001.

[21] T. K. Ghosh and R. G. Carter, "The Effect of Secondary Electron Emissions in Multistage Depressed Collectors," in *Proceedings of PREP 2001*, April 2001, pp. 69-70.

[22] R. Forman, "Secondary-electron-emission properties of conducting surfaces with application to multistage depressed collectors for microwave amplifiers," NASA TP-1097, 1977.

[23] A. N. Curren and K. A. Jansen, "Secondary Electron Emission Characteristics of Ion-Textured Copper And High-Purity Isotropic Graphite Surfaces," NASA TP-2342, 1984.

[24] A. N. Curren, "Carbon and Carbon-Coated Electrodes for Multistage Depressed Collectors for Electron-Beam Devices - A Technology Review", *IEEE*

Transaction on Electron Devices, vol. ED-33, no. 11, November 1986, pp. 1902-1913.

[25] P. Ramins and B. T. Ebihara, "Improvement in MDC and TWT Overall Efficiency Through the Application of Carbon Electrode Surfaces", *IEEE Transaction on Electron Devices*, vol. ED-33, no. 11, November 1986, pp. 1915-1924.

[26] N. Stankiewicz, "Analysis of Spent Beam Refocusing to Achieve Optimum Collector Efficiency," *IEEE Transaction on Electron Devices*, vol. ED-24, no. 1, January 1977, pp. 32-37.

Chapter 5

Design Optimisation - Part I: Optimisation of Electrode Potentials

5.1 INTRODUCTION

It is necessary to optimise the collector performance for airborne and space applications where the weight and volume of the total system are extremely important. This can be done in three steps. At first, the number of electrodes is chosen according to the application and efficiency requirement of the collector. Sometimes a compromise in the efficiency is necessary to reduce the complexity in the fabrication. In the second step, the potentials of the electrodes are optimised based on a spent beam distribution curve that can be generated by a large signal model (LSM). The potentials are optimised to recover maximum power from the spent beam by forcing the electrons to land softly on the electrodes, which reduces the amount of heat generated in the collector by the bombardment of electron trajectories. Finally, the geometry of the collector is optimised through a number of iterations keeping the electrode potentials fixed. The efficiency of the collector for this optimised geometry is close to the theoretical maximum efficiency achieved through the optimisation of the collector potentials. In Chapter 6, the optimisation technique of collector geometry is discussed in detail.

In this chapter an approach is presented to optimise the number of electrodes and their potentials. Techniques to find the collector efficiency and the electrode potentials are described in sections 5.3 and 5.4. The features of the computer code developed are illustrated in section 5.5 and the algorithm is validated in section 5.6. This code is used in section 5.7 to choose a suitable number of electrodes for a specific collector. The sensitivity of the collector performance at different input drive levels is analysed in section 5.8. This chapter is concluded with a summary.

5.2 EFFECT OF ELECTRODE POTENTIALS ON COLLECTOR EFFICIENCY

In Chapter 2 it was shown that a multistage collector recovers more power than a single stage collector. It was assumed that the electrode potentials of the collector were optimised. A technique to optimise the collector performance is discussed here. Figure 5-1 shows the spent beam energy distribution and the potentials of a 4-stage collector. A designer has to choose the electrode potentials V_1, V_2, V_3 and V_4 on the curve such that the shaded area is maximised. This gives maximum collector efficiency for a specific number of electrodes.

To recover the power from the accelerating electrons in the spent beam it is necessary to have one or more electrode potentials lower than the cathode potential. With the conventional power supply it is not possible to have an electrode at a potential more negative than the cathode potential. In conventional power supply rectifiers are used which allow the flow of current only in one direction. If any electrode potential is more negative than cathode, then the flow of current will be in the reverse direction from the tube to the supply. So the power supply needs to allow the current to flow both ways. It is not known if it is possible to make such a supply, but the advantage of having one or more electrodes below the cathode potential is observed. In this chapter, the electrode potentials are optimised by choosing one or more electrode potentials lower than the cathode potential.

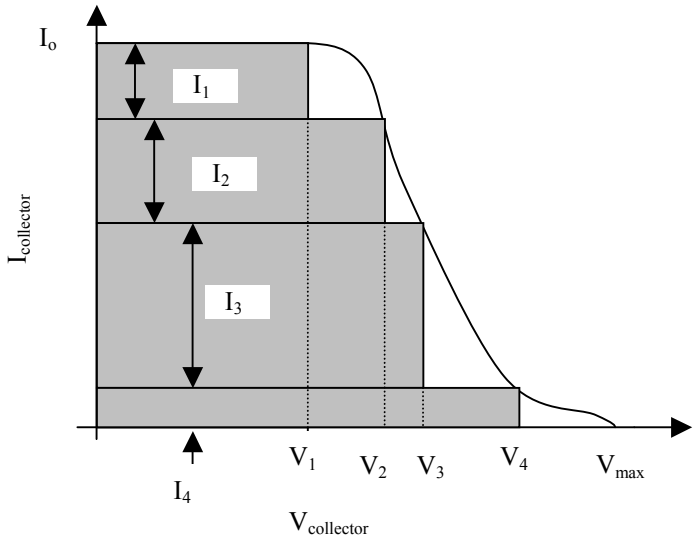

Figure 5-1: Electrode potentials of a 4-stage collector

5.3 HOW TO CALCULATE THE COLLECTOR EFFICIENCY

The collector efficiency can be calculated analytically using the formula presented by Kosmahl [1], but the efficiency of the collector is an "educated" estimate with some assumptions. A spent beam distribution curve and the assumptions are shown in Figure 5-2. In this case the true spent beam energy distribution curve $I(V)/I_o$ versus V/V_o is approximated as a triangular distribution and the potentials at different stages of the collector are placed in equal steps. These two assumptions are quite inaccurate.

A more accurate numerical method of predicting the collector efficiency is described here. A spent beam distribution curve is shown in Figure 5-3, which is used as an example for demonstration purposes. The normalised voltage (horizontal axis) and current (vertical axis) for the curve are discretised to form very small rectangular strips as shown in the figure. The area under the curve can be estimated as the sum of the rectangular strips and the triangular area between the adjacent strips. To calculate the total area of the curve, the rectangular area of the strips (OC_1CC_2, $C_2A_1AA_2$, $A_2B_1BB_2$ etc.) and the triangular area between the strips and the curve (CA_1A, AB_1B etc.) are added together. The total area under the curve computed in this way (calculated including the high energy tail) gives the total power remaining in the spent

beam. The method used for the purpose of integration is *Trapezoidal Rule*. In mathematical terms it can be expressed as

$$\int_{x}^{x+\Delta x} f(x)dx = \Delta x/2\left[f(x) + f(x+\Delta x)\right] \tag{5-1}$$

It is possible theoretically to recover all power from the spent beam if a large number of electrodes are taken with all possible electrode potentials. Therefore the theoretical maximum efficiency of the collector is 100%, though it is not possible to achieve this due to practical limitations.

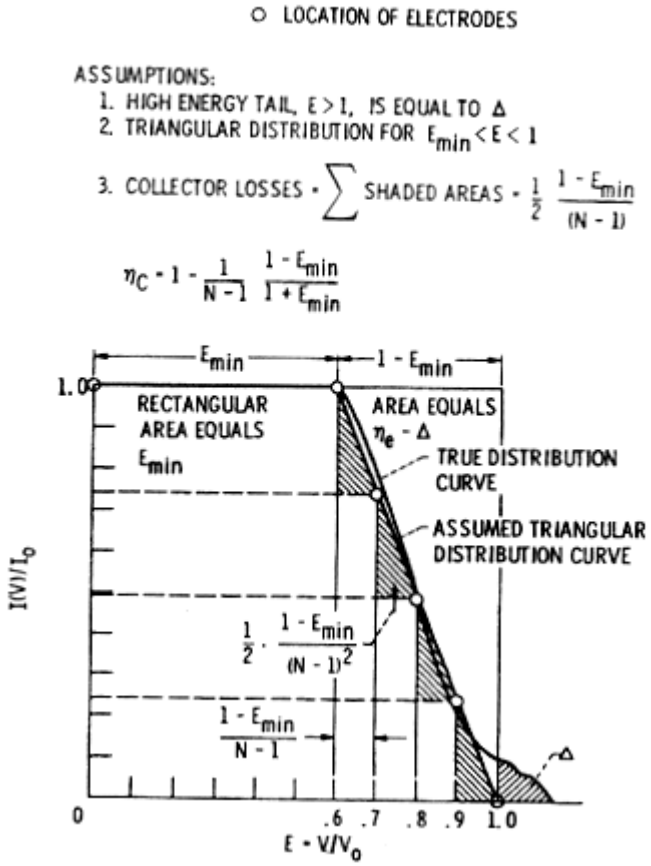

Figure 5-2: Derivation of the collector efficiency from the assumed triangular energy distribution curve [2].

To calculate the theoretical maximum efficiency of the collector the following assumptions are made:

- Collector electrodes are made of materials with a very low secondary electron emission co-efficient ($\delta << 1$) that makes the effect of secondary electron emission negligible.
- The connecting lines between the discrete points on the curve are straight lines e.g., the connecting line between A and B. This assumption is more accurate if the number of discrete points is increased so that the points become close.
- One or more electrodes are assigned potentials lower than the cathode potential.
- The body current of the tube is negligible.

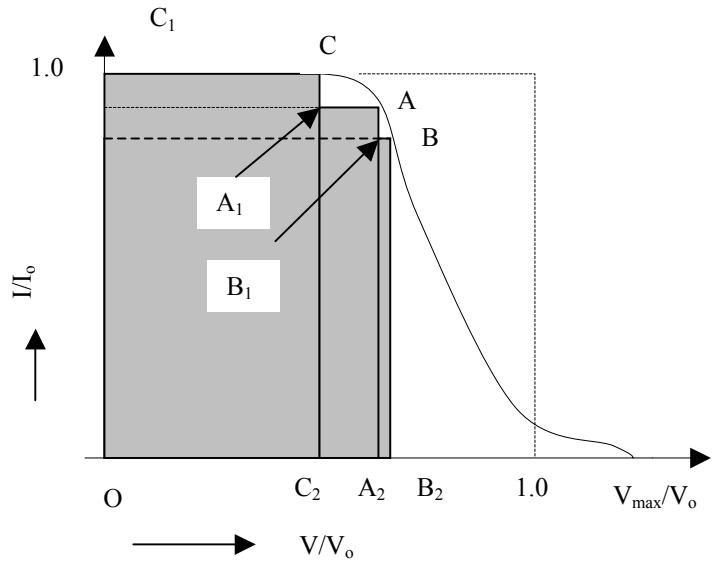

Figure 5-3: Plot of spent beam curve and discretisation

The above discussions assume that the collector has recovered all possible power from the spent beam. So to calculate the actual efficiency of any collector it is necessary to calculate only the area of those rectangular strips as shown in Figure 5-1 (depending on the electrode potentials).

5.4 HOW TO CHOOSE THE ELECTRODE POTENTIALS

To recover maximum power from the spent beam, the potentials of the collector electrodes should be selected in such a way that the area under the spent beam curve covered by these electrodes is maximised. Given the energy distribution *I(V)*, the energy recovered is

$$E(V_1, V_2 \ldots V_n) = \sum_{i=1}^{n} I(V_i)[V_i] \tag{5-2}$$

Where V_i is the potential of the i-th electrode

$I(V_i)$ is the current collected by the i-th electrode

n is the number of collector stages

The purpose is to maximise *E* by adjusting the values of V_i. An algorithm has been developed to choose the optimum potentials on the electrodes, which is shown in Figure 5-4. The first electrode potential is chosen at the knee of the spent beam curve (point C_2 in Figure 5-3). If the potential of the first electrode is increased beyond this limit, the slower electrons cannot reach the collector electrode and are repelled towards the interaction region; this increases the body current. Therefore the first electrode potential remains the same for any number of stages in the collector, e.g. the first electrode potential remains the same for a two-stage and a three-stage collector but the potential of the second electrode for these two collectors varies for optimised design. The knee is not sharply defined for any collector as the spent beam curve changes due to the RF modulation in the beam. In practice the first electrode potential is operated well below the knee voltage to avoid back streaming.

- *Two-stage collector*

It is easy to find the second electrode potential for a two-stage collector, the first being already assigned the knee voltage. The combined power recovered (area covered) by the two electrodes is calculated for each possible potential on the second electrode keeping the first electrode potential fixed. Out of these values the combined maximum power is considered as the optimised design and the second potential corresponding to it is chosen as the second electrode potential.

- *Three-stage or more*

It is a complex procedure to find the electrode potentials for a collector with three or more stages. In a three-stage collector the choice of a third electrode potential keeping the two other electrode potentials fixed at the same potentials of an optimised two-stage collector will not yield the optimised result. Instead, the total power is calculated adding the maximum power recovered by the second and third electrode combined together and the power recovered by the first electrode. For all different potentials between the knee voltage and the maximum potential assigned to the second and the third electrodes, the values of combined power recovered (area covered) by them are compared. The second and third electrode potentials corresponding to the maximum power are chosen as the optimised potentials. Similarly for an n-stage collector the maximum area covered by (n-1) electrodes combined together is added with the area covered by the first electrode for maximum power recovery. The corresponding potentials at different electrodes are the optimised potentials.

5.5 THE COMPUTER CODE

- *Structure of the code*

Based on the algorithm discussed in Figure 5-4 a computer code has been developed. The code operates in four steps. First the spent beam data is discretised. In the second step the area under the spent beam curve is calculated using the Trapezoidal Rule. The electrode potentials on the curve are optimised next and finally the sensitivity analysis is carried out (if required).

There are several optimising algorithms that can be used to optimise the electrode potentials. Among them, the hill-climbing method (calculus based method) cannot be used for our purpose, as it does not guarantee the maximum value. It finds a local maximum and to get an optimised value it is necessary to repeat the process several times changing the starting point of computation. On the other hand the enumerative method, which looks for all points in the space by changing one variable at a time, guarantees the maximum value. This is the reason why this algorithm is used for our

computation purpose. The advantages and disadvantages of several optimising techniques are described in detail in Chapter 6.

Instead of developing the new algorithm for the optimisation of electrode potentials the code could have been developed using a library routine (if there is one available). In that case the code would be dependent on the library routine and the operating system in which the library routine works. The same program would be of no use in other operating systems or even in the same operating system where the library routine is not available. Therefore the program would have lost its portability.

- *Features of the code*
  - Computes the collector efficiency for different number of stages
  - Optimises the electrode potentials and does the sensitivity analysis
  - Module contains two programs including the graphics
  - Postscript option is created
  - Language used is FORTRAN

- *Reliability*

In this algorithm all possible combinations of the electrode potentials are considered. That is why the algorithm is robust and reliable. It is also simple to implement. But one drawback is that it takes a long time to compute the values of optimised potentials if the number of collector electrodes is increased beyond seven stages. For the present purpose this is not a serious problem as nearly all modern multistage collectors use either 4 or 5 stages. In that case the computation time is less than 10 seconds, which is quite reasonable.

- *Example*

The electrode potentials of a 5-stage collector have been optimised using this algorithm. A spent beam distribution curve and the electrode potentials are plotted in Figure 5-6. The area in the curve in different shades represents the power that can be recovered by different electrodes. Optimised potentials of the electrodes and the currents recovered by the electrodes are shown in the Table 5-1. The computed collector efficiency is 94.2%.

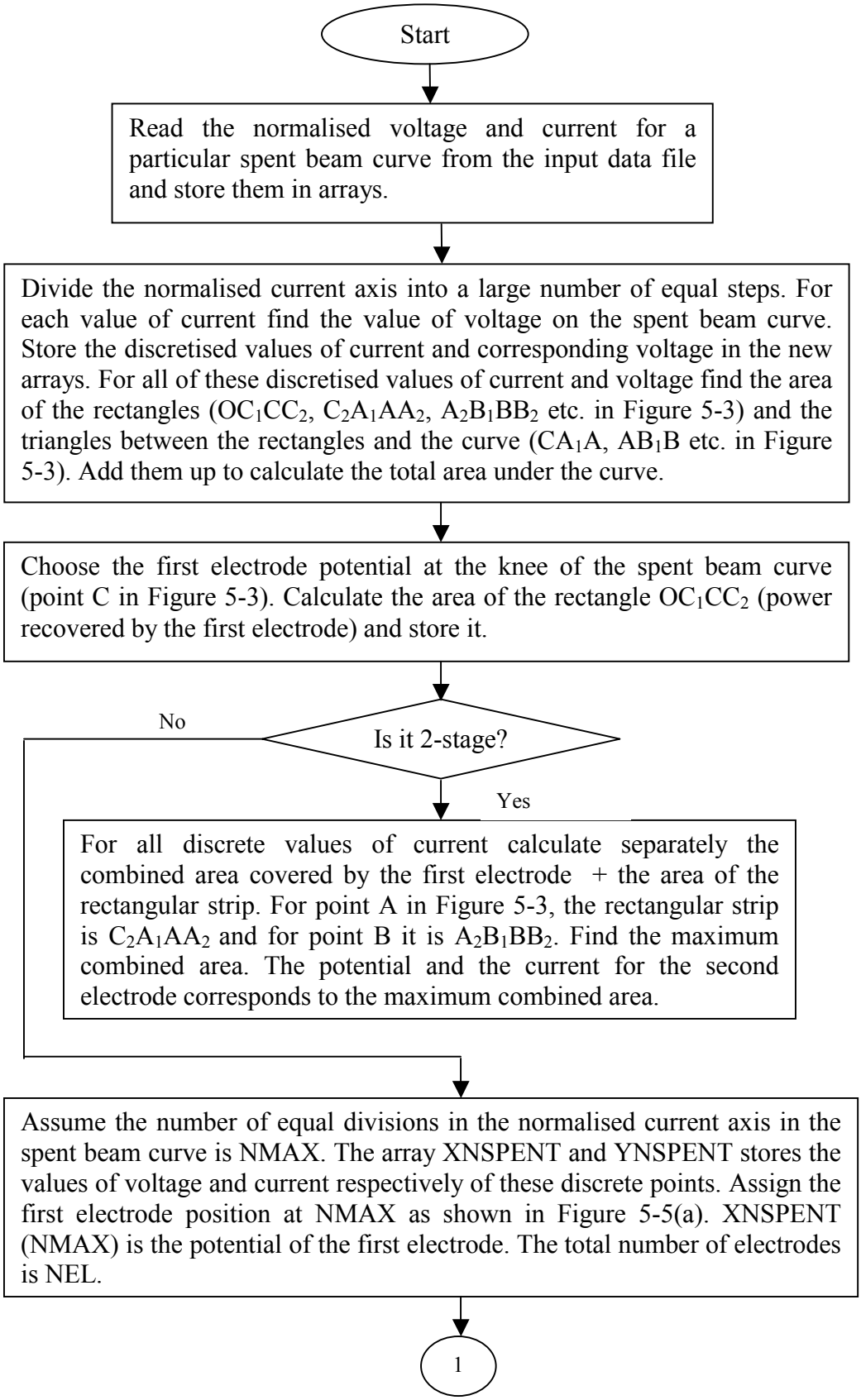
Start
Read the normalised voltage and current for a particular spent beam curve from the input data file and store them in arrays.
Divide the normalised current axis into a large number of equal steps. For each value of current find the value of voltage on the spent beam curve. Store the discretised values of current and corresponding voltage in the new arrays. For all of these discretised values of current and voltage find the area of the rectangles (OC_1CC_2, $C_2A_1AA_2$, $A_2B_1BB_2$ etc. in Figure 5-3) and the triangles between the rectangles and the curve (CA_1A, AB_1B etc. in Figure 5-3). Add them up to calculate the total area under the curve.
Choose the first electrode potential at the knee of the spent beam curve (point C in Figure 5-3). Calculate the area of the rectangle OC_1CC_2 (power recovered by the first electrode) and store it.
No
Is it 2-stage?
Yes
For all discrete values of current calculate separately the combined area covered by the first electrode + the area of the rectangular strip. For point A in Figure 5-3, the rectangular strip is $C_2A_1AA_2$ and for point B it is $A_2B_1BB_2$. Find the maximum combined area. The potential and the current for the second electrode corresponds to the maximum combined area.
Assume the number of equal divisions in the normalised current axis in the spent beam curve is NMAX. The array XNSPENT and YNSPENT stores the values of voltage and current respectively of these discrete points. Assign the first electrode position at NMAX as shown in Figure 5-5(a). XNSPENT (NMAX) is the potential of the first electrode. The total number of electrodes is NEL.
1

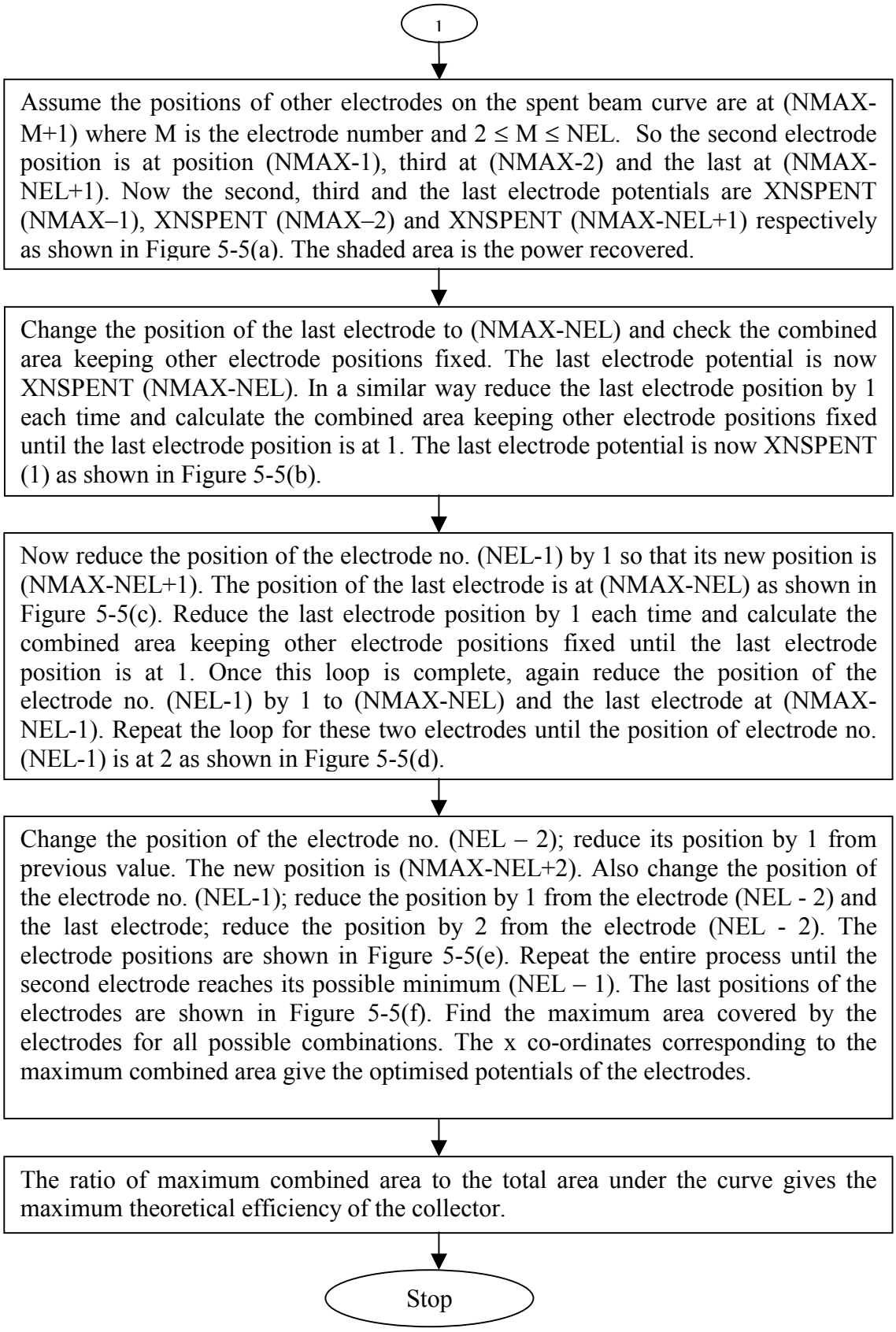

Figure 5-4: Basic flow diagram to find the optimised electrode potentials

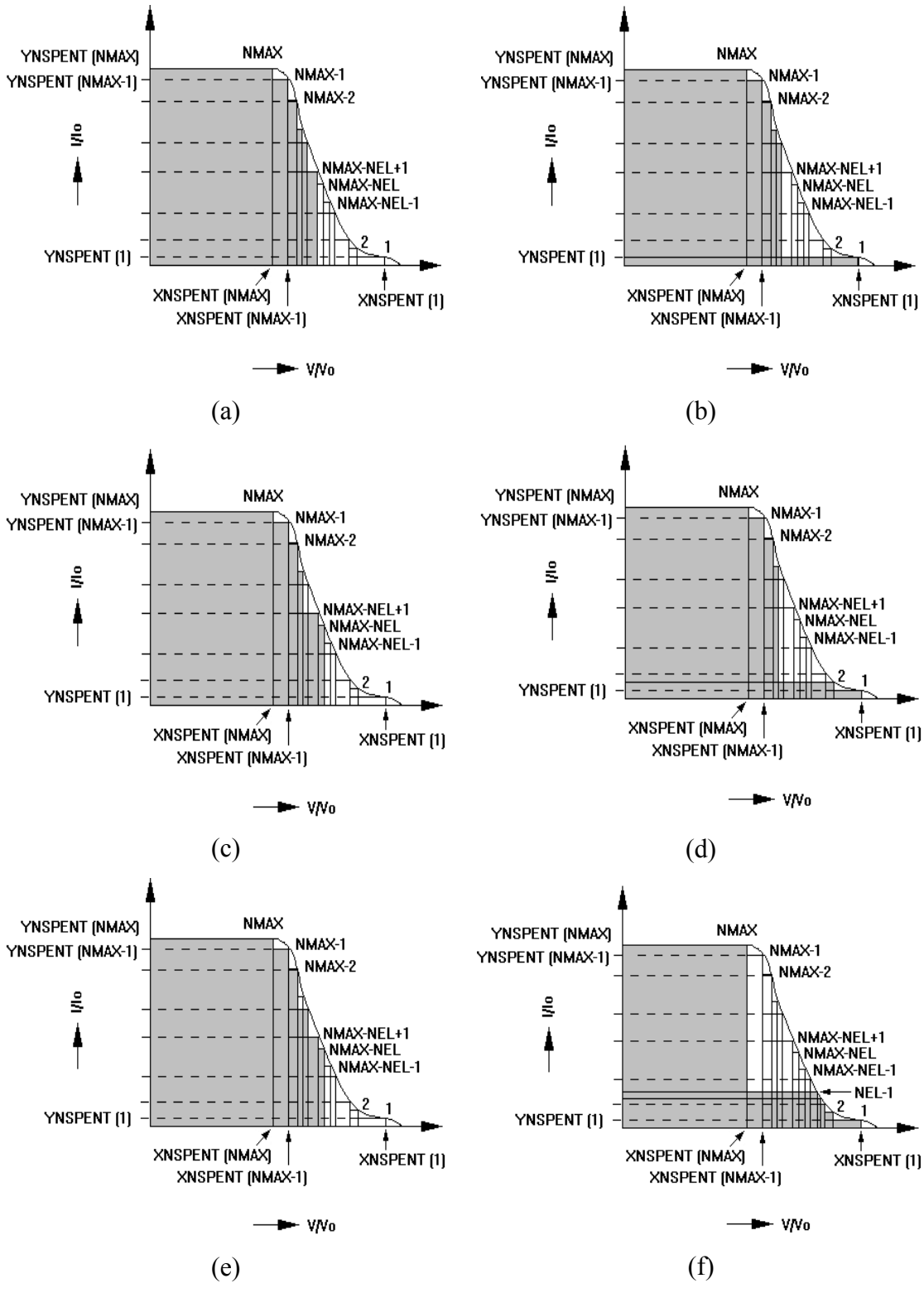

Figure 5-5: Different positions of the electrodes on the spent beam curve during the execution of the algorithm

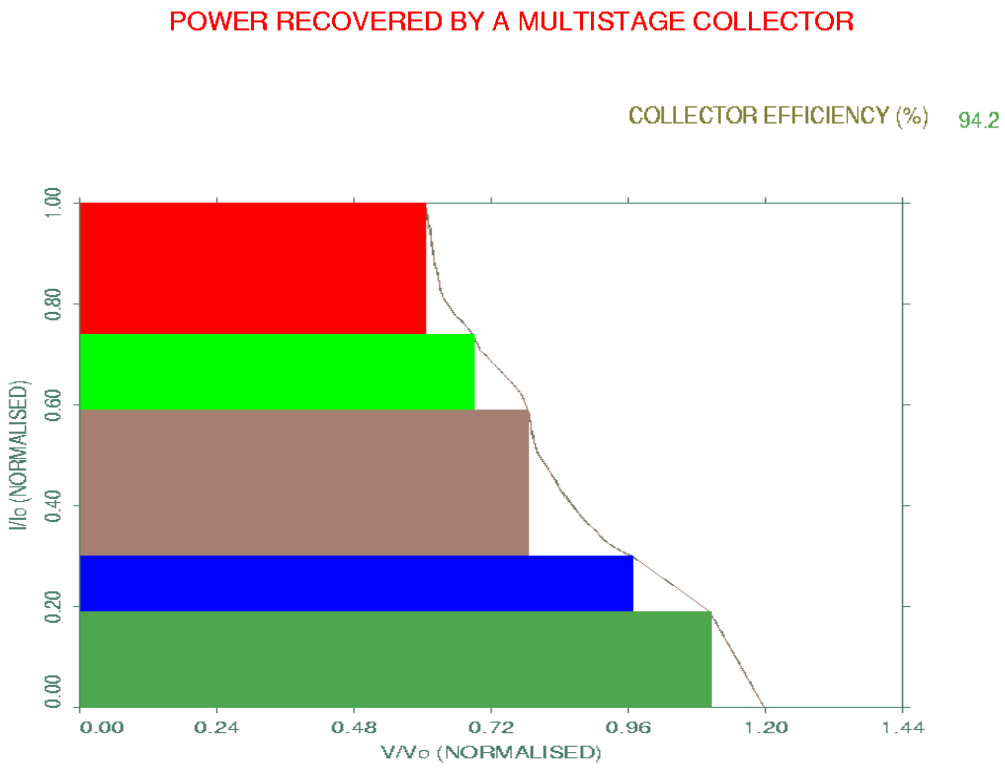

Figure 5-6: Selection of optimised potentials in a 5-stage collector

Table 5-1: Normalised currents and potentials of the electrodes in a 5-stage collector

Electrode Number	Normalised Current	Normalised Potential
1	0.26	0.61
2	0.15	0.69
3	0.29	0.79
4	0.11	0.98
5	0.19	1.11

5.6 VALIDATION OF THE ALGORITHM

The computer code, based on this algorithm, is tested here to check its accuracy in calculating the area encircled by a curve. Some known regular curves are used for this purpose. The value of the computed area enclosed by a curve is compared with the value obtained using the analytical formulae. Two different types of curves are considered to compare these results. The first curve is a circle and the other is an ellipse.

- *Circle*

A circle with centre at (0,0) and radius 1.0 unit is considered for the evaluation. A quarter of the circle is used instead of any spent beam curve for testing purposes. The x- and y- co-ordinate points for the circle are generated from the analytical formulae. Another set of data is generated by the computer code after discretisation. The actual and the discretised data are plotted together in Figure 5-7(a). From the plot it is observed that there is no significant difference between these two curves.

- *Ellipse*

Another curve is an ellipse with centre at (0,0). The major axis and the minor axis are 2.0 units and 1.0 unit respectively. The x- and y- co-ordinate points of the first quadrant of the ellipse are generated both by the analytical formulae and the computer code separately. These two curves are now plotted together in Figure 5-7 (b). It is observed in the figure that these curves are not distinguishable.

The area of one quarter of a circle and an ellipse are computed both analytically and numerically (using the computer code). These results are compared in Table 5-2. It is observed that the values are close with accuracy up to three decimal places. An error in the collector efficiency due to the difference in the values of the area should be negligible (at the second or higher decimal place). Therefore the computer code is accurate enough to serve our purpose.

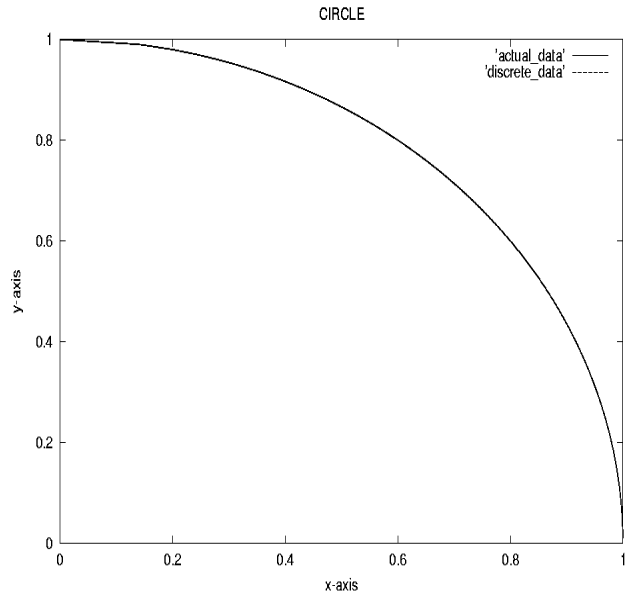

(a)

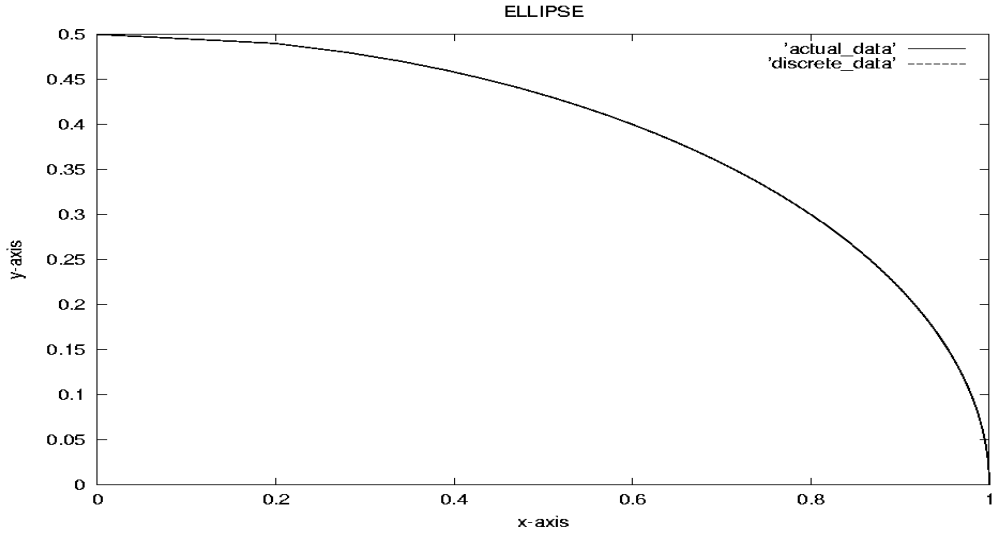

(b)

Figure 5-7: Comparison between the computed and actual curves

(a) circle of radius 1.0 unit (centre at (0,0))

(b) ellipse of major axis 2.0 units and minor axis 1.0 unit (centre at (0,0))

Table 5-2: Comparison between the results obtained numerically and analytically

Shape of the curve	*A quarter of the area in sq unit (Computed by program)*	*A quarter of the area in sq unit (Computed by analytical formulae)*
Circle	0.7851	0.7853
Ellipse	0.3922	0.3926

5.7 SELECTION OF THE NUMBER OF STAGES FOR AN MDC

The collector should recover the maximum amount of power from the spent beam. In theory it is possible to achieve close to 100% collector efficiency if the number of collector stages is large and the electrodes are made of materials with very low secondary electron emission properties. But in practice the number of stages is limited to 4 or 5 considering the complexity in fabrication of the collector geometry and the power supply. The weight of the collector is also an important parameter for space applications. So there should be a compromise between the efficiency and the number of stages in a multistage collector.

An example of a multistage collector is shown here where the electrode potentials are optimised using the computer code mentioned earlier. A spent beam distribution curve is used to optimise the potentials of the electrodes. The spent beam data is generated by the 1-D LSM at 0 dBm input drive level. In Figure 5-8(a), the actual spent beam curve, the discretised spent beam curve and the optimised electrode potentials for a 3-stage collector are plotted together. A similar plot for a 4-stage collector using the same spent beam data is shown in Figure 5-8(b). The actual and the discretised spent beam curves cannot be separated in the plots. The area in different shades in the spent beam curve represents the power recovered by different stages of the collector.

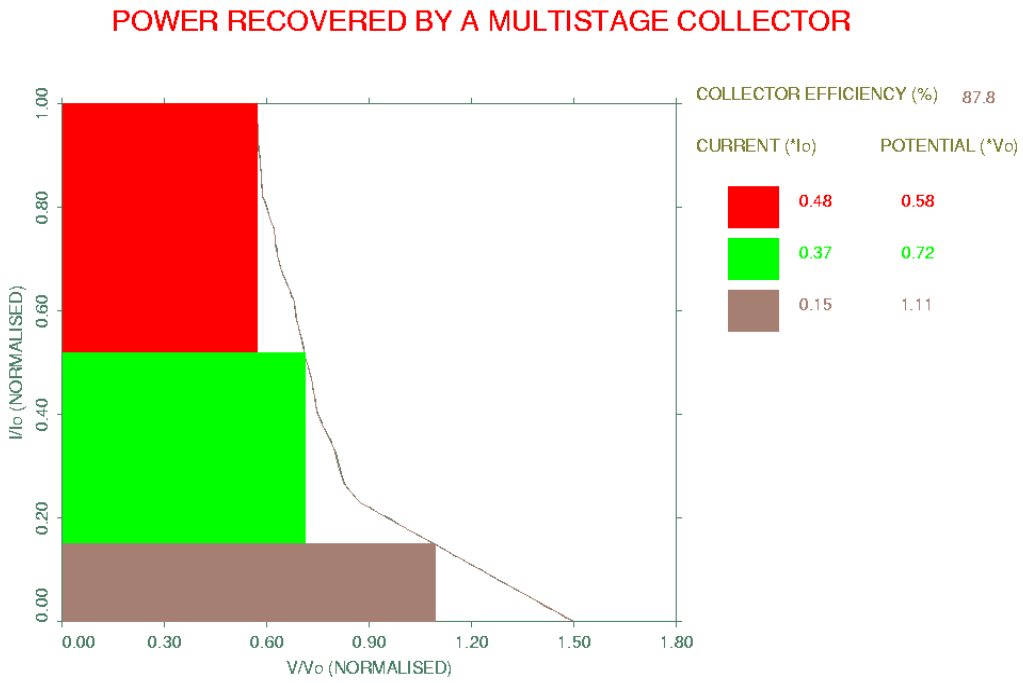

(a)

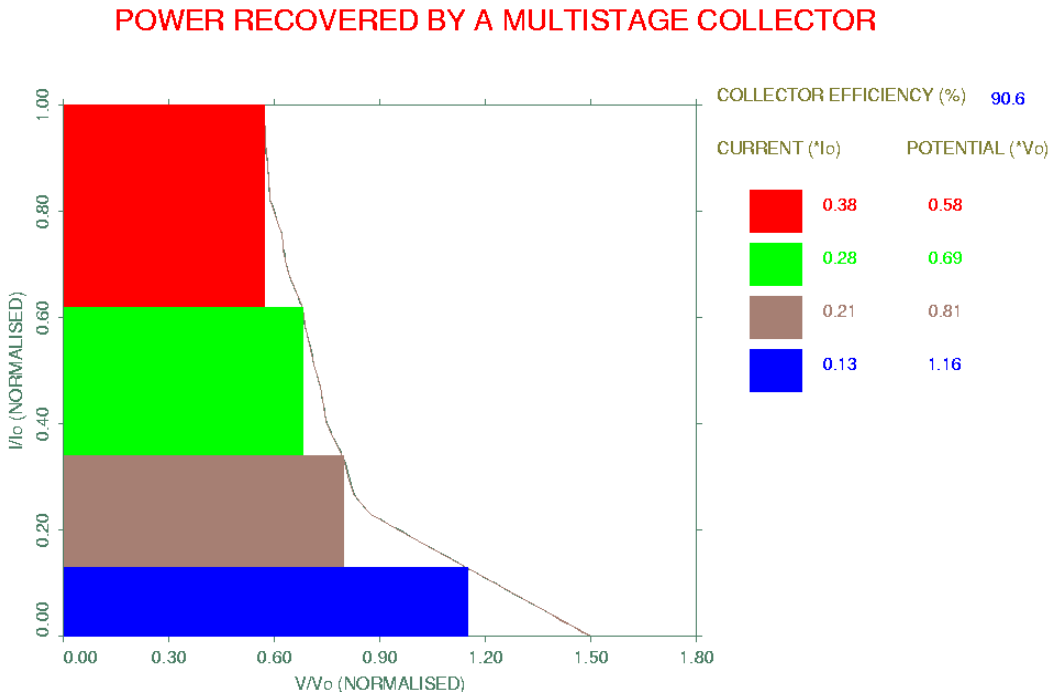

(b)

Figure 5-8(a): Plot of electrode potentials and the power recovered (a) 3-stage collector (b) 4-stage collector

The normalised current and potential for each stage and the efficiency of the collector are shown in the upper right corner of the plot. The difference between the corresponding electrode potentials in the 3-stage and 4-stage collectors can be clearly observed. These two plots show that the second electrode potential for a 3-stage collector is not the same as that for a 4-stage collector. This proves that the inclusion of a fourth stage (with optimised potential) in a 3-stage collector with all its potentials (optimised) fixed will not yield the optimised collector efficiency. These two plots also show that the efficiency of the collector is increased from 87.8 % to 90.6 % due to the increase in collector stages from 3 to 4.

The variation in the collector efficiency due to the change in the number of stages is shown in Table 5-3. These values are obtained using the same spent beam curve as described earlier. It is observed that the increment in collector efficiency is not very significant if the number of stages is increased beyond three stages. This information is quite useful from the design point of view. The designer can make a compromise between a fourth stage in the collector and an improvement of nearly 3% points in collector efficiency. Increment in collector efficiency with the increase in the number of collector stages is shown in Figure 5-9. A sharp increase in collector efficiency is observed in the plot up to three stages, but it becomes less effective afterwards.

Table 5-3: Change in collector efficiency with the change in collector stages

Collectors	**Efficiency in %**
Single-stage	71.5
2-stage	81.4
3-stage	87.8
4-stage	90.6
5-stage	92.5
6-stage	93.4

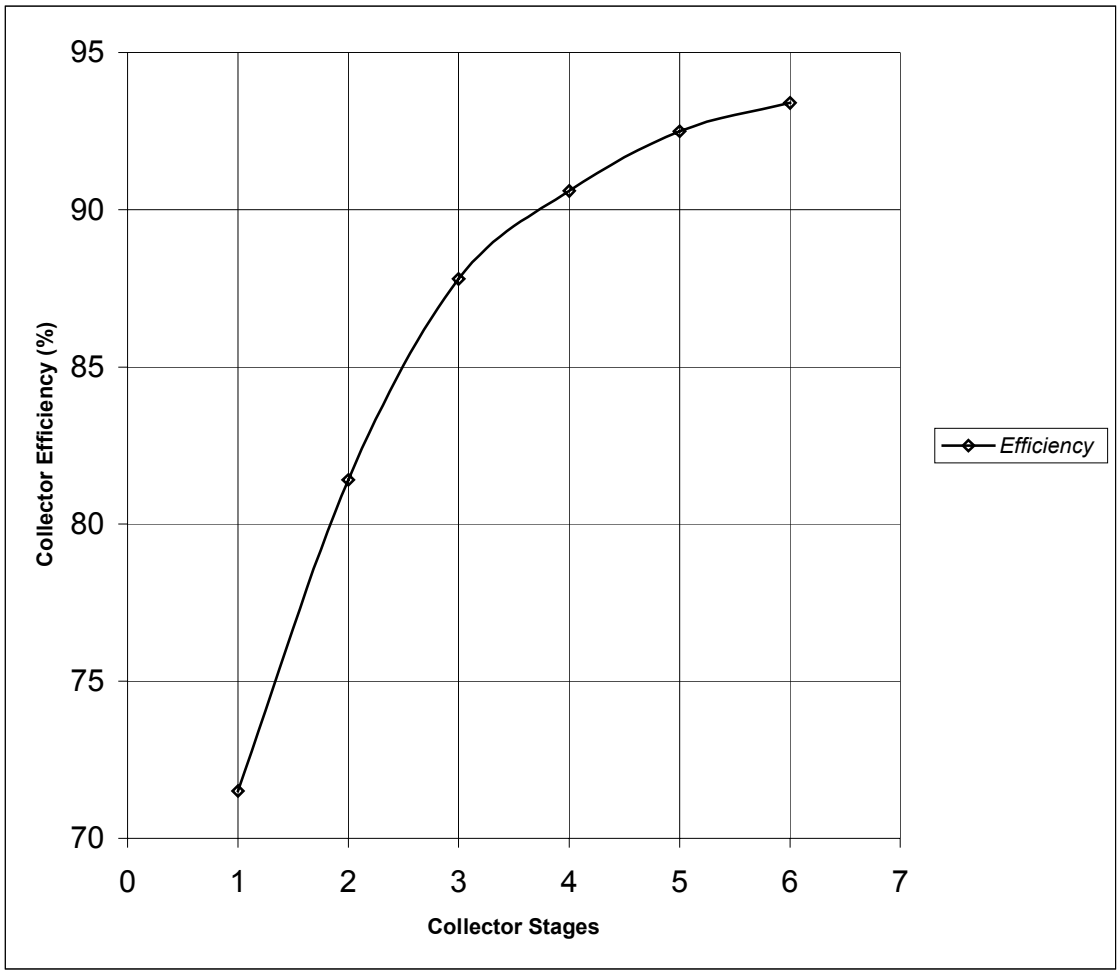

Figure 5-9: Increment in collector efficiency with the increase in the number of stages

5.8 SENSITIVITY OF MDC AT DIFFERENT DRIVE LEVELS

Due to the modulation in the RF wave, the amplitude of the output signal varies. So the energy in the spent beam also varies. A collector designed for the best performance at a certain RF level may not be able to give maximum efficiency at other RF levels. However it is desirable for some applications that the overall efficiency be maintained at a maximum level. An example of this kind is a dual mode TWT where it has to provide two different RF signals at a difference of nearly 10 dB. The dual mode TWT is mostly desirable for airborne electronic counter measure

(ECM). Therefore it is necessary to ensure that the overall efficiency of the TWT is maintained.

The overall efficiency of the tube can be expressed in terms of the electronic efficiency (basic tube efficiency) and the collector efficiency. Equation 2-4 has been re-written for the overall efficiency

$$\eta = \frac{\eta_e}{1-\eta_{coll}(1-\eta_e)}$$

Where η_{coll} and η_e are the collector and basic tube efficiency respectively

If the input driver level is varied, then both η_o and η_{coll} also vary. So to maintain a high overall efficiency it is necessary to keep the η_{coll} value as large as possible for the lowest drive whilst the η_{coll} can be lower (but not too much) at high drive. The value of collector efficiency should be nearly 99% to maintain 50% overall efficiency at 10% electronic efficiency. This gives an idea of the value of collector efficiency one is looking for. It is worth mentioning here that the effect of secondary electrons is not considered in the computation. This has been discussed in detail in Chapter 4.

The sensitivity of the collector has been investigated through different cases. Three different sets of electrode potentials have been optimised for a 4-stage collector. These sets are obtained by optimising the collector at three different input drive levels 0 dBm, -7 dBm and –14 dBm which correspond to the highest, middle and the lowest values of the input drive levels. In the first case a comparison of the performances at different drive levels is shown in Figure 5-10(a) for the collector optimised at input drive level 0 dBm. The efficiency for this collector is 90.6 %. Keeping all electrode potentials fixed, the collector performance has now been tested for five different input drive levels, namely –2 dBm (curve sp2), -4 dBm (curve sp4), -7 dBm (curve sp7), -10 dBm (curve sp10) and -14 dBm (curve sp14). The efficiency of the collector at different input drives is shown at the right side of the plot. In the second case the electrode potentials are optimised at -7 dBm input power and the performance is tested for five different input power levels as shown in Figure 5-10(b). Finally, the potentials of the collector electrodes are optimised at a -14 dBm and tested for five different input drives as shown in Figure 5-10(c).

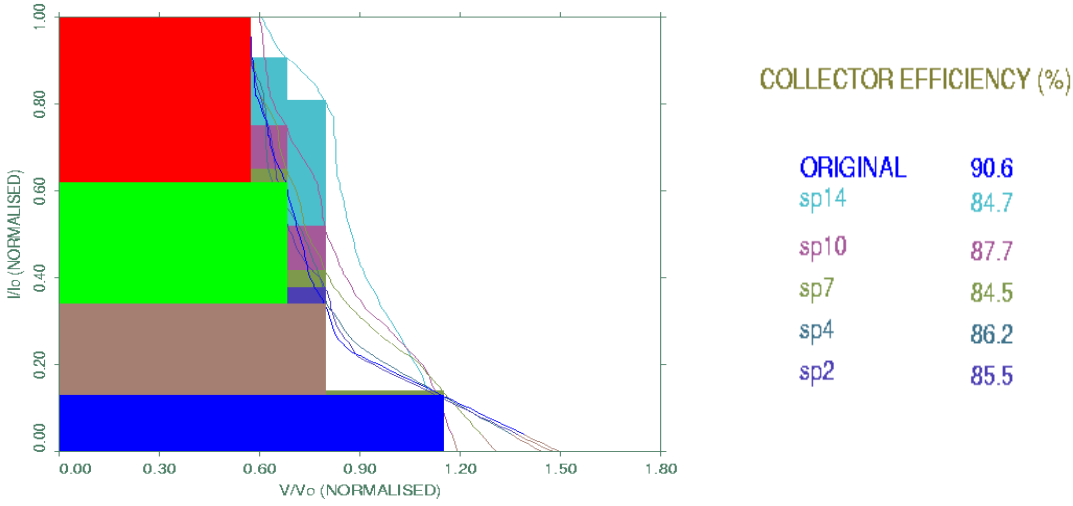

(a)

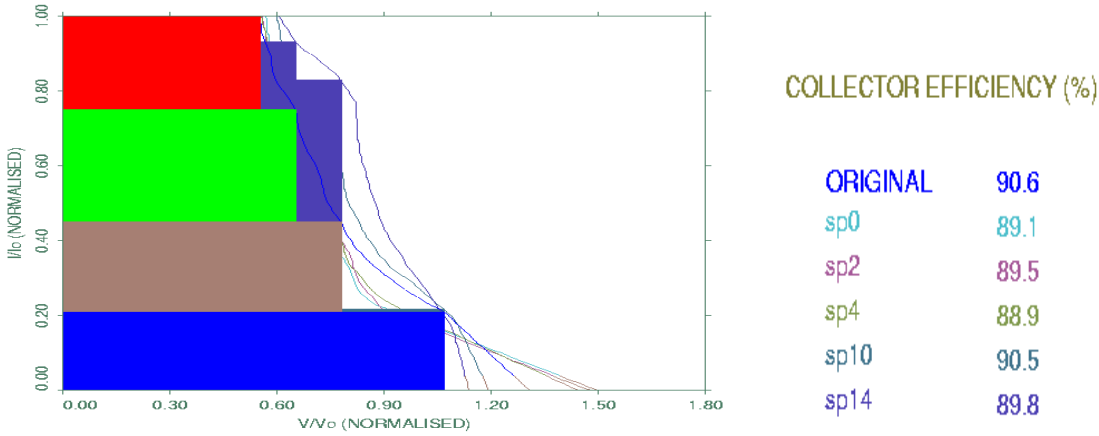

(b)

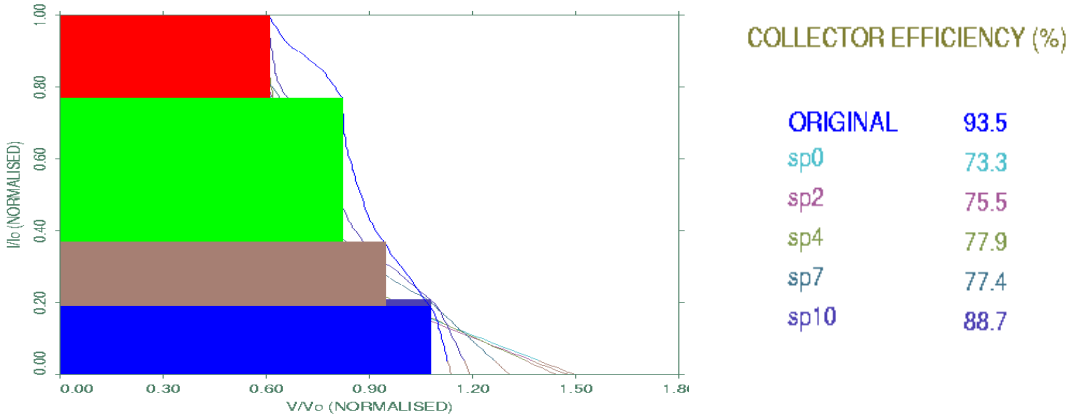

(c)

Figure 5-10: Comparison of power recovered by a 4-stage collector at input drive level 0 dBm, -2 dBm, -4 dBm, -7 dBm, -10 dBm and - 14 dBm. Collector electrode optimised at (a) 0 dBm (b) -7 dBm (c) -14 dBm

In Figure 5-11 the electronic efficiency versus the input power is plotted. It shows that the electronic efficiency is increased with the increase of input drive power and become saturated at 0 dBm input power. The computed results for the collector and the overall efficiency versus the basic tube efficiency are potted in Figure 5-12. The dashed curves in the plot represent the collector efficiency and the solid curves represent the overall tube efficiency. The same symbol is used for representing the collector efficiency and its corresponding overall tube efficiency. Curves with a similar set of symbols "triangle", "cross" and "circle" correspond to cases 1, 2 and 3 respectively. It is observed from the plot that both in the first and second cases the overall tube efficiency drops more than 20% points from the maximum value at the lowest basic tube efficiency though the collector efficiency is more than 80%. However in the third case the overall tube efficiency drops only 10% points from the maximum value in this range. But the saturation efficiency in the third case is considerably lower compared to the other two cases. It should be noted that the maximum theoretical collector efficiency at the lowest basic tube efficiency is higher in comparison with the collector efficiency achieved at a very high electronic efficiency. This plot supports the statement mentioned earlier in Chapter 2 that the collector efficiency decreases with the increase in electronic efficiency.

The collector and the overall tube efficiency are plotted against the output power in Figure 5-13. These plots are very similar to the plots in Figure 5-12 because the basic tube efficiency is directly proportional to the output power. The plot in Figure 5-13(b) shows that the overall efficiency varies within 10% for the variation of the output power in the third case as opposed to 20% in the second case and 40% in the first case. In Figure 5-14 the collector and overall efficiency are plotted against the input drive power for all three cases. It is observed that the collector and overall efficiency drop significantly at a low drive power when the electronic efficiency is also low. This results in a low overall efficiency at low input drive. But in the third case the collector is optimised at the lowest input drive and gives the highest collector efficiency. So the overall efficiency does not drop much at the lowest input drive even though the basic tube efficiency is low. The collector pulls up the overall tube efficiency and maintains a nearly constant level for all input drives.

From the above discussions it is clear that the collector designed at the lowest input drive performs well over all the operating input drive power. In this case, the overall efficiency varies very little due to the variation in the input drive level. It is also observed that the electronic efficiency plays a significant role in determining the collector efficiency.

- *Importance of sensitivity analysis in multi-carrier operation*

In a multi-carrier operation the intermodulation products are generated which are multiplies of the frequency separation of the carriers. These are called intermodulation products. For two-carrier system with frequencies f_1 and f_2 the third order intermodulation products are $(2f_2 - f_1)$ and $(2f_1 - f_2)$. Other higher order modes also exist. If the tube is operated at saturation then the amplitude of the third order intermodulation product is very high. As it is very close to the carrier frequency it introduces distortion to the signal. To reduce this effect the tube is generally "backed of" 8-10 dB that means the tube is operated 8-10 dB below saturation by reducing the input drive power. Because of this the electronic efficiency of the tube reduces and thus the overall efficiency. The multistage collector has to be designed to cope with this situation so that the overall efficiency is maintained to a maximum level. The sensitivity analysis of a collector (which is designed for one drive condition) helps in estimating the overall efficiency of the tube for different input drive levels.

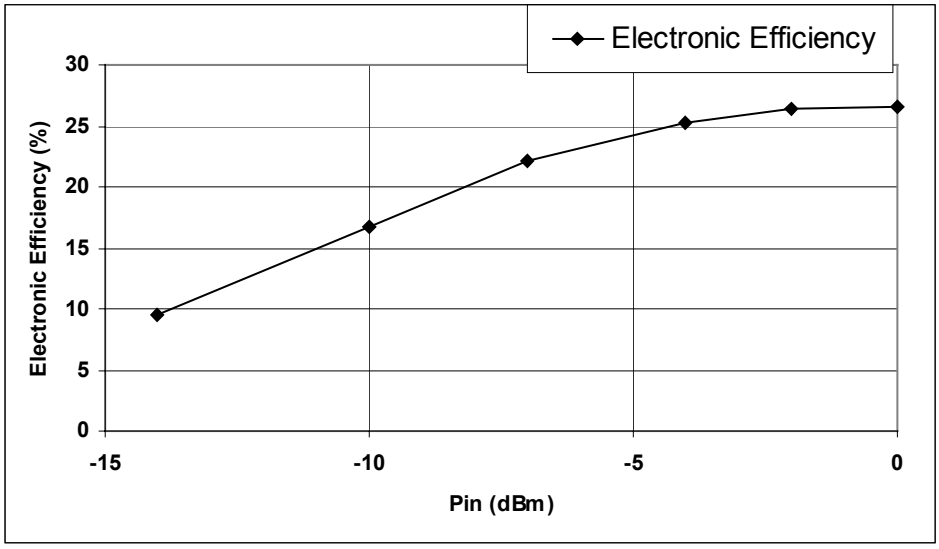

Figure 5-11: Electronic efficiency versus input power

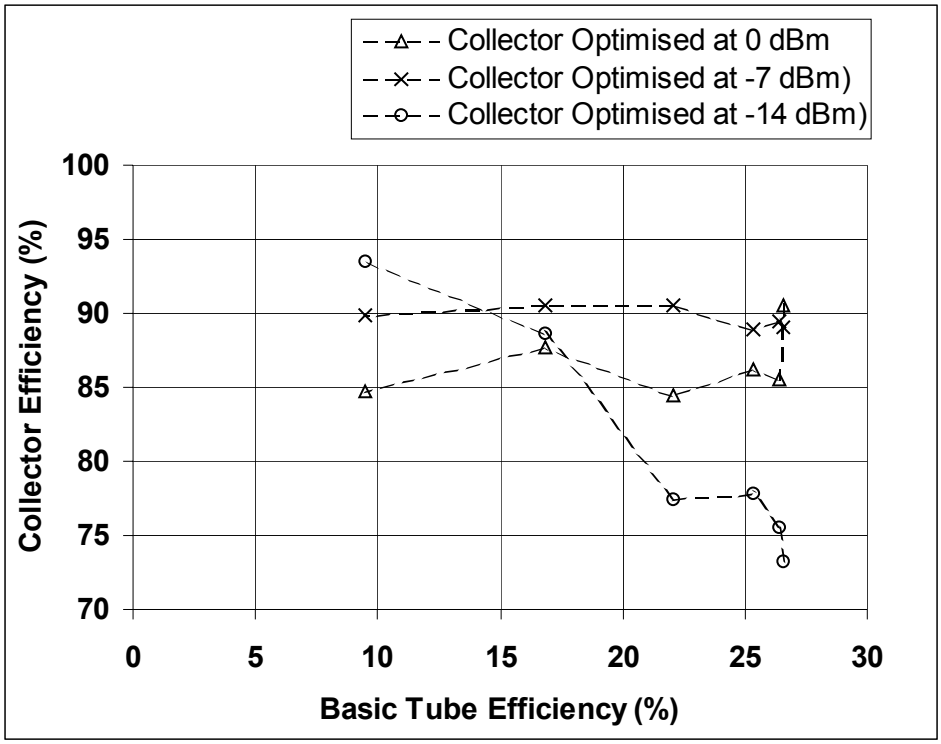

(a)

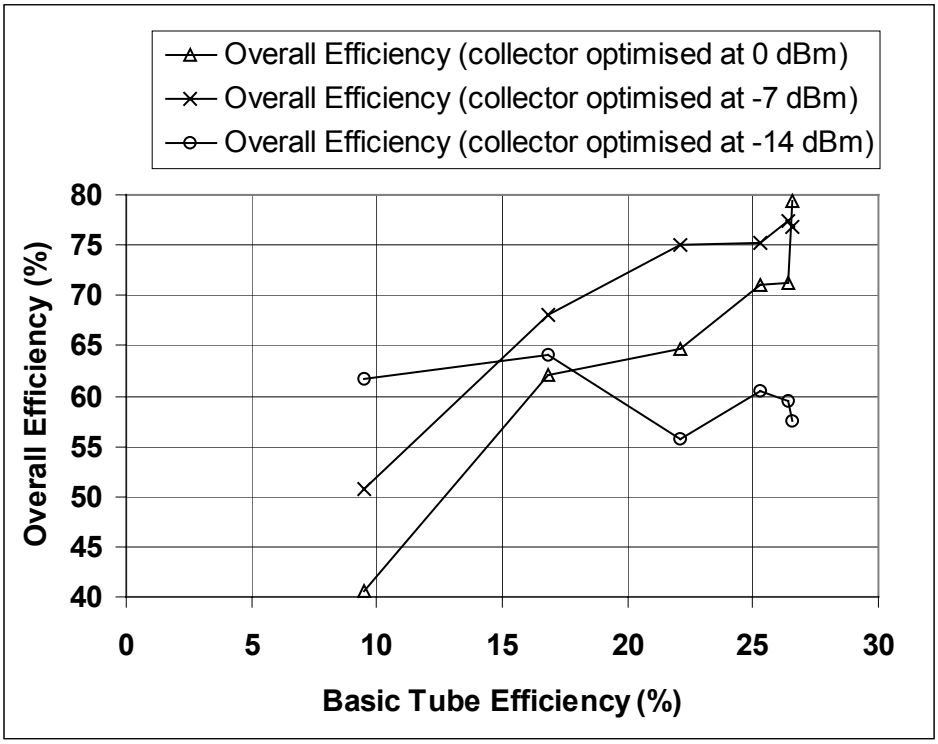

(b)

Figure 5-12: At different input drive levels (a) collector efficiency versus basic tube efficiency (b) overall efficiency versus basic tube efficiency

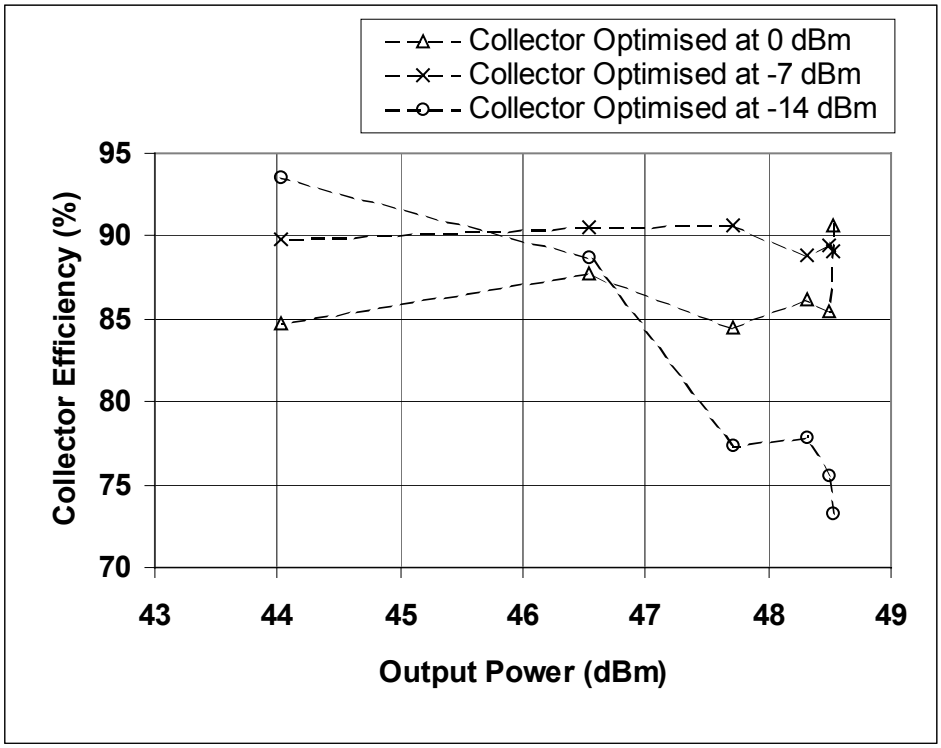

(a)

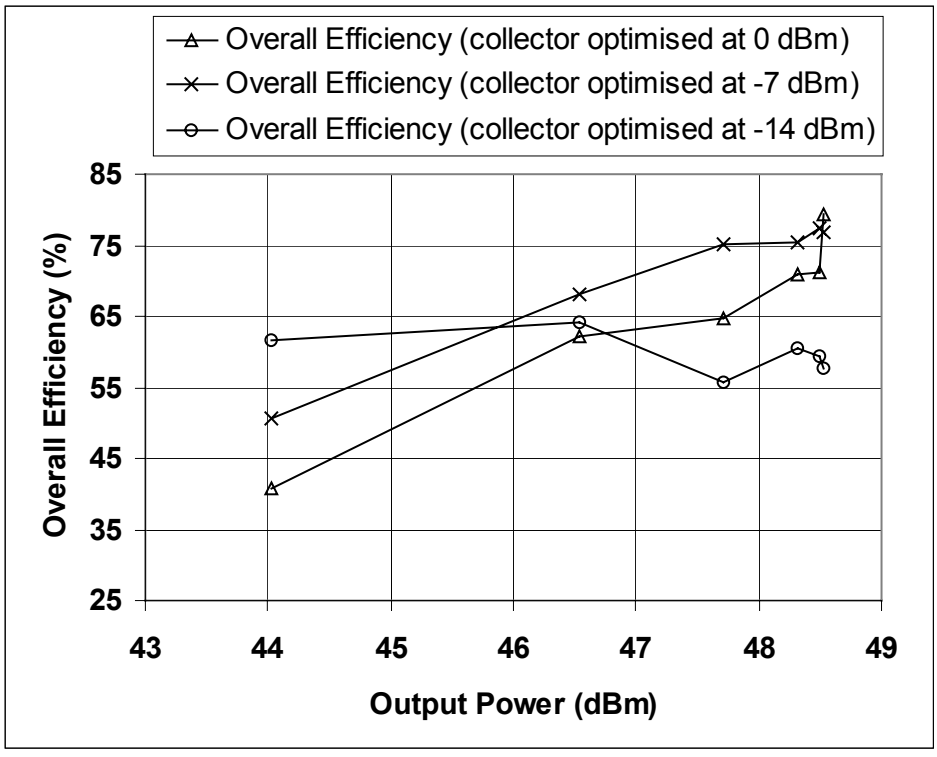

(b)

Figure 5-13: At different input drive levels (a) collector efficiency versus output power (b) overall efficiency versus output power

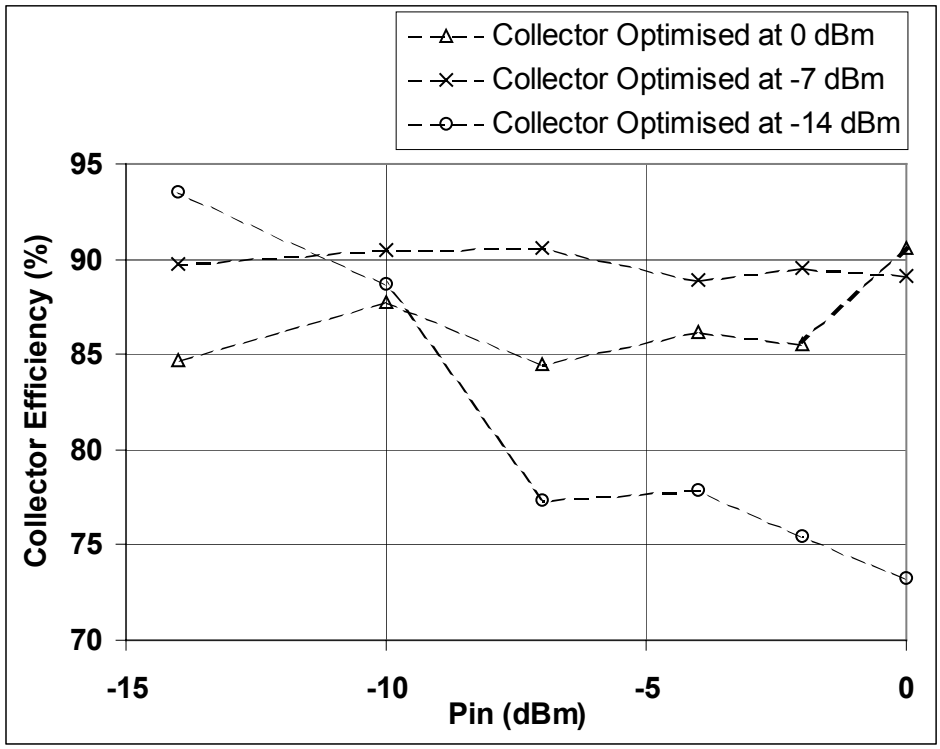

(a)

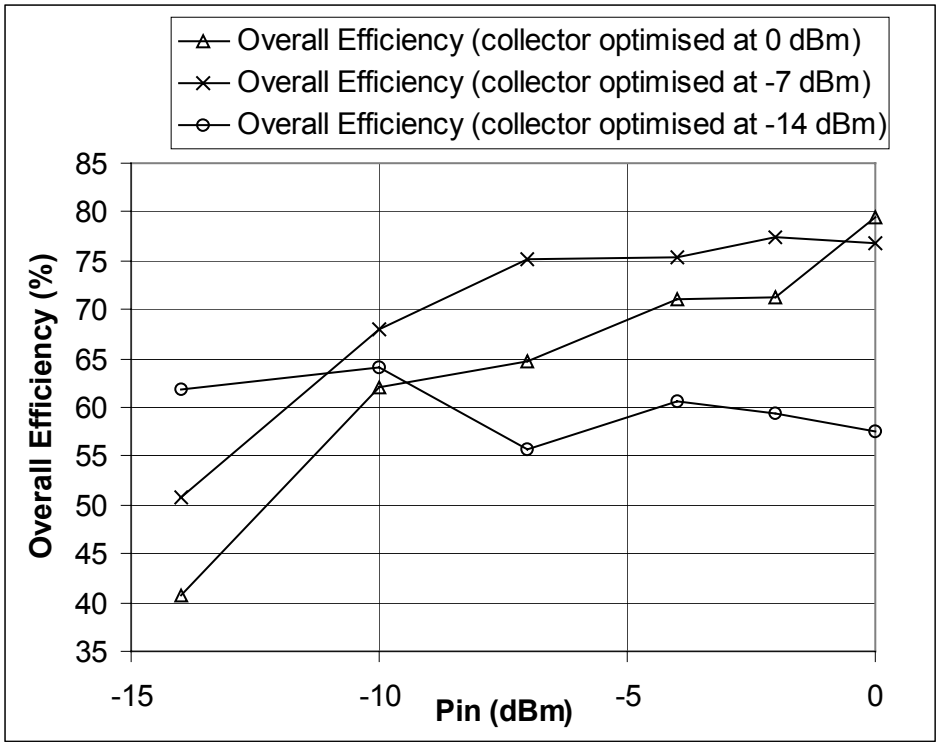

(b)

Figure 5-14: At different input drive levels (a) collector efficiency versus input power (b) overall efficiency versus input power

5.9 SUMMARY

An algorithm has been developed to optimise the number of stages and the electrode potentials of a multistage collector as a first step to design optimisation. The number of stages in a collector is determined through a compromise between the improvement in collector efficiency and the increase in complexity of fabrication and weight. As an example, a quick calculation with a given spent beam has shown that the improvement in collector efficiency is not significant after 3 or 4 stages. It is possible to choose the electrode potentials based on either a single spent beam curve or a set of spent beam curves. The potentials of a five-stage collector have been optimised for a given spent beam curve using this algorithm. With the help of this algorithm the sensitivity analysis of the collector can be easily done using multiple spent beams generated at different input drive levels. The collector potentials, optimised at the highest input drive, offers low collector and overall efficiency at the lowest input drive. However the potentials, optimised at the lowest input drive, ensures little fluctuation in the overall efficiency for all input drive levels. It also ensures a higher minimum overall efficiency than the previous case.

In this chapter the electrode potential was assigned lower than the cathode potential for optimisation purpose and a clear advantage is observed. In all cases the optimum potential for the last electrode is beyond the cathode potential. However the possibility of making the new type of power supply is to be explored for this purpose. In the meantime a choice of optimising the electrode potentials at lower than the cathode potential is made optional in the computer program. If the value of the electrode potential flag is set to “1”, then the lower potentials than the cathode are considered for optimisation; otherwise it follows the conventional method and restricts the electrode potential up to the cathode potential.

The second step to optimise a collector is to optimise the electrode geometries i.e. the length, inner diameter, outer diameter angle of inclination with the axis etc. A new algorithm has been developed based on the genetic algorithm, which can be used for the automated optimisation. The details of this algorithm are described in the next chapter.

REFERENCES

[1] H. G. Kosmahl, "How to Quickly Predict the Overall TWT and the Multistage Depressed Collector Efficiency," *IEEE Trans. on Electron Devices*, vol. ED-27, No. 3, pp. 526-529, March 1980.

Chapter 6

Design Optimisation - Part II: Optimisation of Electrode Geometry

6.1 INTRODUCTION

There are several methods for optimising problems related to different practical applications. For complex optimisation problems a probabilistic algorithm can be a very good choice. These algorithms do not guarantee the maximum value but it is always possible to reduce the error in the optimised value by randomly choosing a sufficiently large number of iterations. Optimisation of collector geometry is such a complex problem.

The optimisation of the collector performance is done in two steps. First the electrode potentials are optimised to recover maximum power from the spent beam. Then, the electrode geometry is optimised to achieve the maximum theoretical collector efficiency. A procedure to optimise the number of electrodes and their potentials has been illustrated in the previous chapter. The method for optimising the electrode geometry is presented in detail in this chapter. Different methods of optimisation are discussed in section 6.2. Two optimisation techniques namely random walk and genetic algorithm are discussed in sections 6.3 and 6.4 respectively. In these sections the basic theory and their implementation procedure for optimising the multistage

collector are described in detail. Finally the advantages of the genetic algorithm and the summary of the chapter are presented in sections 6.5 and 6.6 respectively.

6.2 DIFFERENT OPTIMISATION METHODS

Probable methods, available for optimising the performance of a multistage collector are shown below [2]:

- *Calculus based method*

This method is widely known as hill-climbing technique that follows the steepest slope until an apparent best result is obtained. The process is repeated from another starting point until no further improvement is obtained.

- *Enumerative method*

In this method the object function value is searched in a finite space at each point by changing one variable at a time in small steps. The object function value is a type of pay off value. It is similar to the method applied in the previous chapter for optimising the electrode numbers and their potentials.

- *Random method*

Unlike the previous two methods the random method changes all variables randomly at a time and search for the improved result in the problem space. The following methods are mostly used for optimisation:

- Random walk

When an apparent better result is obtained the process is repeated from this point until no further improvement is obtained.

- Simulated annealing

This is a probabilistic approach and the solutions do not depend on the starting point of the search. A probability of acceptance is computed from the object function value. The probability is 1 if the object function value is better than

the previous value and it is greater than 0 for other values. In the second case the probability is a function of old and new values of object function and an additional parameter "temperature" denoted as "T". During the execution of the algorithm the value of T is lowered and terminates after a certain user specified value is reached after which no change is accepted. The lower the temperature value the lower the probability of acceptance. In this method the solutions are nearly close to the optimum [1]. A relation between this method and the genetic algorithm has been illustrated by Davis in his book [4].

- *Genetic algorithm*

Genetic algorithm is based on natural genetics and natural selection. This works from a population of strings. A string in the genetic algorithm is analogous to a chromosome in the natural system. It is a binary number consisting of 0s and 1s. Each string is a potential solution of the problem. A fitness value (object function value) is obtained for each string through an evaluation process. Strings with higher fitness values contribute more whereas the strings related to lower fitness values die out in the next generation like the theory of survival of the fittest. The process continues until an optimum value is obtained.

The hill-climbing technique has a few inherent limitations as it needs the derivative of a function and the function has to be continuous in the search space. But this is not quite true in most of the complex problems. Further the scope is limited due to the local scope of search.

Out of these search methods, the enumerative technique is easy to implement. This method is very useful when the number of variables is small. Sometimes it is not feasible to use this algorithm for solving problems with a large numbers of variables as the computational time becomes too long and sometimes unrealistic. A major disadvantage of this algorithm is its efficiency. The optimisation of collector geometry is complex in nature and deals with a large number of variables. Due to the limitations of the hill-climbing technique and the enumerative scheme, these methods are not considered here. In the following sections the random walk and the genetic algorithm

methods are discussed in detail. Based on these two methods computer packages have been developed and tested. The performance of these two methods is also compared.

The simulated annealing is a different approach and extra efforts are needed to implement it for optimising collector efficiency, which is beyond the scope of the thesis. However this method has been proved to be working well for this purpose [5].

6.3 RANDOM WALK

As the name suggests this is a random method. The idea is very simple. In a finite search space the algorithm looks for the object function values at different points and one at a time. All the variables in the problem are changed together randomly and the object function value is calculated. If the value of the object function is better than the previous value, then the search operation starts again from this point. This algorithm is most effective in cases where the search space and the number of possibilities are small.

6.3.1 Principle – How It Works

A basic flow chart for the design optimisation package using the random walk approach is shown in Figure 6-1. The pre-processor of this package reads the geometry and trajectory data from two separate files and converts it into an input data file in a format suitable for the mainframe version of the 3-D simulator KOBRA3. Once the simulation is complete, the performance of the collector is analysed using the post-processor of the package. The collector efficiency computed thus is used as an object function value for that specific collector geometry. The target is to maximise the object function value. Based on this value a decision is taken in the random walk algorithm whether the present point can be used as the new base for future computation or whether it should start from the previous point. The amount of change in different dimensions of the collector electrodes is chosen randomly, but with small steps to facilitate the procedure for searching for all possible combinations. A clear

advantage of this method over enumerative method is that all dimensions of the collector electrodes are changed at a time unlike the other method. The critical dimensions of the collector electrodes and the assumptions to chose the limits of change in each dimension are discussed later in this section. The detailed flow chart of the random walk section is shown in Figure 6-2.

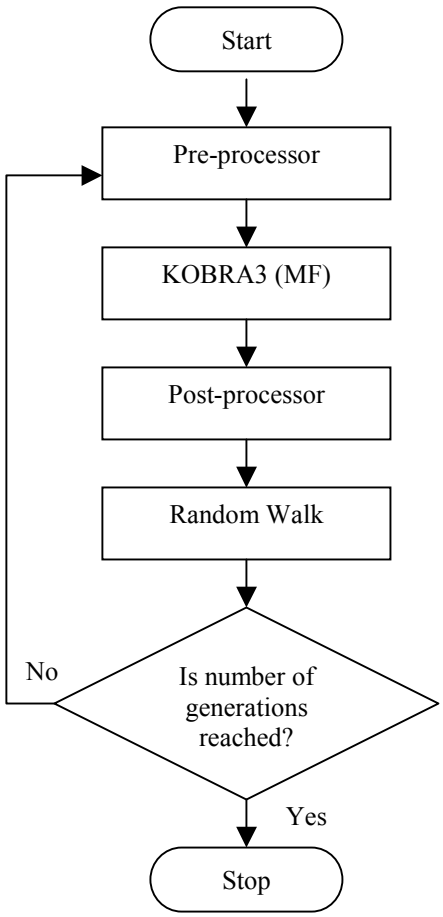

Figure 6-1: Basic flow chart for the random walk process as used in our problem

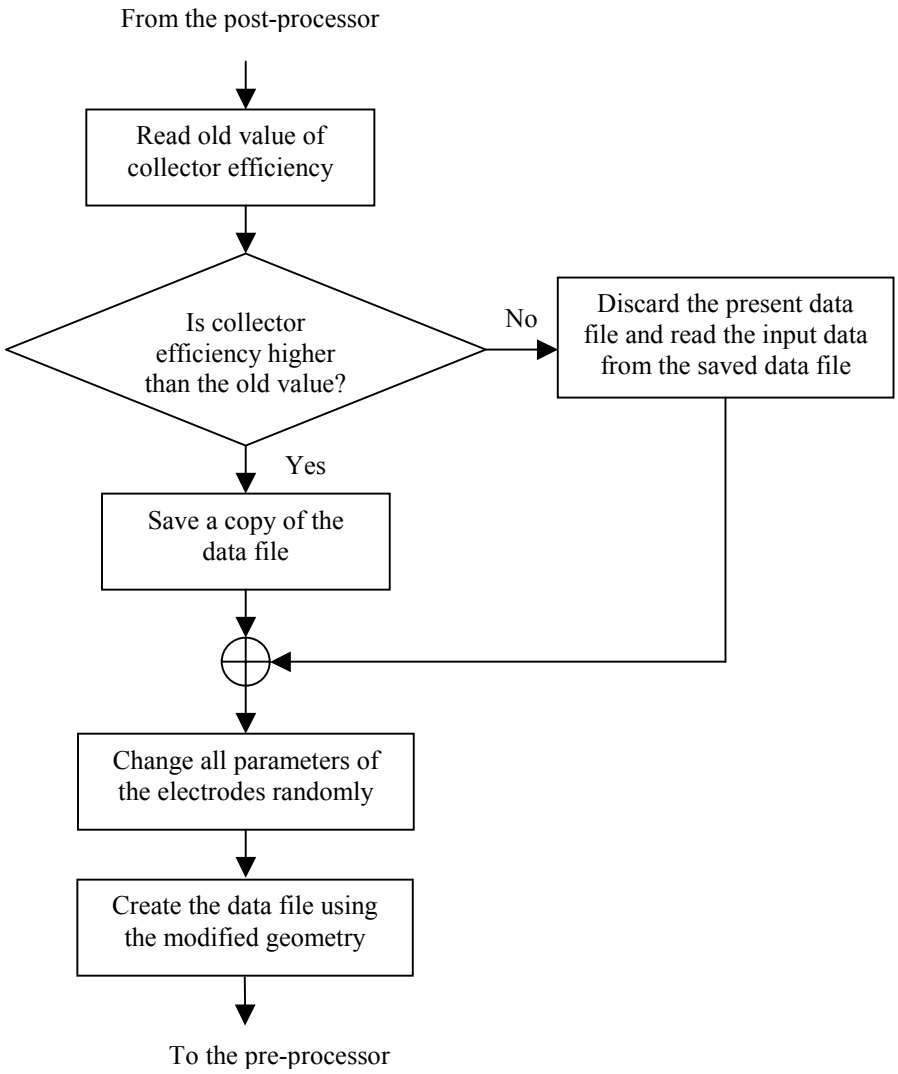

Figure 6-2: Detail flow chart of the random walk section

6.3.2 How to Create a New Geometry

The main purpose of the random walk approach is to generate the geometry of a new collector each time and test its performance to optimise it. A new collector can be generated in different ways (a) by changing the geometry of a single electrode (b) by changing the geometry of all electrodes simultaneously. The second method is more suitable as the change in collector performance may be a significant amount. In the second case the amount of change in the dimensions of the collector electrodes has to be very little to search through all possible points in the space. The electrode

dimensions are read from an intermediate data file, where all dimensions of the electrodes, the mesh information and the electrode potentials are stored. This file can be converted into an input file suitable for the simulator by the newly developed pre-processor. This part of the pre-processor (converter) has been developed recently. And detail can be found in Chapter 3. Once the geometry data for the collector is read from the intermediate data file the following steps are taken to create the geometry of a new collector:

- The electrode dimensions to be changed are chosen, e.g., length, inner diameter, outer diameter, angle of inclination with the axis etc.
- From the previous experience of modelling and simulation of collectors the dimensions, which change the collector performance significantly are chosen. Based on that, a decision is taken on what should be the amount of change in different dimensions in each step.
- A random number generator generates a set of random integer numbers between 0 and 1 for each electrode. Each random number should be associated with one dimension of the electrode.
- Based on the value of the random number a dimension of the electrode is changed as follows:
    - If the random number is 0 then the dimension is decreased
    - If the random number is 1 then the dimension is increased

All new electrode dimensions are written in the intermediate data file in a suitable format replacing the old data file. Using this data the pre-processor generates the input file for the simulator. The performance of the newly generated geometry is evaluated and analysed. The whole process is repeated as shown in the flow diagram in Figure 6-1.

6.3.3 Critical Parameters of the Electrodes

Figure 6-3 shows the dimensions of the first electrode of a 3-stage symmetric collector, which are commonly changed to create a new geometry. However these

parameters may be different depending upon the shape of the electrode. In this case the first electrode is a combination of a funnel and a cylinder whereas the second electrode is a combination of a cone, a hole and a cylinder. The complexity of the problem can be understood from the number of dimensions to be changed for a 4 or a 5-stage collector.

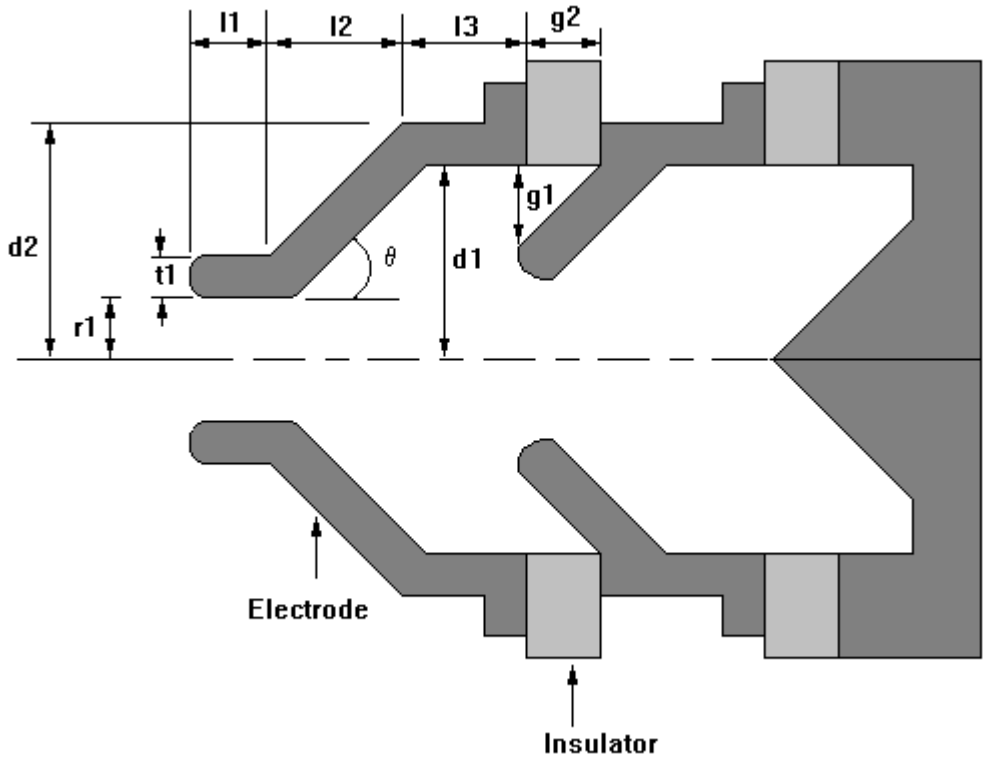

Outer Radius	d2
Inner Radius	d1
Beam Hole	r1
Length of Electrodes	l1,l2,l3

Thickness	t1
Gap Between Electrodes	g1, g2
Angle of Inclination	θ

Figure 6-3: Dimensions of a 3-stage collector

Some precautions are taken while changing the dimensions of the electrodes in an old geometry. These are as follows:

- *Gap between the electrodes*

In multistage collectors it is common to have an electrode entered inside the previous electrode (in the direction of the interaction circuit). This is to avoid the accidental hitting of ceramic insulators by the electrons, which may cause damage to them. A minimum value for g2 ensures a gap between the high voltage electrodes to avoid

sparking and a maximum gap prevents the electrons from hitting the high voltage insulator.

- *Outer radius*

The outer radius remains fixed to avoid excessively large or small collector volumes.

- *Inner radius*

In the case of a cylindrical electrode the inner radius (d1) should be large enough to maintain a reasonable gap (g1) between the electrodes. As the outer radius is fixed the maximum inner radius is also fixed. It is generally 1 or 2 mm smaller than the outer radius to allow for the thickness of an electrode.

- *Beam hole radius*

This dimension should be higher than the beam radius to accommodate the expanded beam. The spent beam electrons must not be allowed to strike on the top face of the electrode (surface toward the interaction circuit). Otherwise the secondaries and the reflected primaries generated here see an accelerating field, which causes them to stream back towards the interaction circuit.

- *Thickness of the electrodes*

Minimum electrode thickness should be fixed to a practical value.

- *Angle of inclination*

The minimum and maximum value is set to some practical values.

Other than the parameters mentioned here several other parameters, like the length of different parts of an electrode and the angles of the two faces of the electrodes, are also changed. The change in the angles of the faces is necessary for the optimisation of asymmetric tilted electric field (TEF) collectors. However for symmetric collectors these angles are always kept fixed at 90^0 with the axis of the collector.

6.3.4 Design Automation – Implementation of Random Walk Algorithm

The random walk approach has been implemented as a computer package. To implement this algorithm it is necessary to integrate the simulator (the geometry generator, the Poisson solver and the trajectory solver), the pre- and the post-processor and the random walk code. It is a huge task to integrate the whole set of codes as the

package transfers data through several common statements inside the subroutines and also through different programs. Several new files are also opened to store the data in the intermediate steps which are used either in the next phase of the same run or in the next run. After each cycle, the input data (i.e. the collector geometry data) file is stored in a separate file along with the performance analysis data. This helps in analysing the collector geometries and their performances in different intermediate stages of the program. The package runs in the unix operating system in a batch mode. A facility has been introduced to run the package in the background that terminates only after the user specified iteration number is reached. It is also possible to terminate the package once the targeted collector efficiency is achieved. The value of the optimised efficiency and the corresponding collector geometry data are stored separately. A documentation file has been included that illustrates the structure of the package and how to operate it.

6.3.5 Results and Validation

This package has been tested to optimise the design of a 4-stage symmetric and a 2-stage asymmetric collector. After several runs it is seen that the present package is capable of achieving a significant improvement in efficiency for a 4-stage collector. The collector efficiencies for different cases are shown in Table 6-1. In all these cases the starting point is the same. Figure 6-4 shows the collector efficiency at intermediate steps versus the number of iterations for all four cases. The difference between the optimised efficiencies for all four cases is prominent from this figure. The amount of change in the dimensions of the collector electrodes is random in any iteration in a specific run. Because of this, the intermediate steps are different. The maximum value of efficiency among all these can be considered as an optimum value. In this case the optimum value of collector efficiency is 89.20%. But the difference between the optimum and actual maximum can be reduced if the number of trials is increased. It should be mentioned here that the optimisation of the collector is carried out using 3-D simulation and it does not include the secondary electrons. This is to reduce the total computation time. If however the secondaries are included then the efficiency may be reduced by a few percent depending on the material used as the collector electrodes. The symmetric 4-stage collectors before and after optimisation are shown

in Figures 6-5(a) and (b) respectively. These figures do not include the secondary electrons. The efficiency for the geometry shown in Figure 6-5(a) is nearly 70%. The collector efficiency has been improved by a factor of 1.27. All trajectories in the plots are colour-coded; different colours represent different energy class.

In the second case a two-stage asymmetric tilted electric field (TEF) collector is chosen for optimisation purposes. The computed efficiency after different iterations is shown in Table 6-2. For this collector the optimised efficiency is about 82%. Figure 6-6 shows the collector efficiency at different intermediate steps for all four cases. These plots show that no improvement in collector efficiency was achieved after 200 iterations. The asymmetric 2-stage collector before and after optimisation is shown in Figures 6-7(a) and (b) respectively. In both case the colour-coded trajectories are plotted to show their energies. This gives an idea about where the trajectories are expected to land. These computations do not include the secondaries. The collector efficiency for the geometry shown in Figure 6-7(a) is nearly 79%. The improvement in efficiency is by a factor of 1.04.

6.3.6 Conclusion

The random walk approach has been proved to be working well for the optimisation of the performance of both symmetric and asymmetric collectors. However the end points are different in each case for a specific collector though the starting points are the same. A large number of trials is necessary to reduce the difference between the optimum and actual maximum efficiency. There is a possibility that the search may be trapped on a local maximum. This can be avoided by changing the starting points for different trials.

Table 6-1: Improvement in collector efficiency for different cases starting from the same geometry for a 4-stage symmetric collector (random walk method)

After Iteration	Case 1	Case 2	Case 3	Case 4
	Efficiency	Efficiency	Efficiency	Efficiency
1	73.03	71.29	72.87	73.55
50	83.41	83.57	85.94	83.11
100	83.45	83.57	87.45	83.11
150	83.46	83.57	87.45	83.11
200	83.77	84.30	87.45	83.90
250	84.88	84.30	87.45	87.37
300	84.88	85.52	87.45	88.97
350	84.88	85.52	87.45	89.20
400	84.88	86.24	87.45	89.20
450	84.91	86.24	87.45	89.20
500	84.91	86.24	87.45	89.20

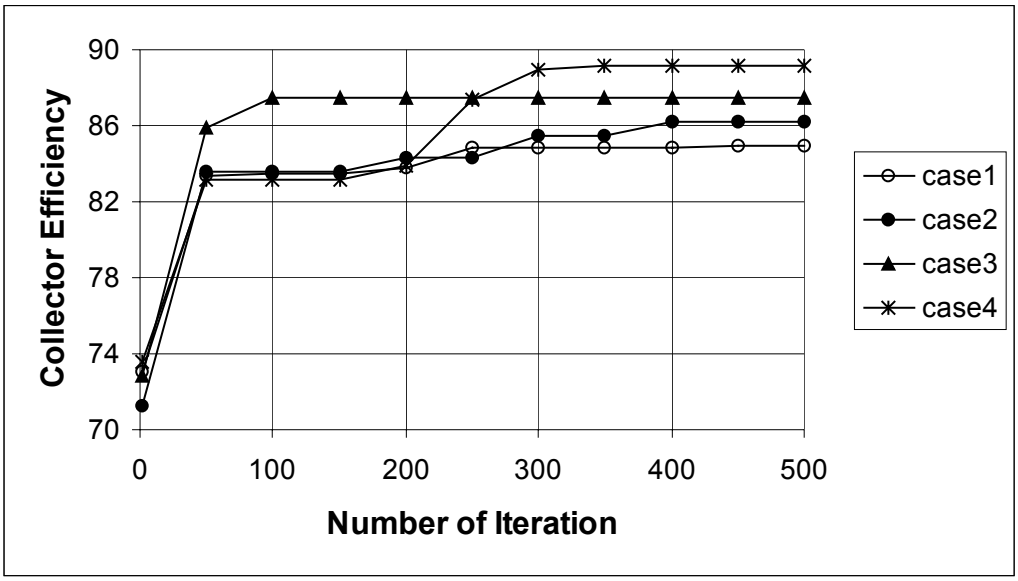

Figure 6-4: Collector efficiency versus the number of iterations

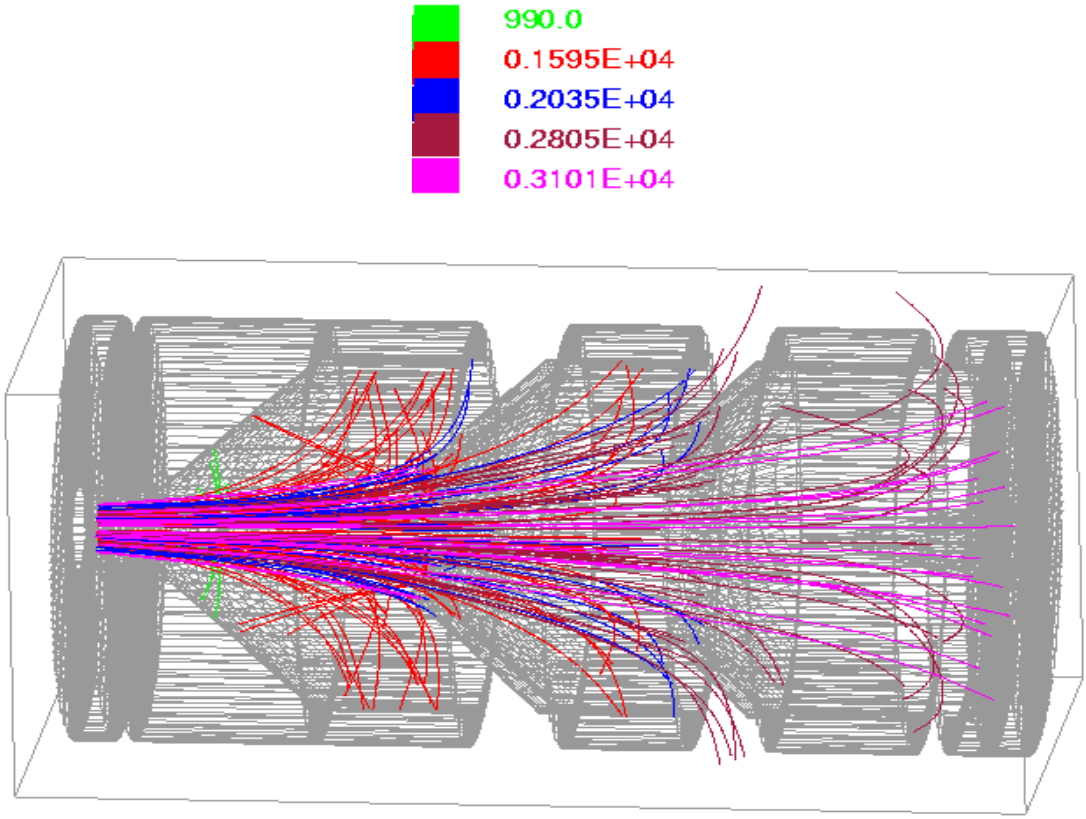

(a)

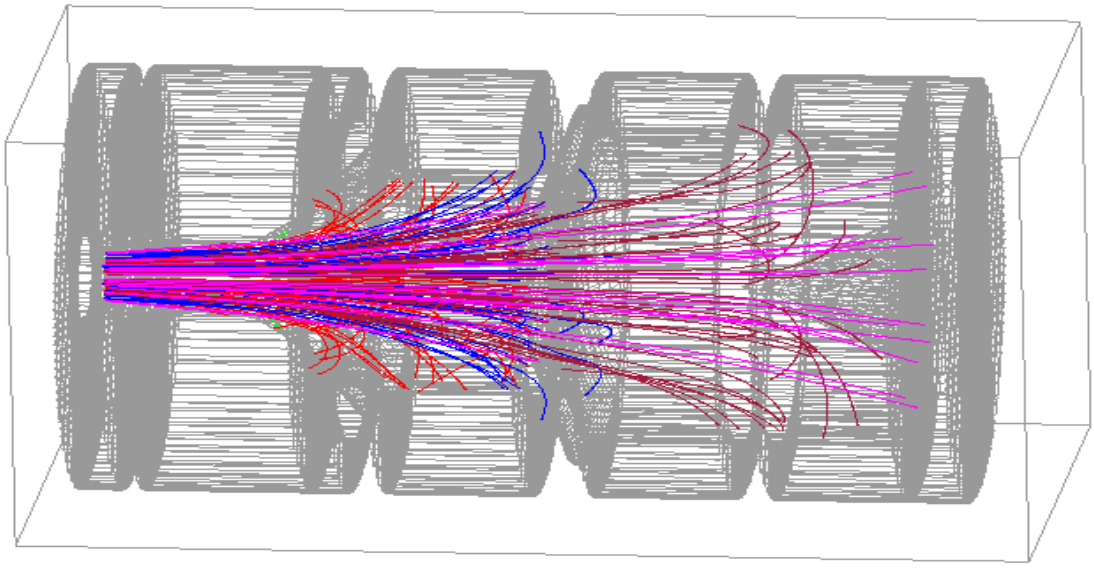

(b)

Figure 6-5: 4-stage axi-symmetric collector (a) initial geometry (b) optimised geometry using random walk method.

Table 6-2: Improvement in collector efficiency for different cases starting from the same geometry for a 2-stage asymmetric collector (random walk method)

After Iteration	Case 1	Case 2	Case 3	Case 4
	Efficiency	Efficiency	Efficiency	Efficiency
1	78.90	78.97	79.25	79.13
50	82.05	82.42	81.50	81.87
100	82.05	82.42	81.87	81.87
150	82.05	82.42	81.87	82.05
200	82.05	82.42	81.87	82.24
250	82.05	82.42	81.87	82.24
300	82.06	82.42	81.87	82.24
350	82.06	82.42	81.87	82.24
400	82.06	82.42	81.87	82.24
450	82.06	82.42	81.87	82.24
500	82.06	82.42	81.87	82.24

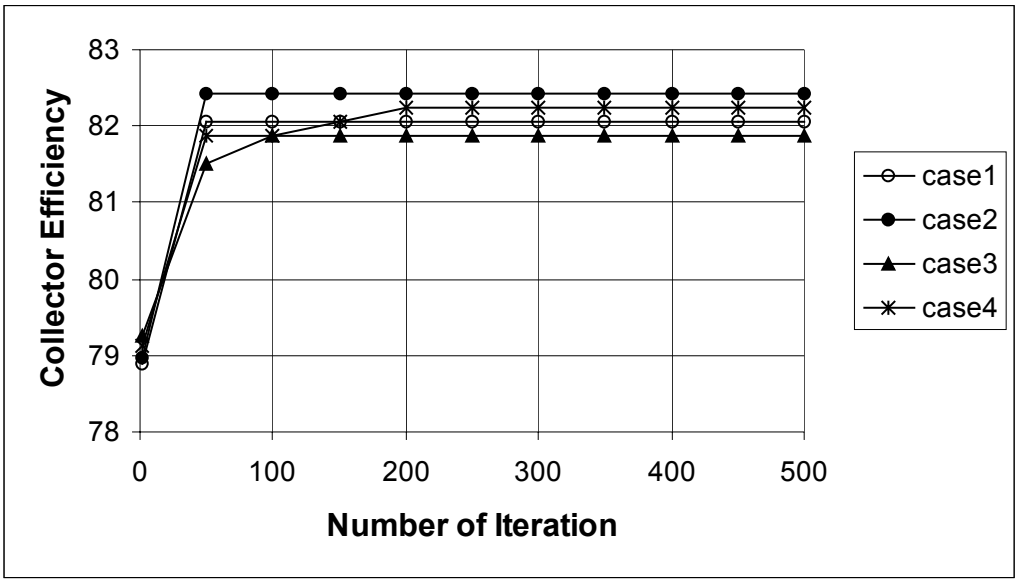

Figure 6-6: Collector efficiency versus the number of iterations

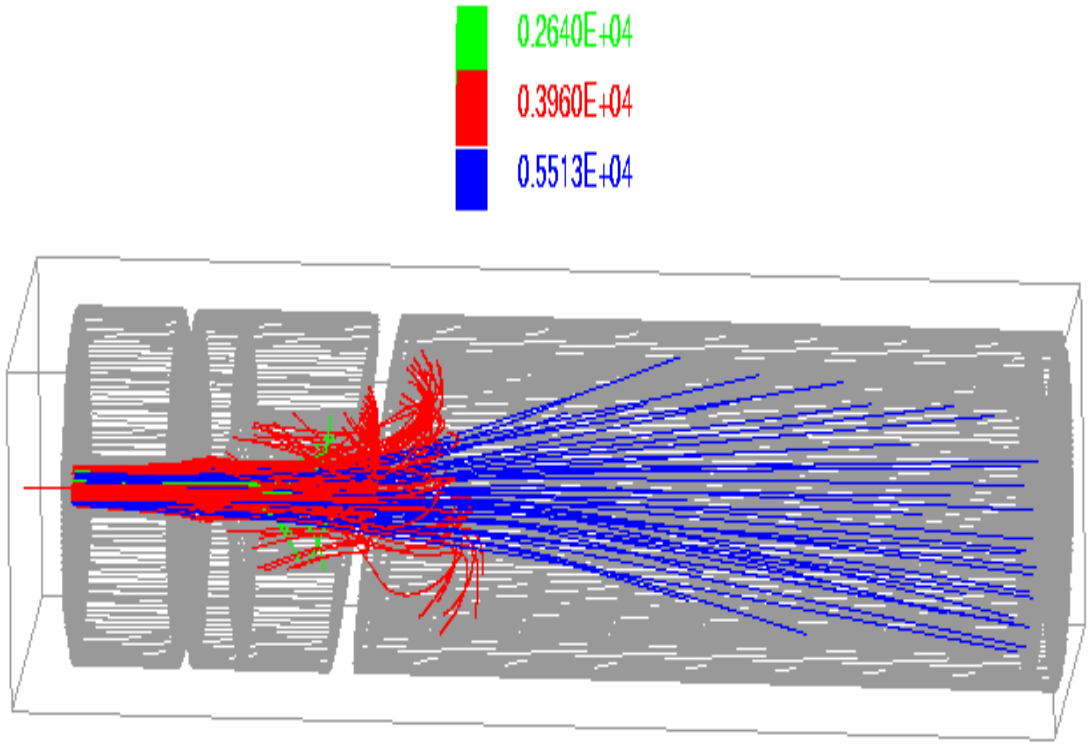

(a)

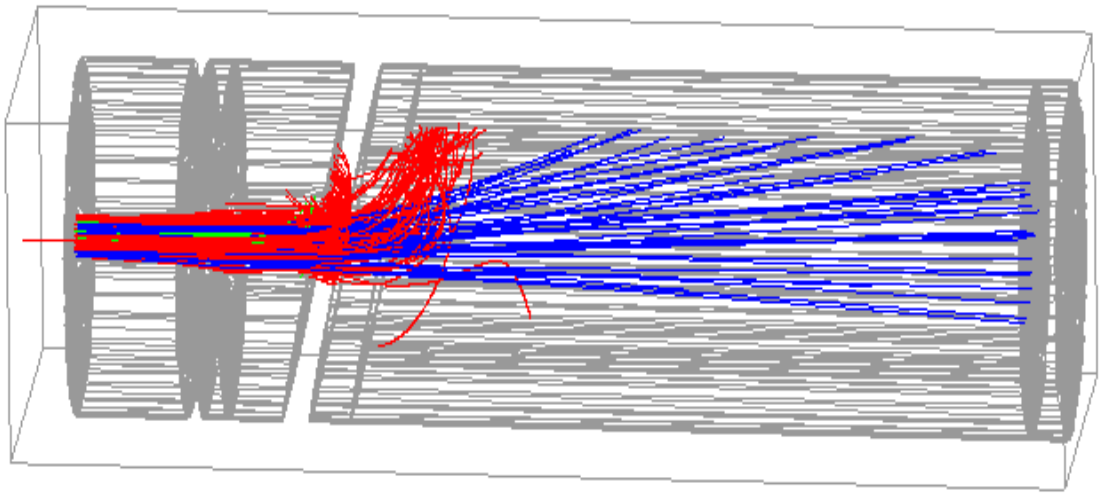

(b)

Figure 6-7: 2-stage asymmetric collector (a) initial geometry (b) optimised geometry using random walk method.

6.4 GENETIC ALGORITHM

There are many different complex problems, which can be perceived as a search through a space of potential solutions to find the best one [1]. As it is very difficult, sometimes impossible, to find the exact solution to these problems, the best possible solution is sought. So this can be viewed as an optimisation problem. For large spaces a special approach is required to reduce the time taken to solve the problem. One such technique is the genetic algorithm, which is based on some natural phenomena (natural selection and natural genetics) and the Darwinian theory of the survival of the fittest. The genetic algorithm generates a new set of data through a search procedure that uses random choice as a tool through a coding of a parameter space. Though it uses random choice as a tool for the search, it is still not directionless [2].

6.4.1 Principle – How It Works

The genetic algorithm works from a population of strings simultaneously unlike other methods where the search operation is carried out from a single point. The initial population is created randomly. Each member of the population is a string of binary data, which is called a chromosome. The size of the population and the length of each chromosome are defined by the user at the beginning. Generally these parameters remain always constant for a specific problem. All subsequent strings are generated using the three operators, namely (a) reproduction (b) crossover and (c) mutation.

In the reproduction process the strings are copied to the next generation according to the objective function or the fitness value. The fitness values are generally some measure like profit, utility, efficiency etc. A higher fitness value means a higher probability of contributing one or more offspring to the next generation. The most common way of implementing the reproduction process is through the roulette wheel, where the pie shaped slices are allocated to the members of the population, with each slice proportional to the fitness of the member [3]. A member of the population is selected as a parent if the spin on the wheel ends up on its slice of the wheel. Once the reproduction is over the strings are entered into the mating pool.

Crossover is an extremely important operator that is used to produce a set of children from the parent chromosomes. A one-point crossover is carried out in two steps. At first, two parent chromosomes are chosen at random for mating. In the next step the position of crossover is chosen. If it is the m-th position in the parent strings then all characters between (m+1) and 1 are swapped between the parents to create a new set of children. In an extreme case when the parents are the same, the crossover operator can introduce no diversity in the children.

Mutation has a secondary role in the genetic algorithm procedure and its probability is sometimes quite small. If at any time any member of the population loses any vital information then mutation is introduced to retrieve it. Every bit in the chromosomes of the population has the same probability to undergo the mutation when the bits are changed from 0 to 1 or vice versa. A number (floating point) between 0 and 1 is generated randomly which determines whether the mutation is to be done. If the number is higher than the mutation probability set by the algorithm then mutation is carried out.

The process of a simple genetic algorithm is summarised below:

(1) Initialise a population of chromosomes randomly based on the data supplied for the population size and the chromosome length.
(2) Calculate the fitness value for each chromosome using the object function. Use this value as a fitness parameter for reproduction.
(3) Generate a new population using the three basic operators reproduction, crossover and mutation.
(4) Repeat the process (2) and (3). Stop when the number of iterations is the same as the user specified number of generations or the fitness value is within a tolerable limit of the actual maximum value.

There are different variations of the basic formation of a genetic algorithm. In some cases a whole new population is not created in the new generation. Instead, only a few (one or two) chromosomes are replaced in the old population at a time. A genetic algorithm rarely repeats its performance as the initial population is started randomly. If any variation in the algorithm is made to solve a specific problem then it should be

run several times before coming to any conclusion. As a single run may result in a lucky hit, or it may give misleading information about the hypothesis the user makes [2].

6.4.2 Implementation of the Genetic Algorithm

A basic flow chart for the genetic algorithm package is shown in Figure 6-8. It has a similarity with Figure 6-1 except for the random walk box, which has been replaced by the genetic algorithm box. But the present method is more complex in comparison with the random walk approach and it is also difficult to implement.

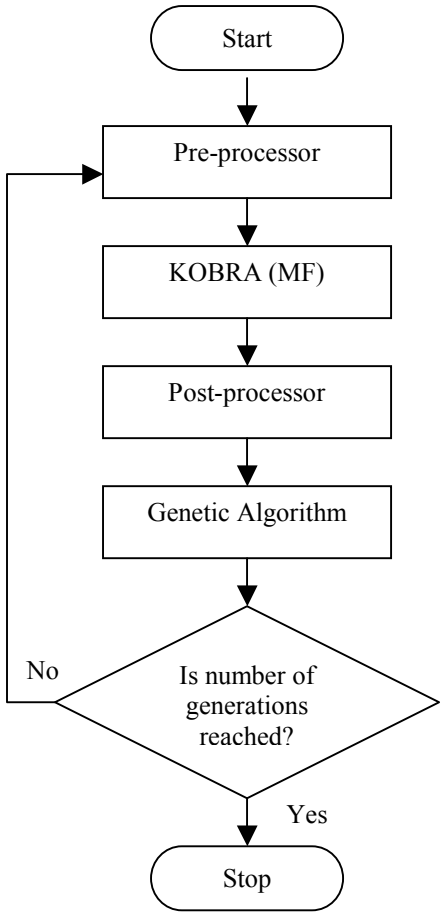

Figure 6-8: Basic flow chart for the genetic algorithm process used in our problem

Initially a population is generated randomly based on the input data. A non-repetitive random number generator produces the initial population in such a way that no two members in the population are same. The detail flow diagram of the genetic algorithm process is shown in Figure 6-9.

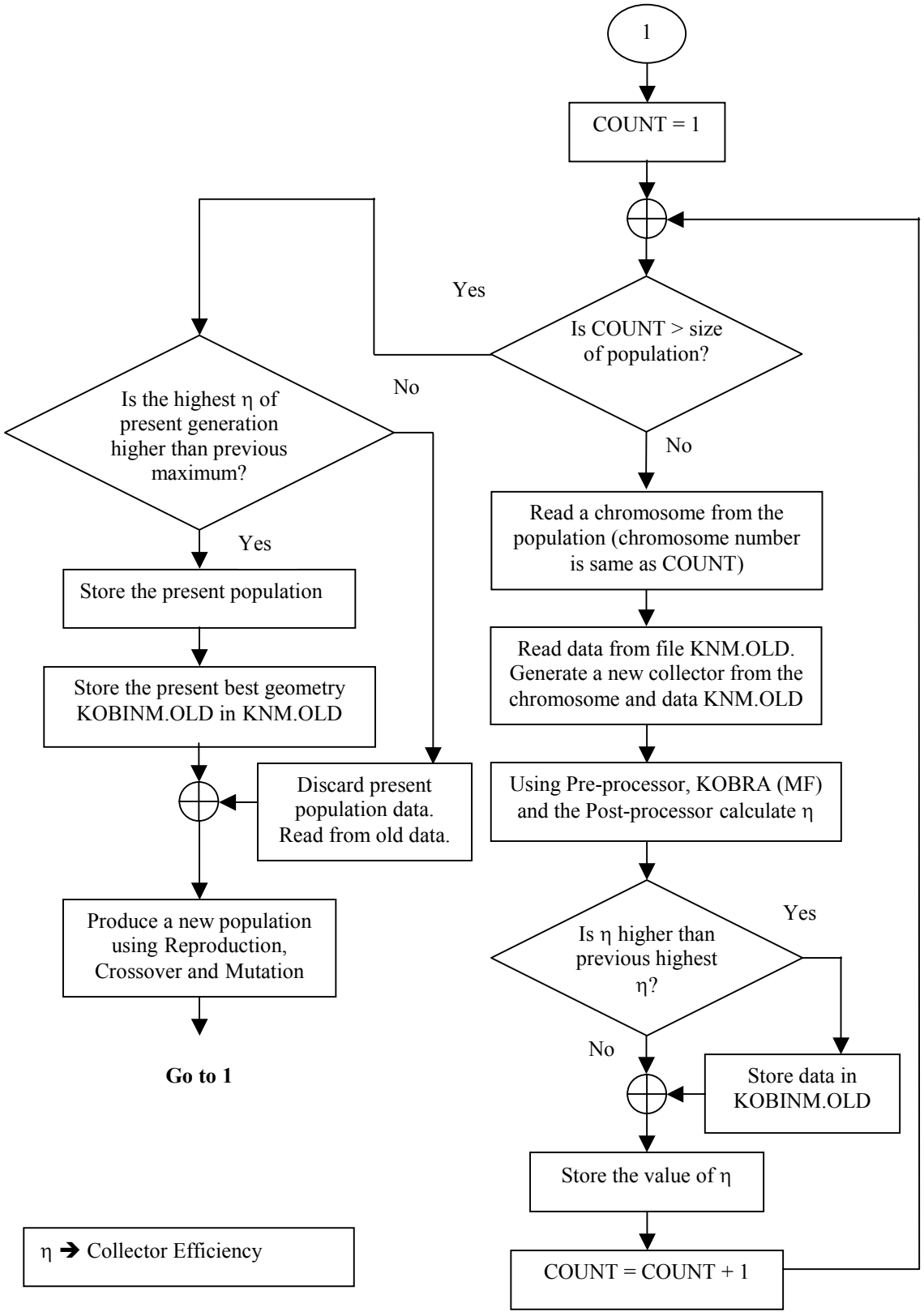

Figure 6-9: Detail flow chart for the genetic algorithm section

The sequence of events in the flow chart is described in steps for better understanding of the total procedure.

Sequence of Operations

1. First, the size of the population, the length of the chromosome, and the total number of generations are chosen.
2. Using a random number generator a set of binary numbers is generated each of a length equal to the length of the chromosome. The size of the population is as set earlier. These two parameters remain the same throughout the computation.
3. A set of basic collector geometry data is created from the previous experience and used as its preliminary design. This can also be done by scaling an existing collector.
4. Using each chromosome and the basic collector geometry data a set of new collectors is generated. The number of collectors is the same as the population size.
5. The pre-processor of the simulator creates one input data file using each set of geometry data and the trajectory data. The starting conditions of the trajectories are stored separately and these values remain the same throughout the computation. Only the geometry of the collector is changed according to the member chromosome of the population.
6. For each input file the geometry generator of the package creates the mesh and defines the boundary at all six faces of the collector. The potential and trajectories are solved through several iterations using the Poisson and trajectory solvers respectively.
7. Once the converged solution is achieved the efficiency of the collector is calculated using the post-processor of the package. This quantity is used as the object function value for the corresponding chromosome. Thus each chromosome now has an object function value or a fitness value. From the second generation onwards, a new population is generated from the previous population through the three main operators - reproduction, crossover and mutation. These three operators are discussed in detail in the next section.
8. If all members of the new population are the same then a single bit mutation is carried out on all members to introduce diversity among the members. A random

number between 1 and the chromosome length is generated which determines the position of mutation. This number is different for each chromosome.

9. The function of the genetic algorithm for this generation is over and the process is repeated for the next generation. The best collector geometry data corresponding to the best efficiency achieved in the present generation is used as the basic geometry data for the next generation.
10. Now the steps from 3 to 9 are repeated till the number of generations (user specified) is reached. If at any generation the best efficiency is not better than the previous best, then the total population is discarded and a new population is created from the previous population.
11. The chromosome and the corresponding efficiency values are written for any population after each generation. The optimised geometry and the efficiency are stored in a separate file to track the progress easily.

6.4.3 How to Create a New Geometry

To introduce diversity in the optimisation procedure the search is started from a population instead of from a point and the size of the population is chosen to be large. A large population means a large number of geometries that covers a number of points in the search space for possible solution. It also provides a large number of alternative paths towards the convergence. With chromosome length 10 there are $2^{10} = 1024$ points in the search space. The larger the length of the chromosome the larger the number of points it covers in the search space. In the multistage collector problem, it is assumed that the chromosome length is same as the number of simple electrodes. In the LKOBRA package the number of electrodes is not considered to be the same as the number of collector stages as the complex electrode geometry is created combining the pre-defined simple electrodes. An example is shown in Figure 6-10 where a funnel is combined with a cylinder to form an electrode.

In any population each chromosome corresponds to a different geometry of a collector. Each member chromosome has a binary bit specified for each electrode, which is used to change the basic collector geometry (e.g. funnel or cylinder in Figure 6-10). It is also possible to associate each binary bit with a dimension of electrode. In

that case the chromosome length will be large. All dimensions of an electrode (e.g. length, angle, inner diameter, outer diameter etc.) are increased if the bit is 1, and the reverse will occur if the bit is a 0. The amount of increment (or decrement) varies for different dimensions. But generally it is done in very small steps to account for the little changes in the collector efficiency due to the changes in the electrode dimensions. Thus a new geometry for the collector is formed corresponding to each member of the population. The critical dimensions of the electrodes have been identified in section 6.3.3.

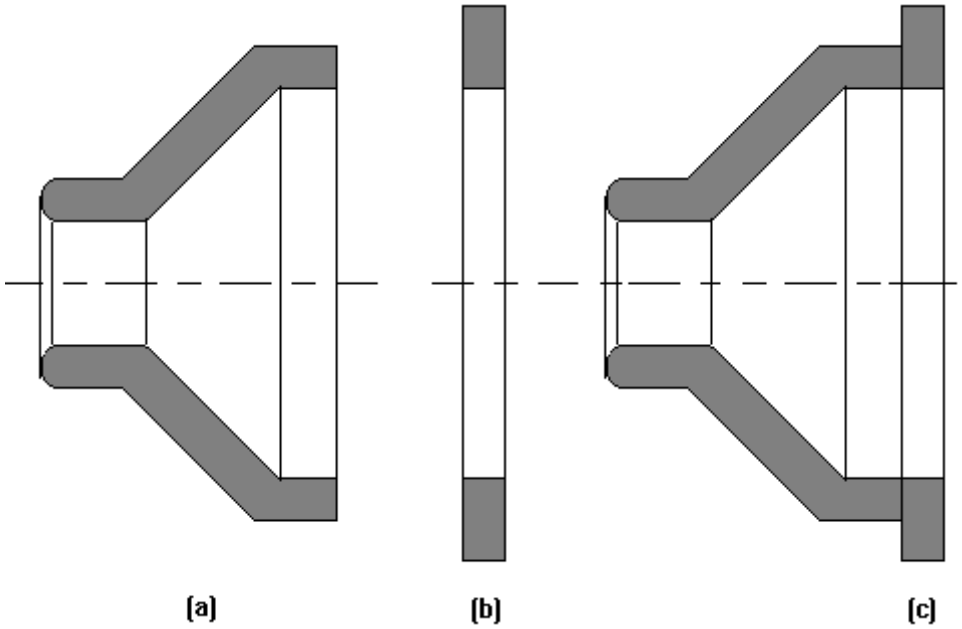

Figure 6-10: Electrode shapes (a) funnel (b) cylinder (c) complex shape formed by combining funnel and cylinder

6.4.4 Reproduction, Crossover and Mutation

Each member of the population produces a number of its offspring in the next generation with a probability proportional to the collector efficiency, which corresponds to that member of the population. These members are entered into the mating pool where the pair of parents is chosen randomly from the population. The number of pairs is made half of the population to maintain its size constant. This process is called reproduction. The process of reproduction is demonstrated below with an example. A typical population is shown in Table 6-3 where the size of population is 4 and the length of each chromosome is 10.

Table 6-3: A typical reproduction process

String No.	Randomly Generated Initial Population	Fitness Value	Number of Offspring Generated
1	1010110111	75	2
2	0101001100	45	1
3	0011010110	40	1
4	0001110001	20	0

The fitness value corresponding to each chromosome of the population is shown in the third column, which is chosen randomly as an example (in practice these values are some pay-off values). The number of offspring generated in each case is shown in the fourth column. In the first case the number of offspring is two as the best get more copies and in the second and third case the number of offspring is one, whereas the member of the last population with worst fitness value dies off.

The next process is crossover. In this problem we have used a single point crossover. A number generated randomly between '1' and the 'chromosome length' is used as the point of crossover. All digits between the point of crossover and 1 are swapped between the pair of parents to produce two children. These children form the new population. The crossover process is shown in two steps in Tables 6-4(a) and 6-4(b). In Table 6-3 the first chromosome has generated two offsprings and the third and the fourth chromosomes have generated one offspring each. Therefore in Table 6-4(a) the first two chromosomes are same as the first chromosome in Table 6-3. Similarly the third and fourth chromosomes in Table 6-4(a) are same as the second and the third chromosomes in Table 6-3. Out of these chromosomes in Table 6-4(a) pairs are chosen randomly. In this case the first and third chromosomes make a pair and the second and the fourth chromosomes make the second pair. A random number generator generates a number between 1 and the chromosome length that is used as the point of crossover. All members of the chromosomes between 1 and 7 (point of crossover 6) are swapped in the first case to produce a pair of children. The old and the new populations are shown in Table 6-4(c).

Mutation is carried out when all chromosomes in a population are same. A random number is generated between 1 and the length of the chromosome that determines the position of the bit where mutation is to be done. This position is different for each chromosome.

Table 6-4: (a) reproduction (b) crossover (c) old and new population

String No.	Population After the Reproduction	String No.	Randomly Selected Pairs
1	1010110111	1	1010110111
2	1010110111	3	0101001100
3	0101001100	2	1010110111
4	0011010110	4	0011010110

(a)

Parent 1	1010110111	Child 1	0101001111
Parent 2	0101001100	Child 2	1010110100
Crossover at 6 (Randomly Chosen)			
Parent 3	1010110111	Child 3	0011110111
Parent 4	0011010110	Child 4	1010010110
Crossover at 3 (Randomly Chosen)			

(b)

String No.	Old Population	New Population
1	1010110111	0101001111
2	1010110111	1010110100
3	0101001100	0011110111
4	0011010110	1010010110

(c)

6.4.5 Some Assumptions

During the optimisation process a few assumptions are made to reduce the complexity of the algorithm. Present population is not always used to produce a new population for the next generation. The suitability of the population in producing a new generation depends on the maximum value of the collector efficiency achieved during that generation. If this value is higher than the previous maximum then it is accepted as the parent population to produce a new generation. Otherwise the present population is discarded altogether and the previous population is used as the basis for generating the new population. The following assumptions are made in the implementation of the genetic algorithm:

- The population size is constant. Though this is in contrast with the natural procedure, this assumption is made as it is simple to implement and it takes less storage space.
- The population size is an even number.
- Each string is of equal length; the length is constant throughout the computation.
- A single point crossover is used and the probability of crossover is always 1.
- Mutation is used only when the chromosome loses vital information and all members in the population become the same.

6.4.6 Results And Validation

A fully automated computer package has been developed using the genetic algorithm. Designs of a 4-stage symmetric and a 2-stage asymmetric collector have been optimised using that package. These are the same collectors, which have been earlier optimised using the random walk technique. This package has been tested in a similar way as the random walk package. For the symmetric collector the population size, chromosome length, probability of crossover and the maximum generation are assumed 8, 12, 1 and 50 respectively; in the case of the asymmetric collector these values are 8, 6, 1 and 50 respectively.

- *Symmetric collector*

After four trials it has been seen that the present package is capable of achieving an efficiency of more than 90% for the 4-stage symmetric collector. In all four cases the amount to be changed in a specific dimension in each step is not the same. A maximum and a minimum limit have been set for the amount to be changed in each step. Any value between these limits can be chosen randomly to make a change in that dimension of the electrode. In Table 6-5 the results for four different trials are shown. As the initial population in the genetic algorithm is created randomly and it is non-repetitive (each time the package is run, the initial population is different) the intermediate steps are different although the optimised results are nearly the same. The improvement of collector efficiency is plotted versus the number of generation in Figure 6-11 to show the convergence in each case. This shows the intermediate steps towards the convergence.

The geometry of the 4-stage collector with the primary trajectories before and after optimisation is shown in Figures 6-12(a) and (b) respectively. The geometry of the collector in Figure 6-12(b) corresponds to the results as shown in case 1 in Table 6-5. In this case, an improvement by a factor of 1.3 in collector efficiency was achieved due to optimisation of its geometry. None of these computations include secondary electron emissions. The potentials for this collector are 0 V, -900 V, -1450 V, -1850 V and –2550 V for the interfacing ring (body), electrode 1, electrode 2, electrode 3 and electrode 4 respectively. The trajectories with green colour should be collected at electrode 1 because their energy range is within 10% limit of 900 V. Similarly trajectories with red colour should be collected at electrode 2, trajectories with blue should be collected at electrode 3 and rest (brown and pink) should be collected at electrode 4. It is clear from the Figure 6-12(a) that the trajectories are not collected at the right electrodes where they should be. Some red and blue trajectories are collected at electrode 1, and electrode 2 respectively. The energies of these electrons are not recovered fully which will cause excessive heating and reduce the collector efficiency. Some brown and pink trajectories are collected at the front of the third and second electrode respectively because of the smaller aperture diameter. The secondaries generated from these trajectories will either be collected at a higher potential or stream back towards the interaction region that will degrade the collector performance. The simulated results for this collector are shown in detail in Appendix B.

In the optimised design (Figure 6-12(b)) the trajectories with red colour are mostly collected at electrode 2, trajectories with blue colour are collected at 3, trajectories with brown are collected either inside electrode 3 or at electrode 4 and the final group of trajectories with pink colour are collected at electrode 4. Sorting of electrons is better in case of the optimised design and this is the reason why the collector performance is better in this case than the previous one. A careful observation to the two figures reveals that the length of the optimised collector is shortened by nearly 30%, which has reduced both the volume and the weight of the collector. This is quite significant for space and airborne applications.

- *Asymmetric collector*

For the 2-stage asymmetric collector the optimised efficiency is about 84%. The optimum collector efficiencies for different cases are shown in Table 6-6. The best collector efficiency at intermediate steps for all four cases is plotted in Figure 6-13. As in the previous example, the starting geometry is the same in all four cases. The geometry of the 2-stage asymmetric collector before and after optimisation is shown in Figures 6-14(a) and (b) respectively. The geometry in Figure 6-14(b) corresponds to the collector as shown in case 2 in Table 6-6. The improvement in collector efficiency is about 5% points. None of these computations included the secondary electrons.

- *Repeatability*

To check the repeatability of the results the best collector efficiency for all four trials (from case 1 to case 4) are plotted versus the trial number in Figure 6-15. For both collectors the optimum efficiency remains nearly the same. This repeatability feature of the algorithm makes it a better choice over other random methods.

Table 6-5: Improvement in collector efficiency for different cases starting from the same geometry for a 4-stage symmetric collector (using genetic algorithm)

After Generation Number	Case 1	Case 2	Case 3	Case 4
	Efficiency	Efficiency	Efficiency	Efficiency
1	79.97	79.62	80.22	79.73
5	83.22	81.79	83.68	82.10
10	83.48	82.21	85.80	84.39
15	83.64	83.67	89.12	85.17
20	86.01	86.95	89.12	88.56
25	86.69	87.95	89.13	89.71
50	90.92	90.62	89.46	90.32

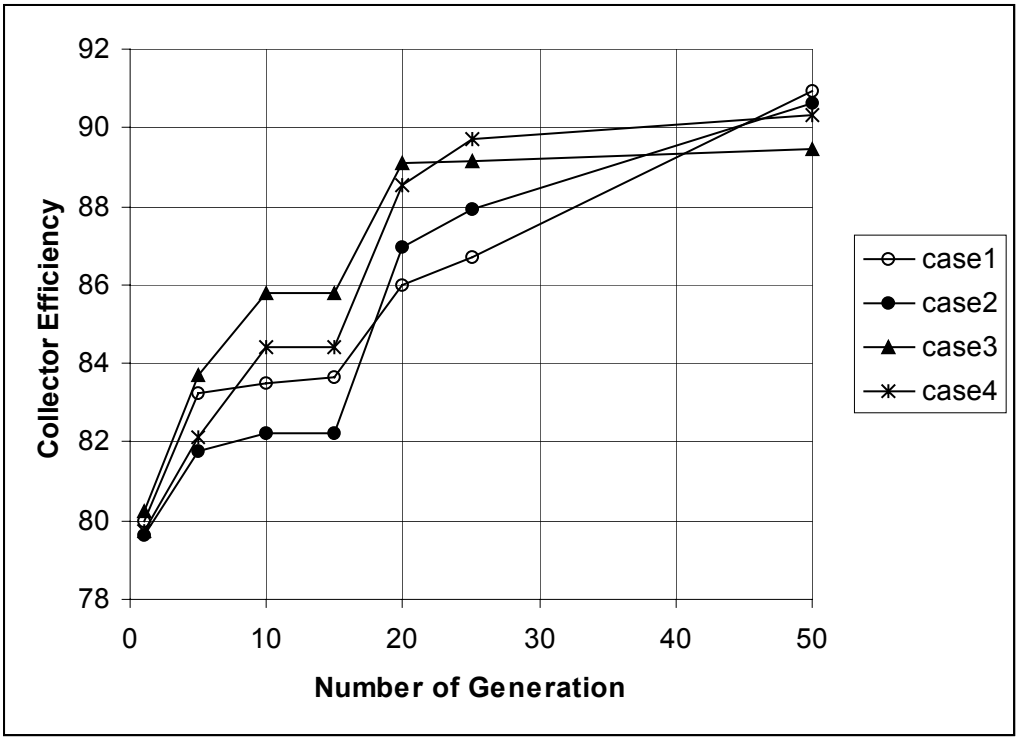

Figure 6-11: Improvement of collector efficiency versus the number of generation for the 4-stage symmetric collector

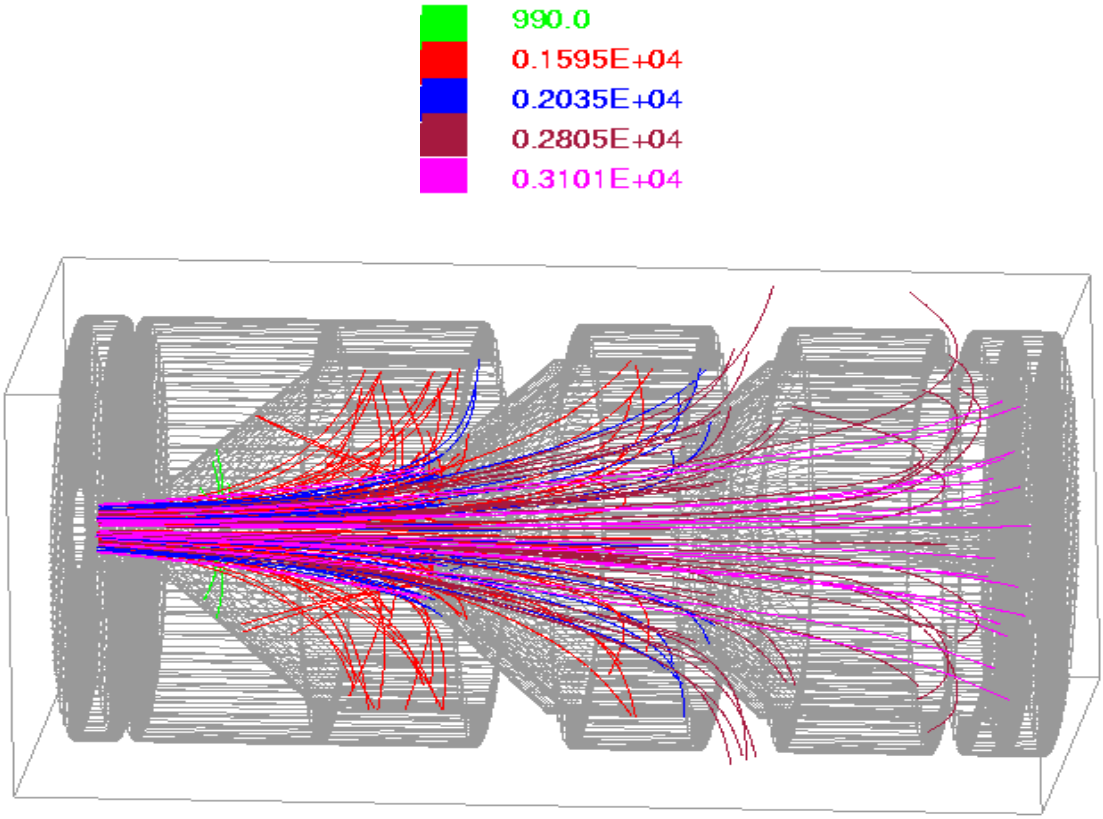

(a)

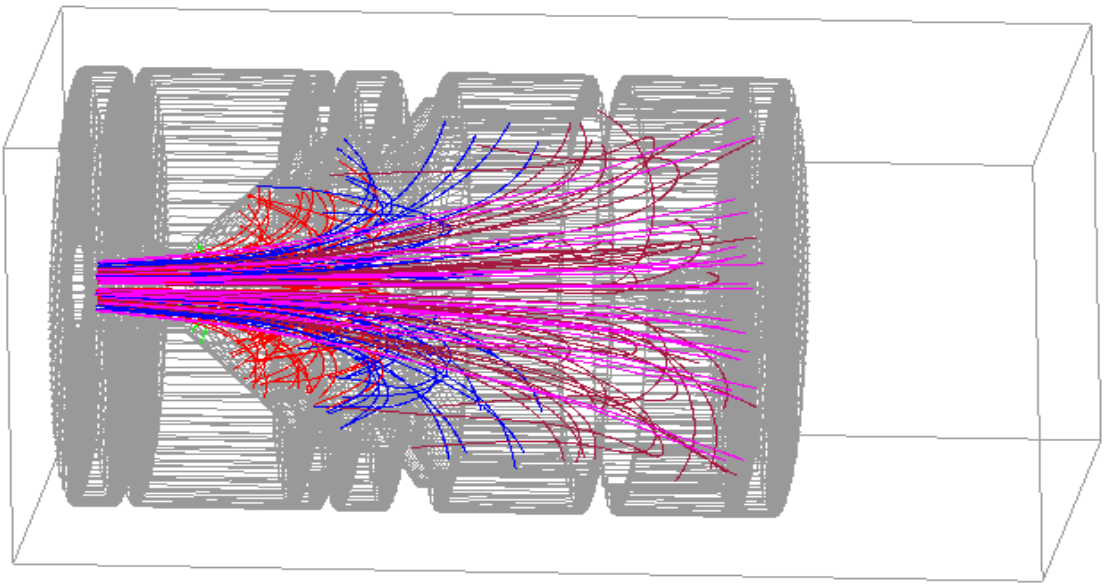

(b)

Figure 6-12: 4-stage axi-symmetric collector (a) initial geometry (b) optimised geometry using genetic algorithm.

Table 6-6: Improvement in collector efficiency for different cases starting from the same geometry for a 2-stage asymmetric collector (using genetic algorithm)

After Generation Number	Case 1	Case 2	Case 3	Case 4
	Efficiency	Efficiency	Efficiency	Efficiency
1	78.90	78.93	79.10	78.96
5	82.60	81.13	81.14	81.68
10	82.60	82.42	82.42	82.60
15	82.60	83.16	82.42	82.79
20	82.60	83.34	82.42	82.79
25	82.60	83.52	82.60	82.79
50	82.60	83.70	82.79	82.79

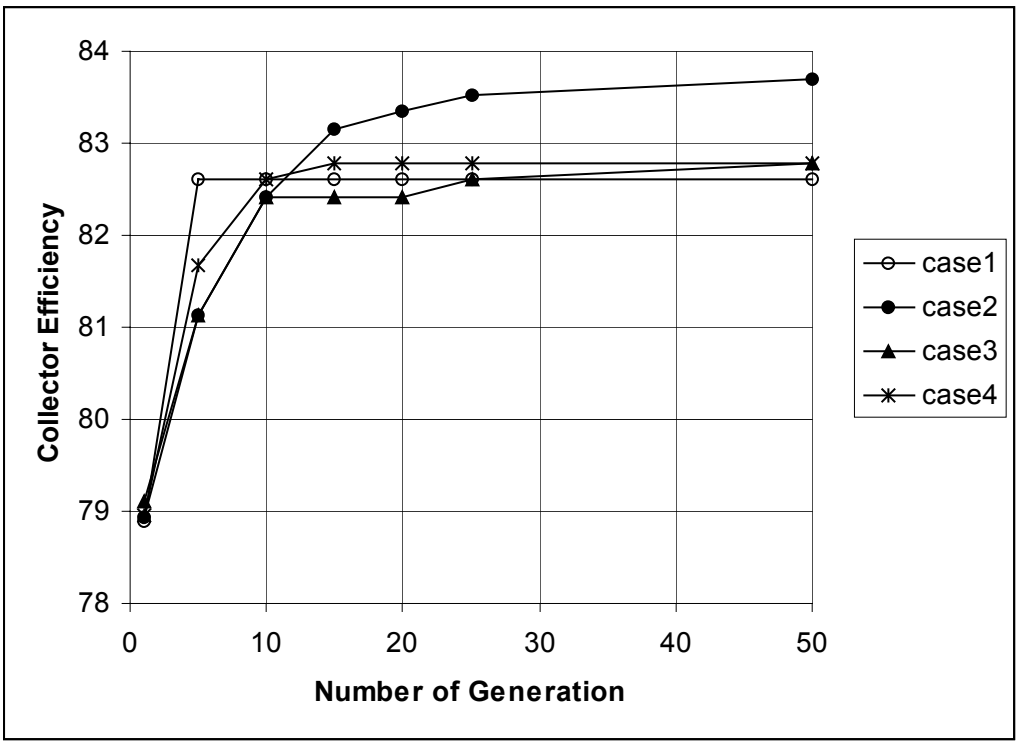

Figure 6-13: Improvement of collector efficiency versus the number of generation for the 2-stage symmetric collector

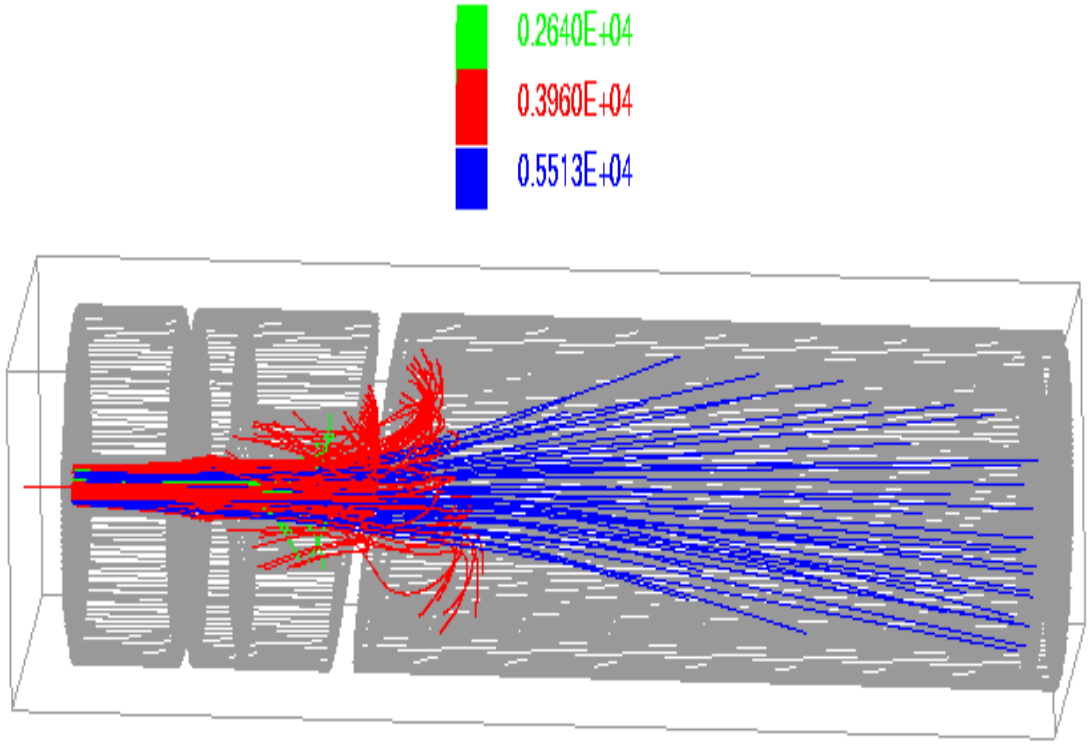

(a)

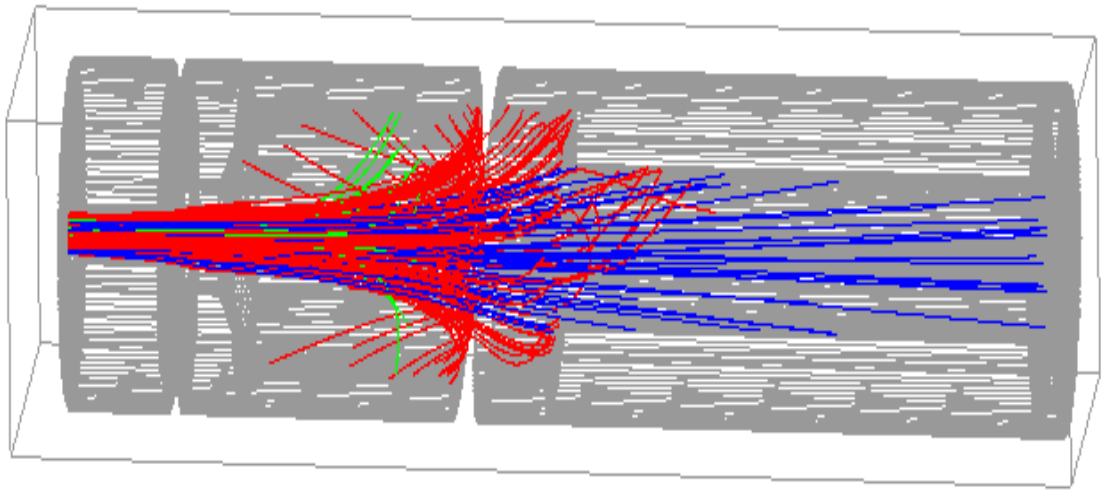

(b)

Figure 6-14: 2-stage asymmetric collector (a) initial geometry (b) optimised geometry using genetic algorithm.

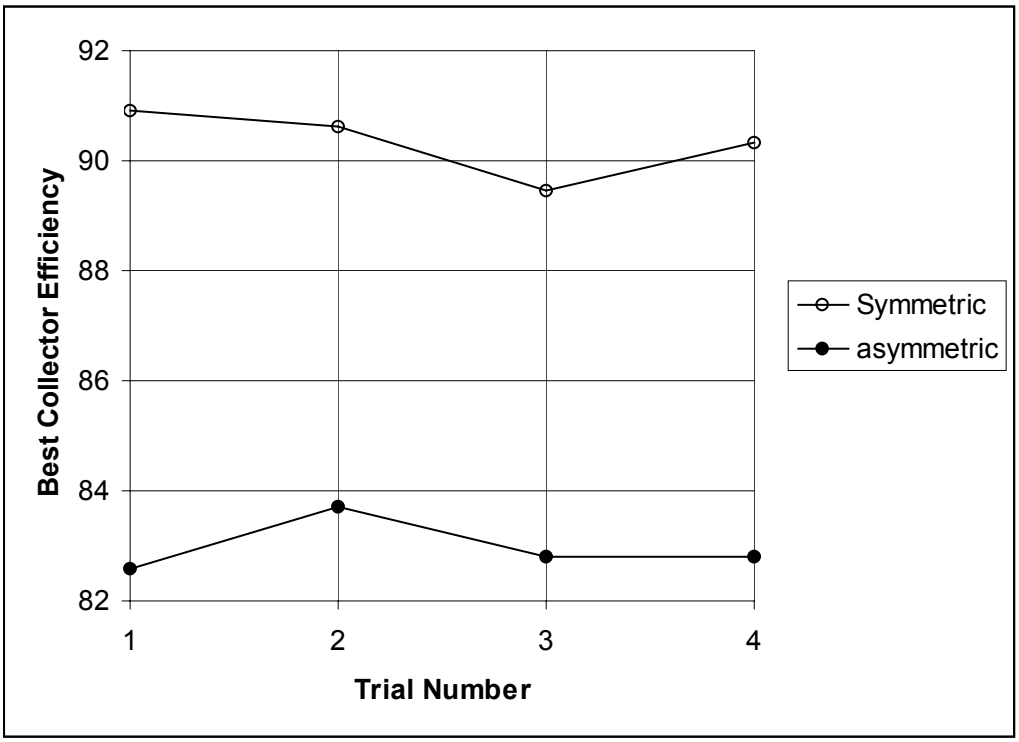

Figure 6-15: Best collector efficiency in each trial versus the trail number showing the reproducibility of the results.

6.4.7 Conclusion

The genetic algorithm has been proved to be a powerful tool for optimising the performance of the multistage collectors. For complex problems where both the number of variables and the search space are large the genetic algorithm can be the prime choice if used efficiently. Previous experience in design and simulation may be helpful in implementing this algorithm for optimisation purposes. Different variations of this algorithm may be tried to reduce the time taken to solve the complex problems. Each time the genetic algorithm follows a different path towards the optimisation, as the intermediate steps are different. The starting population is also generated randomly. But the targets are nearly the same. Both symmetric and asymmetric collectors were successfully optimised using this algorithm and the repeatability of the results was achieved. But the effects of the secondary electrons were not included in

the simulation. The loss in the collector efficiency due to the secondary electrons can be estimated to be a few percent depending on the material of the collector electrodes.

6.5 ADVANTAGES OF GENETIC ALGORITHM OVER OTHERS

In the hill-climbing technique the improvement in the value of the objective function is obtained through iterations. It is a single point search technique in the search space. In any iteration a single point is searched in the neighbourhood of the current point (that is why it is called a neighbourhood search or the local search) [1]. If the new point has a better value of the object function then it can be accepted as a new base point. The hill-climbing routines always find the local maximum and the maximum value depends on the starting point of the search. In the simplest hill-climbing technique a single variable is changed each time in the space. This makes it completely unsuitable for complex problems where the number of variables is large.

A better method called random walk can be used for relatively complex problems. If the number of variables is large then it is not possible to check all possible combinations of the variables to search the exact solution. Instead of that the random walk method can be used where the next point in the search space is obtained by changing all variables simultaneously. This method is totally random and may also end up in a local maximum like the hill-climbing technique. To make this method effective it is necessary to start the operation from different points in the search space.

Simulated annealing is a global optimisation method. This has been successfully applied for the optimisation of collector geometries [5] but there is a possibility of getting trapped in the local minima. This can be avoided by starting the computation from more than one point instead of a single point. In that respect this method has a similarity with the genetic algorithm.

Genetic algorithms employ an artificial version of the natural selection procedure and they are used to solve complex problems where the optimisation is of prime importance rather than the exact solution. They use the theory of probability for search

operations. In this method a population of strings is used to search for the better object function value, which is in contrast with other methods where the search operation is carried out using a single point. The previous value of object function is used to select the next point with improved value. The three basic operators generate a new population on the basis of the previous fitness parameter. This makes this algorithm more intelligent and robust. In that sense the other methods (except the simulated annealing method) are random.

6.6 SUMMARY

The random walk method and the genetic algorithm have been used successfully to optimise both symmetric and asymmetric collectors. The first method can be used if a sufficiently large number of trials are carried out and the best result out of these trials can be used as the optimised value. But in the second case the end result for each trial is nearly the same. Several assumptions are made to implement the algorithms for the optimisation of the collector. None of the optimisation methods include the effect of secondary electrons.

REFERENCES

[1] Z. Michalewicz, *Genetic Algorithm + Data Structure = Evolution Programs*. Berlin: Springer-Verlag, 1992, pp. 1-200.

[2] D. E. Goldberg, *Genetic Algorithms in Search, Optimization, and Machine Learning.* Addison-Wesley Publishing Company, Inc., 1989, pp. 1-170.

[3] L. Davis, *Handbook of Genetic Algorithms*. Van Nostrand Reinhold, 1991, pp 1-101.

[4] L. Davis, *Genetic Algorithms and Simulated Annealing*. London: Pitman Publishing, 1990, pp. 1-216.

[5] K. R. Vaden, J. D. Wilson, and B. A. Bulson, "A Simulated Annealing Algorithm for the Optimisation of Multistage Depressed Collector Efficiency," in *Proc. of 3rd IEEE International Vacuum Electronics Conference 2002*, April 23-25, 2002, pp. 164-165.

[6] T. K. Ghosh and R. G. Carter, "Design Optimisation of Multistage Depressed Collectors for High Efficiency Travelling Wave Tubes Using Genetic Algorithm," in *Proc. of 3rd IEEE International Vacuum Electronics Conference 2002*, April 23-25, 2002, pp. 158-159.

Chapter 7

Conclusion and Future Work

7.1 INTRODUCTION

The thesis has demonstrated the modelling and simulation of multistage depressed collectors including the effects of secondary electrons and the magnetic field. A fully three-dimensional simulator LKOBRA (MF) has been developed for this purpose. This is based on an ion-source simulator KOBRA3. The mainframe version of the original simulator and the pre-processor of the package have been modified. Some new options have also been created in the pre-processor. The post-processor of the package has been created afresh; this includes the secondary electron emission model and the analysis package.

A new technique has been developed for the optimisation of multistage collector performance. The number of electrodes can be determined and their potentials can be optimised using the computer code developed during this project. This code can also be used for the sensitivity analysis of the collector. Finally, the geometry of multistage collectors has been optimised using an advanced search algorithm called genetic algorithm. A fully automated three-dimensional package has been developed for this purpose, which includes the pre- and post-processor, mainframe version of the simulator KOBRA3 and the genetic algorithm program. The package has been written in FORTRAN. Presently, it runs in unix. A batch file has been written that makes it possible to run the package in the background.

7.2 SUMMARY OF THE THESIS

The first chapter of the thesis introduced the concepts of TWTs and multistage collectors and their applications. Some basic principles on the way the multistage collector works and the difficulties in designing them were discussed. The objectives of the project and the novelty of the thesis were described at the end of this chapter.

A list of criteria to choose a computer code for its suitability to simulate the multistage collectors was presented in Chapter 2. Based on the criteria a literature review on the existing three-dimensional computer codes was carried out. A background study on the modelling and simulation of both symmetric and asymmetric collectors was carried out and the findings were presented in this chapter. Finally, the importance of the present research was discussed in the light of these findings.

A three-dimensional package and its pre- and post-processors was developed to achieve the aim of the project. The DOS version of the package was modified and transferred to unix to increase the speed of computation. Different properties and the evaluation test results of this package were discussed in detail in Chapter 3. A 2-stage asymmetric collector was simulated and the computed results were compared with the experimental values. The fact that these agree well validates the package.

The post-processor of the package includes a secondary electron emission model, which was developed afresh. The details of this model were discussed in Chapter 4. A 2-stage asymmetric collector was simulated with and without the effects of the secondary electrons. This shows the effects of secondary electrons in the collectors. The effect of the transverse magnetic field on the primary and secondary electrons was also presented in this chapter.

An algorithm based on the enumerative technique was developed to optimise the electrode potentials in the multistage collector. A detailed description of this algorithm is presented in Chapter 5. This algorithm is also capable of doing the sensitivity analysis of the collector performance. An example was presented to demonstrate its capability for the sensitivity analysis of collectors at different input drive levels.

Different techniques for the optimisation of the collector performance were discussed briefly at the beginning of the Chapter 6. A computer code based on the random walk algorithm was developed. The automated package was tested for both symmetric and asymmetric collectors. This package has been proved to be useful if the number of trials is large. A new technique called genetic algorithm was used to optimise the collector geometry. A fully automated computer code was developed using this package. This package demonstrated its suitability by optimising a 2-stage asymmetric and a 4-stage symmetric collector. Finally the advantages of the genetic algorithm over other optimisation techniques were discussed.

7.3 MAIN CONTRIBUTIONS

The objectives of the thesis are the modelling and simulation of multistage collectors and the optimisation of their performance. To fulfil these objectives some major work has been done.

- *Development of a three-dimensional simulator*

A three-dimensional package LKOBRA (MF) has been developed. The DOS version of the original package has been transferred to unix. The mesh generator and the trajectory solver have been modified for better accuracy. All graphics programs have been modified and coloured to improve their quality. Several new options have been introduced for better representation and understanding of the simulated results. An option to generate the postscript files has been introduced for both two-dimensional and three-dimensional graphics.

- *Development of the pre- and post processors*

The pre-processor has been modified to make it more user-friendly. The option to create an input file using the data file has been introduced. The post processor that includes a secondary electron emission model and an analysis program has been developed afresh.

- *Mapping of the 2.5D LSM data into the 3-D beam data*

An input interface between the LSM and the simulator has been developed. This enables the simulator to use the LSM generated trajectory data directly.

- *Development of the secondary electron emission model*

A secondary electron emission model has been developed based on some experimental results and empirical formula. This model calculates the starting conditions of the secondary trajectories. The effects of secondary electrons have been tested in an asymmetric collector. The simulated results have been compared with experimental data to validate the model.

- *Evaluation of the simulator*

The accuracy of computation using this package has been evaluated through some basic tests. One such test is like a mass spectrometer test that computes the effect of a transverse magnetic field on the electron trajectories. The accuracy is within the desired limit. This package has been validated by comparing the simulated results of an asymmetric collector with the experimental data, which are in good agreement. The effect of secondary electron emission on multistage collector performance has been evaluated.

- *Optimisation of electrode potentials and sensitivity analysis of the collector*

A procedure has been developed to optimise the collector performance. As part of the process the electrode potentials are optimised first. An algorithm has been developed based on the enumerative technique where a single variable is changed at a time in the search space. It finds the optimised potentials on a spent beam power distribution curve for maximum power recovery. A computer code has been developed based on this algorithm for the optimisation purpose. The computer code includes the graphics and the postscript options. It is also capable of doing the sensitivity analysis of the collector for different input drive levels.

- *Optimisation of electrode geometry*

In the second part of the optimisation process the geometry of the collector has been optimised using two different random techniques. These are based on random walk

method and genetic algorithm respectively. Two separate fully automated packages have been developed using these two different techniques. Each of them has been used to optimise a symmetric and an asymmetric collector. The random method is proved to be useful if the number of trials is large. Optimisation using the genetic algorithm has been proved to be more effective than the random walk method. After several trials it has been observed that the optimised results achieved using the present method are nearly the same for a specific problem.

7.4 FUTURE PLAN

- *Extension of the same project*

The simulated results of an asymmetric collector have been compared with the experimental data to validate the three-dimensional simulator. Experimental data for any other collector was not available for further validation of this package. Though a 4-stage symmetric collector was modelled using this package still the computed results could not be validated due to the lack of experimental data. However this collector has been used as a test case for the optimisation of its performance.

Due to the non-availability of a three-dimensional magnetic field simulator it was not possible to verify if the collector simulator is capable of dealing with different magnetic fields at different mesh points. This has to be checked with an example. It is worth mentioning here that the simulator is capable of handling a constant transverse magnetic field, which has been tested while simulating the asymmetric collector.

In the present thesis the optimisation of the collector performance is carried out based on the primary trajectories only. The secondaries have to be considered during the optimisation so that the effect of secondaries on the optimised collector performance is minimal. As the automated procedure works well if only the primary electrons are considered so there is no reason to believe why it will not work if the secondary electrons are also included. However some changes in the trajectory solver, the analysis part of the post-processor (this should include the secondaries) and the secondary generator are necessary to include the secondary trajectories in the

simulation. Again this package has to be tested in a few trials for different collector geometries including the secondaries.

Only one set of input parameters (e.g., population size, chromosome length, crossover probability, point of crossover) has been tried for the implementation of the genetic algorithm. Due to the lack of time other combinations could not be tried. It is necessary to try other sets of combinations to check if the computation time can be reduced. Further, it is necessary to try different variations of the genetic algorithm for better optimisation and faster convergence.

- *Related area of research*

The modeling has been carried out for steady state condition assuming that the time rate of change of phase of the RF is very less than the transit time of the beam in the collector. It is necessary to have a 3-D time domain PIC code to study the collector performance before the steady state is reached. This may be a future area of research for analyzing the collector performance in dynamic condition.

The design and modelling of the collector has been carried out on the basis of a single set of spent beam data and under steady state conditions. But in practice the nature of the spent beam changes due to the change in the input drive levels. This indicates that any collector with the same set of electrode potentials cannot recover maximum power from the spent beam. Therefore a mechanism should be in place to change the potentials of the electrodes as the input drive changes. This mechanism has to be intelligent enough to compute the optimised electrode potentials based on the spent beam curve and it has to be quick enough to make the change in the electrode potential effective. This should give constant collector efficiency over a range of input drive levels, which will result in higher minimum overall efficiency at the lowest input drive. The dynamic analysis of the collector for such conditions will be helpful for the design purpose. In a recent paper it has been shown by Y. Goren et al [1] that the helix voltage is being varied to keep the phase of the output signal constant. The same principle may be applied to vary the electrode potentials with the variation of the input drive power.

REFERENCES

[1] Y. Goren, C. Jensen, T. Chen, P. M. Lally, and D. Gagne, "A Novel Technology for Linearizing Travelling Wave Tube Amplifiers," in *Proc. of 2nd IEEE International Vacuum Electronics Conference 2001*, April 2-4, 2001, pp. 278-279.

Appendix A

Glossary of Terms

Back streaming	Electrons are sometimes repulsed by the collector electrodes and stream back towards the interaction region. These electrons introduce noise in the output signal that is undesirable.
Electronic Efficiency (η_e)	The efficiency for converting the dc beam power to RF power is called the basic or electronic efficiency of the tube.
Beam Power	The product of the dc cathode voltage and the cathode current gives the dc beam power.
Body Current	The body current is the electron current intercepted either by the RF interaction circuit or the anode in the electron gun.
Brillouin Field	If the electron gun of the tube is shielded from the magnetic flux and the electron beam has no radial velocity component when it enters the magnetic field region then the amount of magnetic field required to exactly balance the space charge force within the beam is called the Brillouin field.
Collector	One of the three major components of the linear beam tube that collects the spent electron beam and recovers the power from it.

Collector Efficiency (η_c)	The ratio of the power recovered to the total spent beam power.
Collector Stage	Electrodes at potentials other than the ground potential.
Depressed Collector	The electrode potentials are kept lower than the body potential to recover power from the spent beam by retarding the velocity of the electrons.
Electron Gun	One of the three major components of a TWT or Klystron, which produces the dc electron beam.
Multistage Collector	A collector with more than one electrode with different potentials other than the ground potential.
Overall Efficiency (η)	Ratio of output RF power to total input power in a tube.
Perveance	A function of the geometry of the electron gun defined by $P=I/V^{3/2}$.
PPM	Periodic permanent magnet, a type of focussing used mainly in linear beam tubes where the adjacent magnets are kept at the same polarity.
Slow-wave-structure	The region in a TWT between the electron gun and the collector that reduces the velocity of the input RF signal to facilitate the interaction between the RF and the dc electron beam.
Spent Beam Power	The power remaining within the beam after the RF signal has been amplified.
TWT	Travelling wave tube, a linear beam tube where the RF wave travels through a slow wave structure and is amplified due to its interaction with the electron beam.

Appendix B

3-D Simulation of a 4-stage Symmetric Collector

To demonstrate the capability of the package a 4-stage axi-symmetric collector has been simulated using the mainframe version of the LKOBRA package. The geometry and the trajectory data for this collector were supplied in two-dimensional format by Dr Vishnu Srivastava of CEERI. Both the geometry data and the trajectory data have been converted into a three-dimensional format suitable for the simulator. However the computed results could not be verified due to the non-availability of experimental data. It should also be mentioned here that the geometry is not optimised. The interfacing ring between the collector and the body (cylindrical shaped) is kept at the body potential whereas the four electrodes are depressed to that of the ground potential. The electrode potentials are -900 V, -1450 V, -1850 V and -2550 V for the first, second, third and fourth stages respectively. The cathode potential is –3000 V.

Figure B-1 shows how the complex electrodes were represented by combining the simple electrode shapes. A funnel is combined with a cylinder to form the shape of the first electrode. The second and the third electrodes are formed by combining a cone with a hole and a cylinder. Finally, a cone, a cylinder and a circular disc are combined to form the fourth electrode. The collector geometry at two different Euler's angles is also shown in this figure.

The trajectories of primary and secondary electrons are plotted in Figure B-2. In the first two plots the geometry and the primary trajectories are shown at different angles. All the primary trajectories are plotted in Figure B-2(c) with different colours for different energy classes. The secondaries are plotted separately in Figure B-2(d) and they are superimposed on the primaries in Figure B-2(e).

A better view of the primary trajectories according to the energies is shown in different plots in Figure B-3. The primaries in the energy group between 700 eV and 1400 eV are plotted in Figure B-3(a) where the depressed potentials at the first and second stages allow some of the electrons to be collected at the first stage and the rest at the second stage. Some electrons in this group are reflected back from second electrode and are collected at the first electrode. Ideally there should not be any reflection of the primaries; primaries with lower energy in this group should be collected on the back of the first electrode and the rest should be collected on the back of the second electrode. In a similar way the other groups are plotted. A number of primaries in the third group with energies between 1700 eV and 2200 eV are collected on the insulator between the second and the third electrode which is highly undesirable (Figure B-3(c)). Some electrons in this group are also collected at the front of the second electrode. The primaries of this group should be collected at the third electrode. Finally, a number of primaries in the fourth group with energies between 2200 eV and 4000 eV are collected at the front of the second and the third electrodes (Figure B-3(d)). These are to be collected on the sidewalls of the fourth electrode.

In Figure B-4 both primary and secondary trajectories are superimposed according to their energy. The higher energy primary electrons in the first group (700 eV to 1400 eV) are collected on the front surface of the second electrode. Due to the accelerating field (potential at the first electrode is higher than the second electrode) the secondaries generated here are either collected at the first electrode or stream back. This causes the deterioration of the collector performance. A similar logic applies for the third group (1700 eV to 2200 eV) and the fourth group (2200 eV to 4000 eV) of primaries. The collector performance could be improved by increasing the aperture diameter in the third and the fourth electrode.

Equipotential lines at different planes are plotted in Figure B-5. In the first and second plots the equipotential lines are shown in the yz plane at the middle and at the end of the first electrode respectively. The second electrode penetrates inside the first one, which is clear in the second plot. The equipotential lines xy and xz planes are shown at the axis of the collector. It is observed from these figures that the equipotential lines at the gap are nearly vertical which makes the lens effect week. Because of this, the electron trajectories are diverged only under the influence of the space charge forces.

The energies of the primary trajectories versus path length are shown in the plots in Figures B-6. In the first plot the total energy is shown constant throughout the path length, as it ought to be. The transverse energy in the second plot is low; in ideal case it should be zero. The kinetic energies of the electron trajectories are shown in Figure B-6(c). As the trajectories move along the path they loose their kinetic energy so the curves are falling in nature. Some trajectories gain energy after attaining a minimum level when they are repulsed by an electrode and then accelerated by the adjacent electrodes. All trajectories should be collected at the lowest kinetic energy. The energy at the end point of each trajectory denotes the kinetic energy of the electrons with which they strike the electrode surface. The potential energies of all trajectories are shown in Figure B-6(d). All of them are increasing in nature. Some of the trajectories attain a maximum potential energy then repulsed by the electrodes and collected at the higher potential (according to magnitude it is low). Because of that the potential of these trajectories are shown falling. The energy of the end point of each trajectory denotes the electrode potential where the electrons are collected. The primaries are plotted in Figure B-7 according to their energy.

Finally, the computed results of the collector with and without the secondary trajectories are shown in Table B-1. For the computation of the secondary electron emission it was assumed that the electrodes are made of OFHC (oxygen free high carbon) copper. The simulated plots and the computed results are shown here for demonstration purposes.

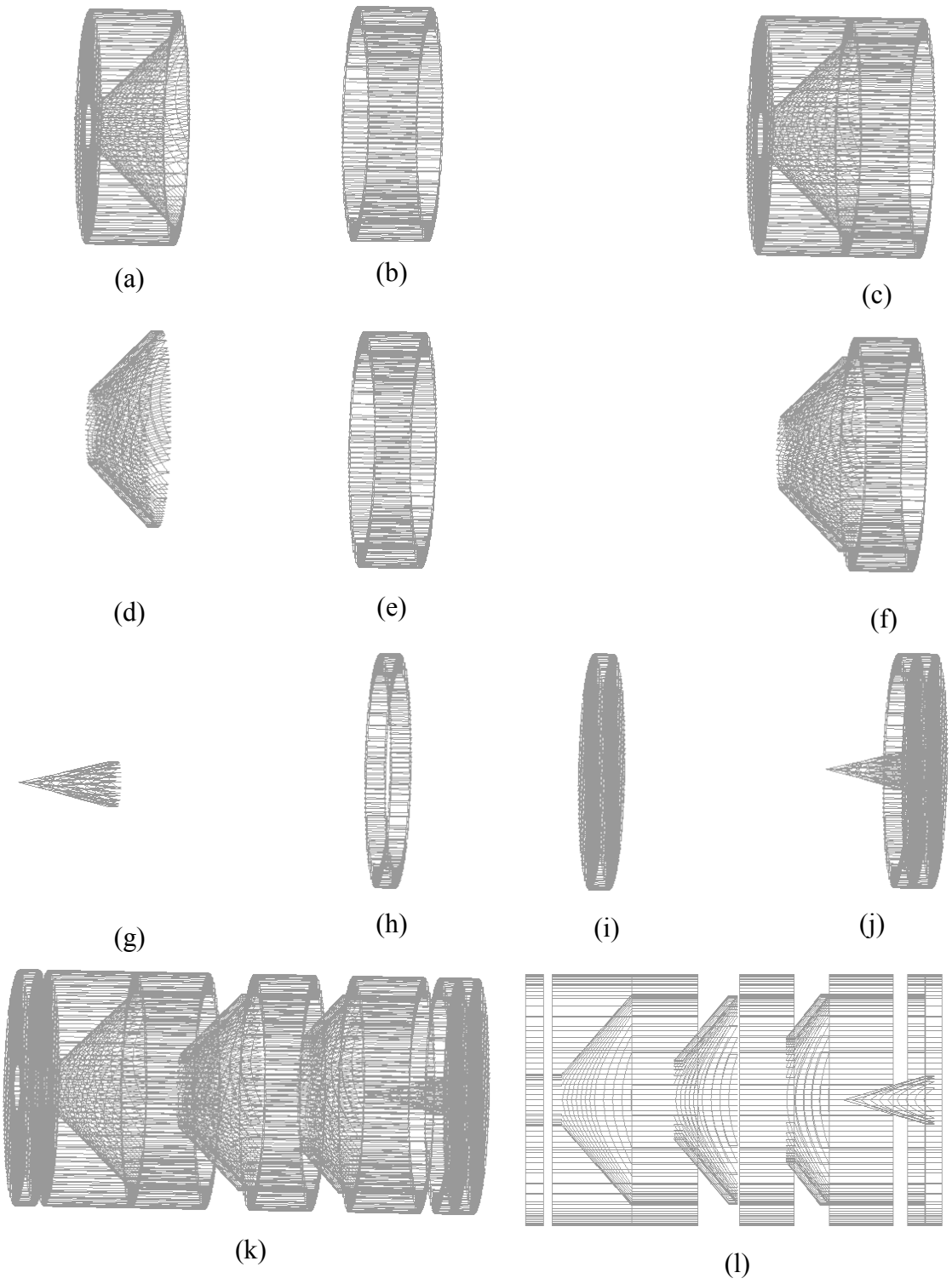

Figure B-1: Geometry of a 4-stage collector (a) funnel (b) cylinder (c) funnel and cylinder combined to make the second electrode (d) cone with a hole (e) cylinder (f) cone and the cylinder makes the third and fourth electrode (g) cone (h) cylinder (i) disc (j) cone, cylinder and disc make the fourth electrode (k) collector at an Euler's angle 20, -20, 20 (l) collector at an Euler's angle 0, 0, 0

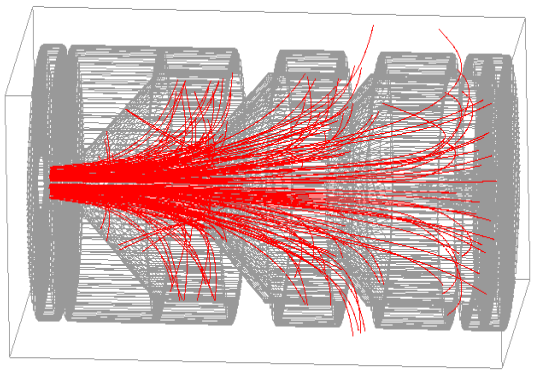

(a)

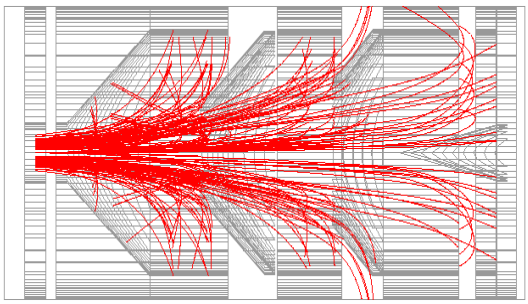

(b)

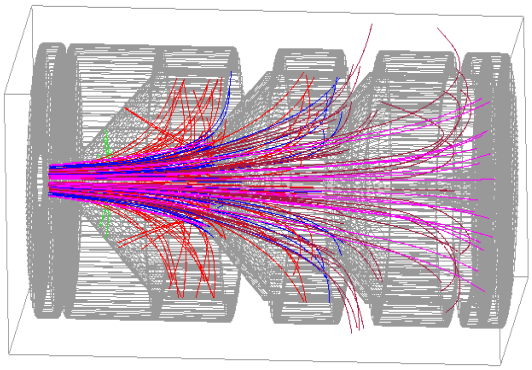

(c)

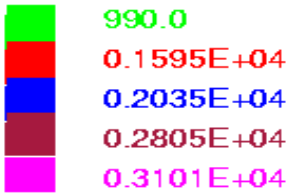

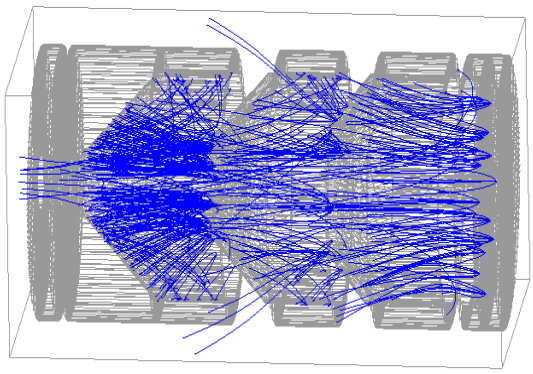

(d)

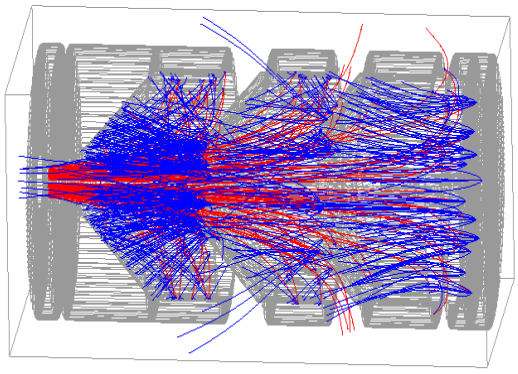

(e)

Figure B-2: Trajectories in a 4-stage collector (a) primaries at Euler's angle 20, -20, 20 (b) primaries at Euler's angle 0, 0, 0 (c) primaries with different energy in different colours (d) secondaries only (e) both primaries and secondaries

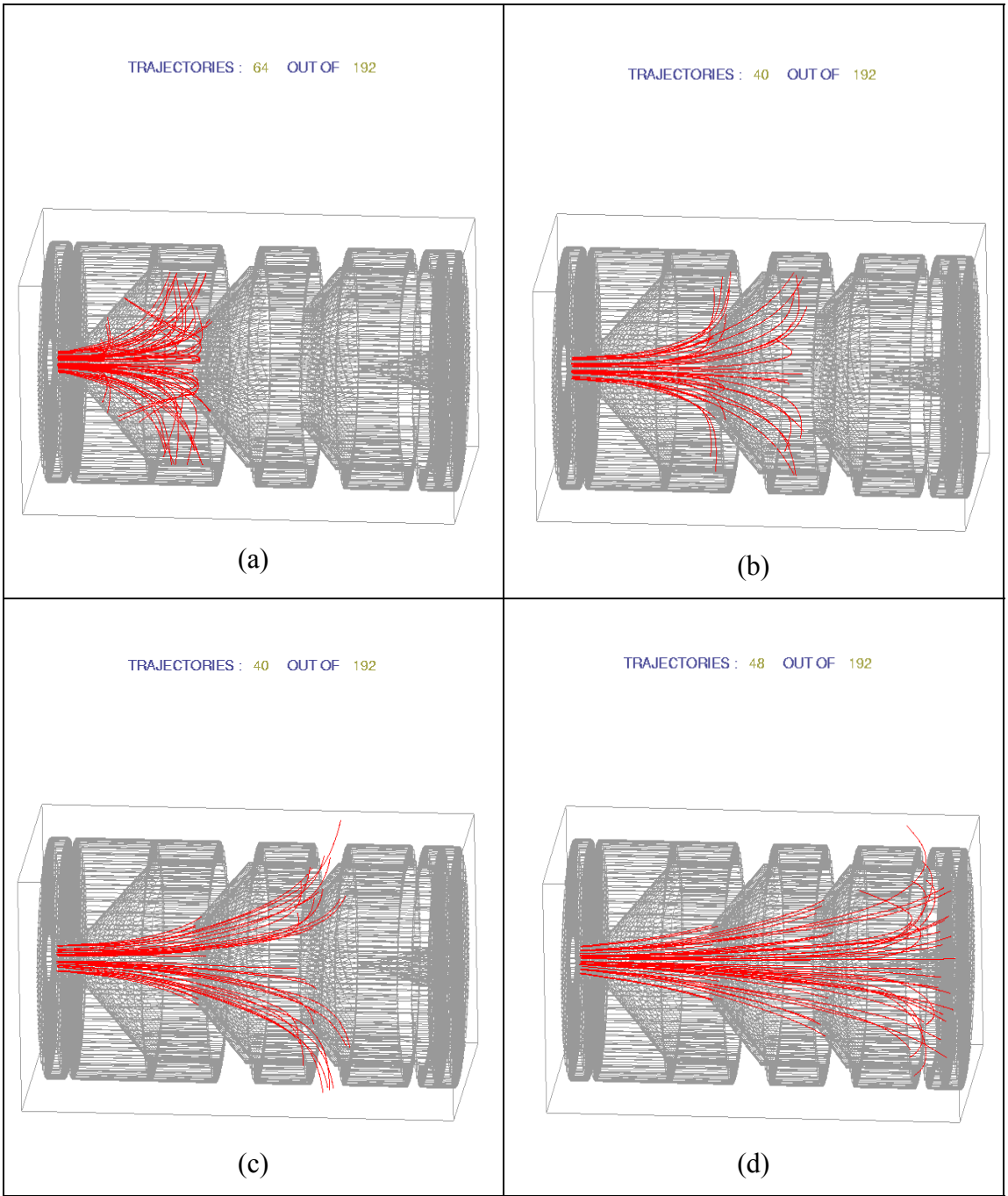

Figure B-3: Primary trajectories according to their energies in a 4-stage collector (a) 700 to 1400 eV (64 trajectories) (b) 1400 to 1700 eV (40 trajectories) (c) 1700 to 2200 eV (40 trajectories) (d) 2200 to 4000 eV (48 trajectories)

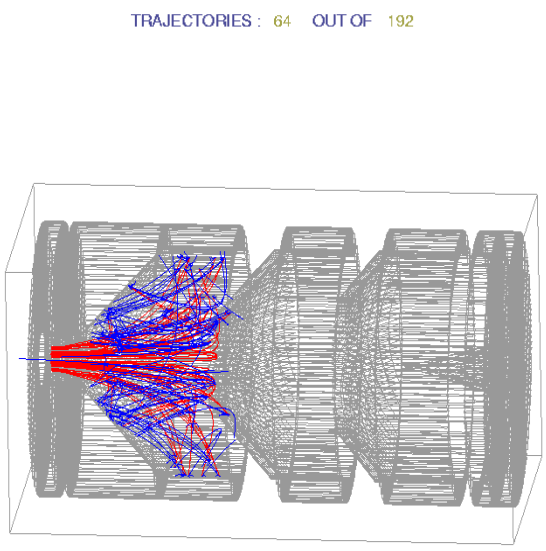

(a)

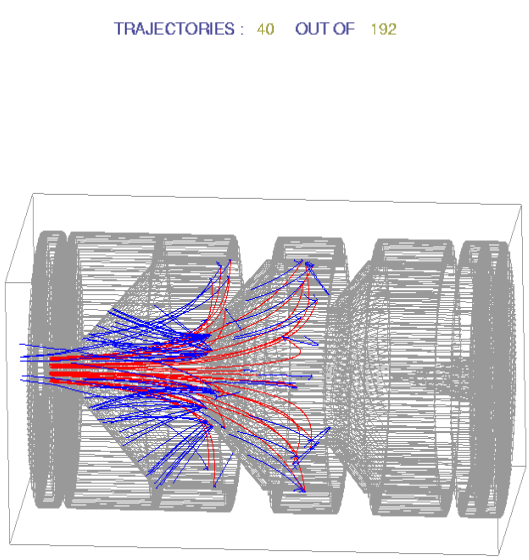

(b)

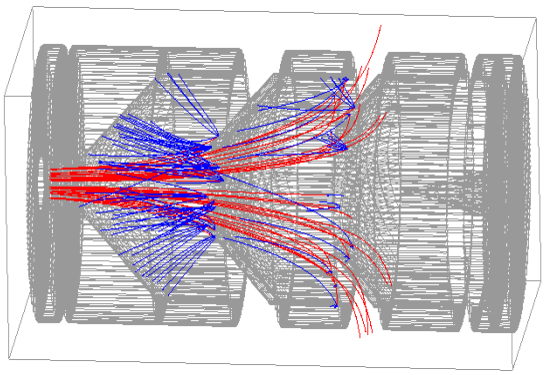

(c)

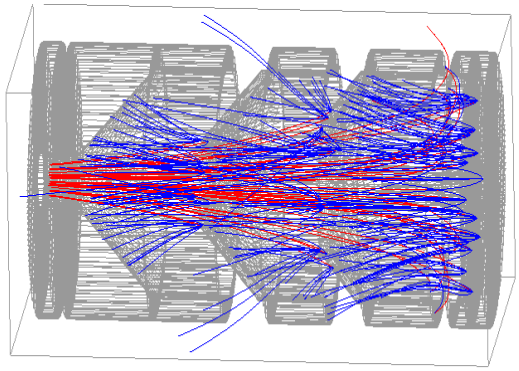

(d)

Figure B-4: Primary and corresponding secondary trajectories according to the energies of the primaries in a 4-stage collector (a) 700 to 1400 eV (b) 1400 to 1700 eV (c) 1700 to 2200 eV (d) 2200 to 4000 eV

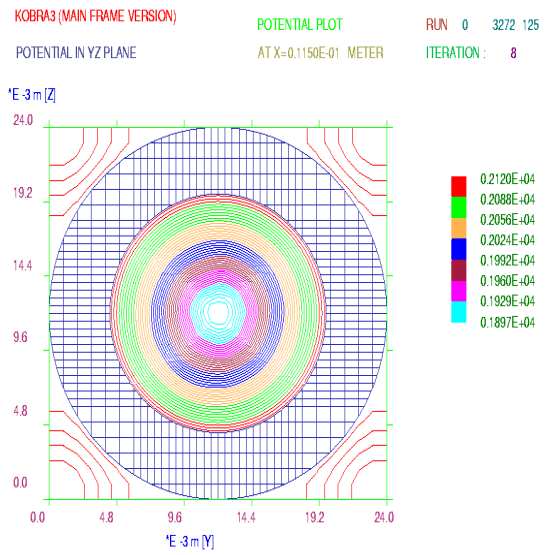

(a)

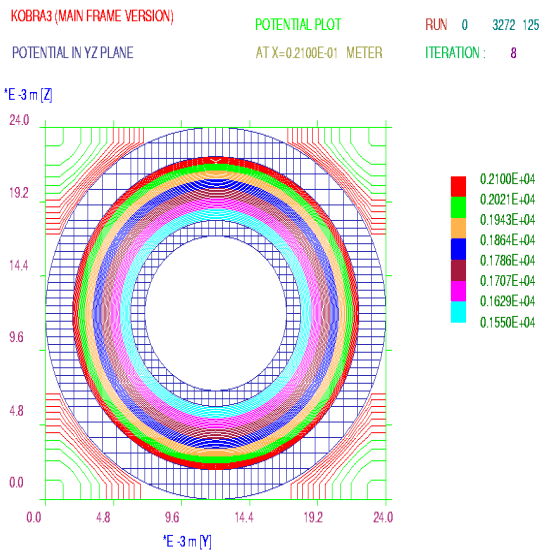

(b)

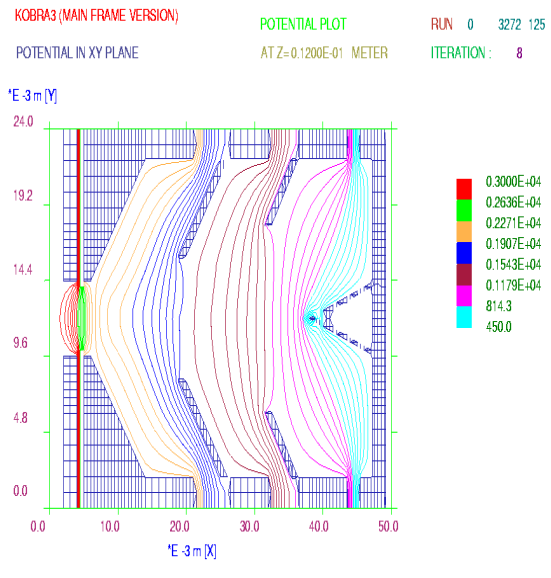

(c)

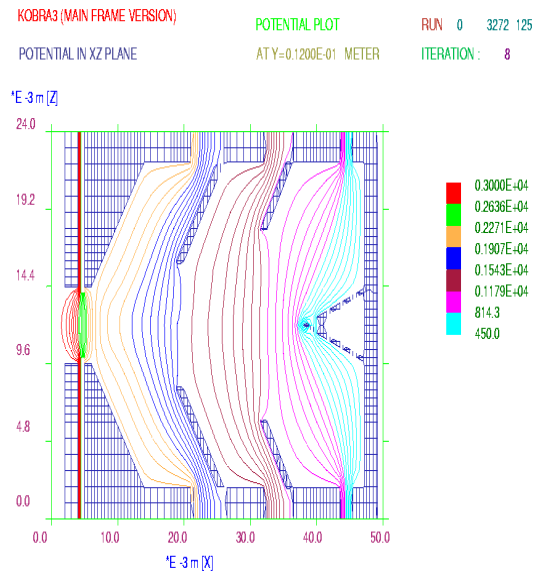

(d)

Figure B-5: Equipotential plot (a) yz plane - near the middle of the first stage (b) yz - plane overlapping section where the second stage enters the first stage (c) xy - plane at the middle of z (d) xz- plane at the middle of y

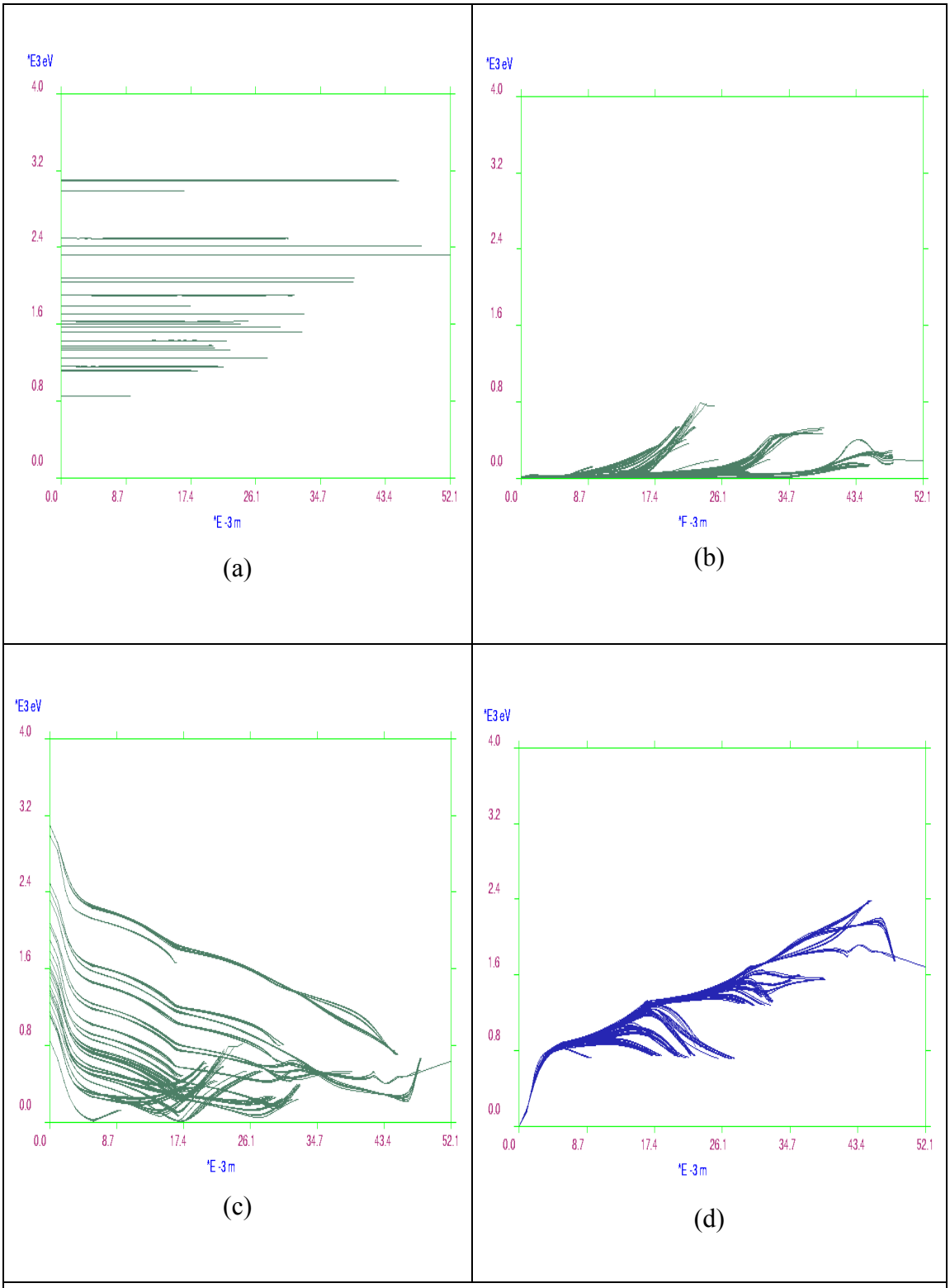

Figure B-6: Energy versus path length in a 4-stage collector (a) total energy (b) transverse energy (perpendicular to x) (c) total kinetic energy (d) total potential energy

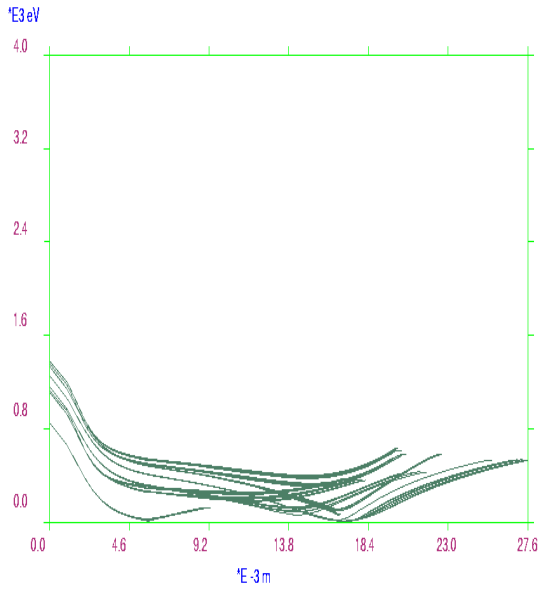

(a)

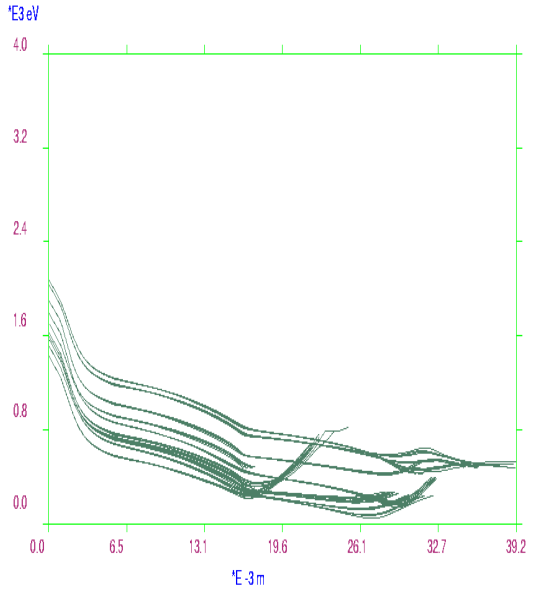

(b)

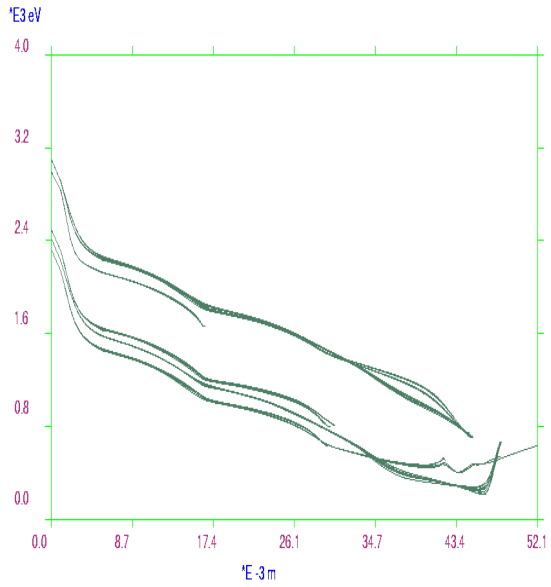

(c)

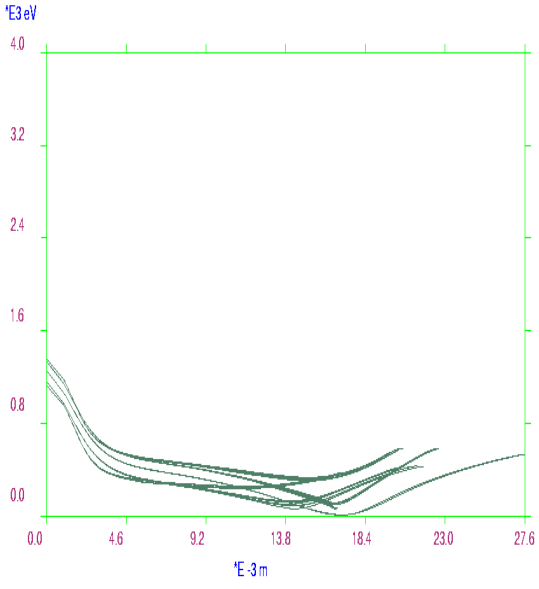

(d)

Figure B-7: Energies in a 4-stage collector (a) total kinetic energy between 700 and 1400 eV (b) total kinetic energy between 1400 and 2200 eV (c) total kinetic energy between 2200 and 4000 eV (d) total kinetic energy (trajectory number 20 to 50)

Table B-1: Computed performance of the 4-stage axi-symmetric collector

QUANTITY	COMPUTED VALUE KOBRA (MF) (MODULATED BEAM)	
	Without secondaries	With Secondaries
Total Power Entering the Collector	135.2 W	135.2 W
Back streaming Current	0.0 mA	0.4 mA
Current at Body Electrode	5.9 mA	7.1 mA
Current at Stage 1	28.5 mA	44.3 mA
Current at Stage 2	24.6 mA	18.3 mA
Current at Stage 3	9.8 mA	6.9 mA
Current at Stage 4	6.3 mA	-2.1 mA
Power Recovered at Body	0.0 W	0.0 W
Power Recovered at Stage 1	25.6 W	39.8 W
Power Recovered at Stage 2	35.7 W	26.5 W
Power Recovered at Stage 3	18.0 W	12.8 W
Power Recovered at Stage 4	15.9 W	-5.2 W
Power Dissipated at Body	12.2 W	12.3 W
Power Dissipated at Stage 1	9.8 W	-3.5 W
Power Dissipated at Stage 2	9.2 W	18.1 W
Power Dissipated at Stage 3	5.2 W	10.1 W
Power Dissipated at Stage 4	3.4 W	24.1 W
Back streaming Power	0.0 W	0.17 W
Total Power Recovered	95.3 W	73.9 W
Total Power Loss	39.8 W	61.7 W
Total Power out of the collector	135.2 W	135.15 W
Collector Efficiency	70.54 %	54.70 %

Appendix C

Publications and Award

Before starting my Ph D studies, I was a member of a space TWT project. I was associated with the design of the electron gun, the PPM focusing structure and the multistage collector. Some of the work was continued while I was at Lancaster and was reported in the second year report. A paper arising from the work on the space TWT was published in the journal [1]. Several papers have been presented in national and international conferences based on different chapters of this thesis. Two reports describing in detail the achievements were submitted to the Engineering Department, Lancaster University, after the first and second year of the project [8], [9]. Four papers [2], [3], [6] and [7] were published (based on the development of a three-dimensional package and simulation of collectors) from the earlier version of Chapter 3. A paper was published on the secondary electron emission model as described in Chapter 4 [5]. The optimisation of collector performance was carried out using the genetic algorithm. This algorithm has been used for the first time for optimisation of the performance of any component of microwave tubes. A paper on the optimisation technique was published based on the earlier version of Chapters 5 and 6 in [4]. An article on the overall progress of the project is published in [10].

During the third year of this project I became one of the first three winners (world-wide) of the prestigious *2001 IEEE Electron Devices Society Graduate Student Fellowship*. This was awarded by the IEEE EDS, USA. A copy of each of the following documents is shown here: (a) plaque (b) award letter and (c) IEEE EDS newsletter (January 2002 issue) announcing the award.

LIST OF PUBLICATIONS

Journal:

[1]. V Srivastava, TK Ghosh, MJ Akhtar, "Design of High Efficiency Space TWT," *IETE Technical Review*, vol.-16, No. 2, pp. 249-254, March-April 1999.

International Conference:

[2] T. K. Ghosh and R. G. Carter, "3-D Simulation of Asymmetric Multistage Depressed Collectors with Secondary Electron Emission Effects for High Efficiency Space TWTs," in *Proc. ITG Conference on Displays and Vacuum Electronics*, May 2-3, 2001, pp. 67-71.

[3] T. K. Ghosh and R. G. Carter, "Improved Three Dimensional Simulation of Multistage Depressed Collectors for High Efficiency Travelling Wave Tubes," in *Proc. of 2nd IEEE International Vacuum Electronics Conference 2001*, April 2-4, 2001, pp. 215-220.

[4] T. K. Ghosh and R. G. Carter, "Design Optimisation of Multistage Depressed Collectors for High Efficiency Travelling Wave Tubes Using Genetic Algorithm," in *Proc. of 3rd IEEE International Vacuum Electronics Conference 2002*, April 23-25, 2002, pp. 158-159.

National Conference:

[5] T. K. Ghosh and R. G. Carter, "The Effect of Secondary Electron Emissions in Multistage Depressed Collectors," in *Proceedings of PREP 2001*, April 2001, pp. 69-70.

[6] T. K. Ghosh and R. G. Carter. (2001, July). Multistage Depressed Collectors for helix TWTs. Presented at The Northern Vacuum Electronics Conference, UK [Online].
Available:
www.comp.lancs.ac.uk/engineering/research/microwave/conference/tushar.pdf

[7] T. K. Ghosh and R. G. Carter. (2000, April). 3-D Simulation of Multistage Depressed Collectors for High Efficiency Space TWT. Presented at The Northern Vacuum Electronics Conference, UK [Online].
Available: epicentre.tay.ac.uk/NVEC2000/tghosh.pdf

Technical Report:

[8]. TK Ghosh and Prof. RG Carter, "3-D Simulation of Multistage Depressed Collectors for High Efficiency Space TWTs (Progress Report 1)," Engineering Department, Lancaster University, MRG/2000/2, March 2000.

[9]. TK Ghosh and Prof. RG Carter, "3-D Simulation of Multistage Depressed Collectors for High Efficiency Space TWTs (Progress Report 2)," Engineering Department, Lancaster University, MRG/2001/1, Jan. 2001.

Newsletter:

[10] Progress Report on "3-D Simulation and Design Optimisation of Multistage Depressed Collectors for High Efficiency Travelling Wave Tubes," *IEEE Electron Devices Society Newsletter,* July 2002, page 13.

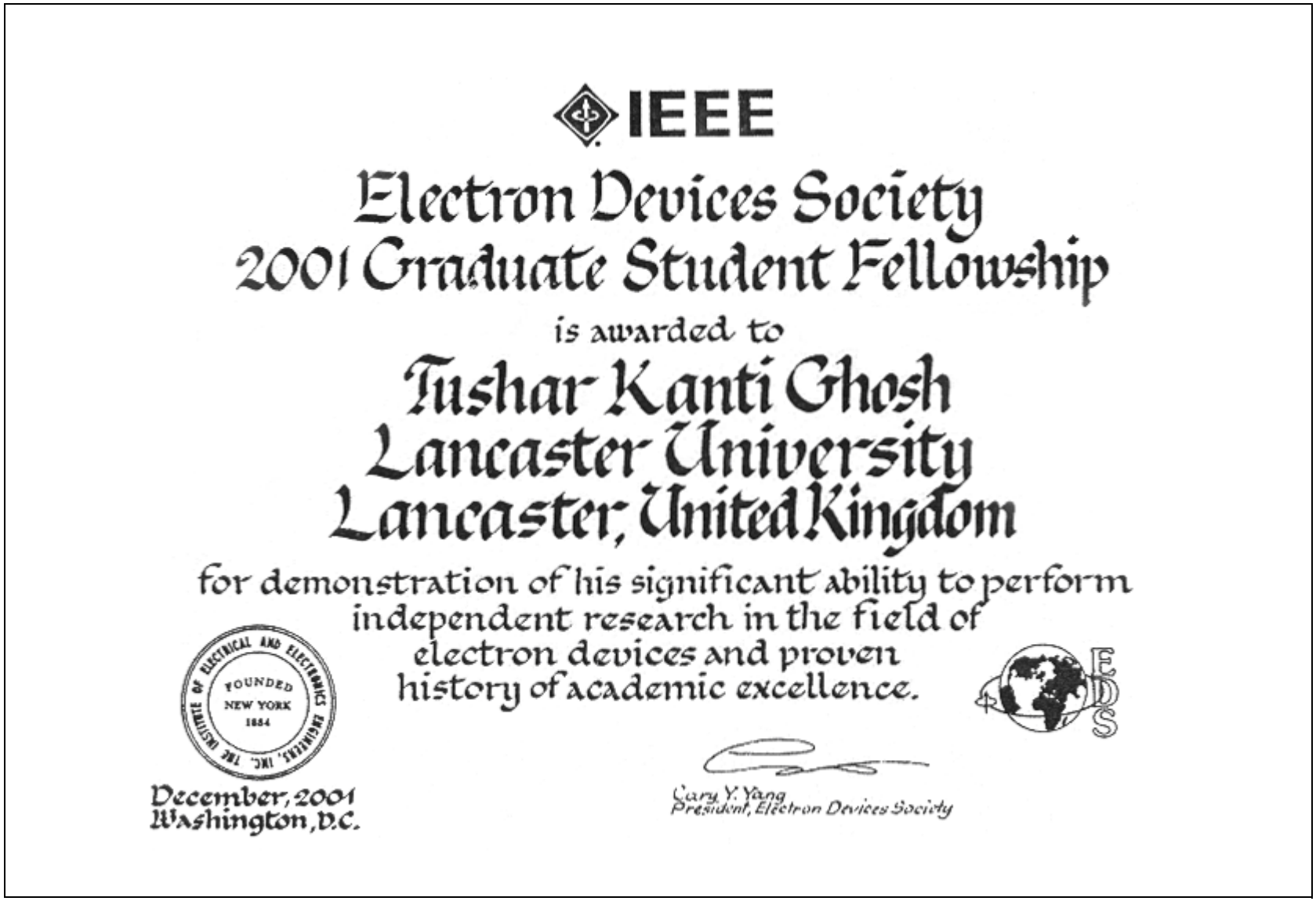

IEEE

Electron Devices Society
2001 Graduate Student Fellowship

is awarded to

Tushar Kanti Ghosh
Lancaster University
Lancaster, United Kingdom

for demonstration of his significant ability to perform independent research in the field of electron devices and proven history of academic excellence.

THE INSTITUTE OF ELECTRICAL AND ELECTRONICS ENGINEERS, INC. FOUNDED NEW YORK 1884

December, 2001
Washington, D.C.

Gary Y. Yang
President, Electron Devices Society

EDS

ELECTRON DEVICES SOCIETY®

20 June 2001

Mr. Tusharkanti Ghosh
Engineering Department
Lancaster University
Lancaster – LA14YR
United Kingdom

Dear Mr. Tusharkanti:

I am delighted to inform you that you have been selected as a recipient of an IEEE Electron Devices Society Graduate Student Fellowship for 2001. The Fellowship Program was established to promote, recognize, and support graduate study and research within the Electron Devices Society's field of interest. I congratulate you on being selected for this prestigious award.

The fellowship will be presented at the 2002 IEEE International Vacuum Electronics Conference (IVEC), 23 - 25 April, at the Double Tree Hotel, Monterey, CA. It will consist of a plaque and a check for US $5,000. The plaque will be presented at the IEDM and your check will be mailed to you by mid-August. In addition, Lancaster University will receive a $2,000 grant, of which $1,000 will be used to help support, the activities of your department and the other $1,000 for your specific research project. The grant check will be mailed to your nominator, Richard Carter, by mid-August as well.

I strongly urge you to attend the ceremony to receive the Fellowship in person. Please contact the EDS Executive Director, William F. Van Der Vort, at (732) 562-3926 or e-mail w.vandervort@ieee.org to let him know if you will be able to attend. If necessary, funds are also available to assist you in covering your travel and accommodation costs. You can discuss the matter with Mr. W. F Van Der Vort.

We would like to announce your fellowship in the January issue of the EDS Newsletter. We will need a good photograph of you (glossy black and white preferred) and a short biographical sketch (about 100 words). In order to meet the schedule for publishing in our Newsletter, we will need your bio and photograph by 15 September. If you have a photo available, please mail that now, and you can send the bio later by e-mail. The photo and bio should be sent via express mail to: Christopher Salicco, IEEE Operations Center, 445 Hoes Lane, PO Box 1331, Piscataway, NJ 08855. His e-mail address and numbers are c.salicco@ieee.org and 732-235-1626, respectively.

Again, my congratulations for having been selected to receive an EDS Graduate Student Fellowship.

Sincerely,

Cary Y. Yang
EDS President

cc: Richard G. Carter, Nominator for Tusharkanti Ghosh
EDS Graduate Student Fellowship Committee
Ilesanmi Adesida, EDS Educational Activities Chair
Steven J. Hillenius, EDS Vice President
Alfred U. Mac Rae, EDS Awards Chair
Richard True, 2002 IVEC General Chair
Ralph Nadell, 2002 IVEC Conference Manager
William F. Van Der Vort, EDS Executive Director

IEEE The IEEE Electron Devices Society
EDS Executive Office • 445 Hoes Lane • P.O. Box 1331 • Piscataway NJ 08855-1331, USA
Phone +1 732 562 3926 • Fax +1 732 235 1626 • E-mail eds@ieee.org • www.ieee.org/eds/

January 2002
Vol. 9, No. 1 ISSN:1074 1879
Editor-in-Chief: Krishna Shenai

IEEE Electron Devices Society Newsletter

Table of Contents

Contributions Welcome

Readers are encouraged to submit news items concerning the Society and its members. Please send your ideas/articles directly to either the Editor-in-Chief or appropriate Editor. All contact information is listed on the back cover page. Whenever possible, e-mail is the preferred form of submission.

Newsletter Deadlines

Issue	*Due Date*
January	October 1st
April	January 1st
July	April 1st
October	July 1st

2002 IEEE International Reliability Physics Symposium (IRPS)

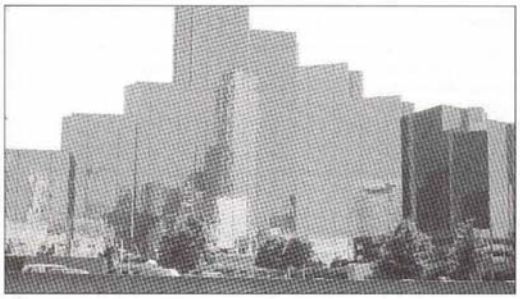

Plan to attend the 40th International Reliability Physics Symposium (IRPS) at the Hyatt Regency in Dallas, Texas, April 8-11, 2002!

The IRPS is now the major forum for exchanges between engineers (development and manufacturing) and scientists to share new information and findings regarding reliability and performance of integrated circuits and microelectronic assemblies for both existing as well emerging technologies. Started in the early 1960's by the military and aerospace community, the IRPS's sponsorship moved to the IEEE in 1967 to best serve the world wide community eagerly engaged in research, development and manufacturing of commercial integrated circuits. As the premier conference event for reliability, the IRPS provides an open and professional forum dedicated to serve the worldwide community in the areas of:

- Reliability implications of integrated circuit scaling
- Failure and degradation mechanisms of microelectronic assemblies
- Correlation of reliability with the properties of electronic materials

Reliability optimization by circuit design, modeling, simulation and defect reduction efforts and techniques

Here are some highlights of what will be included in the 2002 IRPS Symposium:

- **Technical Program:** Keynote presentation, a new panel discussion, and high-quality, carefully selected and peer-reviewed technical presentations
- **Tutorials and Workshops:** a highly diverse collection of cutting-

(continued on page 3)

Your Comments Solicited

Your comments are most welcome. Please write directly to the Editor-in-Chief of the Newsletter at the address given on the back cover page.

Electron Devices Society

EDS ADCOM ELECTED MEMBERS-AT-LARGE

Term Expires:

2002	2003	*2004
C. L. Claeys (1)	I. Adesida (2)	M. Estrada del Cueto (1)
J. A. Dayton, Jr. (1)	T. Hiramoto (1)	K. F. Galloway (2)
M. Fukuma (1)	L. Lunardi (1)	S. J. Hillenius (2)
K. M. Lau (1)	A. A. Santos (2)	C. Jagadish (2)
K. Lee (1)	S. C. Sun (2)	J. K. O. Sin (1)
M. L. Östling (1)	H. S. P. Wong (1)	R. Singh (2)
D. L. Pulfrey (1)	P. K. L. Yu (2)	N.D. Stojadinovic (1)
K. Shenai (2)		

Number in parenthesis represents term.
* Members elected 12/01

Announcement of the EDS Graduate Student Fellowship Winners for 2001

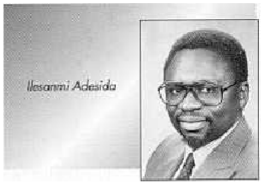

In 2000, the IEEE approved the establishment of the Electron Devices Society Graduate Student Fellowship Program. It is designed to promote, recognize, and support graduate level study and research within the Electron Devices Society's field of interest: Compact Modeling, Compound Semiconductor Devices and Circuits, Device Reliability Physics, Displays, Electronic Materials, Microelectromechanical Systems, Nanotechnology, Optoelectronic Devices, Photovoltaic Devices, Power Devices and ICs, Semiconductor Manufacturing, Technology Computer-Aided Design, Vacuum Devices, VLSI Technology and Circuits.

EDS announced its first winners of the award. Detailed articles about each graduate fellow and their work will appear in forthcoming issues of the EDS Newsletter. The following are brief biographies of the 2001 recipients:

Tushar Kanti Ghosh, received his Beng (1990) and Meng (1993) degrees in Electronics and Tele-Communication Engineering from Bengal Engineering College and Jadavpur University, India, respectively. Currently he is studying for a PhD at the Lancaster University, UK, under the Commonwealth Scholarship and Fellowship Plan. His research area is computer-aided design

(continued on page 23)

IEEE Electron Devices Society Newsletter is published quarterly by the Electron Devices Society of the Institute of Electrical and Electronics Engineers, Inc. Headquarters: 3 Park Avenue, 17th Floor, New York, NY 10016-5997. Printed in the U.S.A. One dollar ($1.00) per member per year is included in the Society fee for each member of the Electron Devices Society. Periodicals postage paid at New York, NY and at additional mailing offices. **Postmaster:** Send address changes to IEEE Electron Devices Society Newsletter, IEEE, 445 Hoes Lane, P.O. Box 1331, Piscataway, NJ 08855-1331.

ence Center, Fiera di Milano, Milano, Italy Contact: Giovanni Ghione, Politecnico di Torino, Corso Duca degli Abruzzi 24, 10129 Torino, Italy Tel: +39 011 564 4064 Fax: +39 011 564 4099 E-Mail: ghione@polito.it Deadline: Not Available www: http://www.eumw.com

September 23 - 26, 2002, T **International Conference of Actual Problems of Electronics Instrument Engineering** Location: Novosibirsk State Technical University, Novosibirsk, Russia Contact: Alexander Griddin, Tel: +7 3832 46 0877 Fax: +7 3832 46 0209 E-Mail: algrid@ref.nstu.ru Deadline: 4/15/02 www: http://www.nstu.ru

September 24 - 26, 2002, T **European Solid-State Device Research Conference** Location: Florence Conference Center, Florence, Italy Contact: Giorgio Baccarani,University of Bologna, Viale Risorgimento 2, 40136 Bologna, Italy Tel: +39 051 209 3012 Fax: +39 051 209 3074 E-Mail: gbaccarani@deis.unido.it Deadline: Not Available www: http://www.essderc.org

September 29 - October 1, 2002, * **IEEE Bipolar/BiCMOS Circuits and Technology Meeting** Location: Doubletree Hotel, Monterey, CA, USA Contact: Janice Japke, CCS Associates, 6611 Countryside Drive, Eden Prairie, MN, USA 55346 Tel: +1 612 934 5082 Fax: +1 612 934 6741 E-Mail: jjopke@aol.com Deadline: Not Available www: Not Available

October 6 - 10, 2002, T **Electrical Overstress/Electrostatic Discharge Symposium** Location: Charlotte Convention Center, Charlotte, NC, USA Contact: Steven Voldman, IBM Microelectronics, 1000 River Street, MS 972 F, Essex Junction, VT, USA 05452 Tel: +1 802 769 8368 Fax: +1 802 769 9659 E-Mail: a108501@us.ibm.com Deadline: 1/14/02 www: Not Available

October 7 - 11, 2002, T **European Symposium on Reliability of Electron Devices, Failure Physics and Analysis** Location: Riminu, Italy Contact: Ing Fantini, Universita degli Studi di Modena e Reggio Emilia, Via Vignolese 905, 41100 Modena, Italy Tel: +39 059 2056 165 Fax: +39 059 2056 129 E-Mail: fantini@dsi.unimo.it Deadline: Not Available www: Not Available

October 7 - 10, 2002, * **IEEE International SOI Conference** Location: Colonial Williamsburg Lodge, Williamsburg, VA, USA Contact: Bobbi Armbruster, BACM, 520 Washington Blvd. Suite 350, Marina Del Rey, CA, USA 90292 Tel: +1 310 305 7885 Fax: +1 310 305 1038 E-Mail: bacm@mediaone.net Deadline: Not Available www: Not Available

October 8 - 12, 2002, * **International Semiconductor Conference** Location: Sinaia Hotel, Sinaia, Romania Contact: Doina Vancu, IMT-Bucharest, CAS Office, PO Box 38-160, Bucharest, Romania 72225 Tel: +40 1 490 82 36 Fax: +40 1 490 82 38 E-Mail: CAS@imt.ro Deadline: 4/15/02 www: http://www.imt.ro/CAS

October 10 - 13, 2002, T **International Seminar/Workshop on Direct and Inverse Problems of Electromagnetic and Acoustic Wave Theory** Location: Tbilisi State University, Tbilisi, Georgia, Ukraine Contact: Mykhalyo Andriychuk, Inst. of Applied Problems of Mech. & Math. Of NASU, 3"b" Naukova str, 79601 Lviv, Ukraine Tel: +380 322 651944 Fax: +380 322 637088 E-Mail: andr@iapmm.lviv.ua Deadline: Not Available www: Not Available

* = Sponsorship or Co-Sponsorship Support
T = Technical Co-Sponsorship Support

@ = Alternates support between 'Sponsorship/Co-Sponsorship' and 'Technical Co-Sponsorship'
# = Cooperation Support

Announcement of the EDS Graduate Student Fellowship Winners for 2001

(continued from page 2)

(CAD) and 3-D simulation of multistage depressed collectors for high efficiency space travelling wave tubes.

From 1993 to 1994 he worked on electromagnetic pulse sensors as a Senior Research Fellow at Jadavpur University. He joined the Central Electronics Engineering Research Institute, India in 1994 as a Project Scientist and he has been a Scientist since 1995.

His research interests include CAD of microwave tubes in general and design and simulation of multistage collectors, electron guns and periodic permanent magnet focussing systems in particular.

He is a member of the Indian Physics Association and a student member of IEEE.

Sergei Kucheyev, was born on January 3, 1976 in the U.S.S.R. In 1997, he graduated from St. Petersburg State Technical University (the former Leningrad Polytechnical Institute) in Russia. After receiving a Master of Physics degree from the same university in 1999, he continued working there as a researcher for several months before starting a Ph.D. project at the Australian National University (Canberra, Australia) under the supervision of Profs. J.S. Williams and C. Jagadish. The Ph.D. project of S.O. Kucheyev has focused on ion-beam processing of III-nitride-based semiconductor devices.

Yee-Chia Yeo received the BEng (first class honors) and MEng degrees from the National University of Singapore, and the M.S. degree from the University of California, Berkeley, all in Electrical Engineering. He is working towards a PhD degree in Electrical Engineering at the University of California, Berkeley.

He has conducted research on sub-100 nm CMOS device fabrication, strained SiGe-channel MOS transistors, alternative gate dielectrics, process integration of dual-metal gates, and novel device structures such as the ultra-thin body transistor. He has authored or co-authored 30 journal/conference papers, and has written a book chapter on MOS transistor gate oxide reliability with Professor Chenming Hu.

July 2002
Vol. 9, No. 3 ISSN:1074 1879
Editor-in-Chief: Ninoslav D. Stojadinovic

Table of Contents

Contributions Welcome

Readers are encouraged to submit news items concerning the Society and its members. Please send your ideas/articles directly to either the Editor-in-Chief or appropriate Editor. All contact information is listed on the back cover page. Whenever possible, e-mail is the preferred form of submission.

Newsletter Deadlines

Issue	*Due Date*
January	October 1st
April	January 1st
July	April 1st
October	July 1st

IEEE Electron Devices Society Newsletter

2002 IEEE Bipolar/BiCMOS Circuits and Technology Meeting

Wireless communications is a burgeoning market area and a major driver behind the semiconductor industry, and SiGe BiCMOS and III-V technologies have emerged as the manufacturing processes of choice for many wireless ICs. If you work or are interested in this exciting area, then the IEEE Bipolar/BiCMOS Circuits and Technology Meeting (BCTM) is a conference you want to attend.

BCTM has historically been held in Minneapolis, MN. However, due to popular demand the conference is now on the road. In 2002 it will be held 30 September – 1 October at the Doubletree Hotel in Monterey, CA, and in 2003 it will be in Europe, in Toulouse, France. The Doubletree Hotel in Monterey is just a few steps from Fisherman's Wharf, a pleasant stroll from Cannery Row and sandy beaches, and the area is widely known through the works of John Steinbeck. So Monterey is not just a new and exciting place for BCTM; it's a great place to bring the family as well.

The technical program for BCTM consists of one day of short courses (Sunday Sep. 29) given by noted industry experts, and two days of invited and contributed technical presentations. Also for 2002, we will follow a tradition established in 2001 of having a Conference Banquet on the Monday evening. For 2002, this will be at the Monterey Bay Aquarium, a world famous marine institute. The Banquet will actually be a strolling dinner, where you can wander among the exhibits, munch on Californian gourmet specialties, and socialize with other conference attendees.

For the Short Courses this year, we have three noted experts who will present 2-hour courses on various aspects of bipolar devices and technology. Dr. Peter Zampardi of Conexant Systems, Inc., will present a designer's

(continued on page 3)

Your Comments Solicited

Your comments are most welcome. Please write directly to the Editor-in-Chief of the Newsletter at the address given on the back cover page.

Status Report from the 2001 Graduate Student Fellowship Winners

In 2000, the IEEE approved the establishment of the Electron Devices Society Graduate Student Fellowship Program. The Program is designed to promote, recognize, and support graduate level study and research within the Electron Devices Society's fields of interest: which include: Compact Modeling, Compound Semiconductor Devices and Circuits, Device Reliability Physics, Displays, Electronic Materials, Microelectromechanical Systems, Nanotechnology, Optoelectronic Devices, Photovoltaic Devices, Power Devices and ICs, Semiconductor Manufacturing, Technology Computer-Aided Design, Vacuum Devices, and VLSI Technology and Circuits. In deference to the increasing globalization of our Society, at least one fellowship is to be awarded to students in each of three geographical regions: Americas, Europe/Mid-East/Africa, and Asia-Pacific.

In July 2001, EDS announced the first winners of the Fellowship awards. The three winners are: T.K. Ghosh of Lancaster University in the United Kingdom, Sergei Kucheyev of the Australian National University, and Yee-Chia Yeo of the University of California, Berkeley. The winners are pursuing distinctly different research topics for their doctoral degrees. The following are brief progress reports on the activities of the winners.

Yee-Chia Yeo

Yee-Chia Yeo is a student in the Department of Electrical and Computer Engineering at the University of California, Berkeley and his supervisor is Professor Chenming Hu.

Yee-Chia Yeo's research interests are related to semiconductor devices and electronic materials, with focus on front-end issues in complementary metal-oxide-semiconductor (CMOS) device technology. He has previously conducted research on solid-state physics and optoelectronic devices. Currently, he works on the design, fabrication, characterization, and modeling of CMOS transistors, with specific engagement on the diverse challenges faced in device scaling for improved performance and density of integrated circuits. Issues addressed in his recent projects include: channel engineering using novel materials such as silicon-germanium (SiGe), novel device structures such as the ultra-thin-body transistor, alternative gate dielectrics for reduction of direct tunneling gate leakage current, and CMOS process integration involving a dual-metal gate technology. His research encompasses experimental device fabrication and process development, as well as theoretical modeling of materials interfaces and device simulation.

In his work on strained-channel transistors, he developed a simple and novel bulk CMOS process that integrates a pseudomorphically-strained SiGe channel layer for transistor performance enhancement. He has also worked on the integration of the SiGe heterostructure channel in a novel device structure, the ultra-thin-body MOS transistor. The ultra-thin-body transistor relies on a body thickness of 20 nm or thinner to suppress short-channel effects. Some highlights of this project were the demonstration of the first ultra-thin-body MOS transistor incorporating a SiGe heterostructure channel, and the report of the smallest heterostructure MOS transistor to date. The ultra-thin-body was formed by a novel solid-phase epitaxy technique. From June 2001 – January 2002, he was with the Exploratory Technology Department of Taiwan Semiconductor Manufacturing Company, Taiwan, where he led a team of engineers on strained-channel MOS transistors research and development.

Another area of his research relates to alternative gate dielectrics and metal gates, their process integration issues and impact on device performance. The direct tunneling gate current in transistors with alternative gate dielectrics is investigated, and important material parameters such as the tunneling effective masses are extracted. He recently explored the scaling limits of alternative gate dielectrics based on their direct tunneling figures-of-merit and gate leakage requirements for future CMOS technology generations. Guidelines are provided for the selection of gate dielectrics to satisfy the off-state leakage current requirements of future high-performance, low operating power, and low standby power technologies. He has also worked on the integration of two different metal gates in a CMOS process in an attempt to eliminate the problems of poly-silicon gate depletion, high gate resistance, and dopant penetration. This work resulted in the first demonstration of a dual-metal gate CMOS technology using titanium and molybdenum gate electrodes. He also employed the interface dipole theory to explain the experimental observation that metal workfunctions on high-k dielectrics differ appreciably from their values on SiO2 or in vacuum, and provided additional guidelines on the choice of gate materials for future CMOS technology incorporating high-k gate dielectrics.

He has authored or co-authored more than 30 journal and conference papers, and has written a book chapter on MOS transistor gate oxide reliability with Professor Chenming Hu.

Sergei Kucheyev

Sergei Kucheyev is a student in the Department of Electronics Engineering at the Australian National University in Canberra and his supervisor is Professor Chennupati Jagadish.

Sergei Kucheyev's research has focused mainly on ion-beam processing of group-III-nitride and ZnO

semiconductor devices. Ion-beam-produced defects can severely alter all material properties. Hence, an understanding of ion-irradiation-produced defects is essential if potential applications of ion implantation for the fabrication of III-nitride- and ZnO-based electronic devices are to be fully exploited. Emphasis of Sergei's project has been on an understanding of (i) the evolution of defect structures in III-nitrides and ZnO during ion irradiation and (ii) the influence of ion irradiation on structural, mechanical, optical, and electrical properties of these materials. In addition to ion-beam processes, Sergei's current research interests include the deformation behavior of brittle semiconductors (in particular, GaN and ZnO) and basic properties of defects in wide band gap semiconductors.

His project has resulted in the identification of a range of new and technologically important phenomena in group-III-nitrides and ZnO during ion implantation. These phenomena include (i) an unexpected and rather complex behavior of damage accumulation during ion irradiation, (ii) ion-beam-induced phase transformations in III-nitrides, (iii) local stoichiometric imbalance and associated material decomposition during ion implantation as well as during post-implantation thermal annealing, (iv) an intriguing microstructure of defects in ion-irradiated III-nitrides and ZnO, and (v) the evolution of implantation-produced defects during thermal annealing. An understanding of these phenomena is important for a successful application of ion implantation in the fabrication of electronic devices. Sergei's research on mechanical properties has led to a significantly improved understanding of the plastic deformation behavior of GaN and ZnO, which is crucial for the estimation and control of contact-induced damage in GaN- and ZnO-based electronic devices. During his Ph.D. work, Sergei has published more than thirty papers in prime journals in the field.

He has recently been awarded a highly prestigious postdoctoral fellowship at Lawrence Livermore National Laboratory (LLNL) in the U.S.A. Only up to two Fellowships in all fields of research are awarded each year with typically several hundred applicants from all over the world for the three-year program. Sergei is planning to start his appointment as a Distinguished Lawrence Fellow at LLNL in the latter part of 2002.

TK Ghosh

T. K. Ghosh is a student in the Engineering Department at Lancaster University, Lancaster, UK and his supervisor is Professor R. G. Carter.

T. K. Ghosh's research interest is on 3-D simulation and design optimisation of multistage depressed collectors for high efficiency travelling wave tubes. Travelling wave tube (TWT) is a linear beam microwave device and it is an important part of any satellite and air-borne communication system. Multistage depressed collector (MDC) is one of its major components; other two are electron gun and slow-wave structure. A dc beam, generated from the electron gun, transfers some its energy to the input rf wave through a complex process and the rf gets amplified during its travel through the length of the slow-wave structure which is then taken out from the interaction region. The purpose of a collector is to recover most of the remaining power from the spent beam and thereby increase the collector and the overall efficiency. A well-designed multistage collector sorts electrons in the spent beam according to their energy and allow them landing softly which otherwise hit the electrode surface with sufficient energy to generate heat and knock out secondary electrons. Secondary electrons play the detrimental role in collector efficiency if they are collected at a lower depressed electrode from where they were generated. They introduce noise to the amplified signal if stream back towards the interaction region, which is highly undesirable. Experimental results have shown that graphite and carbon, which have low secondary electron emission properties, can be used as electrode materials to suppress the secondary electron emission successfully to a significant level. Use of asymmetric collector geometries and the application of magnetic field in the collector region have proved to be effective in recapturing the secondaries. A fully 3-D simulator LKOBRA (MF) – mainframe version of Lancaster KOBRA has been developed at Lancaster University, UK, which is capable of simulating the multistage collectors including the effects of secondaries and the magnetic field. It is based on KOBRA3 (originally developed for the simulation of ion sources) that has been modified and the pre- and post-processors of the package have been included.

Efficiency is a prime concern in space applications; TWT is no exception. It is always desirable to optimise the collector performance to maximise the overall amplifier efficiency. At first the potentials at different electrodes are optimised to achieve maximum possible theoretical efficiency. The number of collector stages is restricted due to the compromise among efficiency, weight and complexity in fabrication and power supply. A computer code based on the well-known hill climbing technique has been developed where all possible combinations of the electrode potentials are considered in such a way that the area under the spent beam curve covered by the electrodes is maximum for maximum power recovery. This makes the algorithm robust and reliable. It is also simple to implement. In the next step the geometry of the collector electrodes is optimised using an automated design package that is based on the 3-D simulator LKOBRA (MF). This package has been developed using a genetic algorithm. A genetic algorithm creates a new geometry through a search procedure that works from a population simultaneously. New set of geometries is generated using three basic operators, namely reproduction, crossover and mutation. The efficiency is used as the fitness parameter in the genetic algorithm that produces a new population of geometries. It acts as the deciding parameter for the changes in the collector geometry to be made. This package has been used to optimise the efficiency of a 4-stage symmetric collector to about 90% and for a 3-stage asymmetric collector to nearly 84%. In both cases the effect of secondary electron emission has not been considered which will be included in the future work.

As our current winners finish their Fellowship terms, we wish them success in their research and future endeavors. The competition for 2002 EDS Fellowship Awards is ongoing; the winners will be announced in July 2002.

Ilesanmi Adesida
EDS Educational Activities Chair
University of Illinios
Urbana, IL, USA

Third IEEE International Vacuum Electronics Conference Banquet

Wednesday, April 24, 2002

Dinner

Salinas Valley Greens

With Bleu Cheese Crumbles, Spiced Walnuts, Shaved Fennel and Port Wine Dressing

Grilled Swordfish

With Papaya-Lime Relish

Cappuccino Mousse Cake

Awards

IEEE Electron Devices Society

2001 Graduate Student Fellowship

Tushar Kanti Gosh

2002 IVEC Award for Excellence in Vacuum Electronics

To be announced

Entertainment

"A Tribute to the History of Vacuum Electronics"

Tushar
Carry on the research on Gallecta design that I started 25 yrs. ago. Jim Asmus

Tushar,
Congratulations.
This is WELL DESERVED!
Carol Kory

Hi Tushar - It was great meeting you at IVEC this year. Congratulations! You have a spectacular future ahead of you!
Keep up the good work R.S. Symons

Tushar,
I see 95% collection efficiency in your future.
-Will Menning

congratulations
Yingqin Miao

Your paper was excellent. A great combination of very separate disciplines. Thank you
Stephen Dick Tsue

Congratulations Tushar
Richard Carter

Well done Tushar
best wishes for the future
Richard Jenkins

Well done, dear boy
(& congratulations to Sutapa, too) Andrea

Wonderful!
our best congratulations
Jan Todd

My best wishes to all future achievements
Carlos Hernandez

The life is wonderful
Enjoy your life and dream of many outstanding tubes
Philippe THOUVENIN